MODULATING LIPID FLUX SENSITIZES TUMOURS IN A FATTY TUMOUR MICROENVIRONMENT TO ONCOLYTIC VIRUS THERAPY

ABERA SURENDRAN

Thesis submitted to the University of Ottawa in partial fulfillment of the requirements for the Doctorate of Philosophy in Microbiology and Immunology

Department of Biochemistry, Microbiology and Immunology
Faculty of Medicine
University of Ottawa

ABSTRACT

The tumour microenvironment (TME) is an important determinant of successful drug intervention. In 'fatty' tumours such as breast cancer, adipocytes are abundant and active in the TME. Ovarian cancers demonstrate an overwhelming metastasis to the omentum (a site of abdominal fat storage), indicating a propensity for a fat rich TME. Adipocytes are well known for their rich source of energy and endocrine function but there is a growing body of evidence for a role in driving resistance to anti-cancer therapies across a diverse range of treatment modalities. Oncolytic viruses (OVs) are a unique class of immunotherapeutic drugs that selectively lyse cancer cells and initiate a host anti-tumour immune response. We sought to determine the effects of adipose tissue and adipocyte-secreted factors on responses to OV therapy. Here, we found that tumours in a fat rich TME *in vivo* or receiving adipocyte-secreted factors *in vitro* are strongly resistant to OV infection. By employing a protease or using lipid-depletion strategies, we determined that the inhibitory effect derives from lipid constituents in adipocyte conditioned media (ACM). Closer examination of cells receiving ACM revealed that cancer cells become strikingly accumulated with lipids and this coincides with a metabolic shift favouring lipid metabolism. In an effort to overcome adipocyte mediated OV resistance, we briefly evaluated the effect of limiting *de novo* lipogenesis and, more extensively, blocking fatty acid (FA) uptake by FA transport proteins (FATPs). We found that blocking FA uptake, specifically FATP2-mediated FA transport, can mitigate the OV inhibitory effects of adipocyte secreted factors *in vitro* and *in vivo*, in our models. The findings from this thesis highlight the therapeutic advantage of incorporating lipid modulating strategies in combinatorial approaches with OVs.

ACKNOWLEDGEMENTS

The work presented in this thesis would not be possible without the support of numerous people both in and outside of the lab. First and foremost, I would like to thank my supervisor and co-supervisor, Drs. Carolina Ilkow and John Bell, for your mentorship. I am grateful to have had the opportunity to conduct research in your esteemed labs and fulfill my 'mad scientist' dreams. I would also like to acknowledge my thesis committee members, Dr. Barbara Vanderhyden, Dr. Morgan Fullerton and Dr. Tommy Alain, whose diverse backgrounds were instrumental in shaping the progress of this interdisciplinary research project.

Thank you to all of my lab mates at the Cancer Center and the greater OHRI for your support and encouragement. I would especially like to thank Dr. Harsimrat Birdi, Dr. Leonard Angka and Nouf Alluqmani for your technical assistance and patience with flow cytometry experiments. Thank you to Christine Lawson and Dr. Lee-Hwa Tai for your collaboration and expertise on Seahorse experiments. I would also like to acknowledge the indelible contributions of hard-working summer students, Victoria Taylor and Ben McSweeney. Julia Petryk and Christiano Tanese de Souza were critical for the completion of mouse work. Christiano, in addition to your technical expertise, your humour and moral support were very much appreciated throughout my studies.

Thank you to all past and present Ilkow and Bell lab members for fostering a friendly and collaborative work environment. I would especially like to thank Dr. Joanna Poutou, Dr. Taylor Jamieson-Datzkiw, Dr. Serge Neault, Dr. Ragunath Singaravelu, Jaahnavi Dave, Emily Brown, Xiaohong He, Bradley Austin, Shainyn Garrett, Marie-Eve Wedge, Hayley McKay, Sarah Tucker, Elaine Rose, Brian Laight and Dr. Brian Keller for your guidance and benchside comradery. Thank

you to Dr. Taha Azad for your collaborative spirit and encouragement to broaden my research activities.

Finally, this milestone would not have been possible without the support of my dearest friends and family. My parents, Thirunavukkarasu Surendran and Sumathy Surendran, and my brother, Aravind Surendran, have been a pillar of strength throughout this journey. Though we were physically apart, I never felt too far from the warmth of your love and support. Your phone calls and care packages of heartwarming home-cooked meals were instrumental in carrying me through the past 5 years. Thank you for your unrelenting support in helping me fulfill my dreams.

TABLE OF CONTENTS

LIST OF ABBREVIATIONS

ACC – acetyl-CoA carboxylase
ACM – adipocyte conditioned media
ACS – acetyl-CoA synthetase
ADSC – adipose-derived stem cells
AKG – α-ketoglutarate
ATGL – adipose triglyceride lipase
CAA – cancer-associated adipocyte
CD36 – fatty acid translocase
CMC – caroboxylmethyl cellulose
CoA – Coenzyme A
CPT1 – carnitine palmitoyltransferase I
CRAT – carnitine o-acyl transferase
DAG – diacylglycerol
DDX58 – DExD/H-Box Helicase 58
Dpi – days post-infection
EGCG – Epigallocatechin gallate
ER – endoplasmic reticulum
Eto – Etomoxir
FA – fatty acid
FAS – fatty acid synthase
FATP – fatty acid transport protein
FBS – fetal bovine serum
FCCP – trifluoromethoxy carbonylcyanide phenylhydrazone
FP – fat-pad
G – glycoprotein
GFP – green fluorescent protein
GM-CSF – granulocyte macrophage colony stimulating factor
GOT2 – glutamate oxaloacetate transaminase 2
HFD – high-fat diet
HI – heat inactivated
Hpi – hours post-infection
Hpt – hours post-transfection
HSL – hormone sensitive lipase
HSV – Herpes Simplex virus
IB – intrabursal
IFIT1 – interferon regulatory factor 1
IFIT2,3,4 – interferon induced proteins with tetratricopeptide repeats
IFITM1 – interferon-induced transmembrane protein 1
IFN-α – interferon- α
IFNAR – interferon-α/β receptor
IL-1β – interleukin-1β
IL-6 – interleukin-6

ISG – interferon-stimulated gene
JAK/STAT – Janus kinase/signal transducer and activator of transcription
JAK1-3 – Janus kinase 1-3
JAKi – JAK inhibitor
L – large polymerase
L-Asp – L-aspartate
lncRNA – long non-coding RNA
LRA – lipid removal agent
M – matrix protein
MAG – monoacylglycerol
MDSC – myeloid derived suppressor cells
MeV – measles virus
MG1 – oncolytic Maraba virus
MOI – multiplicity of infection
MX1 – interferon-induced GTP-binding protein Mx1
NCS – newborn calf serum
OAS1-3 – 2'-5' – oligoadenylate synthetases
OCR – oxygen consumption rate
OV – oncolytic virus
PFU – plaque forming unit
PK – proteinase-K
PPAR-γ – proliferator-activator receptor γ
PUFA – polyunsaturated fatty acids
RD – regular diet
RT – room temperature
SC – subcutaneous
SLC27A1-6 – solute carrier family 27 1-6
STAT1 – signal transducer and activator of transcription 1
STOSE – spontaneously transformed ovarian surface epithelial
TAA – tumour associated antigen
TAG – triacylglyceride
TCA – tricarboxylic acid
TME – tumour microenvironment
TNBC – triple negative breast cancer
TNF-α – tumour necrosis factor alpha α
TOFA – 5-tetradecyloxy-2-furoic acid
TXNIP – thioredoxin interacting protein
Tyk2 – tyrosine kinase 2
VACM – visceral adipocyte conditioned media
VACV – Vaccinia virus
VLP – virus-like particle
VSV – vesicular stomatitis virus

LIST OF FIGURES

LIST OF TABLES

COPYRIGHT STATEMENT

This thesis contains published and unpublished work.

Figure 2 was published in the following review article and has been included in this thesis in accordance with Elsevier's policy on the use of published text in a dissertation.

> Achard C*, Surendran A*, Wedge M-E, Ungerechts G, Bell J, Ilkow CS. Lighting a Fire in the Tumor Microenvironment Using Oncolytic Immunotherapy. *EBioMedicine* 2018; 31: 17–24.

The following published article is included Appendix IV of this thesis with written permission from JoVE.

> Rezaei R, Surendran A, Singaravelu R, Jamieson TR, Taklifi P, Poutou J, Azad T, Ilkow CS. Detection of SARS-CoV-2 Receptor-Binding Domain Antibody using a HiBiT-Based Bioreporter. Journal of Visualized Experiments: Jove. 2021 Aug 12(174).

All schematics and diagrams were produced with a paid subscription of BioRender.com which permits publication.

CHAPTER 1 – INTRODUCTION, RATIONALE & OBJECTIVES

INTRODUCTION

A Brief Introduction to Cancer

Cancer arises when healthy cells escape the mechanisms in place to keep uncontrolled growth and genetic integrity in check, and is often simply defined as an uncontrolled division of abnormal cells.[1] Typically, a cancer develops over decades, with at least half a dozen mutations in the genes affecting cell growth as well as epigenetic alterations that contribute to gene dysregulation.[1,2] Cancer incidence or increased risk of cancer can be inherited, can be a result of exposure to toxins, exposure to radiation, due to some medical interventions, hormones, chronic infections, diet or oncogenic viruses. [3,4]

The epidemiological prognosis for cancer incidence is bleak. In Canada, nearly half of the population is expected to receive a cancer diagnosis in their lifetime.[5,6] Despite advancements in anti-cancer therapies which surmounted in a peak in cancer mortality rates in the late 1980s, it remains a leading cause of death in this country and globally.[5] Thus, the persistent need for effective and durable anti-cancer therapies cannot be understated.

The Tumour Microenvironment

The field of cancer biology has evolved substantially from the longstanding model of a homogenous mass of tumour cells. It is now well documented that tumours are highly complex entities with heterogenic diversity and are supported by a diverse array of infiltrating cells that support its growth and proliferation. Immune cells (T cells, B cells, NK cells, dendritic cells, macrophages), endothelial cells, cancer-associated fibroblasts, cancer stem cells, cancer-

associated adipocytes (CAA) and the scaffolding extracellular matrix shape the tumour and its larger microenvironment.[7] The non-random nature of metastatic spread was first described by Stephen Paget where he outlined that tumour cells ("the seed") preferentially grow in selective microenvironments ("the soil"), and metastatic sites occur when this requirement is met.[8] Together, the complex interplay of the tumour cells and stromal elements of the microenvironment form a complex niche termed the tumour ecosystem or tumour microenvironment (TME).

Targeting stromal cells in the TME can improve anti-cancer therapeutic outcomes

Concerted efforts of tumour cells and cells of the TME create a supportive environment for tumour progression.[7] Targeting stromal cells in the TME is a proven strategy to promote tumour eradication. To this end, approaches that seek to "wake up" or activate the immune system aim to recruit and exploit the host immune system to help eliminate the tumour. For example, increasing the bioavailability of pro-inflammatory cytokine granulocyte-macrophage colony-stimulating factor (GM-CSF) stimulates antigen presentation by antigen presenting cells to ultimately supporting the anti-tumour functions of pro-inflammatory T-cells.[9,10] Checkpoint inhibitors, such as those that target checkpoint proteins CTLA-4 or PD-1/PD-L1, aim to override the negative regulation of T-cells induced by dysregulated checkpoint protein expression often observed in tumours.[11] Moreover, selective ablation of immunosuppressive cell types like myeloid derived suppressor cells (MDSCs) and tumour-associated macrophages have shown to be promising approaches to diminish the pro-tumour benefits of these cells in the TME.[12–14] Outside of immune-driven approaches, several trials have found success in targeting other stromal cell types. For instance, the targeting of tumour neovascularization with the use of anti-angiogenic

targeting compounds can promote anti-tumour effects in the TME.[15] Extracellular matrix remodelling in the TME increases tumour stiffness and inhibits the penetration of anti-cancer therapies into the tumour.[16–18] Using agents to block extracellular matrix protein production, such as an inhibitor of collagen I production, can improve the distribution and therapeutic impact of traditional nanotherapies and emerging immunotherapies, including oncolytic viruses (OVs).[19] Given the interwoven nature of the tumour and its supporting TME, it is unsurprising that the incorporation of strategies to target elements of the TME can significantly improve therapeutic outcomes. Incorporating TME stromal cell targeting strategies paves the way for a holistic approach in the way tumours are treated.

Adipocytes

Adipocytes are an underappreciated and often overlooked player in the TME. Typically recognized for their role in energy storage and endocrine functions, a growing body of evidence suggests that this dynamic cell type is a critical player in shaping the TME to influence tumour progression.[20–22]

Adipose tissue is largely comprised of adipocytes, but also harbours macrophages, monocytes, pluripotent stem cells, pericytes and endothelial cells.[23,24] There are two main types of adipose tissue, white adipose tissue and brown adipose tissue. Brown fat surrounds the heart and vessels in infancy and disappears with aging.[25] White adipose tissue, the dominant subtype in adulthood, is specialized in the storage of triacylglycerides (TAGs), the major energy reserve in eukaryotes.[26] TAGs are comprised of three fatty acids (FAs) esterified onto a glycerol molecule (Figure 1A). They make up the core of lipid droplets, where they are stored along with other

neutral lipids and encased in a phospholipid bilayer.[27] Perilipin proteins on the surface of lipid droplets act as gatekeepers, controlling the access of lipases to liberate stored lipids.[28]

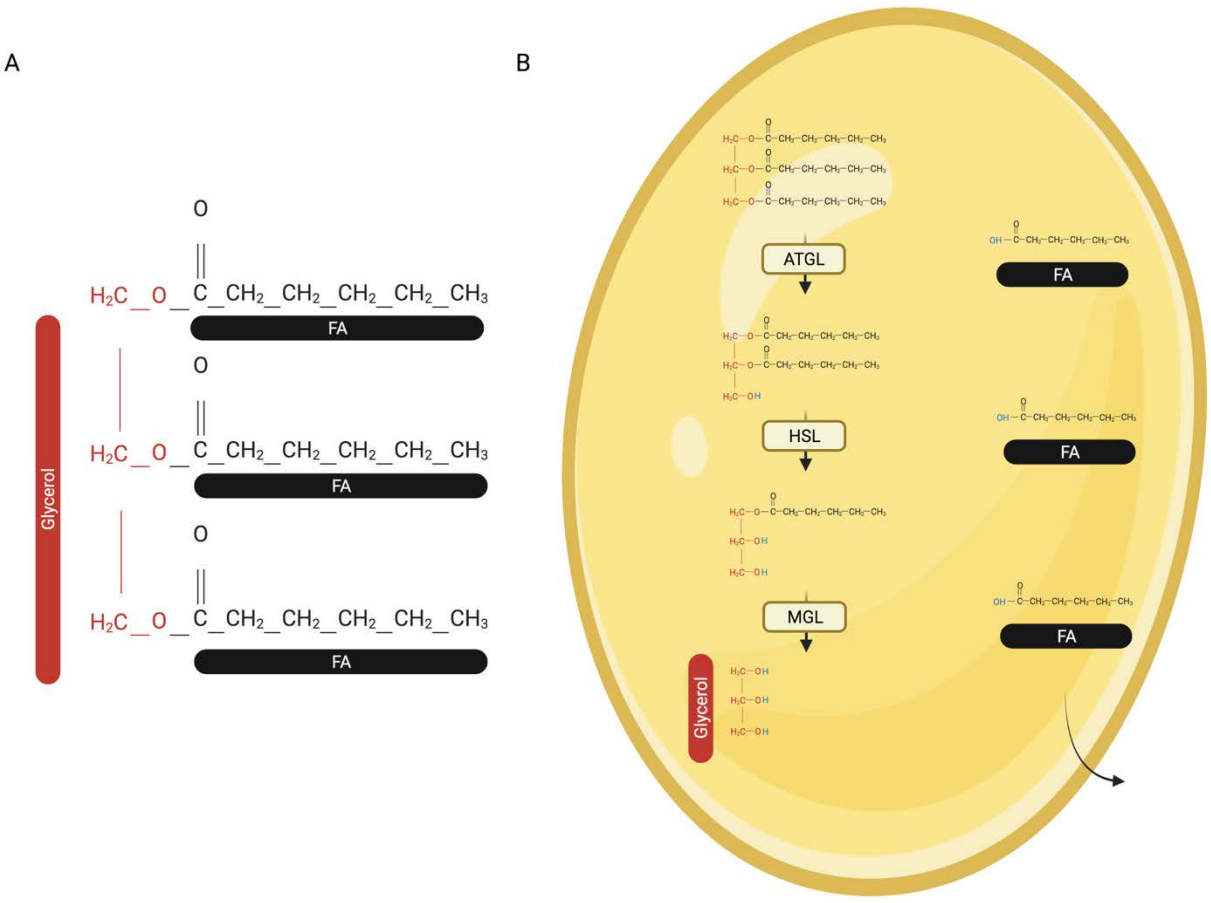

Figure 1: FAs are stored in TAGs and can be liberated by lipolytic enzymes. TAGs are made up of a 3 FAs that are esterified onto a glycerol molecule (A). FAs in lipid droplets can be liberated by lipolytic enzymes that hydrolyze TAGs into glycerol and free FAs. First, TAG is hydrolyzed into DAG by ATGL. DAG is then broken down into MAG by the action of HSL and finally, MAG is relieved of the last FA molecule by MGL to produce a glycerol molecule. The free FAs can now leave the lipid droplet for downstream metabolic processes.

Mature adipocytes are achieved from the differentiation of pre-adipocytes, a fibroblast-like cell type which arise from the mesenchymal lineage. Green and Kehinde showed that mature adipocytes can be obtained *in vitro* by providing a cocktail of FBS, dexamethasone,

isobutylmethylxanthine and insulin to 3T3-L1 murine adipocytes.[29] This cocktail activates adipogenic transcription factors and cell cycle regulators, including the expression of proliferator-activator receptor γ (PPAR-γ), a central regulator of adipocyte differentiation.[23,30] A critical step of the adipogenesis program is terminal differentiation. When pre-adipocytes are differentiated into mature adipocytes, they are characterized by lipid droplet accumulation and a specific metabolic program.[31]

Adipocytes play an important role in the tight control of energy storage and release. They adjust their secretory profile to respond to nutrient requirements of their environment by releasing a milieu of adipokines and adipo-cytokines such as leptin, adiponectin, visfatin, retinol-binding protein-4, resistin, tumour necrosis factor alpha (TNF-α), interleukin-6 (IL-6) and others, that play functional roles in regulating energy and metabolism. Control of adipocyte energy storage is regulated by hormonal and sympathetic signals. Specifically, the role of insulin and catecholamines (ex. Epinephrine and norepinephrine) are the best studied. Briefly, in calorie-rich circumstances, insulin promotes the storage of lipids by inducing the esterification of FAs into TAGs and inhibiting lipolysis, the hydrolysis of TAGs into glycerol and free FAs. In times of nutrient shortage, catecholamines and glucocorticoids initiate a series of events that results in the activation of proteins involved in lipolysis, like hormone sensitive lipase (HSL) and adipose triglyceride lipase (ATGL). Systemic regulation of adipocytes is complimented with autocrine and paracrine signaling to inform local adipocyte metabolic regulation.[23,32]

Release of adipocyte-stored FAs – lipolysis

Adipocytes are in a constant state of flux, toggling between re-esterification (storage of lipids) and lipolysis (release of stored lipids). They are highly efficient at storing energy, containing

more energy per unit mass than carbohydrates.[25] In times of nutrient demand, the stored energy is released into circulation in the form of free FAs and glycerol, broken down from TAG stores.[26] The breakdown of lipids is achieved in an orderly and sequential fashion. ATGL converts TAG into diacylglycerol (DAG) by liberating a free FA molecule. DAG is subject to further breakdown by removal of another free FA molecule by HSL, to produce monoacylglycerol (MAG). Finally, monoacylglycerol lipase catalyzes MAG to glycerol by releasing the remaining free FA chain (**Figure 1B**).[26] When FAs are found in their free form and not in their esters, they are referred to as free FAs or as non-esterified FAs. Free FAs and non-esterified FAs will simply be referred to as FAs in this thesis. The presence of lipolytic products glycerol and FAs are accepted as one of the most direct methods of detecting lipolysis.[33]

In the TME, cancer cell crosstalk with infiltrating adipocytes induces adipocyte lipolysis to liberate stored FAs into the microenvironment. The FAs are uptaken by cancer cells to support tumour progression (discussed further in 'Cancer-associated adipocytes' section).

FA Transport & Metabolism

FA transport by fatty acid transport proteins

Numerous proteins involved in FA transport are now being recognized as an important driver of tumour progression and targeting FA transporters as an anti-cancer strategy has shown promise.[34–38]

Small and medium chain FAs can be transported across the plasma membrane by passive diffusion. The translocalization of larger FAs like long-chain and very long chain FAs requires facilitated transport. This is achieved by transmembrane or membrane associated proteins like

plasma membrane associated fatty acid binding protein, fatty acid translocase (FAT/CD36) and fatty acid transport proteins (FATPs).[39]

FATPs are one of the most well studied group of proteins that transport FAs. They are members of the solute carrier family 27 (SLC27A1-6) commonly referred to as FATP1-6.[40] The predominant substrate of FATP proteins are long-chain fatty acids.[40,41] There is high degree of homology between these isoforms, sharing 3 distinguished regions: a transmembrane region, a FATP/very-long-chain acyl-CoA synthetase region thought to contribute to FA binding, and an ATP/AMP region which has a shared motif with acyl CoA synthetase (ACS).

In normal physiological conditions, the expression of FATPs are regulated in response to nutrient levels, hormones and even cytokines.[40,41] FATP1 is highly expressed in adipose tissue and skeletal muscle, with evidence for regulation by insulin.[42] FATP2 is most highly expressed in the liver and kidney.[43] There is accumulating evidence for FATP3 as a peroxisomal very long chain acyl-CoA synthetase but devoid of FA transport activity.[44] Similar to FATP1, FATP4 is also highly expressed in adipose tissue and skeletal muscle but includes the cardiac tissue. It has been linked to insulin resistance and obesity and to this end, has been a target for anti-obesity drug development.[43] FATP5 is proposed to aid FA transport and condense bile acids with Coenzyme A (CoA) for downstream metabolism in the liver.[40,45] FATP6 thus far appears to be isolated to cardiac tissue. Its FA transport and activation functions are not yet fully understood.[40,41,43]

Tapping into energy rich FAs – FA Oxidation

Fatty acids are carboxylic acids with an aliphatic chain (**Figure 1**). Following transport or concurrently with transport, FAs must be activated before being utilized in downstream metabolic processes. FATPs are bifunctional proteins that are well known to participate in vectorial acylation,

the concomitant activation of FAs into Acyl-CoAs during FA uptake.[46–48] Activation of FAs is achieved by the activity of ACS enzymes as shown below:

$$FA + ATP \rightarrow \text{fatty acyl-AMP} + PPi \qquad \text{(Adenylation Reaction)}$$

$$\text{fatty acyl-AMP} + CoA \xrightarrow{ACS} \text{fatty acyl-CoA} + AMP \qquad \text{(Thioester Formation Reaction)}$$

The energetic demands of the TME favour oxidation of FAs.[49] β-oxidation is a catabolic process which occurs in the mitochondria and, to a lesser extent, in peroxisomes. In mitochondrial β-oxidation, long and very long chain activated FAs are transported into the mitochondrial matrix by the efforts of carnitine palmitoyltransferase I (CPT1) and carnitine palmitoyltransferase II, on the outer and inner mitochondria membranes, respectively. In the mitochondrial matrix, the fatty acyl-CoAs undergo a series of oxidation reactions to generate acetyl-CoA molecules. Acetyl-CoAs feed into the TCA cycle to produce ATP.

CPT1 is the rate-limiting enzyme in β-oxidation and evidence is mounting for a tumour promoting role in cancer.[50,51] As such, CPT1 inhibitors are being actively investigated as a therapeutic tool to reduce the progression of disease.[52]

Cancer-associated adipocytes (CAAs) & their role in the Tumour Microenvironment

Obesity & cancer

Excess adipose tissue, as characterized in obesity, is an established risk factor for cancer. The correlation between overweight individuals and the incidence of cancer has been observed in endometrial, gastric, liver, kidney, esophageal, colorectal, pancreatic, gallbladder, breast, ovarian, prostate and thyroid cancers, as well as meningioma and multiple myeloma.[53] Obesity is also linked to local and distant invasion of tumours.[54–56] Moreover, inflammatory cell types, such as macrophages, are up to 50% more abundant in obese individuals verses lean individuals. This inflammation likely contributes to the adipocyte dysregulation observed in CAAs.[23,57]

CAAs have characteristic functions in the TME

Adipocytes in the TME take up a specific phenotype and are often referred to as CAAs. CAAs derive from adipose tissue surrounding the tumour, including dysfunctional adipose tissue in obese individuals, adipocytes that were differentiated from tumour-resident mesenchymal stem cells or adipocytes recruited to the tumour tissue as a result of cancer cell signaling.[58,59] Tumour-secreted inflammatory cytokines, such as TNF-α and IL-6, and soluble factors produced by cells in the TME, such as from cancer-associated fibroblasts or tumour-associated macrophages, promote the transformation of adipocytes into a pathogenic phenotype. Crosstalk between the CAAs and cancer cells in the TME promote tumour progression by stimulating pro-survival signaling in cancer cells.[59–63] In fact, co-culture studies revealed that cancer cells induce lipolysis in CAAs and the subsequent availability of FAs in the microenvironment serve as metabolic fuel for proliferating cancer cells. This induces a metabolic switch in cancer cells to favour β-oxidation.[23,58,64–66] The uptake of CAA-released FAs not only serves to meet the energetic demands

of the cell, but also contributes to the invasive and metastatic potential tumours.[38,59,66] Moreover, FAs likely also serve building blocks for plasma membranes and organelle composition.[58,67] Typically, cancer cells produce ATP through the 'Warburg effect', whereby ATP is produced by glycolysis rather than the more efficient oxidative phosphorylation. The phenomenon of acquiring energy from substrates provided by stromal cells of the TME is referred to as the 'reverse Warburg effect'.[21,68] The de-lipidation of CAAs coincides with adipocyte-induced expression of proteins involved in FA transport in cancer cells, like FATP1 and CD36.[36–38]

CAAs also secrete growth factors, adipokines and adipo-cytokines that potentiate tumour growth. These include fibroblast-growth factor, leptin, adiponectin, interleukin-1β (IL-1β), IL-6, TNF-α, CCL2 and CCL5.[23,58,69–71] In fact, adipokines also play important roles in promoting tumour aggressiveness and metastases. In breast cancer, leptin secretion was associated with increased expression of markers associated with epithelial-mesenchymal transition and metastasis.[72] Resistin secretion promotes the metastasis of breast cancer by phosphorylating ezrin, radixin and moesin, proteins involved in maintaining cell structure.[73] Together, CAA secreted lipids and adipokines stimulate proliferation, migration and survival of cancer cells. [23,74]

Histological analysis of numerous tumours with an adipose rich TME, including in breast and ovarian tumours, showed that the CAAs at the tumour front decrease in size and are replaced by tumour cells as well as fibroblast cells that are likely delipidated CAAs that have reverted to their de-differentiated preadipocyte form.[23] This TME remodeling is further potentiated by various CAA-secreted proteases that facilitate invasion of the tumour into neighbouring tissues.[75]

Lipogenic Enzymes in Cancer

High lipogenic activity has been associated with cancer progression, including metastasis. In addition to drawing FAs from the TME, cancer cells can generate intracellular FAs through the actions of *de novo* lipogenic enzymes.[76]

Fatty acid synthase (FAS), for instance, is overexpressed across numerous cancers including breast and ovarian cancer, and is often associated with a poor prognosis.[77] It is a multi-enzyme protein that catalyzes the synthesis of palmitate from acetyl-CoA and malonyl-CoA in the presence of NADPH. There is significant interest in determining appropriate inhibitors to target this proposed oncogene as an anti-cancer strategy.[78,79] Similarly, acetyl-CoA carboxylase (ACC) is overexpressed in numerous cancers.[77,80,81] It provides the malonyl-CoA substrate for the synthesis of FAs. The use of ACC inhibitors have shown promise in curbing tumour progression.[82]

Numerous cancer lipogenic enzymes are under investigation as targets for mitigating tumour growth, including SLC25A1 (blocking citrate supply for FA synthesis), SREBP-1 (blocking overexpression of lipogenic enzymes, SCD1 (inhibiting FA modification enzymes), LPCAT2 (blocking lipid droplet formation), among others.[83]

Breast cancer

Breast cancer is one of the most frequently diagnosed cancers globally, and a leading cause of cancer related deaths in women, second only to lung cancer.[84,85] It is a histologically diverse cancer but molecular studies have identified 3 major groups: luminal, human epidermal growth receptor-2 (HER2)+ and basal-like breast tumours.[86,87] Breast cancer can be highly aggressive, often producing tumour metastasis in the bone, lung, liver and brain.[88] The TME is a crucial player

in breast cancer progression. Fibroblasts, mesenchymal stem cells, adipocytes and immune cells (T-cells, NK cells and macrophages) play unique roles in supporting breast tumour growth.[89,90] Cancer cells secrete cytokines and chemokines that support the recruitment of these cells into the tumour and together, the tumour and supporting TME potentiates colonization of distant sites.[90,91]

CAAs in Breast Cancer

The breast is abundant in fat tissue, and it comes as no surprise that adipocytes play critical roles in breast cancer pathogenesis. Studies with adipose tissue grafts showed that adipose tissue can promote the pathogenesis of a subclinical tumour or regional reoccurrence of the tumour.[92] In a telling experiment by Dirat and colleagues, breast cancer cells that were previously exposed to adipocyte secreted factors through co-culture with adipocytes produced more lung metastases in mice receiving these cancer cells by tail vein injection, than cells that were cultured alone.[59] This aligns with separate reports indicating that adipocytes promote breast cancer cell motility.[93] *In vitro* assays evaluating the effect of adipocyte co-culture with breast cancer cells demonstrated a propensity to increase its invasive properties.[23] Transcriptomic profiling showed an increase in tumourigenic markers associated with cell proliferation (IGF2, FOS, JUN, cyclin D1). Markers associated with cell invasiveness (MMP1, ATF3), survival (A20, NFκB) and angiogenesis were also noted.[94] Specifically, CAA-derived adipokines were implicated in promoting some of these pro-tumour effects. IL-6 and leptin encouraged breast tumour invasion by promoting collagen remodeling and metastasis formation.[95] In triple-negative breast cancer (TNBC), the most aggressive and difficult to treat type of breast cancer, high levels of adipocyte-derived CCL5 was associated with a poorer prognosis.[96]

Adipocytes in co-culture with breast cancer cells show hallmark features of CAAs – de-lipidation, the loss of terminal differentiation markers (adiponectin, resistin and FA binding protein 4) and an increase in the expression of proinflammatory gene expression such as IL-6.[23] In fact, histological evidence further supports the idea of crosstalk in the breast cancer TME that contributes to pronounced tumour aggressiveness. At the invasive front of the tumour there is a visible decrease in adipocyte size. Breast cancer cells in coculture with adipocytes undergo intracellular lipid accumulation, suggesting that the liberated FAs are being uptaken by nearby cancer cells.[51,67,97]

Often breast cancer patient deaths are attributed to the metastatic lesions rather than the primary breast tumour.[98] A main metastatic site of breast cancer is the bone marrow where adipocytes make up the majority of the cell population.[88,99] Adipocytes constitute 70% of the volume in bone marrow and this figure increases with age.[100] There is some evidence to suggest that breast cancer cells are homed to the bone tissue by adipocyte-secreted leptin and IL-1β signaling.[101,102] Here, cancer cells can capitalize on bone-marrow derived FAs to meet their energetic demands.[99] Adipocytes from different sources have distinct secretory profiles, thus the specific impact of bone-derived adipocytes may have distinguishing impacts on metastasized tumours. [103,104]

Although breast tumour metastasis is observed in the adipose-rich bone marrow, metastases in other non-adipose rich regions, such as the brain and lung are also common; thus, breast cancer metastasis is likely a multifactorial phenomenon.

There is a demand for more effective breast cancer treatments

The treatment regimen for the treatment of breast cancer depends on the stage. Depending on the characteristics of the tumour, it may include a lumpectomy, chemotherapy, radiation, a mastectomy, endocrine therapy, immunotherapies, or a combination of these modalities.[105] The advancements in anti-cancer therapies have significantly improved survival among breast cancer patients; however, given the high incidence of breast cancer and the persistence of treatment resistant and aggressive tumours, there remains a undeniable need for more robust and durable therapies.[106]

Ovarian cancer

Ovarian cancer is one of the most lethal gynecological cancers, accounting for 5% of cancer deaths in women despite only making up 2.5% of all malignancies.[107] This is in large part due to diagnosis at later stages when the tumour is widely metastatic.[108]

The ovary has a pro-tumour niche, as evidenced by metastasis at the ovary from primary tumours originating from numerous other tissues including the fallopian tube, breast, colon and gastric cancers. [109–112] Cancer-associated fibroblasts, endothelial cells and immune cells (tumour-infiltrating lymphocytes, MDSCs, macrophages) can be found in the ovarian TME and a high quantity of stromal cells in the TME is associated with a poor prognosis. [113–115]

CAAs in Ovarian Cancer

In ovarian cancer, metastasis in the abdominal cavity is a non-random event. Over 80% of patients exhibit metastatic sites in the omentum, a site of a large abdominal fat pad.[66] In high-

grade serious ovarian cancer, the most commonly diagnosed type of ovarian cancer, metastasis outside of the abdominal region is rare.[116]

There are 5 primary adipocyte deposits in the peritoneum – the omentum, gonadal fat, uterine fat, mesentery and splenoportal fat.[117] When cancer cells from the primary site shed into the peritoneal cavity, the flow of the peritoneal fluids provide access for dissemination throughout the organs in the peritoneum in a process called direct intraperitoneal seeding. Adipocyte secreted factors influence various steps of this process, from detachment of cells from the primary tumour, to its movement and eventual implantation at a metastatic site. [61,118,119] Nieman and colleagues eloquently showed that adipocytes promote the homing of ovarian cancer cells to the omentum through signaling by the adipokines Interleukin-8 (IL-8), IL-6, monocyte chemoattractant protein 1 and adiponectin.[66] IL-6 and IL-8 can induce anti-apoptotic signaling in nearby ovarian cancer cells through the actions of BCL-2 and BCLXL.[120] In addition to homing ovarian cancer cells to distal sites, adipocytes promote tumour growth. When mice are injected with ovarian cancer cells and adipocytes, the tumours grow larger than with tumour cells alone and there is evidence to suggest that this effect could at least in part be attributed to the transfer of FAs from adipocytes. When co-cultured, adipocytes undergo lipolysis and ovarian cancer cells increase their rate of CPT1 expression and β-oxidation.[66] In a separate *in vivo* study evaluating the effect of intraperitoneal injection with ovarian cancer cells, diet-induced or leptin-mutant obese mice had increased tumour burden in comparison to leaner mice.[56] This correlates with clinical data demonstrating that increasing body mass index enhances ovarian cancer.[121] In line with aforementioned evidence of CAA-mediated remodeling of the TME, histological analysis shows that the adipocyte area of

the omentum decreases during the time course of ovarian cancer growth, insinuating CAA-cancer cell crosstalk that promotes de-lipidation of CAAs for cancer cell uptake of liberated FAs.[117]

The interaction of ovarian cancer cells with adipocytes in a fatty TME promotes the expression of genes involved in FA transport. Metastasized ovarian cancer cells were found to be upregulated in fatty acid transport proteins such as FA binding protein 4 and CD36.[36,116,122] FA binding protein 4 inhibition studies revealed that FABP4 inhibition can reduce tumour weight and the number of metastasis.[66] In a separate study, interaction with adipocytes increased the expression of CD36 and its inhibition reduced FA uptake and lipid accumulation.[36] Interestingly, the transcriptional profile of these cells revealed that they were also downregulated for genes associated with endogenous lipid metabolism and cholesterol biosynthesis, suggesting that cells in the vicinity of adipocytes rely more heavily on exogenous lipid sources rather than *de novo* lipogenesis.[36] The 'reverse Warburg effect' in ovarian cancer is further corroborated by alterations to adipocytes in the vicinity of ovarian cancer cells. When ovarian cancer cells are co-cultured with adipocytes, adipocytes are increased in the phosphorylation of HSL, a key enzyme in lipolysis, and increased transcription of perilipin, the gatekeeper of lipid droplets.[123]

<u>There is still a demand for more effective ovarian cancer treatments</u>

Treatment for ovarian cancer often consists of debulking surgery and adjuvant therapy, chemotherapy and poly(ADP-ribose) polymerase inhibitors. [124] Ovarian cancer prognosis directly correlates with the stage of disease at the time of diagnosis.[125] Unfortunately, due to lack of effective early detection methods, patients are often diagnosed in later stages when the tumour is already widespread. Thus, there is a persistent need for more effective and robust anti-cancer therapies to improve outcomes for those diagnosed with this aggressive illness.

Adipocytes impede the efficacy of anti-cancer therapy

Adipocyte-mediated treatment resistance occurs through diverse mechanisms

Adipocytes are emerging as an undeniable player in anti-cancer treatment resistance across numerous tumour types. In mouse models of leukemia, adipocyte conditioned-media (ACM) inhibits vincristine chemotherapy-induced apoptosis by promoting pro-survival signaling.[126] Similar patterns of adipose tissue induced chemoresistance were observed in squamous cell carcinoma of the tongue, breast cancer, acute lymphocytic leukemia and among others.[127–130] The adipocyte secretome has also been implicated in radioresistance and resistance to targeted therapy, such as SAHA, a histone deacetylase inhibitor.[131,132] In targeted therapies like Trastuzumab, a clinically approved humanized antibody drug for the treatment of breast cancer, pre-incubation of HER2-positive breast cancer cells with ACM reduced Trastuzumab-mediated antibody-dependent cellular toxicity.[133] In another targeted therapy L-asparaginase, a first-line therapy for acute lymphocytic leukemia patients, adipocyte secreted factors protected leukemic cells from L-asparaginase mediated cytotoxicity. [134]

The mechanism of adipocyte-mediated treatment resistance has largely been investigated in the context of chemotherapy. Adipokines have been widely implicated in this process.[135] For instance, leptin is linked to chemoresistance.[130,132] Liu *et al.* showed that this is at least in part achieved through autophagy activation. Resistin, another adipokine, promoted multi-drug chemotherapy resistance through the upregulation of ATP-binding cassette transporter expression.[136] Moreover, Major vault protein, an intracellular transporter of molecules, was linked to doxorubicin resistance in breast cancer. [137]Alternative to transport-associated resistance mechanisms, adipocytes have also been shown to metabolize chemotherapy to ultimately deplete

the availability of the drug concentration in the TME.[138] In an eloquent study by Sheng *et al.,* the authors showed that adipocytes diminish the antileukemic activity of daunorubicin by metabolizing it into daunorubicinol, an inactive form of the drug.

Moreover, the metabolic adaptation of cancer cells to uptake FAs from an adipose rich TME can promote chemotherapy resistance. Ye *et al.* showed that chemotherapy resistance was associated with the expression of the FA transporter CD36.[139] In ovarian cancer, the FA arachidonic acid activates the Akt pathway to inhibit cisplatin-induced apoptosis.[140] Similarly, in anti-angiogenic therapy resistance, hypoxic conditions promote adipocyte lipolysis and trigger CD36-mediated FA uptake and β-oxidation in cancer cells.[58,66,141] Given the abundance of fat-deposits in the peritoneal cavity and a described role for adipocytes in promoting ovarian cancer progression, it is reasonable to speculate that adipocyte secreted factors play a role in ascites fluid-mediated resistance to chemotherapy.[66,117] The wide diversity in the mechanisms of adipocyte-mediated treatment resistance across a variety of different anti-cancer therapeutic platforms showcases the complex ways in which CAAs promote anti-cancer therapy resistance and highlights the need for a shift from cancer-cell centered therapy to a holistic approach that also considers CAAs in the TME.

Adipocyte-mediated treatment resistance can be overcome with lipid modulating drugs

Fortunately, the recognized role of adipocytes and specifically, adipocyte-derived FAs in the TME have inspired combination strategies to overcome adipocyte-mediated treatment resistance. For instance, blocking FAS, a *de novo* lipogenesis enzyme, improves chemosensitivity and radiosensitivity in breast and prostate cancers, respectively.[142,143] In anti-angiogenic therapy, pharmacological or shRNA mediated blocking of FAS overcame tumour re-growth and metastasis

following treatment withdrawal.[144] Targeting FAS also showed promise in improving responses to HER2-targeted treatment.[145]

Alternative to modulating *de novo* lipogenesis, attenuating lipid uptake can also alleviate adipocyte-mediated treatment resistance across a variety of different anti-cancer platforms. In prostate and ovarian cancers, monoclonal antibody-mediated blockade of the scavenger receptor CD36, provided control of tumour growth.[38,66] FATP1 blockade reduced tumour growth and invasion in a model of melanoma.[37] Alicea *et al.* discovered that age-related lipid-mediated resistance to BRAF/MEK inhibition can be overcome by blocking FATP2-mediated FA transport.[146] Further, there is some evidence to suggest that blocking FA oxidation with the use of a CPT1 inhibitor, etomoxir, can alleviate treatment resistance, at least in the case of anti-angiogenic therapy.[147] These studies highlight the tremendous value of modulating lipid flux in combination strategies with anti-cancer agents.

The rise of immunotherapy as an anti-cancer treatment modality

Chemotherapy, radiation and surgery have long been the standard of care for anti-cancer therapy. Recent advances have expanded the oncologists' toolkit to include targeted therapies (ex. poly(ADP-ribose) polymerase inhibitors, anti-HER2 antibody therapy), adjuvant therapy as well as immunotherapy.[148]

The field of cancer immunotherapy was catapulted by the promise of immune checkpoint inhibitors. Immune checkpoint inhibitors are molecules that disrupt the cancer-adapted brake on tumour detection by the host's immune system. In Canada, a handful of immune checkpoint inhibitors have been approved for use in advance-stage cancers.[149] Recognizing that the host anti-

tumour immune response is an incredibly powerful anti-cancer agent, the success of immune checkpoint inhibitors have fueled the development of other immune-modulating anti-cancer treatment modalities, such as cancer vaccines, adoptive T-cell therapies and OV therapy.[7,149,150]

Oncolytic Viruses

OVs are replication competent naturally occurring or genetically engineered viruses that specifically infect and kill cancer cells. OVs as an anti-cancer treatment modality emerged from the serendipitous observation that individuals who were simultaneously infected with a pathogenic virus experienced regression of their tumour, such as in the case of lymphoma regression after wild type measles infection. In the 1950s-1970s, deliberate delivery of live viruses into cancer patients was tested and showed some benefit but toxicity remained a significant barrier since the viruses were not adapted for tumour selectivity.[151–153]

Many decades of pre-clinical optimization and clinical testing surmounted in the landmark achievement of the first global regulatory approval of an OV for the treatment of cancer. China approved Oncorine (H10-1) in 2006, an attenuated adenoviral vector for the treatment of head and neck cancer in combination with chemotherapy.[154] Nearly a decade later, T-VEC (Imlygic) was approved by the FDA for the treatment of unresectable melanoma in the United States. This recombinant oncolytic HSV was the first to be approved for clinical use in the US. The number of OV therapies approved for clinical use is steadily increasing, with a multitude more being evaluated in pre-clinical and clinical studies globally.[153,155]

There are over 3000 species of viruses; however, not all viruses can be adapted for oncolytic use. The virus must be non-pathogenic in nature and be intrinsically tumour selective or

be engineered to be tumour selective.[156] The most popular viral platforms for OV development are Measles virus, Newcastle disease virus, Rhabdovirus, Adenovirus, Vaccinia virus, Herpes viruses, Coxsackievirus and Reovirus.[153]

OVs can infect normal cells or cancer cells; however, normal cells have competent innate anti-viral mechanisms to mitigate infection. Alternatively, cancer cells accumulate a plethora of functional properties that contribute to their oncogenesis, aptly termed the hallmarks of cancer. Briefly, the hallmarks of cancer are resisting cancer cell death, sustaining proliferative signaling, evading growth suppressors, activating invasion and metastasis, enabling replicative immortality and inducing angiogenesis.[157] Among the accumulated transformations include cellular changes that, coincidentally make cancer cells more susceptible to virus infection.[158,159] The intrinsic cellular defects in cancer cells provide a selective advantage for viral replication.[158] Tumour selectivity can also be achieved at the level of receptor-mediated cell entry and other host restriction factors.[153,160] Thus, OVs exploit the inherent susceptibility of cancer cells to virus infection. [161]

Cancer cells experiencing successful OV infection eventually succumb to the viral burden and the resulting cytolysis. This facilitates the spread of the OV in the TME for further infection, tumour debulking, and even abscopal effects, where tumour metastases experience regression despite not being directly treated at the site.[162–165] Moreover, tumour lysis and the release of tumour-associated antigens acts as *in situ* vaccination in the TME and contributes to generating a host-mediated anti-tumour immune response to wake up immunologically inert or 'cold' tumours to become inflamed or 'hot' (**Figure 2**).[7]

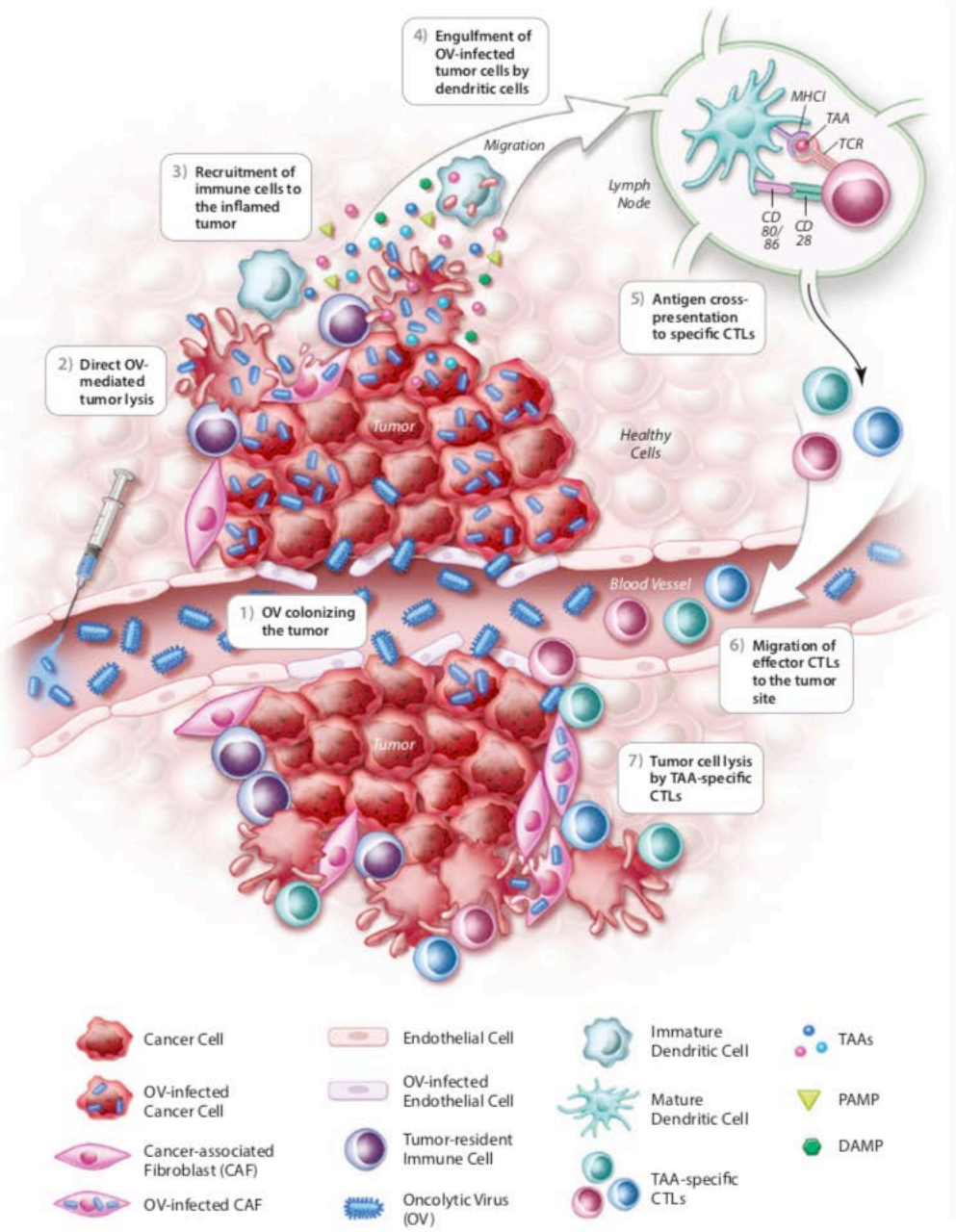

Figure 2: OV infection of the tumor serves as *in situ* vaccination. OVs directly infect and lyse cancer cells and stromal cells of the TME. The release of danger signals [pathogen-associated molecular patterns (PAMPs) and damage-associated molecular patterns (DAMPs)] and pro-inflammatory cytokines as well as the release of tumour-associated antigens (TAAs) from lysed cancer cells activate immune cells. Among them, dendritic cells engulf OV-infected tumor cells and migrate to the lymph node, where antigen cross-presentation to specific cytotoxic lymphocytes will take place. The TAA-specific cytotoxic lymphocytes then travel through the blood stream to reach the tumor, where they can exert their cytotoxic activity against cancer cells displaying specific TAAs. Thus, OV mediated tumour destruction is achieved by direct cytolysis and concerted action with the host immune system to ultimately eradicate the tumor. Adapted from Achard *et al.*[7]

The appeal of OVs also derives from its capacity to act as a replicating gene therapy vector. This platform overcomes the limitations of selectivity and dosing observed in gene therapy strategies since OVs can specifically infect and replicate in cancer cells. Today, we use rational therapy design to maximize the therapeutic impact of OVs by encoding immune stimulating [TNF-related apoptosis-inducing ligand (TRAIL), TNF-α, GM-CSF, tumour-associated antigens] and cancer death promoting payloads ('suicide genes'), without compromising a good safety profile. [7,155,161]

OVs are a unique and promising anti-tumour modality because of their ability to be tumour selective, directly kill cancer cells, induce a host derived anti-tumour immune response and provide potential to kill tumours with targets previously deemed undruggable.[166] In addition to killing cancer cells, this anti-cancer platform has also shown promise in targeting other malignant cell types in the TME, including cancer-associated fibroblasts and tumour vasculature. [167,168]

Clinical testing of OVs for the treatment of breast and ovarian Cancer

Despite significant advancements in therapies for breast and ovarian cancers, the need for new treatment avenues exist due to the persistence of treatment resistant tumour types. Several OV platforms investigated for clinical use either as a monotherapy or in combinatorial strategies include oncolytic HSV, oncolytic adenovirus, oncolytic reovirus, oncolytic vaccinia virus and oncolytic New Castle disease virus.[87,155] The use of OVs in highly resistant breast tumours like TNBC have also shown promise in pre-clinical studies.[169] In ovarian cancer, oncolytic vaccinia virus, oncolytic adenovirus, oncolytic reovirus and oncolytic measles are being tested as monotherapies as well as in combination strategies.[170,171] Many of these platforms have shown a promising safety profile, passing phase I clinical trials, and are actively being pursued for further clinical evaluation.

Despite the promise of OVs, the heterogeneity of cancers, the wide range in anti-tumour immune responses and the diverse TME poses barriers to tapping into the full anti-tumour potential of this treatment modality.

Vesicular stomatitis virus (VSV)

Vesicular stomatitis virus (VSV) is an enveloped, negative sense single stranded virus of the Rhabdovirus family.[172] It has an 11kb genome that is made up of 5 genes which encode the nucleocapsid (N), phophoprotein (P), matrix protein (M), glycoprotein (G) and large polymerase (L). The 5 proteins are encased by a phospholipid bilayer and coated with the transmembrane protein G to form a bullet shaped virus.[173] The natural hosts of VSV are cattle, swine, horses and deer.[174] Seroprevalance in humans is very low and as such makes VSV an attractive platform for therapeutic use in humans.[175]

VSV has broad tissue tropism largely in part due to the ubiquitous expression of its principal host-cell receptor for virus binding, low density lipoprotein receptor (LDLR).[174] LDLR is bound by VSV-G. Following attachment, VSV enters the cell by endocytosis. As it is trafficked through the endosomal pathway in the cell, a drop in endosomal pH occurs. The acidification catalyzes the fusion of viral and cellular membranes, releasing the viral ribonucleoprotein into the cytoplasm. The RNA-dependent-RNA-polymerase complex (nucleoprotein, phosphoprotein, and large polymerase protein) transcribes the viral genes and host ribosomes yield the corresponding proteins. The polymerase complex also synthesizes the positive-strand RNA which generates additional copies of the negative-strand genome. The genomic RNA and viral proteins are

assembled in the cytoplasm and the VSV particle leave the cell by budding through the cell membrane.[173]

The oncolytic VSV platform VSVΔ51

VSV is an attractive oncolytic platform. It is both a potent inducer of interferon and is susceptible to its anti-viral effects, setting the stage for controlled infection as an oncolytic agent.[176] VSVΔ51 is an attenuated version of VSV with a single residue deletion in the M protein. VSV M is a multifunctional protein with roles in virus budding and assembly.[177,178] Stojdl *et al.* showed that VSVΔ51 is unable to replicate in cells with intact interferon signaling; however, cells that have a defective interferon response remain susceptible to VSVΔ51 infection largely due to the mutant strain's inability to block the expression of host cell-derived anti-viral genes.[173,176]

Numerous recombinant VSVΔ51 platforms have been explored with the intention of maximizing oncoselectivity and anti-tumour potential while maintaining safety.[173,179] VSV-IFN-β-NIS (VoyagerV1™), an oncolytic VSV expressing interferon-β (IFN-β) and the sodium iodide symporter (NIS), has shown 'one-shot' curative potential in a murine model of myeloma and has a demonstrated clinical safety and tolerability in dose escalation studies in patients with late-stage endometrial cancer.[180,181] Recently, this platform has shown one shot potential in clinical evaluation of patients with relapsed refractory T-cell lymphoma.[182] VSV-IFN-β-NIS and other VSV platforms are being evaluated as a monotherapy or in combinatorial strategies in the context of numerous cancers including non-small cell lung cancer, colorectal cancer, melanoma, endometrial cancer, acute lymphocytic leukemia, among others.[183]

The oncolytic Maraba platform MG1

Maraba MG1 is an oncolytic Maraba virus that belongs to the rhabdovirus family and shares homology with VSV.[184] Mutations in the sequence of the M and G proteins produced an oncolytic Maraba with faster replication and increased tumour killing potential in comparison to the wild-type virus, while maintaining oncoselectivity.[184,185] Its ability for oncolysis has been validated in pre-clinical and clinical studies.[185] In clinical studies, Maraba oncolytic vaccines have shown a good safety profile (NCT02285816, NCT02879760).[185]

Lipids in anti-viral immunity

As obligate intracellular parasites, OVs rely entirely on host cell metabolism for successful infection and replication. Lipids are important players in virus infection and replication, including in the initial interaction with the host cell plasma membrane, fusion, modification of cellular compartments to facilitate replication and/or assembly and budding.[186,187]

Given the enrichment of CAA-derived FA species in the adipose-rich TME, it is relevant to examine the role of FAs on virus infection. Many viruses require FAs for both their replication and assembly; however, they can have pleiotropic effects on viral growth.[188] Interestingly, one of earliest evidence for anti-viral FAs was observed in breast milk.[189–191] Numerous FA species have been shown to have anti-viral activity across a diversity of viral species. Valproic acid, a small chain FA, impairs both VSV and West Nile virus; however, in the case of VSV, the production of viral RNA or protein synthesis was not compromised.[192] Similarly, lauric acid reduces Junin virus yields.[193] In studies with VSV, lauric acid did not disturb viral RNA or protein synthesis, but inhibited its maturation by impairing virus assembly.[194] Moreover, the level of FA saturation can promote or

hamper genome replication, as observed in the context of Hepatitis C virus.[195] The mechanisms of FA-mediated viral impairment is not thoroughly understood; however, the capacity for FAs to have anti-viral effects is irrefutable given the evidence for a broad range of FAs that can impair a broad range of viruses.

RATIONALE & OBJECTIVES

The TME is an undisputable driver of tumour progression and a key player in the response to anti-cancer therapy. Across numerous therapy modalities, adipocytes have been demonstrated to diminish the anti-cancer effects of various treatment modalities and promote therapy resistance.

This thesis aims to determine the effects of adipose tissue and CAAs on OV infection and OV therapeutic efficacy. As intracellular obligate parasites, OVs rely entirely on the host cell environment for therapeutic success. Given the highly metabolic nature of adipocytes and their ability to shape the TME, it is reasonable to hypothesize that adipocyte secreted factors can alter the impact of OV therapy in adipose-rich TMEs. Our early studies showed that an adipose-rich TME negatively impacts the anti-cancer effects of OV therapy. Correspondingly, we sought to characterize adipocyte-mediated resistance to OV therapy and, ambitiously, determine strategies to improve tumour sensitivity to OV infection in lipid-rich microenvironments.

Objectives:

1. Characterize the phenotypic changes in cancer cells due to co-culture with adipocyte secreted factors that contribute to OV resistance
2. Provide a mechanistic understanding of OV resistance
3. Develop strategies to overcome adipocyte mediated OV resistance

CHAPTER 2 – RESULTS

Section I: A 'fatty' TME or adipocyte secreted factors impede OV infection

1.1 A fat rich TME impedes OV infection *in vivo*

We hypothesized that an adipose-rich TME would influence intatumoural OV infection. To determine the effect of local tumour adiposity on responses to OV infection, we performed *in vivo* studies evaluating the effect of tumour localization on OV titers. Breast tumours were seeded subcutaneously (SC) or in the mammary fat pad (FP) and treated with OV by intratumoural delivery. 72 hours post infection (hpi), the intratumoural viral titer was quantified by plaque assay. In all 3 syngeneic breast tumour models that were evaluated (EO771, EMT6, 4T1), tumours seeded in the fat-rich mammary FP demonstrated significantly less VSVΔ51 infection than their subcutaneous counterparts (**Figure 3A-C**). A similar pattern of resistance was observed in the spontaneously transformed ovarian surface epithelial (STOSE) model of high grade serous ovarian cancer, a murine model of the most commonly diagnosed form of ovarian cancer. Tumours were seeded SC, in the FP, or orthotopic to the ovary (intrabursal, IB). In this study, both FP and IB-localized tumours were significantly more resistant to OV infection than tumours seeded SC (**Figure 3D**).

When tumour localization was held constant at the FP and the global adiposity of C57BL/6 mice were altered with a high-fat diet (HFD), the mice fed a HFD showed >1 log decrease in intratumoural OV titer in comparison to regular diet (RD)-fed mice (**Figure 4**). This finding correlated with an increase in tumour adiposity.

Taken together, the aforementioned studies strongly suggested that a fat-rich TME impedes OV infection at the site of the tumour.

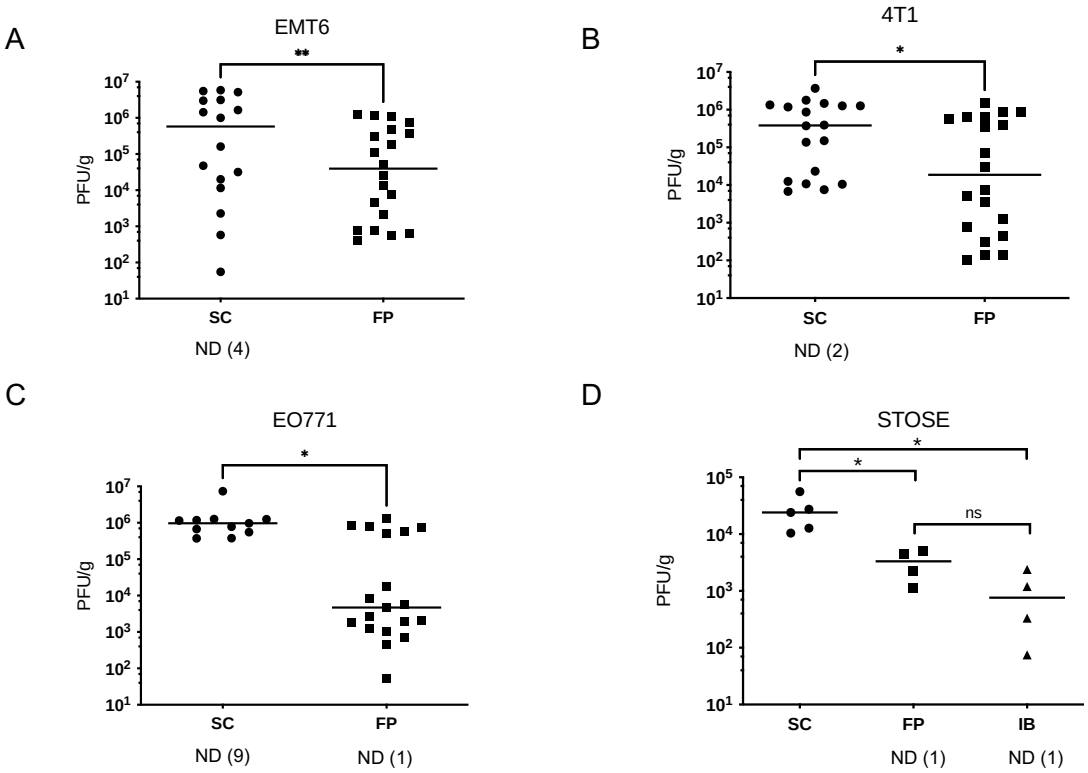

Figure 3: Tumour localization influences sensitivity to OV infection. EMT6 (A), 4T1 (B) or EO771 (C) cells were seeded in the FP and SC of Balb/c or C57BL/6 mice to generate double tumour bearing syngeneic breast tumour models. Tumours were intratumourally treated with VSVΔ51 (1.5E8PFU/tumour). STOSE cells were seeded SC, FP or IB in FVB/N mice and treated with Maraba MG1 (1E7 PFU/tumour) (D). Tumours were harvested 72 hpi for quantification by plaque assay. 20 mice/group harbouring bilateral tumours were used in A-C. 5 mice/group were used in C. ND (not detected) denotes the number of tumours that did not have detectable infectious viral particles by plaque assay. Line indicates median. Two tailed, unpaired t-test for A-C. 1-way ANOVA, Tukey's multiple comparison test for D, *p <0.05, **p <0.01.

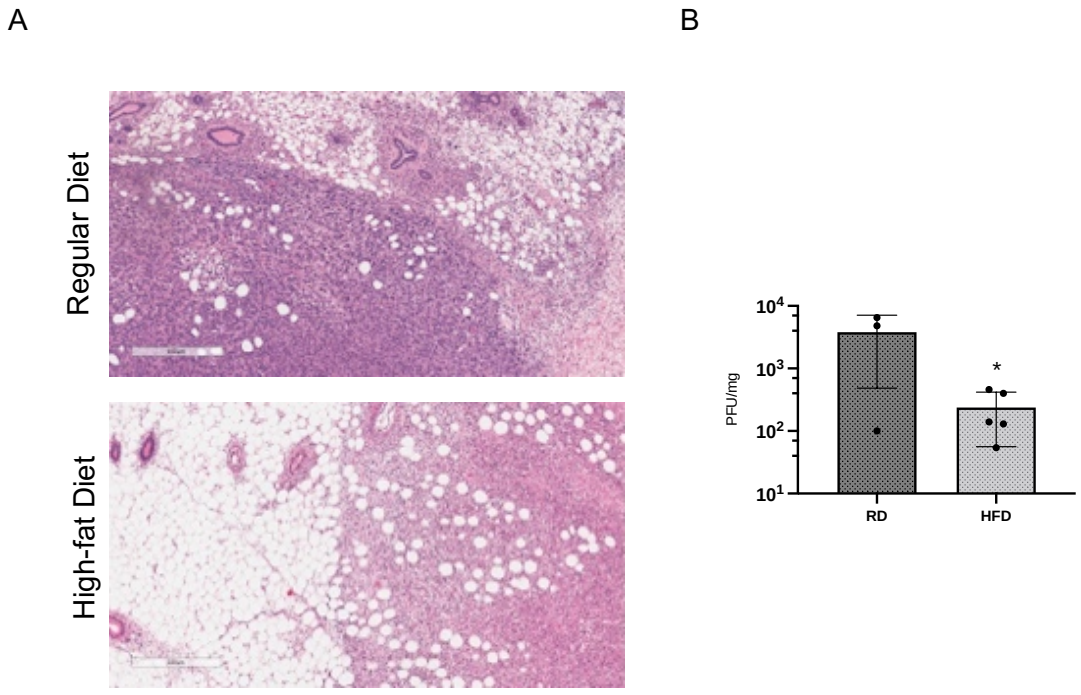

Figure 4: High-fat diet decreases sensitivity to OV infection. Following a period of high-fat (HFD) or regular diet (RD) feeding of C57BL/6 mice, EO771 cells were seeded in the FP. Representative H&E staining of tumours are shown (A). Tumours were intratumourally treated with Maraba MG1 (5E8 PFU/tumour) and harvested for quantification by plaque assay 72dpi (5 mice/group) (B). Tumours that did not have detectable OV infection or were below the limit of detection were excluded. Scale bar denotes 400µm or 500µm as indicated. Error bars represent SD. Two tailed, unpaired t-test, *p <0.05.

1.2 Adipocyte secreted factors impede OV infection *in vitro*

As previously mentioned, adipose tissue contains a myriad of different cell types; however, it is largely comprised of adipocytes. As such, we sought to investigate the role of adipocyte-secreted factors on OV infection.

Mature human adipocytes were obtained by differentiating primary preadipocytes with a proprietary differentiation cocktail (Zenbio). Following differentiation and short-term acclimatization to regular cell culture medium, the adipocyte conditioned media (ACM) containing adipocyte secreted factors were collected periodically (**Figure 5A**). The terminal differentiation to mature adipocytes was characterized by an accumulation of lipid droplets by microscopy (**Figure 5B**).

A small panel of breast and ovarian cancer cell lines (2 breast cell lines, 3 ovarian cell lines) were exposed to ACM and infected with a small, but diverse, panel of OVs belonging to 4 distinct viral families: Rhabdovirus (Vesicular stomatitis virus, VSV), Poxvirus (Vaccinia virus, VACV), Herpesvirus (Herpes simplex virus-1, HSV) and Paramyxovirus (Measles virus, MeV). We observed an overwhelming trend of resistance to OV infection in the presence of ACM in comparison to cells receiving control (CTL) media (**Figure 6A**). Among the cell lines and OV platforms tested, nearly all conditions showed statistically significant or palpable trend towards ACM-mediated resistance to OV infection. The robust nature of this resistant effect was visually apparent in immunofluorescence microscopy (IF) images of GFP-expressing OV-infected OVCAR8 cells (**Figure 6B**). OVCAR8 cells infected with oncolytic VSV, VACV, HSV or MeV showed less GFP expression from OV-infected cells in ACM compared to CTL media receiving cells. These studies strongly suggested that adipocyte secreted factors inhibit OV infection. A dilution series revealed that the

inhibitory effect is concentration-dependent (**Figure 7**) and the inhibition to OV infection is not due to an impairment in cell growth (**Figure 8**).

A

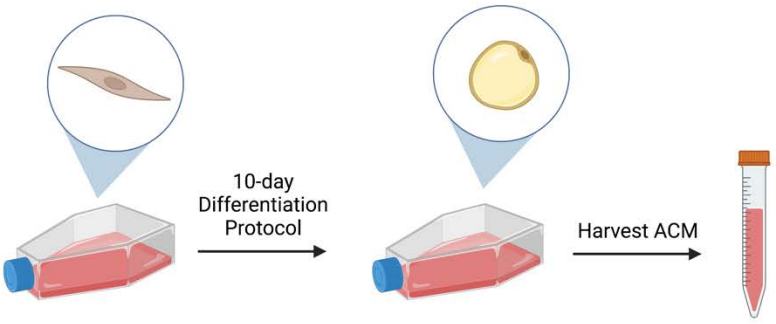

B

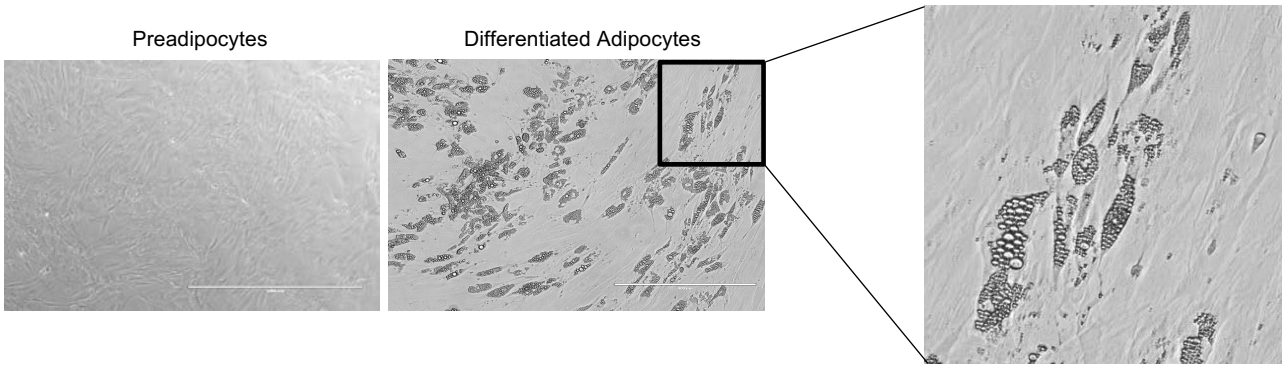

Figure 5: Adipocyte secreted factors are captured in ACM from mature adipocytes. Human adipocytes are differentiated to mature adipocytes over a 10-day differentiation protocol. After a short acclimatization period to regular culture media, the adipocyte conditioned medium (ACM) is harvested (A). Terminal differentiation of human adipocytes is characterized by an accumulation of lipid droplets as shown in (B). Scale bar represents 400µm.

A

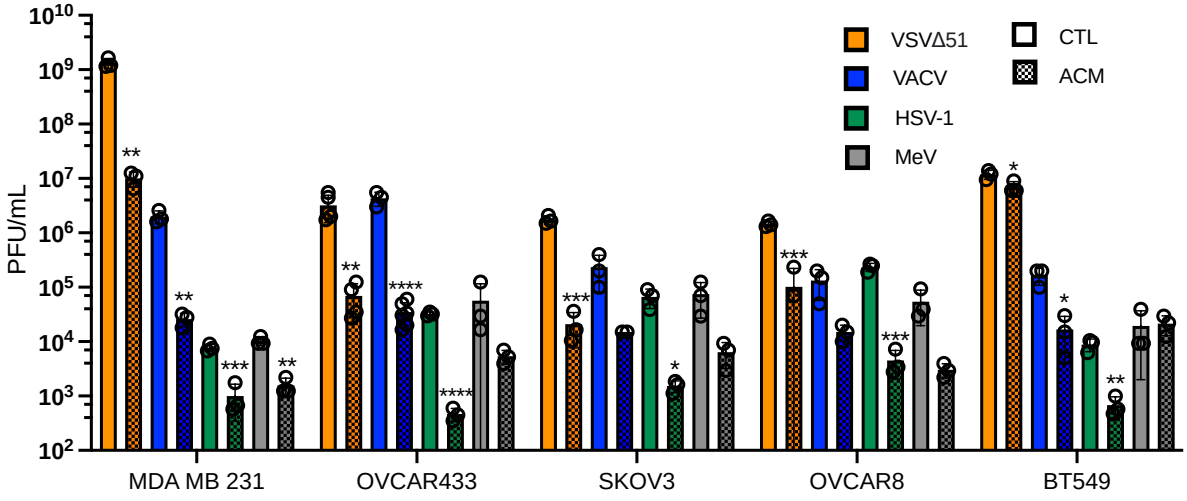

B

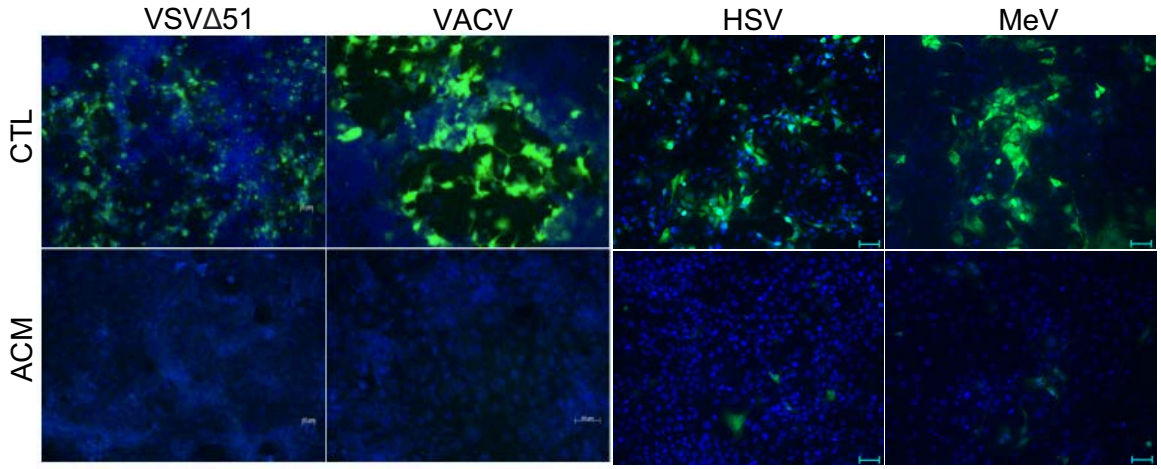

Figure 6: Adipocyte secreted factors inhibit OV infection. Titers from an OV-infected panel of breast and ovarian cancer cell lines were quantified by plaque assay. Titers are expressed as plaque forming units (PFU) per mL except for MeV which is determined as cell infectious units (CIU) per mL (n=3 biological replicates) (A). ACM was transferred to OVCAR8 cells and infected with GFP-expressing OVs (MOI 0.1, 24 hpi) from diverse viral families – VSVΔ51 (Vesicular stomatitis virus; Rhabdovirus family), VACV (Vaccinia virus, Poxvirus family), HSV-1 (Herpes simplex virus 1, Herpesvirus family) and MeV (Measles virus, Paramyxovirus family). Representative immunofluorescence microscopy images of OV-infected OVCAR8 cells are shown (VSV and VACV magnification 40X, HSV-1 and MeV magnification 63X; n=2 biological) (B). Scale bar represents 50μm. Error bars represent SD. Two tailed, unpaired t-test of each CTL vs ACM pair, *p <0.05, **p <0.01 ***p<0.001, ****p < 0.0001.

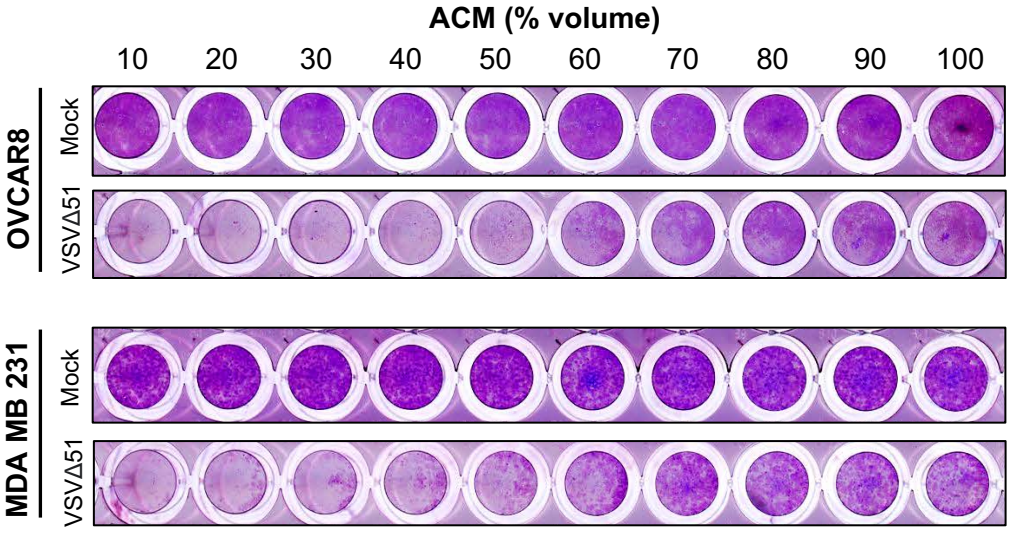

Figure 7: ACM-mediated OV resistance is concentration dependent. The indicated cells were cultured in increasing concentrations of ACM overnight before inoculation with VSVΔ51 (MOI 0.1) for 48hrs. The supernatant was removed, and the cell monolayer was stained with crystal violet for cytotoxicity analysis (n=3 biological replicates).

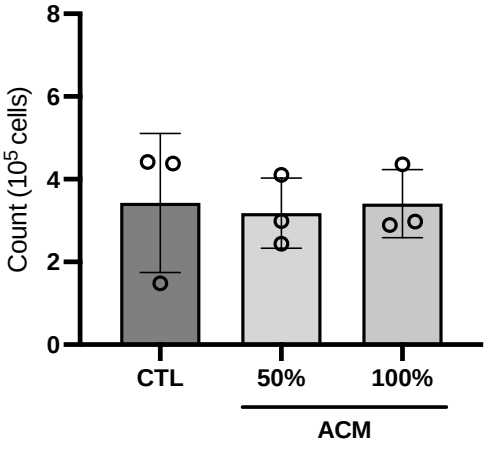

Figure 8: Evaluating the effect of ACM on cell growth. OVCAR8 cells were cultured in the indicated media for 24hrs and the number of viable cells was counted with a ViCell Analyzer (n=3 biological replicates). Scale bar represents SD. 1-way ANOVA, Dunnett's multiple comparisons test.

Moreover, the effect of adipocyte-mediated treatment resistance remained constant across different sources of adipocyte secreted factors. When a small panel of breast or ovarian cancer cells were infected with oncolytic rhabdoviruses (VSVΔ51 or MG1) or vaccinia virus (VACV) after exposure to ACM from visceral adipocytes, they remained strongly resistant to infection as evidenced by a significant reduction in viral titer (**Figure 9**). Ovarian patient ascites cells were also resistant to OV infection in the presence of breast ACM (ACM) or visceral ACM (VACM) (**Figure 10**). This data suggested that a common denominator exists in the secreted products from different sources of ACM that contribute to OV resistance. For simplicity, ACM from human breast adipocytes were used for the reminder of experiments in this study, unless otherwise indicated.

The inhibitory effect of adipocyte secreted factors was also observed in murine lineages. Human cancer cell lines given ACM from murine adipocytes induced a similar pattern of OV resistance observed with ACM from human adipocytes (**Figure 11A**). In the reciprocal scenario, where murine cells were cultured with human ACM, the phenotype of ACM-mediated OV resistance was maintained (**Figure 11B**). This data suggests a conserved phenomenon between human and murine species.

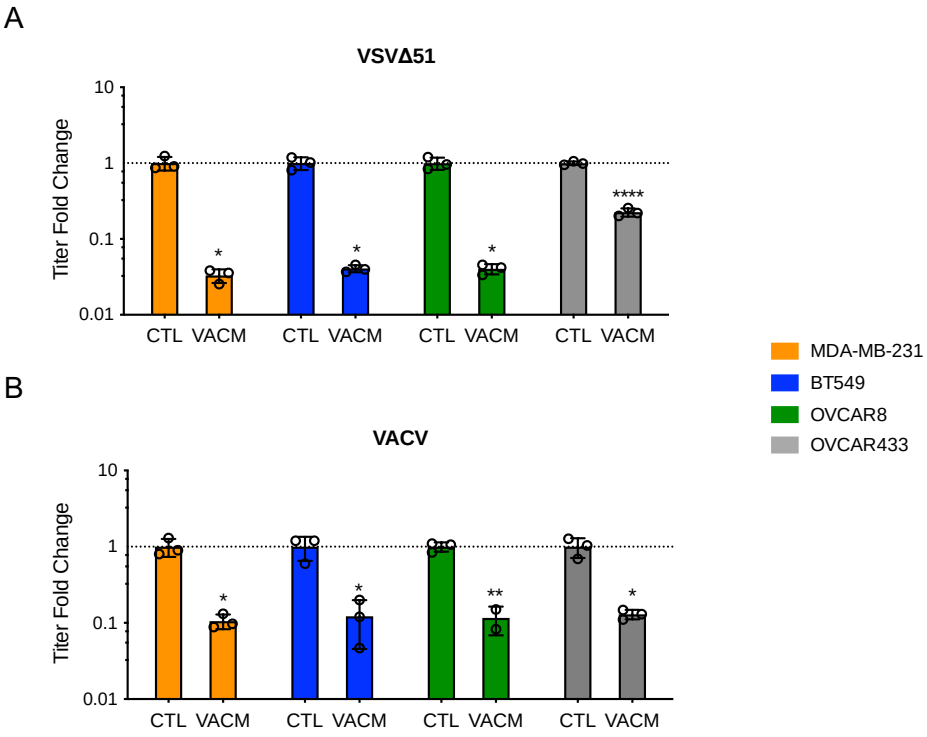

Figure 9: ACM from visceral adipocytes inhibit OV infection. A small panel of human breast or ovarian cell lines were cultured in visceral ACM and infected with VSVΔ51 (MOI 0.01) (A) or VACV (MOI 0.01 except BT549 which was infected at MOI 0.1) for 48hrs (B) (n=3 biological replicates). The viral titer was quantified by plaque assay. Scale bar denotes SEM. Two tailed, unpaired t-test, *p <0.05, **p <0.01, ****p < 0.0001.

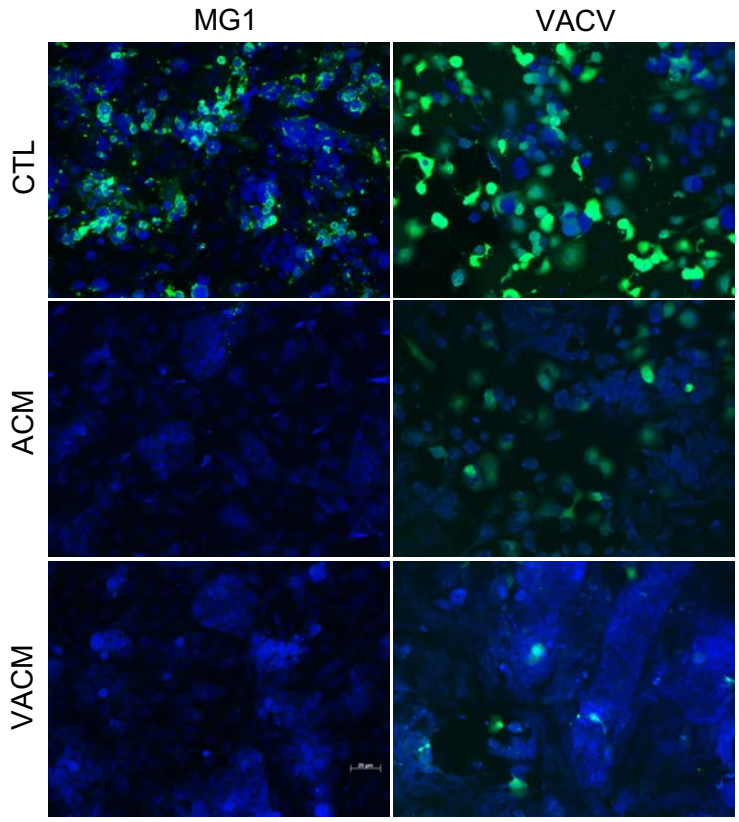

Figure 10: Adipocyte secreted factors inhibit sensitivity to OV infection in ovarian patient ascites cells. Representative immunofluorescence images of patient ascites cells (P2068) cultured in breast ACM or visceral ACM (VACM) and infected with GFP-expressing MG1 (MOI 0.1, 48 hpi) or VACV (MOI 0.1, 48 hpi) (n=2 biological replicates). Scale bar represents 20μm.

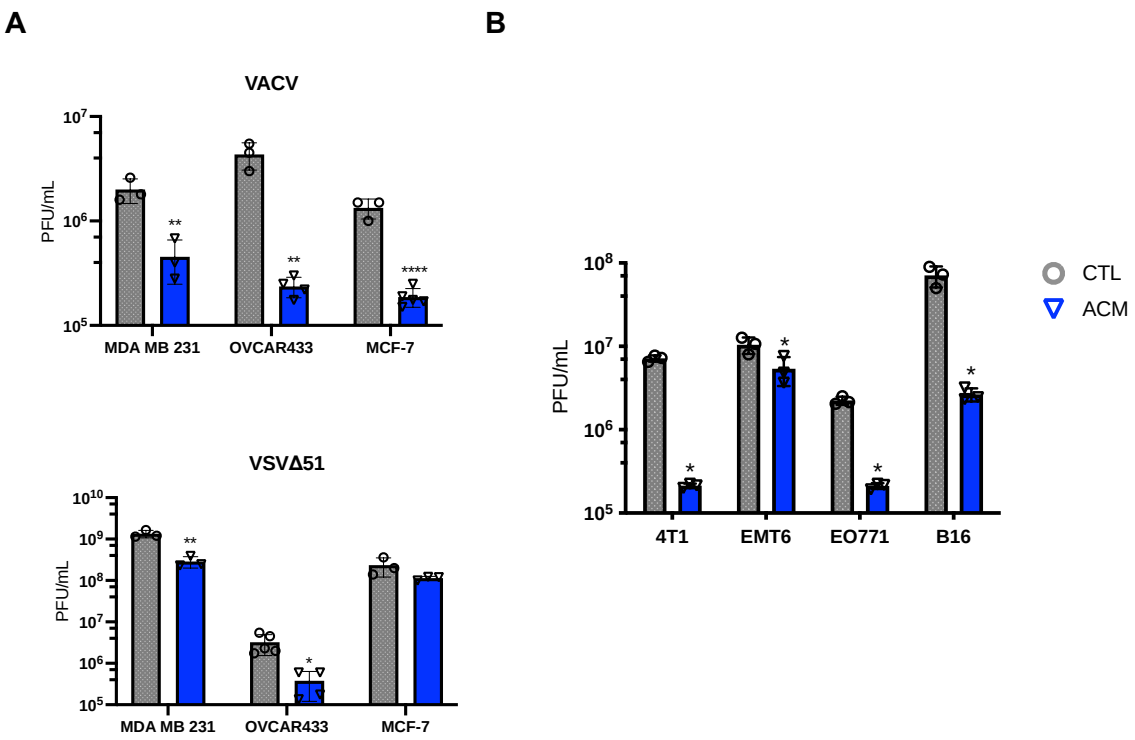

Figure 11: The inhibitory effect of ACM is conserved across murine and human species. ACM from murine adipocytes, 3T3-L1, were transferred to human breast or ovarian cancer cell lines and infected with VACV (MOI 0.01) or VSVΔ51 (MOI 0.01, except OVCAR433 which was infected at MOI 0.1) for 48hrs (A) (n=3 biological replicates). In a reciprocal approach, murine cancer cells were cultured in human ACM and infected with VSVΔ51 (MOI 0.1 for EO771 and B16 and MOI 1 for EMT6 and 4T1, 48hr) (n=3 biological replicates) (B). OV titers was quantified by plaque assay. Error bars represent SD. Two tailed, unpaired t-test, *p <0.05, **p <0.01, ****p < 0.0001.

1.3 Evaluating the impact of ACM on OV infection & replication

In order to gain a better understanding of the observed OV resistance, various elements of virus infection and replication were examined.

To ensure that the virus remained intact and retained the capacity for infection following exposure to ACM, we performed an experiment where VSVΔ51 was pre-incubated at room temperature (RT) or 37°C for various lengths of time in CTL media or ACM prior to transfer to cancer cells. Cytotoxicity analysis revealed that there was no difference in the ability of VSVΔ51 to kill cancer cells with prior exposure to ACM, suggesting that it is unlikely that a direct virus-neutralizing agent in ACM is the driver of ACM-mediated OV inhibition (**Figure 12**). Analogous results were observed with oncolytic Vaccinia virus (VACV) (**Appendix Figure 1**).

In a modified plaque assay experiment adapted from Xu *et al.*, cancer cells were cultured in CTL media or ACM for varied lengths of time prior to infection with OV.[196] The cells were then infected for 1hr and the inoculum containing media was removed and replaced with semi-solid overlay medium containing caroboxylmethyl cellulose (CMC). CMC is a viscous substance that will constrain the movement of virus particles, thereby facilitating the formation of plaques. At 48 hpi, the overlay medium was removed and the cells were fixed and stained with methanol containing crystal violet solution to visualize the plaques. Each counted plaque forming unit (PFU) represents a VSVΔ51 particle that was able to enter the cell under the given conditions. Here, we observed no apparent disadvantage to OV infection when cells were pre-incubated with ACM (**Figure 13**). This study provided the first indication that ACM is unlikely to bar OV entry.

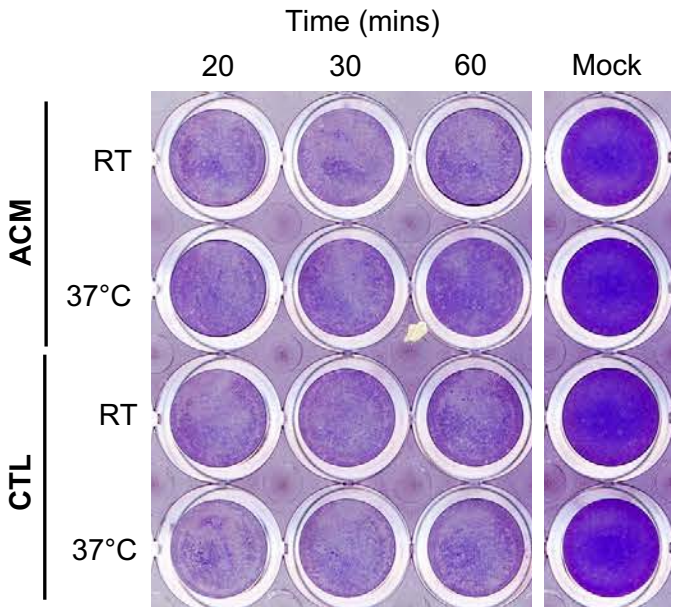

Figure 12: Pre-incubation of OV with ACM does not impact OV-mediated cytotoxicity. VSVΔ51 was pre-incubated in CTL media or ACM at room temperature (RT) or 37° for the indicated lengths of time prior to using the inoculum for infection of OVCAR8 cells (MOI 1). OV-mediated cell death was assessed by crystal violet cytotoxicity assay (48hpi). Representative crystal violet staining of n=2 biological replicates.

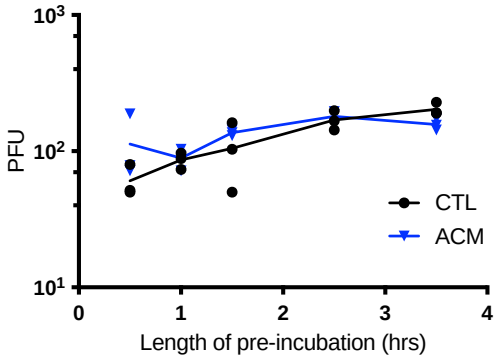

Figure 13: Pre-incubation of cancer cells in ACM does not impair OV infection. OVCAR8 cells were incubated in CTL media or ACM for the indicated amount of time prior to infection with VSVΔ51 (150PFU). Following a 1hr period of infection, the inoculum and media was removed and replaced with semi-solid CMC-containing overlay medium. After 48hrs, the overlay medium was removed and the cells were stained with crystal violet. Each counted PFU represents a VSVΔ51 particle that was able to enter the cell under the indicated conditions (n=3 biological replicates). Modified plaque assay adapted from Xu *et al.*[196] Line connects means. 2-way ANOVA, Sidak's multiple comparison test.

To further investigate the role of ACM on OV entry, we employed virus-like particles (VLPs), a platform of recent interest and under development by colleagues in the Ilkow and Bell labs. VLPs can mimic the structural conformation of native viruses without the capacity for replication since they do not carry the viral genome. The G protein facilitates rhabdovirus entry into the host cell.[197] As such, we sought a VLP platform loaded with GFP and pseudotyped with VSV-G glycoprotein (**Figure 14A**). GFP signal from cells in ACM or CTL media that were transduced with GFP-loaded VLPs or infected with GFP-expressing VSVΔ51 were quantified by flow cytometry. Here, we found that GFP signal from VLP transduced cells was not significantly changed in ACM-receiving cells (>90% transduction across both groups), while GFP from VSVΔ51-infected cells were significantly diminished (<5% in ACM vs >90% in CTL) (**Figure 14B-C**). Hence, G-mediated VSVΔ51 entry appeared to be unhindered in ACM despite a severe impairment to virus replication. This finding strongly suggested that ACM-mediated impairment to VSVΔ51 infection occurs post-viral entry.

In a separate study, cancer cells were infected with an oncolytic rhabdovirus that is deleted for the G protein. G-deleted rhabdoviruses are single-cycle viruses that are incapacitated for viral spread, thereby serving as a useful platform for a closer examination of virus replication in infected cells.[198] OVCAR8 cells were infected with MG1ΔG first, to establish a baseline for virus entry. Following a 1hr period of infection, the media containing inoculum was removed and replaced with CTL media or ACM. Viral replication was gauged by quantification of the viral target gene L by qPCR (**Figure 15**). Here, we found that post-infection exposure to ACM notably impairs viral replication as evidenced by a >50% reduction in L gene transcription. These results furthered accumulating evidence for a post-entry mechanism of ACM-mediated OV resistance.

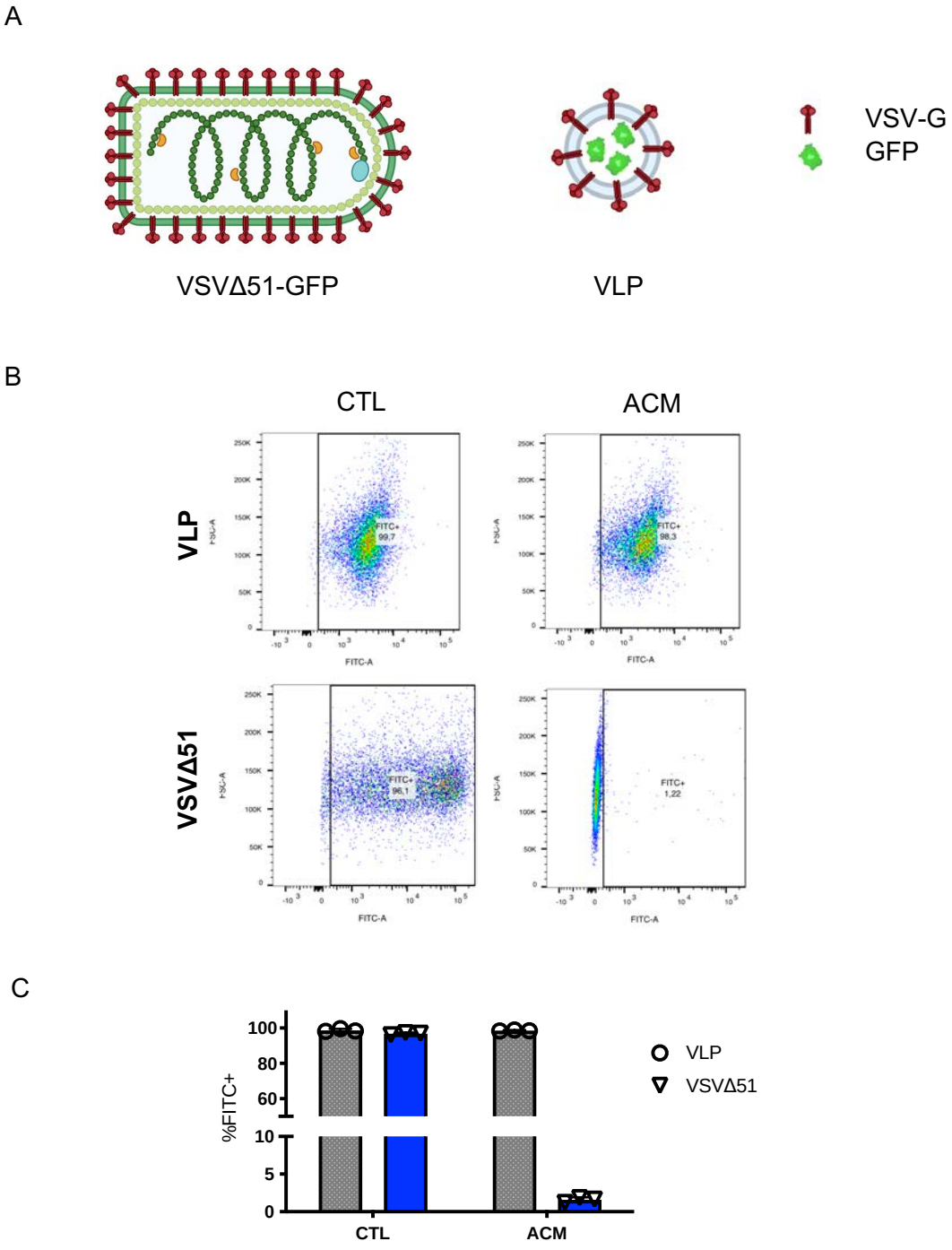

Figure 14: ACM does not impede VSV-G mediated entry. OVCAR8 cells in CTL media or ACM were transduced with GFP-loaded VLPs pseudotyped with VSV-G glycoprotein or infected with VSVΔ51-GFP (MOI 0.1) for 24hrs and assessed by flow cytometry. A schematic of VSVΔ51 and VLP are shown in (A), representative dot plots are shown in (B), and the average FITC signal is represented as a bar graph in (C) (representative n=1 biological, n=3 technical replicates shown; n=2 biological replicates total).

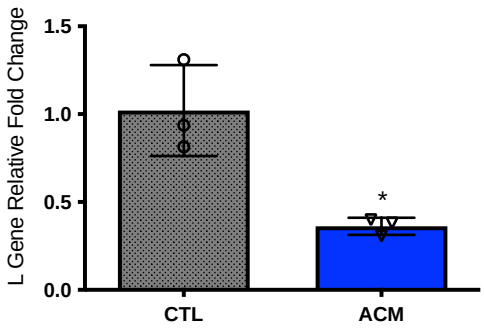

Figure 15: ACM impedes transcription of OV gene. OVCAR8 cells in CTL media were infected with MG1ΔG (MOI 3). After 1hr, the inoculum containing media was removed and changed to CTL media or ACM. The RNA was extracted 24 hpi and the expression of gene L was evaluated by qPCR relative to Rplp0 (n=3 biological replicates). Error bars represent SD. Two tailed, unpaired t-test, *p <0.05.

We then sought to perform a study that more broadly examined the effect of the timing of ACM exposure on OV infection. Cancer cells were exposed to CTL media or ACM overnight (16hrs), and infected with the OV ('pre-infection'). Alternatively, following the removal of CTL media, the cells were cultured in CTL media or ACM before infection with OV ('Peri- and Post-Infection') (**Figure 16**). ACM exposure peri- and post- post-infection had the greatest influence on mounting OV resistance. The findings from this experiment corroborated the accumulating evidence in this section suggesting that the inhibitory effects of ACM on OV infection is likely a post-virus entry phenomenon.

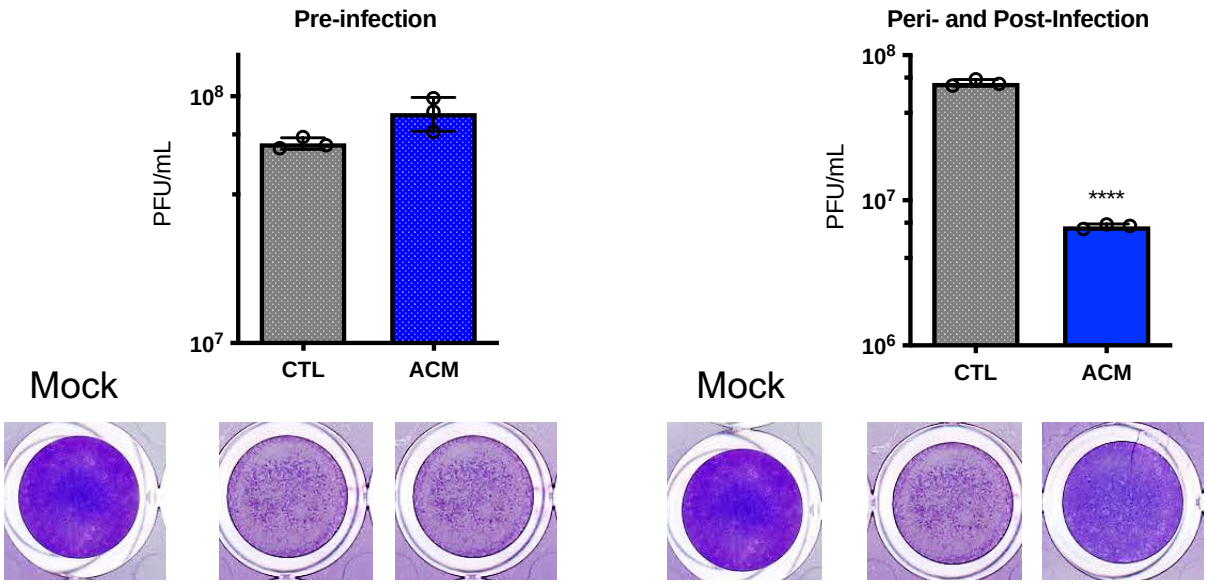

Figure 16: Evaluating the effect of the timing of ACM exposure on OV infection. OVCAR8 cells were cultured overnight (16hrs) in CTL media or ACM, and the media was changed to CTL media at the time of VSVΔ51 infection (A). Alternatively, the media was changed to CTL media or ACM at the time of infection (n=3 biological replicates) (B). The inoculum containing media was removed following 1hr of infection and replaced with the same media at the time of infection. Viral titer from OVCAR8 infected cells was quantified by plaque assay. Representative crystal violet staining of n=2 biological replicates shown. Error bar represents SD. Two tailed, unpaired t-tests ****p<0.0001.

Intracellular pH, specifically the acidification of endosomal compartments, is an important determinant of rhabdovirus uncoating.[173,199] The fusion of the acidic endosomal compartment containing the virus particle, and the cytoplasm of the cell, releases the viral particle from the endosome for downstream viral propagation in the host cell. Using a dye that tracks acidic organelles in cells, Lysotracker, we evaluated the effect of ACM on acidic compartments in the cell. In this preliminary study, we observed that Lysotracker staining is decreased (>60%) upon culture with adipocyte secreted factors (**Figure 17**). This finding alluded to an impairment to viral uncoating as a potential driver of ACM-mediated OV resistance.

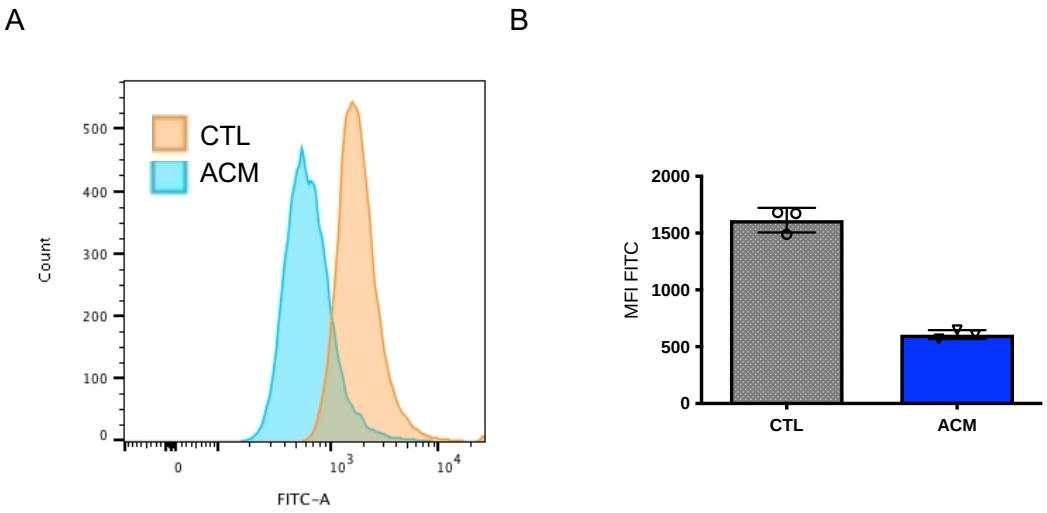

Figure 17: ACM culture decreases Lysotracker staining. OVCAR8 cells that were cultured overnight in CTL media or ACM were stained with Lysotracker, a dye that stains acidic compartments of the cell and analyzed by flow cytometry. Representative histograms (A) and MFI FITC signal (B) are shown (n=3 technical, n=1 biological replicates). Error bars represent SD.

Section II: Elucidating the effect of adipocyte secreted factors on cancer cells that contribute to OV resistance

2.1 ACM-mediated OV resistance is not driven by Type I interferon signaling

RNA sequencing analysis of VSVΔ51-infected OVCAR8 cells in the presence of ACM suggested a vastly different transcriptomic profile from cells receiving CTL media. While a plethora of interferon-stimulated genes (ISGs) such as interferon-induced GTP-binding protein Mx1, 2'-5'-oligoadenylate synthetases 1-3 (OAS1-3), interferon induced proteins with tetratricopeptide repeats (IFIT2, IFIT3, IFIT5), interferon regulatory factor 1, DExD/H-Box Helicase 58 (DDX58) among others were upregulated in CTL media-receiving cancer cells upon VSVΔ51 infection, this effect was notably stunted in ACM-receiving cells (Figure 18A).

Given the robust resistance of otherwise OV-sensitive cancer cells in the presence of ACM, we sought to determine the potential role of interferon signaling, specifically Type I interferon signaling, on ACM-mediated OV resistance. Interferons are a family of cytokines that are critical for mounting a defense against viral infections and can be triggered by a range of biological cues, including viral antigens. To date, three types of interferons have been identified and perform crucial roles in mitigating immunological threats; however, Type I interferon is often the first line of defense in the innate anti-viral response.

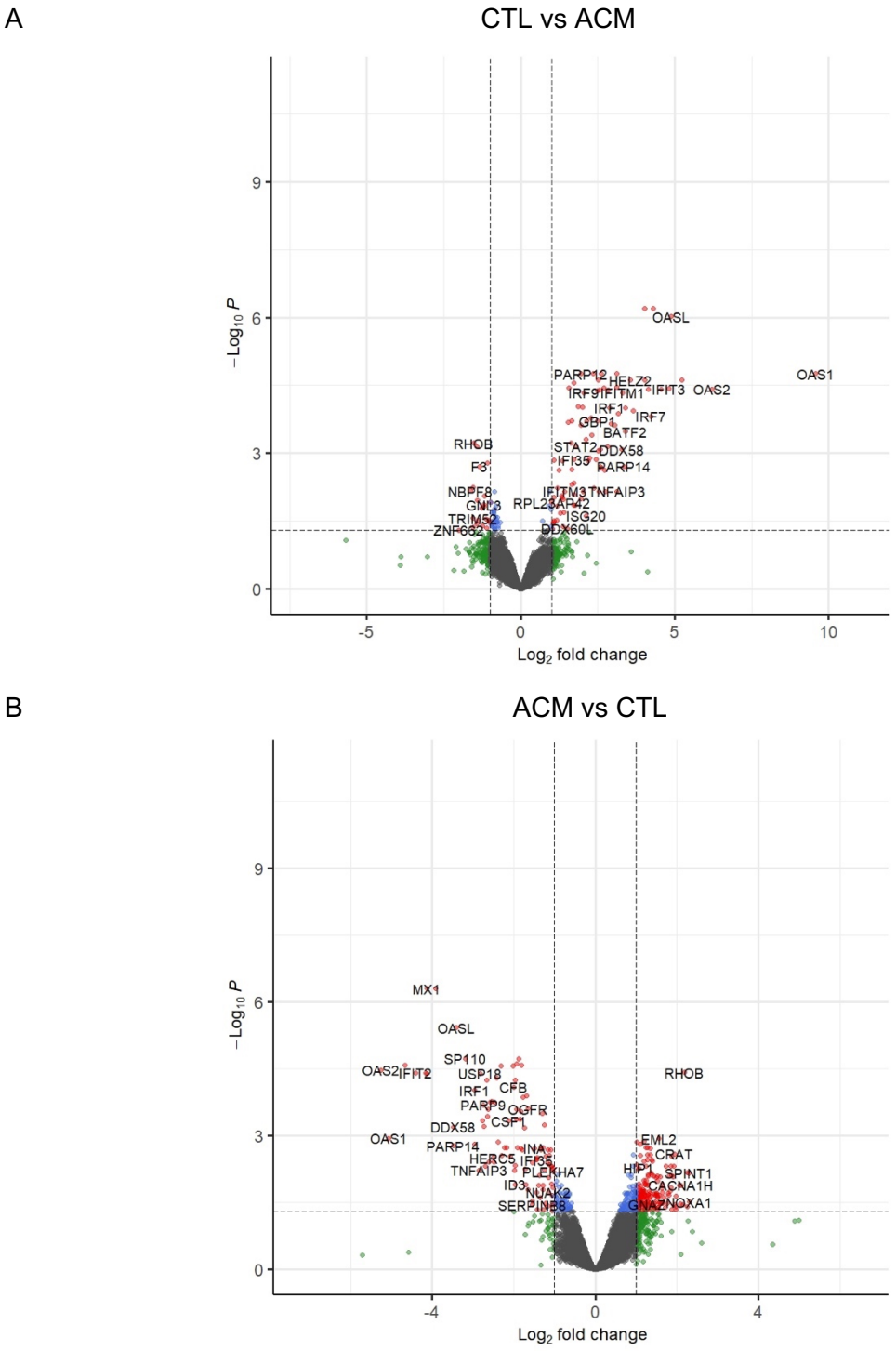

Figure 18: Volcano plots of OV-infected cancer cells in ACM or CTL media. OVCAR8 cells were cultured in ACM or CTL-media for 6hrs prior to infection with VSVΔ51 (MOI 1). The RNA was harvested for RNA sequencing analysis 12hpi. The data was analyzed relative to CTL media (A) or ACM (B) to visualize the relative upregulation or downregulation of genes in each condition (n=2 biological replicates). Y-axis dotted line denotes a p-value cut-off of 0.05. X-axis dotted lines denotes a 2-fold change cut off.

IFN-α is a Type I interferon that engages the interferon-α/β receptor (IFNAR). Topical treatment with IFN-α served as a positive control for engaging anti-viral signaling associated with an IFNAR-mediated interferon signaling cascade. When IFN-α dosed cells were infected with VSVΔ51, little to no infection was observed. Correspondingly, IFNAR blocking antibody (Ab) was used to block engagement of IFNAR. When cells were treated with both IFN-α and IFNAR blocking Ab, the cells became vulnerable to VSVΔ51 infection, suggesting the concentrations of IFNAR blocking Ab used was sufficient to block the binding and engagement of IFNAR ligands. In cells receiving ACM, the addition of IFNAR blocking Ab did not alleviate resistance to VSVΔ51 infection, suggesting an IFNAR-independent mechanism of OV resistance (**Figure 19**). This was further corroborated by an immunofluorescence microscopy study performed in B16-F10 cells that were genetically knocked out for IFNAR (**Figure 20**). Although a murine melanoma cell line is out of the scope of this study, we sought to validate our findings in a genetic knockout model that was previously generated in the Bell lab for a separate project. The data validated the findings observed with IFNAR blocking Ab and further, indicated that the phenomenon of adipocyte mediated OV resistance can be extended to other tumour types. Overall, our IFNAR targeting studies alluded to an IFNAR-independent mechanism of OV resistance.

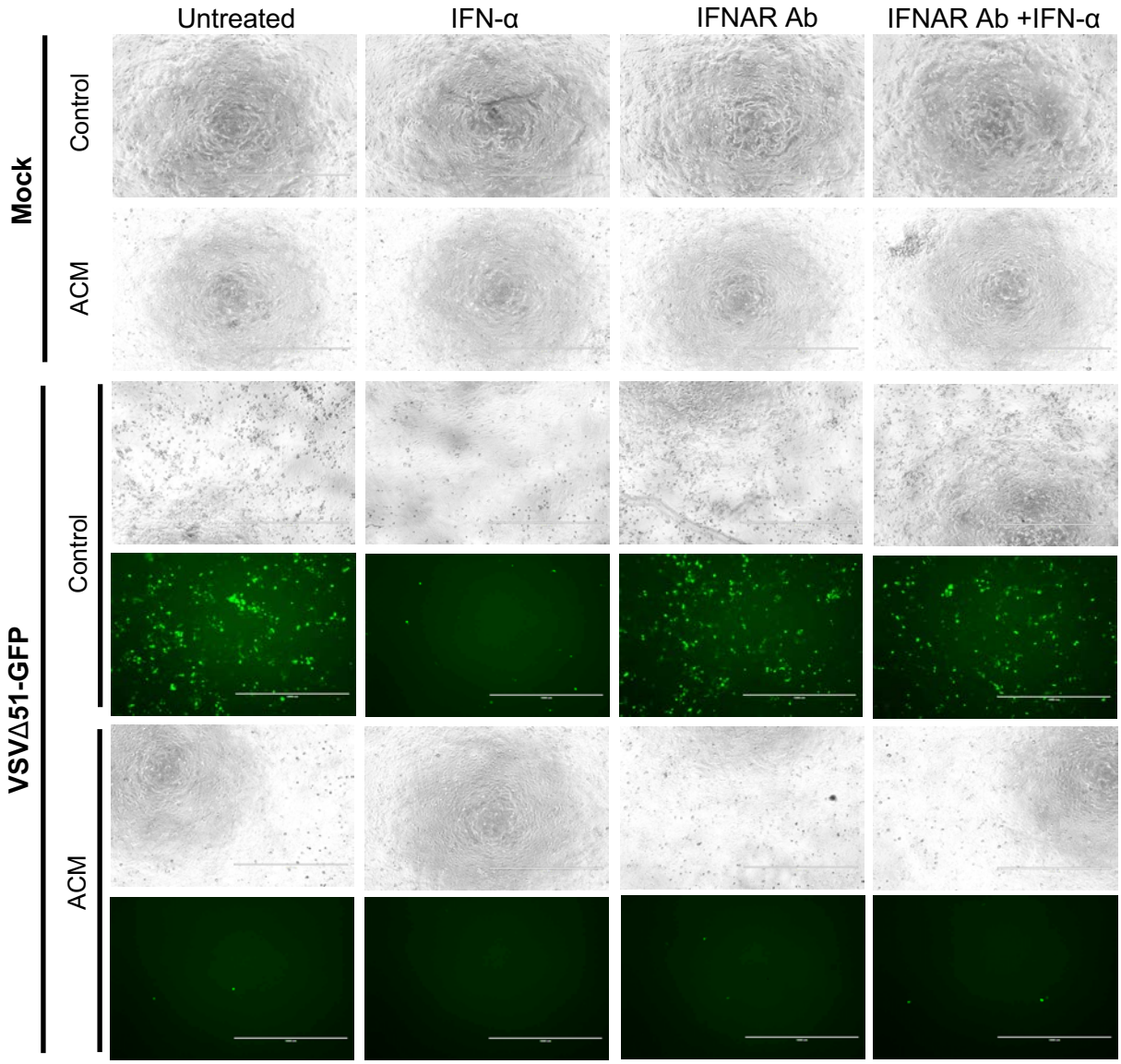

Figure 19: IFNAR blocking Ab does not alleviate ACM-mediated OV resistance. OVCAR8 cells that were incubated overnight in CTL media or ACM, were treated with IFN-α (200U), IFNAR blocking antibody (2μg), or both prior to infection with VSVΔ51-GFP (MOI 1, 48hrs). Representative immunofluorescence microscopy images shown (n=3 biological replicates). Scale bar represents 1000μm.

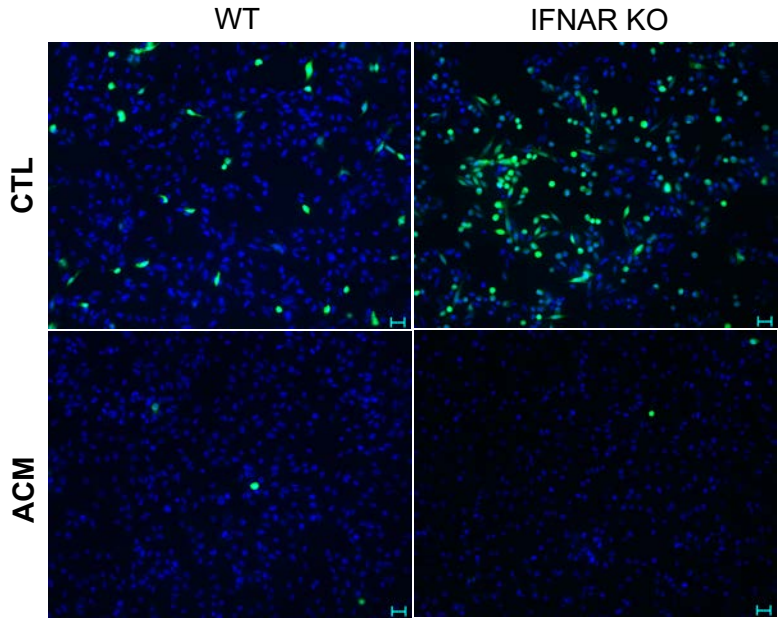

Figure 20: IFNAR knockout does not alleviate ACM-mediated OV resistance. Murine melanoma cells, B16-F10, that were genetically knocked out for IFNAR were cultured in CTL media or ACM overnight and infected with VSVΔ51-GFP (MOI 0.1,24hrs). Representative immunofluorescence microscopy images shown (n=3 biological replicates). Scale bar represents 50μm.

Downstream of IFNAR engagement, interferons activate Janus kinase/signal transducer and activator of transcription (JAK/STAT), which through a series of signaling events, lead to the expression of ISGs that induce anti-viral effects. To complement our experiments evaluating IFNAR receptor engagement, we evaluated the effect of blocking downstream IFNAR-mediated signaling using JAK inhibitors (JAKi) that target JAK1, JAK2, JAK3 and Tyk2. In a small panel of ovarian cancer cell lines (OVCAR8, SKOV3), patient ascites cells (P2149, P2068) and a renal cell carcinoma cell line (786O) cultured in CTL media, JAKi treatment further sensitized the cells to VSVΔ51-mediated cell death; however, it did not perturb the robust resistance to OV infection observed in ACM conditions (**Figure 21**). The utility of JAKi in stunting JAK/STAT-mediated downstream Type I interferon signaling was validated in a preliminary immunoblotting experiment evaluating signal

transducer and activator of transcription 1 (STAT1) phosphorylation in 786O cells, since these cells are well characterized to have a functional interferon pathway.[200,201] (Figure 22).

Although the data presented in this section suggests that ACM-mediated OV resistance is unlikely to be interferon-driven, it stirred the question of whether ACM-receiving cells retained the capacity to mount an interferon response to appropriate stimuli, including non-viral agents. To this end, we evaluated the expression of a small panel of ISGs [DDX58, interferon-induced transmembrane protein 1 (IFITM1), STAT1, OAS1] at baseline levels, and in response to topical IFN-α. The baseline expression of ISGs remained largely similar between CTL media and ACM; however, the dichotomy in their responses to IFN-α treatment was striking. CTL media receiving cells produced a strong increase in ISG expression in response to IFN-α exposure but the magnitude in the ISG response in ACM-receiving cells was noticeably dampened (Figure 23). Similar to our RNA sequencing study with VSVΔ51, ISG expression from ACM-receiving cells dosed with IFN-α was dwarfed due to some unknown mechanism. This data is consistent with accumulating evidence for a mechanism of resistance that is not driven by Type I interferon.

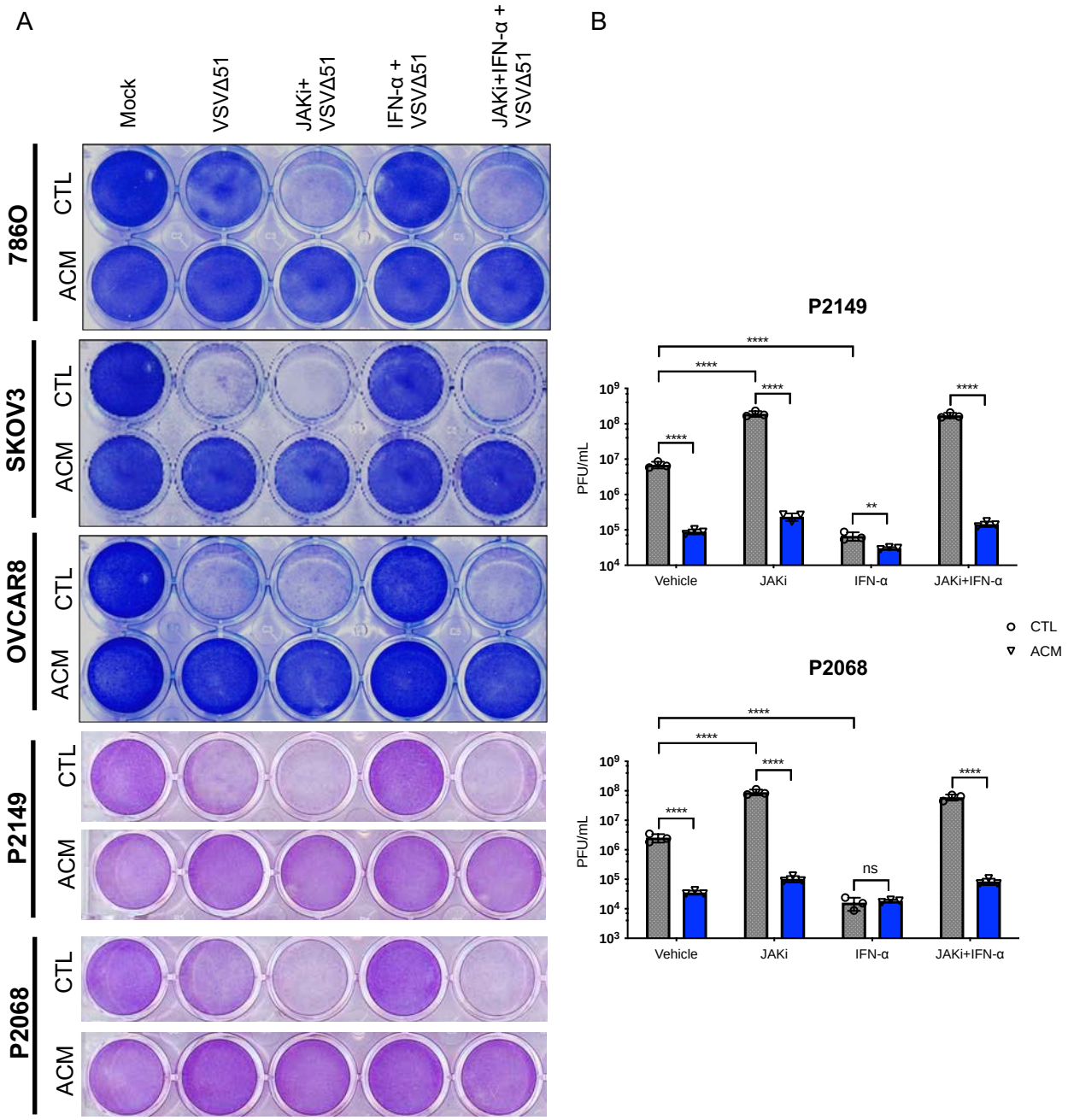

Figure 21: Combinatorial treatment with JAK inhibitors does not perturb ACM-mediated OV inhibition. Ovarian (OVCAR8 and SKOV3) or renal (786O) cancer cell lines (n=2 biological replicates) or ovarian patient ascites cells (P2068, P2149) (n=3 biological replicates) were cultured in CTL media or ACM overnight and treated with JAK I inhibitor (JAKi; 1μM), IFN-α (200U/mL), or both prior to infection with VSVΔ51 (MOI 1 for all except OVCAR8 and SKOV3 which were infected at MOI 0.1) for 48rs. Crystal violet cytotoxicity assay was performed to evaluate VSVΔ51-mediated cell death (A) and the titers from ovarian patient ascites cells were quantified by plaque assay (B). Error bar represents SD. 2-way ANOVA, Tukey's multiple comparison test on log 10 transformed data, **p <0.01, ****p < 0.0001.

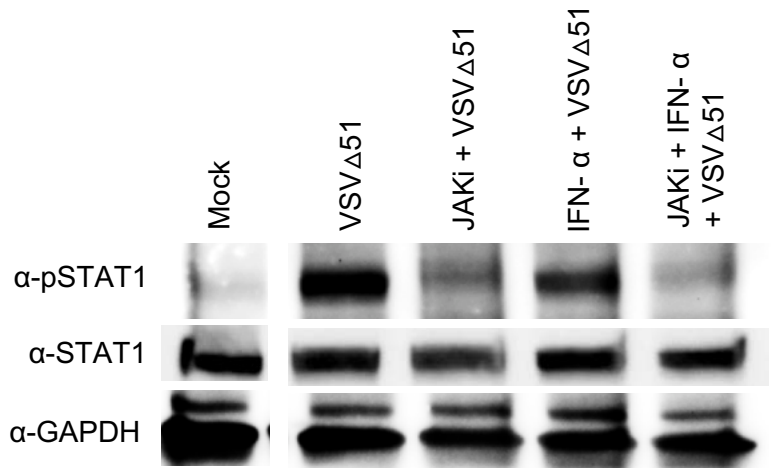

Figure 22: Evaluating the phosphorylation status of STAT1 with JAK inhibition. 786O cells were treated with JAK I inhibitor (JAKi; 1μM), IFN-α (200U) or both and infected with VSVΔ51 (MOI 1, 24hrs). The cell lysates were harvested and blotted for STAT1, phosphorylated STAT1 and the housekeeping gene, GAPDH (n=1 biological).

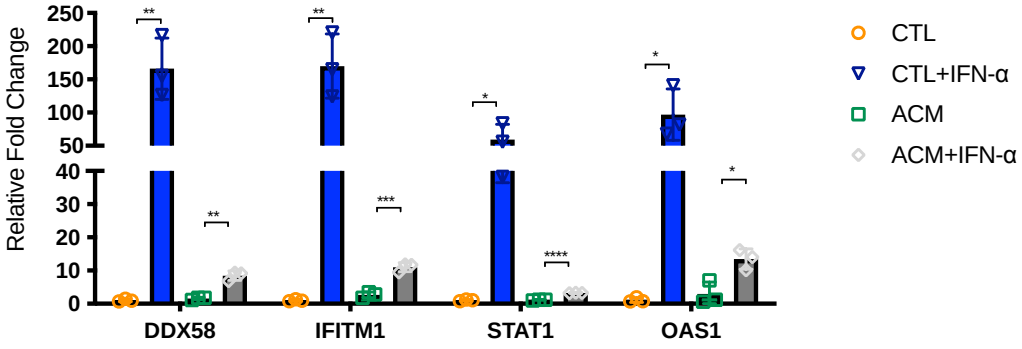

Figure 23: ISG expression induced by IFN-α is dampened in ACM-receiving cancer cells. OVCAR8 cells in overnight culture of CTL media or ACM were dosed with IFN-α (300U) for 8hrs. RNA was harvested for analysis by qPCR (n=3 biological replicates). Fold change relative to Rplp0. Error bars represent SD. Two tailed, unpaired t-tests of CTL or ACM pairs, *p <0.05, **p <0.01 ***p<0.001, ****p < 0.0001.

2.2 ACM induces metabolic changes in cancer cells

Adipocytes are highly metabolic cells involved in the storage and release of lipids. In an effort to better understand the phenomenon of ACM-mediated treatment resistance, we sought to more closely examine the effect of adipocyte secreted factors on receiving cancer cells.

In a fluorescence microscopy experiment using a broad neutral lipid dye, Bodipy, we observed that cancer cells in ACM become accumulated in intracellular lipids over time, with a prominent accumulation of lipids observed at 24hrs (**Figure 24**). When ACM was assessed for FAs, the common substrate in adipocyte storage, we found that ACM was notably enriched in FAs ($p<0.01$, **Figure 25**). Taken together, these results provided the initial indications that lipid components, namely FAs, may be uptaken by cancer cells in ACM culture.

We sought to determine how the intracellular accumulation of lipids may alter the metabolism of ACM-receiving cancer cells by assessing mitochondrial metabolic parameters. Agilent Seahorse technology has become a powerful tool for assessing metabolic parameters of live cells. ACM or CTL media receiving cells underwent the 'Mito Stress Test' protocol which involves the assessment of the oxygen consumption rate (OCR) in response to a meticulous sequence of drug injections that target various proteins in the electron transport chain. The response to these drugs revealed various metabolic parameters, including basal respiration, ATP production, maximal respiration and spare respiratory capacity. We evaluated the OCR in ACM or CTL-media receiving cells in response to the Mito Stress test (**Figure 26A,** black and blue lines).

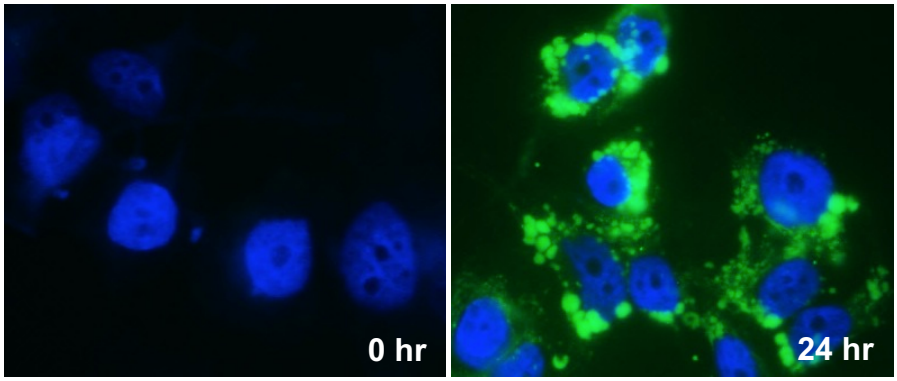

Figure 24: ACM induces intracellular lipid accumulation. OVCAR8 cells cultured in ACM over a 24hr period was stained with Bodipy, a neutral lipid dye, and assessed by immunofluorescence microscopy. DAPI denotes nuclei staining. Representative images shown (n=3 biological replicates).

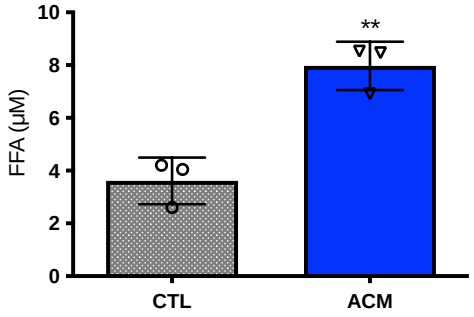

Figure 25: ACM is enriched in fatty acids. The media used to condition adipocytes (CTL media) and ACM wer harvested and the free FA content was determined using a commercially available FA quantification kit (BioVision) (n=3 biological replicates). Error bar represents SD. Two tailed, unpaired t-test, **p <0.01.

A

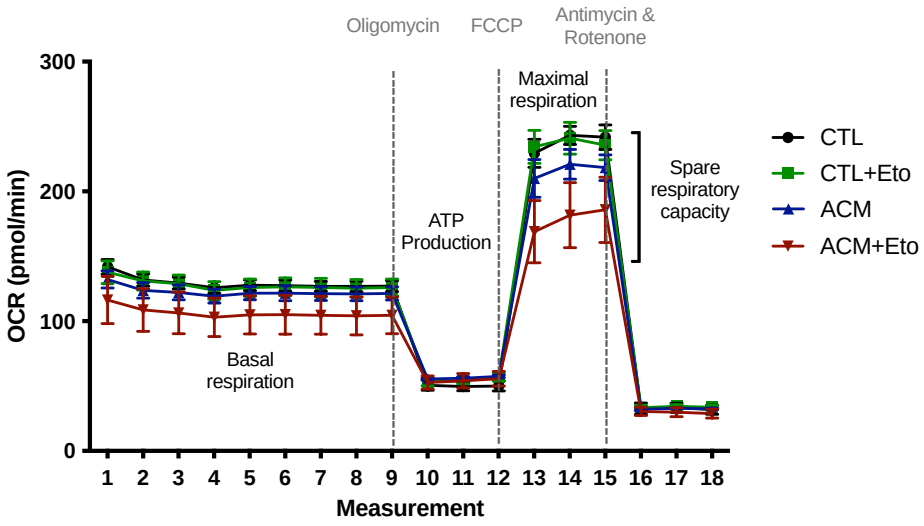

B

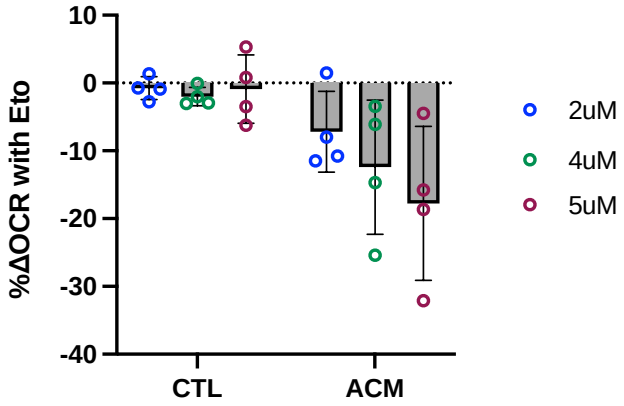

Figure 26: ACM alters mitochondrial respiration. OVCAR8 cells were cultured in CTL media or ACM for 48hrs and assessed for oxygen consumption rate (OCR) using Agilent Seahorse technology with optimized doses of oligomycin (1.5µM), trifluoromethoxy carbonylcyanide phenylhydrazone (FCCP) (0.5µM) and antimycin and rotenone (0.5µM) treatment at designated intervals. Acute dose Etomoxir (Eto; 5µM) was delivered at the start of the experiment. Statistical analysis denotes two-tailed unpaired t-test on measurement 14 (maximal respiration) (representative n=1 biological, n=4 technical replicates shown; representative of total n=2 biological experiments) (A). Percent change in OCR at maximal respiration (measurement 14) when dosed with Etomoxir at indicated concentrations (n=1 biological, n=4 technical replicates) (B). Error bar represents SD.

CPT1 is a critical mitochondrial enzyme involved in the β-oxidation of FAs. When etomoxir, a non-reversible inhibitor of CPT1, was added to cells, CTL media receiving cells showed no significant change in their OCR signature. In contrast, ACM-receiving cells demonstrated a drastic reduction in the assessment of maximal respiration and this effect was titratable with increasing concentrations of Etomoxir (**Figure 26**). These findings were highly suggestive of a reliance of ACM-receiving cells on CPT1-mediated mitochondrial respiration. A qPCR study assessing CPT1 expression showed that ACM culture increased CPT1 expression in at least 2 independent ovarian cancer cell lines tested, including a 2-fold increase in OVCAR8 cells ($p<0.05$, **Figure 27**). Taken together, our data demonstrated a metabolic dependency on FAs as fuel source in ACM-receiving cells and provided functional evidence for a transfer of FAs from ACM to cancer cells.

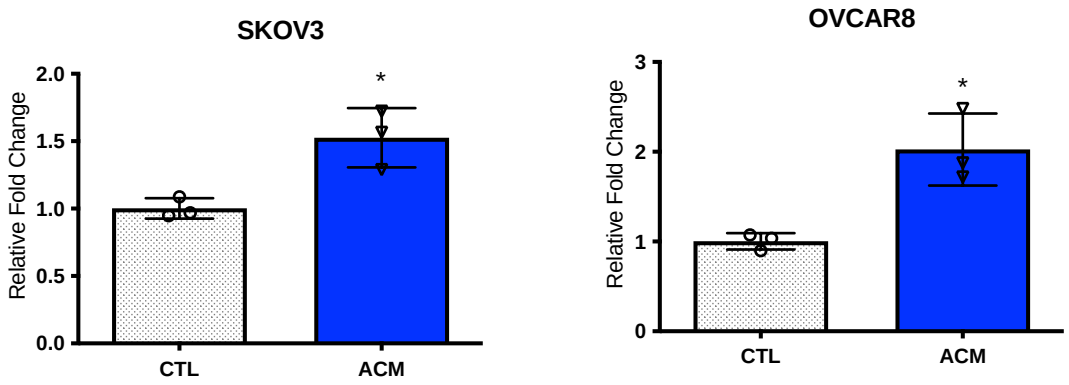

Figure 27: Adipocyte secreted factors increase CPT1 expression. Two human ovarian cancer cell lines were cultured in ACM for 24hrs (SKOV3) or 48hrs (OVCAR8). The RNA was extracted to probe for the expression of mitochondrial protein carnitine palmitolytransferase I (CPT1) by qPCR (n=3 biological replicates). Fold change relative to Rplp0. Error bar represents SD. Two tailed, unpaired t-test, *p <0.05.

RNA sequencing analysis further substantiated the case for ACM-driven metabolic changes favouring FA metabolism. In ACM-receiving OV-infected cells, there was a demonstrated increase in genes associated with FA oxidation, such as carnitine o-acyl transferase (CRAT) (3.6X) and carnitine acylcarnitine translocase (SLC25A20) (2.5X) (**Figure 18B**). Uninfected ACM-receiving cells were also upregulated in genes indicative of FA metabolism, including CRAT (3.2X) and CPT1c (4.1X), a variant of CPT1 associated with cancer (**Figure 28**).[202]

To add, the transcriptome of uninfected ACM-receiving cells showed an upregulation of IFITM1 (2.8X) and thioredoxin interacting protein (TXNIP) (3.9X) (**Figure 28**). IFITM1 is a member of the IFN-induced transmembrane protein family and TXNIP is an important player in redox signaling.[187,203] The potential role of these proteins in ACM-mediated OV resistance is explored in the Discussion.

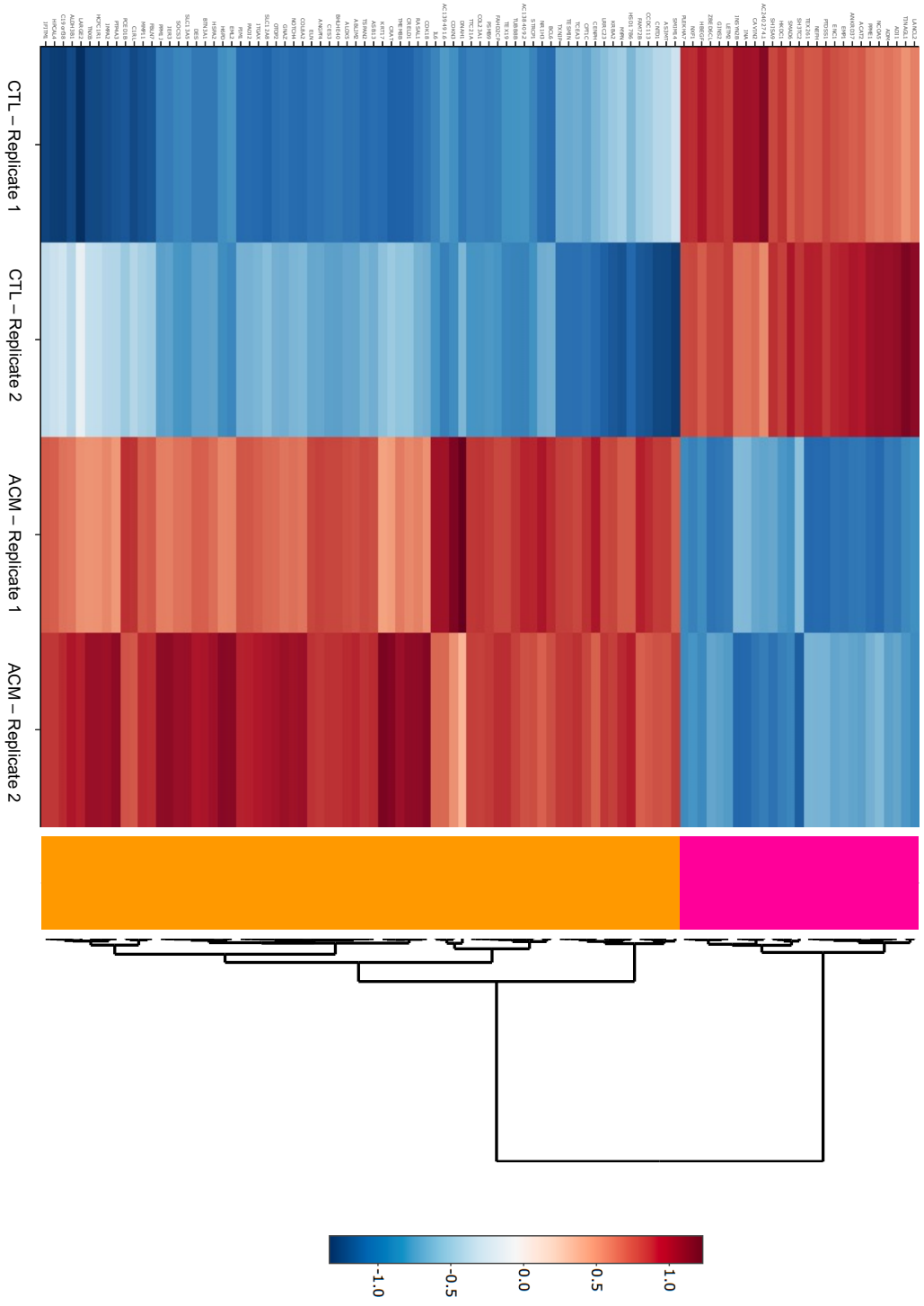

Figure 28: Heatmap demonstrating the transcriptomic changes induced by ACM. OVCAR8 cells were cultured in CTL media or ACM for 18hrs before RNA was extracted for transcriptomic analysis. The heatmap denotes 99 differentially expressed significantly altered genes ($p<0.05$) scaled by z-score (n=2 biological replicates). Heatmap was generated using Heatmaply.

2.3 Adipocyte-mediated OV resistance is largely lipid-driven

2.3.1 Depletion of lipid moieties from ACM increases sensitivity to OV infection

A flow cytometry experiment with Bodipy staining and an RFP-expressing OV facilitated the simultaneous visualization of accumulating intracellular lipids and OV infection to confirm the correlation between high intracellular lipid accumulation and decreased susceptibility to OV infection previously individually described in this thesis (**Figure 29**). Given the phenotypic (fluorescence microscopy) and functional (Seahorse) evidence for the uptake of FAs from ACM, we sought to evaluate the effect of depleting lipid moieties from ACM on OV infection.

Lipid Removal Agent (LRA) is a calcium silicate hydrate that is highly selective for lipids, lipoproteins and lipopolysaccharides in the presence of other biological macromolecules (Sigma Aldrich). ACM was passed through an LRA-mediated lipid depletion protocol prior to transfer to cancer cells. By flow cytometry, we observed that cells receiving lipid-depleted ACM had diminished intracellular lipid accumulation (>20%, $p<0.05$) and the intracellular lipid accumulation was comparable to cells receiving untreated CTL media (ns) (**Figure 30**).

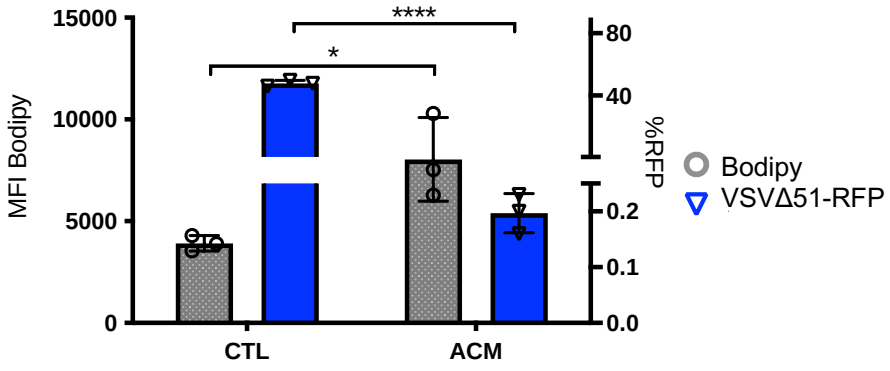

Figure 29: Intracellular lipid accumulation correlates with a decrease in OV infection. SKOV3 cells in CTL media or ACM were infected with an RFP-expressing VSVΔ51 (MOI 3, 18hrs). Intracellular lipid accumulation and VSVΔ51 infectivity were assessed with Bodipy staining and RFP signal, respectively (n=3 biological replicates). Error bar represents SD. Two tailed, unpaired t-test, *p <0.05, ****p < 0.0001.

A

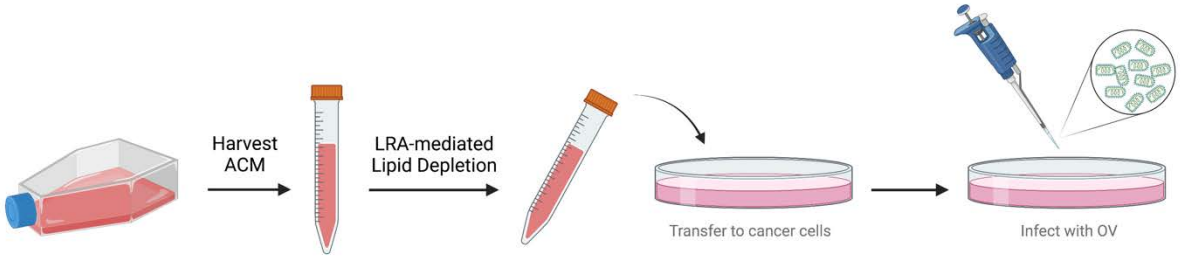

B

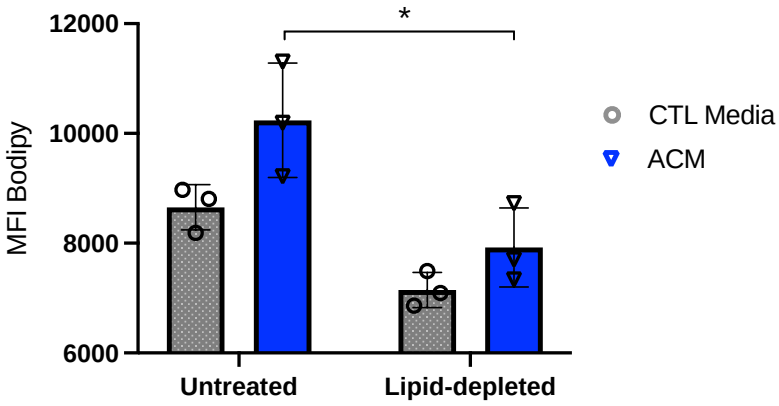

Figure 30: LRA-mediated lipid-depletion of ACM decreases ACM-induced intracellular lipid accumulation. CTL media or ACM were passed through a lipid-depletion protocol using the calcium silicate hydrate product, Lipid Removal Agent (LRA). The untreated or lipid-depleted media was then transferred to SKOV3 cells and incubated overnight. The intracellular lipid accumulation was assessed by flow cytometry with Bodipy staining (n=3 biological replicates). Error bar represents SD. 2-way ANOVA, Tukey's multiple comparison test, *p <0.05.

In a separate study, cancer cells receiving untreated or lipid-depleted ACM or CTL media were infected with OVs and the titers were assessed by plaque assay 48hpi. Here, we observed that OV titers in cells receiving lipid-depleted ACM were dramatically higher than in cells receiving untreated ACM (**Figure 31A**). In lipid-depleted ACM, VSV and VACV infections were boosted by 157.6X ($P<0.0001$) and, more modestly, 5.7X ($p<0.001$), respectively. In VSV, the increase in OV titer corresponded with pronounced OV-mediated cytotoxicity that was comparable to CTL media conditions (**Figure 31B**). The magnitude of recovery in OV infection and the reproducibility across 2 distinct OV platforms strongly suggested that ACM-mediated OV resistance is largely a lipid driven phenomenon. This landmark finding dictated a focus on the role of adipocyte-derived lipids in OV resistance.

A

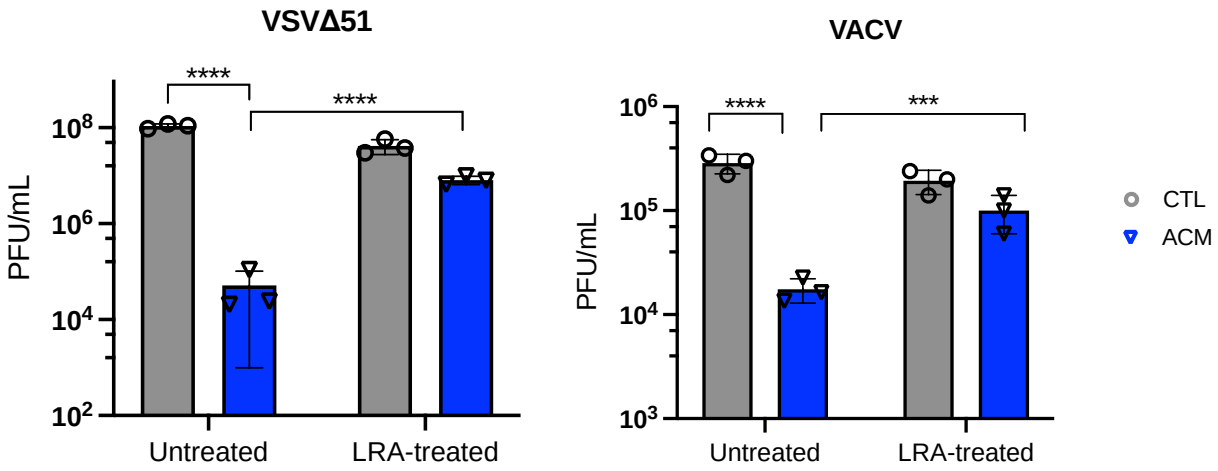

B

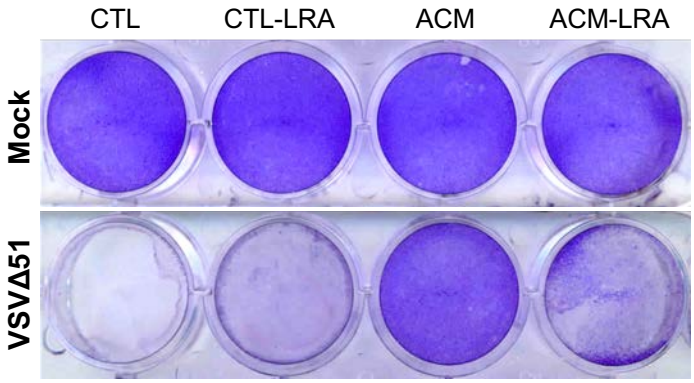

Figure 31: Depletion of lipids from ACM re-sensitizes cancer cells to OV infection. CTL media or ACM were depleted of lipid-derived constituents using LRA and added to OVCAR8 cells for overnight culture. The cells in untreated or lipid-depleted media were infected with VSVΔ51 (MOI 0.1) or VACV (MOI 1). The viral titer was assessed by plaque assay (48hpi; n=3 biological replicates) (A). Representative crystal violet staining of VSVΔ51-infected OVCAR8 cells (MOI 0.01) are shown in (B) (n=2 biological replicates). Error bars represent SD. 2-way ANOVA, Tukey's multiple comparison test on log 10 transformed data, ***p<0.001, ****p < 0.0001.

Given that ACM is enriched in FAs, we evaluated the effect of FA supplementation on OV titers. Palmitate and oleate are among the top three FAs esterified into TAGs in human adipocytes.[204] When cells were cultured in oleate supplemented media, there was discernible lipid droplet formation (**Figure 32A**). Furthermore, the inhibitory effect of ACM was at least partially recapitulated when culture media was supplemented with either palmitate or oleate, and this effect was observed across two different OV platforms tested (**Figure 32B**). At the highest concentration of oleate tested (1.5mM), VSVΔ51 titers were only ~10% of that observed in CTL media conditions but remained ~29.7X higher than the incredibly low VSVΔ51 titers observed in ACM-receiving cells. Despite this disparity, the resistance to VSVΔ51-mediated cytotoxicity remained comparable to ACM conditions ($p=0.9976$).

The potential role of protein-derived adipocyte secreted factors on ACM-mediated OV resistance was evaluated with a broad protease, proteinase K (PK). ACM was treated with PK prior to its transfer to cancer cells and subsequently infected with an OV. PK-treatment of ACM did not recover OV titers in the distinguishable manner observed with LRA-mediated lipid depletion (**Figure 33A-C**). Although a slight increase in OV titer was observed in cells receiving PK-treated ACM in comparison to untreated ACM, this increase is negligible since a similar increase was observed in the CTL media groups. Heat-inactivation or boiling of ACM similarly had no appreciable effects on alleviating OV resistance (**Figure 33D-E**).

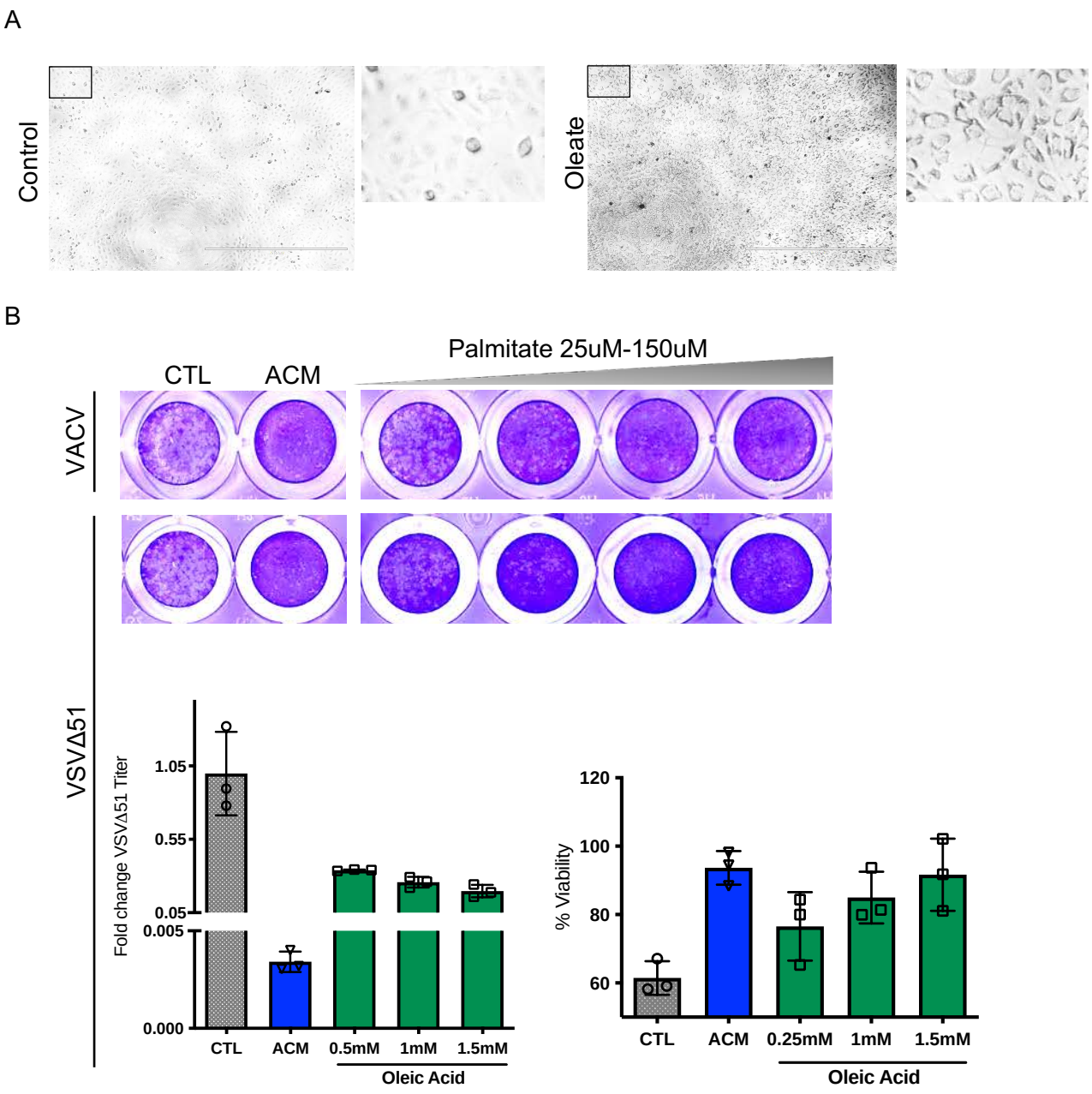

Figure 32: FA supplementation at least partially recapitulates the OV inhibitory effects of ACM. Brightfield images of OVCAR8 cells receiving media supplemented with oleate show lipid droplet formation (A). Crystal violet cytotoxicity assay was performed on cells receiving increasing concentrations of palmitate supplemented media and infected with VACV (MOI 3 for 1 hr; 48hpi) or VSVΔ51 (MOI 3 for 1hr; 24hpi). VSVΔ51 titer and cell viability were quantified by plaque assay and spectrometric analysis of crystal violet staining, respectively (B) (representative n=1 biological experiment shown; total n=2 biological experiments completed). Scale bar represents 1000μm. Error bar represents SD.

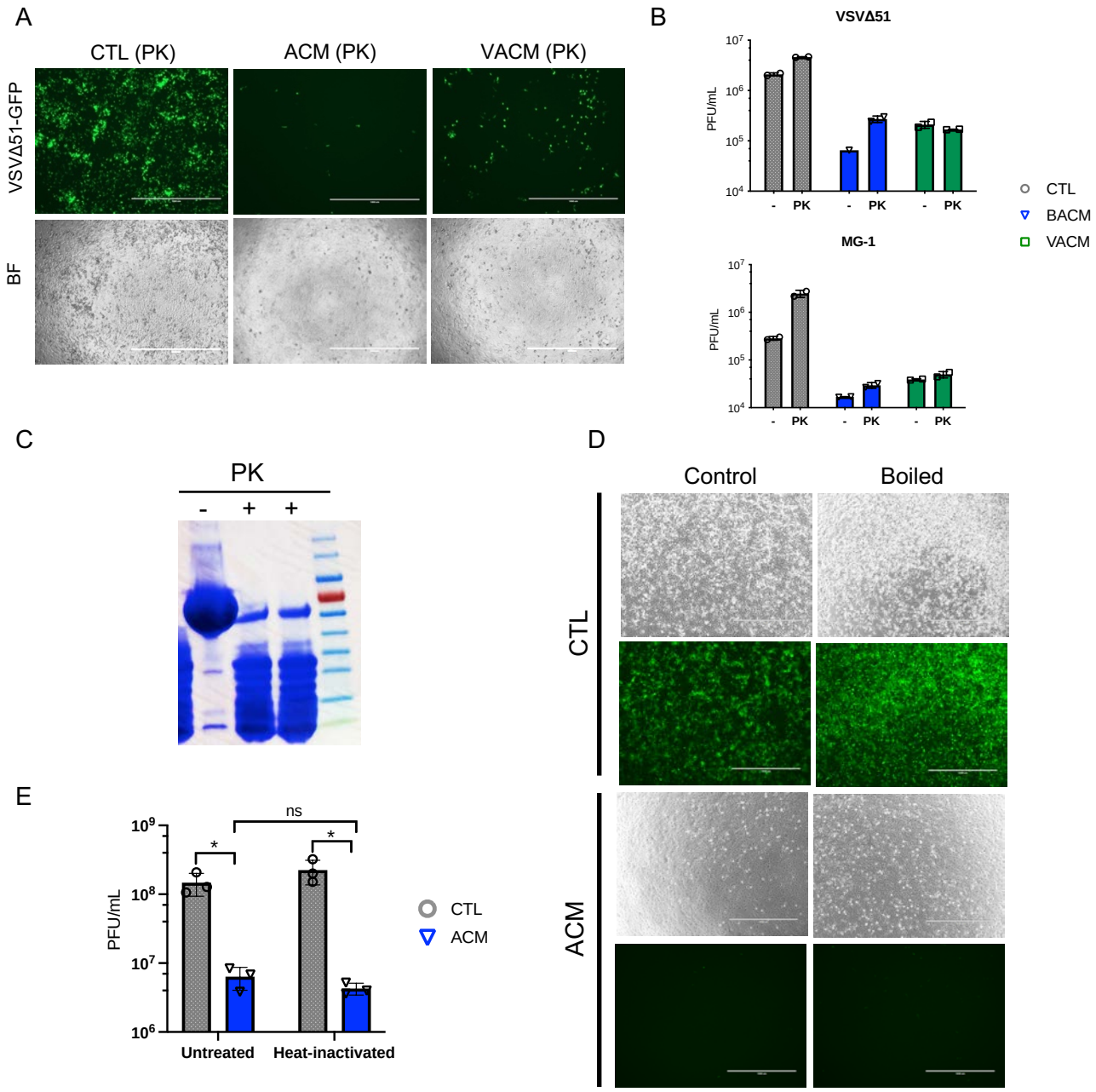

Figure 33: Proteolysis or heat-mediated denaturation does not mitigate ACM-mediated OV resistance. Proteinase-K linked to agarose beads were added to CTL media or ACM. Following incubation at 37°C, the beads were spun down (500g, 5mins) and added to OVCAR8 cells and infected with VSVΔ51 (MOI 0.1) (A) and the titers were quantified by plaque assay (B) (n=2 biological replicates). Proteinase-K treated medias were run on a SDS-PAGE gel and stained with Coomassie blue (n=2 biological) (C). CTL media or ACM were boiled or incubated in a 56°C water bath (heat-inactivation) for 30mins. After cooling to room temperature, the media was added to OVCAR8 cells and infected with VSVΔ51-GFP (MOI 1, 24pi) (D) (representative images shown, n=3 biological replicates) or SKOV3 cells and infected with VSVΔ51 (MOI 0.1, 48 hpi) (E) (n=3 biological

replicates). Bar represents 1000μm. 1-way ANOVA, Tukey's multiple comparison test for panel E. Scale bar represents 1000μm. Error bar represents SD. *p <0.05, **p <0.01, ***p<0.001.

2.3.2 Limiting endogenous lipid synthesis improves the anti-cancer effects of OVs but with limitations

Given the observation that decreased intracellular lipid accumulation as a consequence of depleting lipid sources in ACM corresponds to an increase in OV sensitivity, we aimed to determine the effect of limiting endogenous lipid pools on OV infection.

FAS catalyzes the formation of palmitate from acetyl-CoA and malonyl-CoA in the presence of NADPH. Epigallocatechin gallate (EGCG) is a polyphenolic flavonoid that has garnered significant attention due to its role in mitigating diseases of aging, such as cancer.[205] Some of the positive effects of EGCG has been attributed to its natural FAS inhibitory activity.[206] In the context of OV therapy, combination treatment with EGCG has previously been shown to potentiate oncolytic adenovirus infection.[207] In our studies, EGCG combinatorial treatment with VSVΔ51 increased infection and bolstered VSVΔ51-mediated cell death (Figure 34). Despite its promise as a combinatorial agent, a major limitation of this study was that EGCG has numerous functions aside from its proposed FAS inhibitory activity.[205]

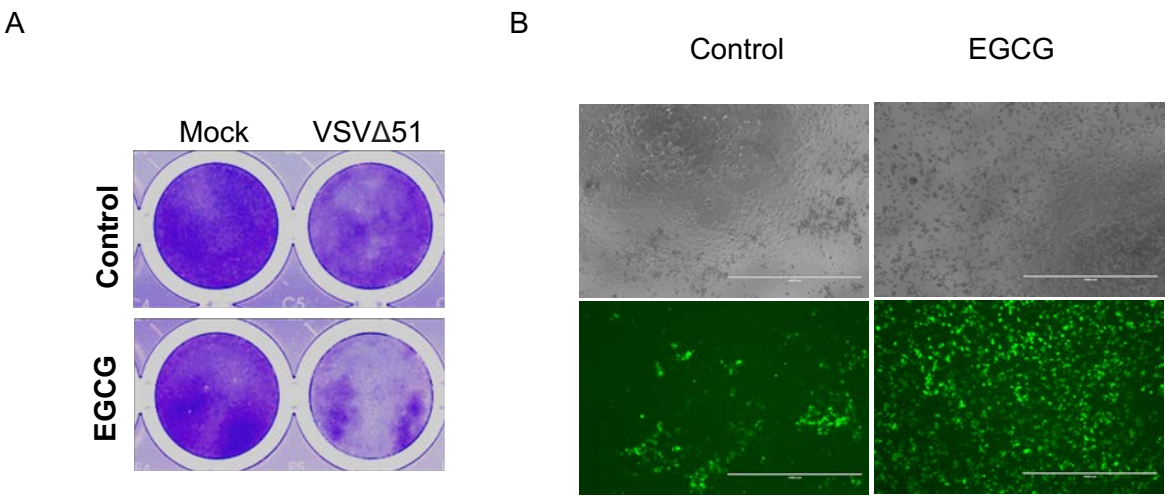

Figure 34: Combination treatment with EGCG enhances sensitivity to OV infection. SKOV3 cells were treated with EGCG (100μM), VSVΔ51 (MOI 0.1 for 1 hr) or both and assessed 48hpi. Cytotoxicity assay (A) and immunofluorescence microscopy (B) were done to assess cytotoxicity and virus infection, respectively. Scale bar represents 1000μm. Representative images from n=3 biological replicates shown.

5-tetradecyloxy-2-furoic acid (TOFA) is an allosteric inhibitor of acetyl-CoA carboxylase (ACC), an enzyme critical for long chain FA synthesis.[208] To determine effect of limiting ACC-mediated *de novo* lipogenesis on OV infection, we dosed cancer cells with increasing concentrations of TOFA and before infecting with VSVΔ51. Here, we found that combination treatment with TOFA increased the susceptibility of cancer cells to OV infection (5.7X, $p<0.0001$) and OV-mediated cell death (**Figure 35**). We then sought to determine whether the OV sensitizing effect of TOFA persists in ACM conditions. In ACM-receiving cells, the sensitizing effect of TOFA was wholly absent ($p>0.9999$). This finding suggested that when limited intracellular lipid pools are replenished by an exogenous source, in this case lipids from ACM, OV resistance is reinstated.

These limited studies using *de novo* lipogenesis inhibitors demonstrated that restricting endogenous lipid synthesis can have beneficial impacts on OV therapeutic efficacy but is limited by the presence of exogenous lipids in the microenvironment.

A

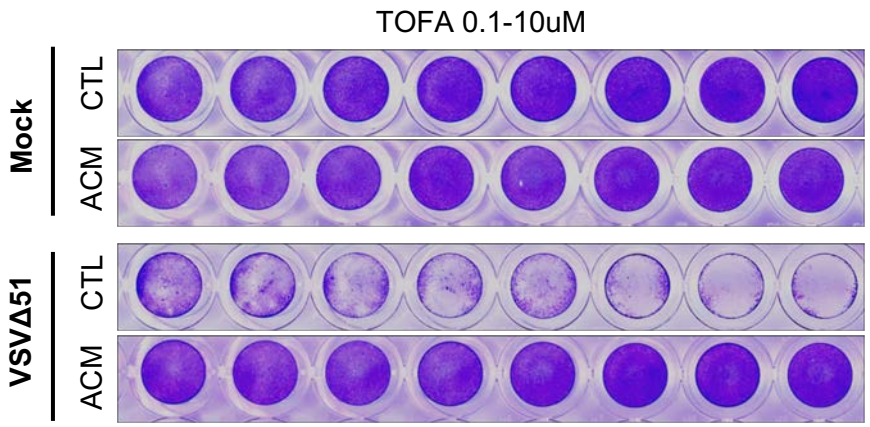

B

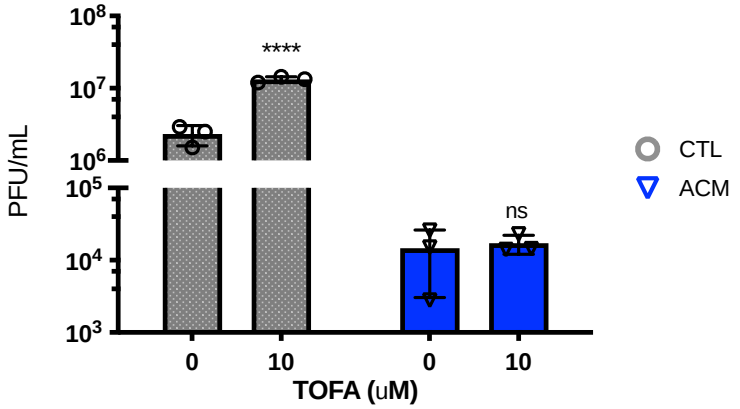

Figure 35: Blocking acetyl-CoA carboxylase increases OV infection but not in ACM. OVCAR8 cells in CTL media or ACM were dosed with increasing concentrations of 5-tetradecyl-oxy-2-furoic acid (TOFA) and infected with VSVΔ51 (MOI 0.1, 48hrs). OV-mediated cell death was evaluated by cytotoxicity assay (A) and viral titer was assessed by plaque assay (B) (n=3 biological replicates). Error bar represents SD. 2-way ANOVA, Bonferroni's multiple comparison test, ****$p < 0.0001$.

Section III: Determining a strategy to overcome adipocyte-derived lipid-mediated OV resistance

3.1 Exploring lipid modulating strategies to improve OV therapeutic outcomes

Part 1 of this section showed that adipose tissue and adipocyte secreted products hamper OV infection *in vitro* and *in vivo*, respectively. In Part 2, using lipid-depletion studies, it was established that adipocyte derived lipids are the predominant drivers of adipocyte-mediated OV resistance. Here, it was also demonstrated that blocking endogenous lipid synthesis in the absence of exogenous lipids can improve OV therapeutic outcomes in combinatorial strategies. The major pitfalls of the aformentioned approaches is the limited clinical translational potential. There are no known ways to deplete CAA derived lipids at the site of the tumour. Additionally, while limiting endogenous lipids may hold some promise, the presence of exogenous lipid sources in a fat-rich TME limits its ameliorative effects. Chapter 3 explores the therapeutic potential of blocking the uptake of adipocyte-derived lipids by cancer cells (Figure 36). The combinatorial effect of blocking FA uptake in the context of OV therapy is explored.

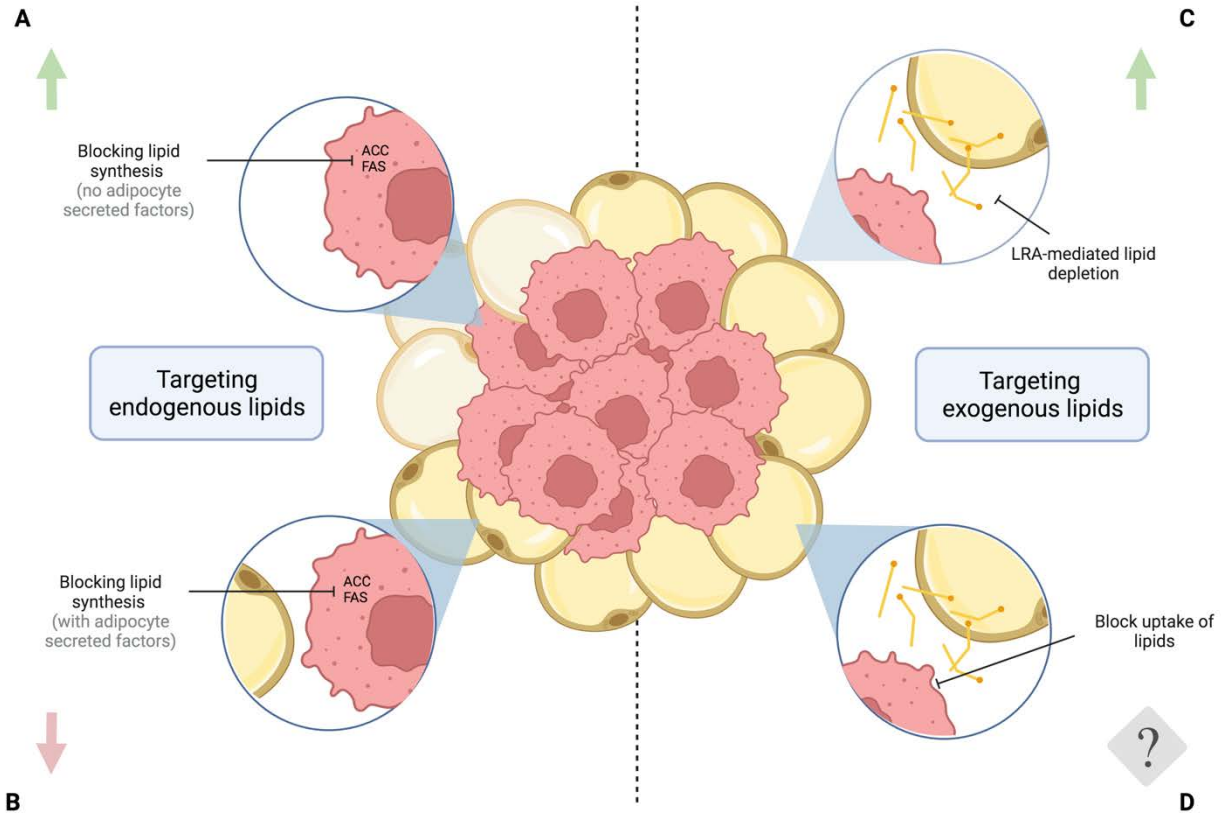

Figure 36: Exploring lipid modulating strategies to improve OV therapeutic outcomes. Blocking endogenous lipid synthesis by targeting proteins associated with endogenous lipid production (ACC, FAS) showed an increase in OV infection (A). This effect was ablated when exposed to adipocyte secreted factors, a source of exogenous lipids (B). When cancer cells received ACM that was depleted of lipid-derived constituents, it increased the sensitivity of cancer cells to OV infection (C). In an effort to develop a strategy with pragmatic clinical translational potential, we sought to investigate the effect of blocking the uptake of lipids by cancer cells (D). Green arrows, red arrows or question mark indicates positive, negative or unknown effects on OV therapeutic outcomes, respectively.

3.2 Evaluating the effect of blocking FA uptake on OV infection in lipid-rich microenvironments

As mentioned in the Introduction section of this thesis, numerous proteins have been implicated in the transport of FAs, including fatty acid transport proteins (FATPs). FATPs are one of the most heavily studied family of proteins involved in the transport of FAs. Of the FATP family, FATP1-6, only FATP1, FATP2 and FATP4 have been shown to directly participate in FA transport, thus presenting as good targets for attenuating FA transport.[48]

The role of FATP1, FATP2 and FATP4 in the context of ACM-mediated OV resistance was evaluated with a knockdown study. Cancer cells were knocked down for FATP1, FATP2 or FATP4 with transient transfection of FATP targeting siRNA pools. While FATP1 or FATP4 knockdown had no apparent effect on bolstering OV infection, FATP2 knockdown noticeably increased the sensitivity of cancer cells to OV infection in the presence of ACM (7.15X, $p < 0.05$) (**Figure 37**). Knockdown efficiency was determined by qPCR analysis of the intended targets (**Figure 38**). Although protein expression analysis is the ideal method to determine knockdown efficiency, I have been unsuccessful in my efforts to obtain a reliable target band with Western blotting. Protein analysis will be further pursued in preparation for submission of a publication.

Quantification of the baseline expression of FATP targets did not show any particular enrichment in FATP2 among a small panel of transporters of FAs evaluated (FATP1, FATP2, FATP4), including CD36, a protein of interest in the context lipid transfer in fat-rich TMEs (**Figure 39**).[36,38]

A

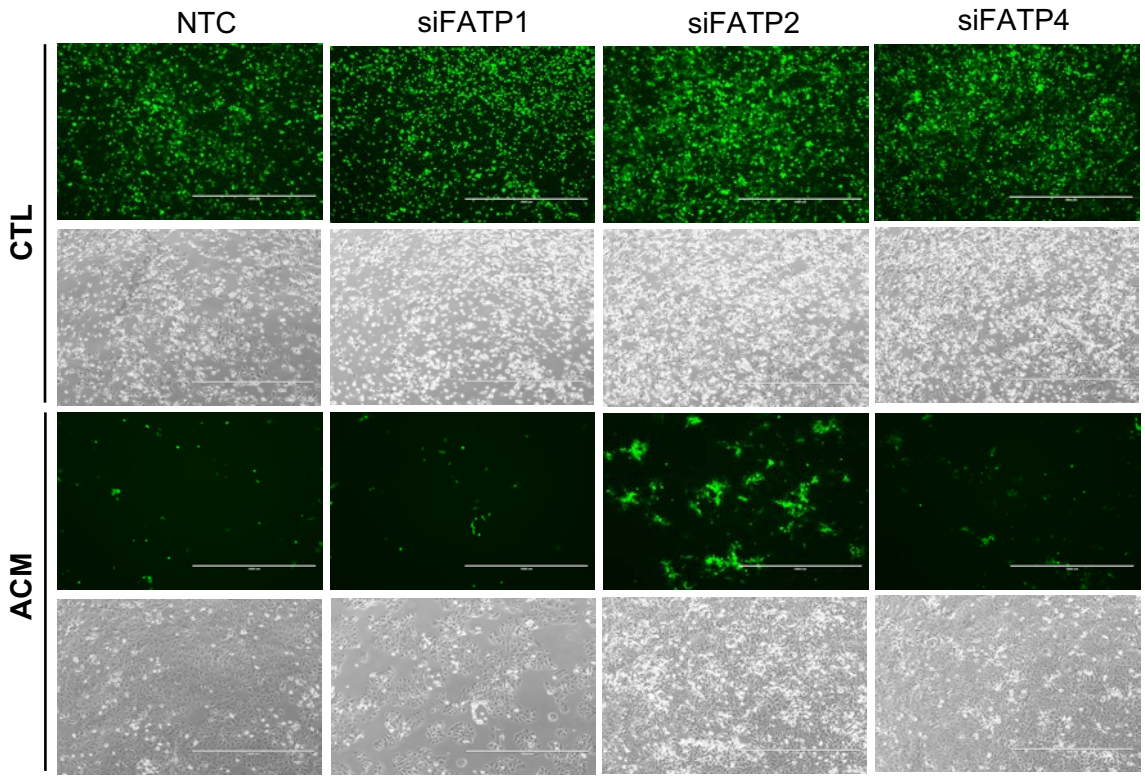

B

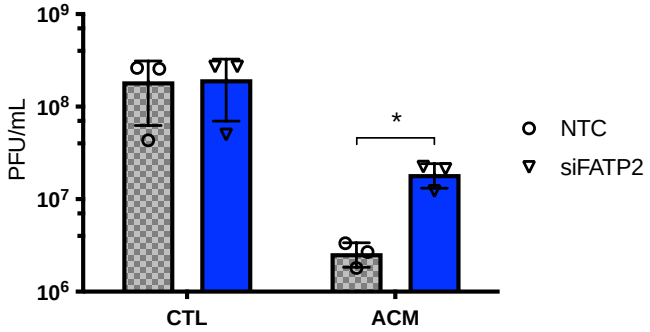

Figure 37: FATP2 knockdown increases OV infection in ACM-receiving cancer cells. OVCAR8 cells were transfected with the indicated siRNAs for 16hr and infected with VSVΔ51 (MOI 0.05). After 1 hr, the inoculum containing media were removed and replaced with CTL media or ACM. VSVΔ51 infection was visualized by IF (A) (representative images; n=2 biological replicates). The supernatant from NTC and siFATP2 transfected cells was quantified by plaque assay (B) (n=3 biological replicates). Scale bar represents 1000μm. Error bar represents SD. 2-way ANOVA, Bonferroni's multiple comparison's test on log 10 transformed data, *p <0.05.

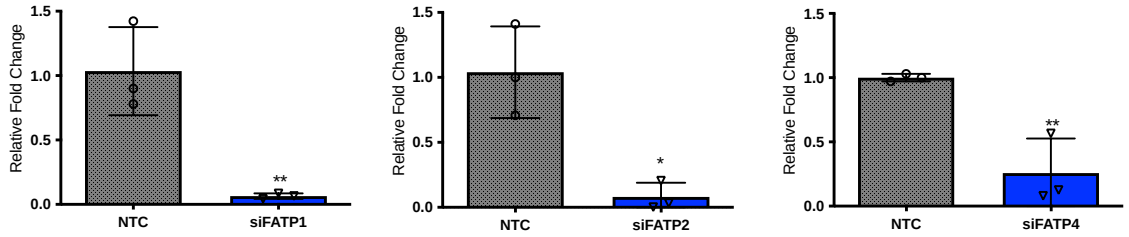

Figure 38: Evaluating FATP target expression following siRNA-mediated knockdown. OVCAR8 cells were transfected with siRNAs targeting the indicated gene targets. The RNA was extracted 48hpt to assess for target gene expression by qPCR (n=3 biological replicates). Fold change to relative Rplp0. Error bars represent SD. Two tailed, unpaired t-test, *p <0.05, **p <0.01.

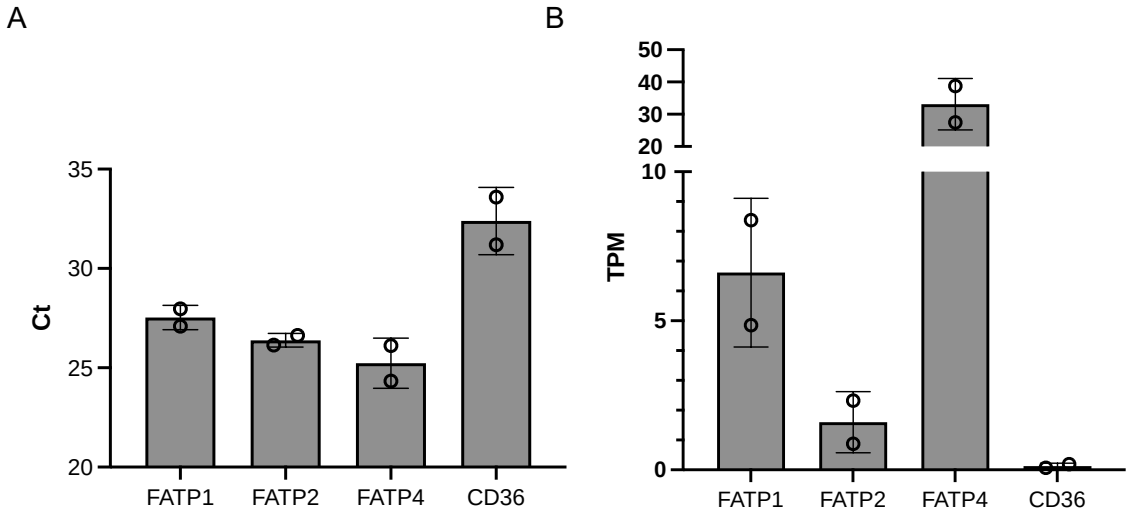

Figure 39: Assessing the baseline expression of select gene targets of proteins involved in FA transport. Ct values of FATP targets and CD36 were determined by qPCR, and pipetting variation was normalized to the ribosomal gene Rplp0 (A) (n=2 biological). The transcript per million (TPM) values of interested targets from RNA sequencing data sets are indicated (B) (n=2 biological). OVCAR8 cells. Error bars represent SD.

3.3 Using FATP inhibitors in combination treatment with OVs – *in vitro*

There has been great interest in developing inhibitors targeting FA transport proteins, particularly in the context of obesity and cardiovascular disease.[209,210] Sandoval *et al.* were triumphant in their efforts to determine FATP2 inhibitors in a yeast system expressing human FATP2 – successfully identifying the FATP2 inhibitors, Grassofermata and Lipofermata.[211]

Grassofermata effectively blocks FA uptake both *in vitro* and *in vivo*.[212] In a flow cytometry study with Bodipy staining, we validated its ability to block FA transport in our model *in vitro* (Figure 40A). ACM-receiving cancer cells treated with Grassofermata in a combination approach with OV infection displayed a marked increase in cancer cell death in comparison to OV infection alone (Figure 40B). Immunofluorescence microscopy with GFP-expressing OV revealed that the increase in cytotoxicity is likely due to an increase in OV infection and OV-mediated cell death (Figure 40C). Grassofermata alone did not affect cell viability, as shown by an unphased monolayer in crystal violet cytotoxicity analysis and microscopy brightfield images. Taken together, the aforementioned data strongly suggests that Grassofermata-mediated attenuation of FA uptake sensitizes cancer cells to OV infection and potentiates OV-mediated cytotoxicity.

A

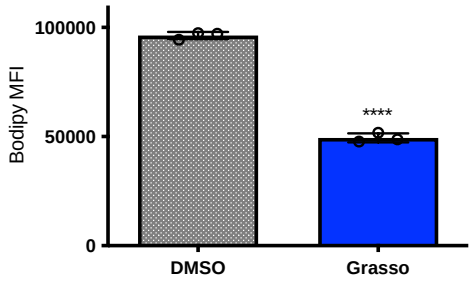
100000
50000
0
Bodipy MFI
****
DMSO
Grasso

B

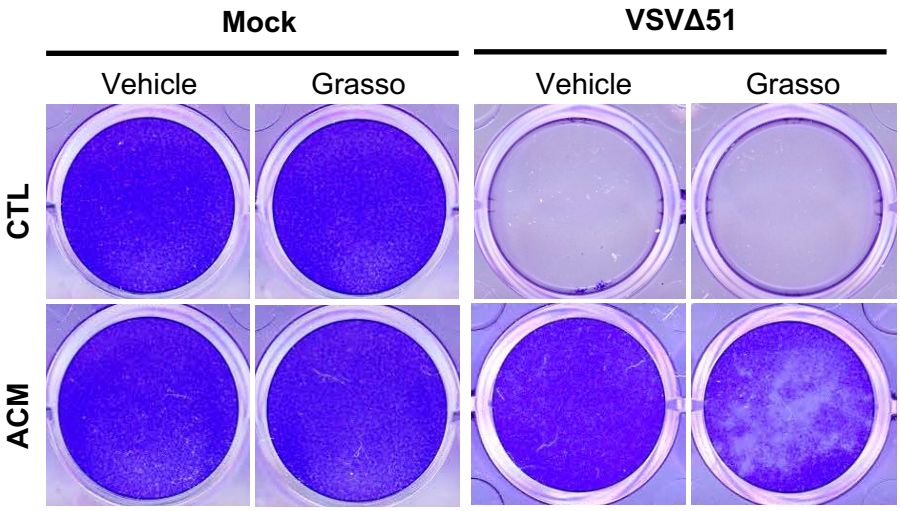
Mock
VSVΔ51
Vehicle
Grasso
Vehicle
Grasso
CTL
ACM

C

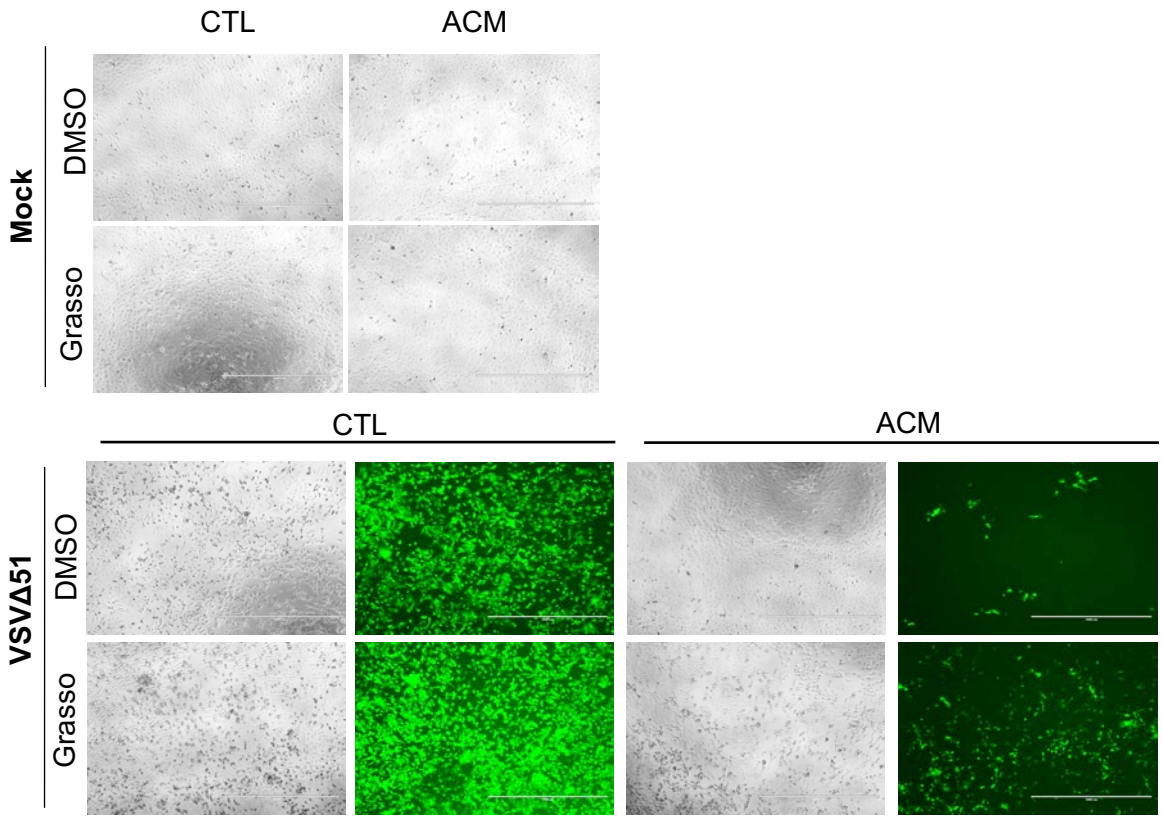
CTL
ACM
Mock
DMSO
Grasso
CTL
ACM
VSVΔ51
DMSO
Grasso

Figure 40: Combination treatment with Grassofermata and OV enhances OV infection. The intracellular lipid accumulation of OVCAR8 cells in CTL media and treated with Grassofermata (Grasso; 2.5μM) was assessed by flow cytometry with Bodipy staining (A) (n=3 biological replicates). Cells receiving Grassofermata alone (2.5μM), VSVΔ51 alone (MOI 0.1) or combination treatment were stained with crystal violet (96hpi) (B) (n=4 biological replicates). IF images of VSVΔ51-GFP infected cells (MOI 0.1, 48hrs) and receiving Grassofermata (5μM) are shown in (C) (representative images of n=3 biological replicates). Scale bar represents 1000μm. Error bar represents SD. Two tailed, unpaired t-test, ****$p < 0.0001$.

In comparison to Grassofermata, the blocking of FAs by Lipofermata have been more widely studied.[213] A preliminary flow cytometry study showed that Lipofermata is effective at blocking lipid accumulation in our model *in vitro* (**Figure 41A**). Echoing the phenomenon observed with FATP2 knockdown or in combination approaches with Grassofermata, cancer cells receiving combination treatment with Lipofermata were more susceptible to OV infection in ACM conditions than with OV monotherapy (**Figure 41B**).

A

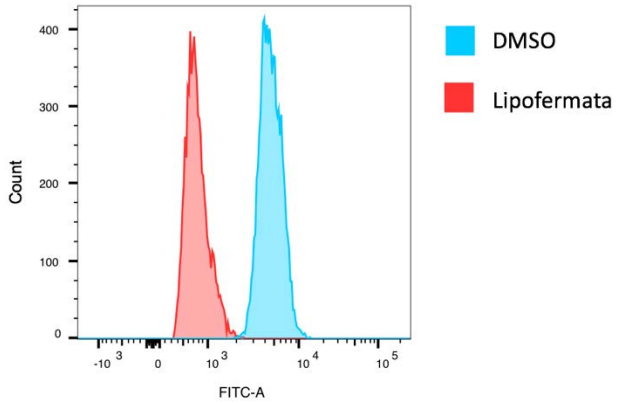

B

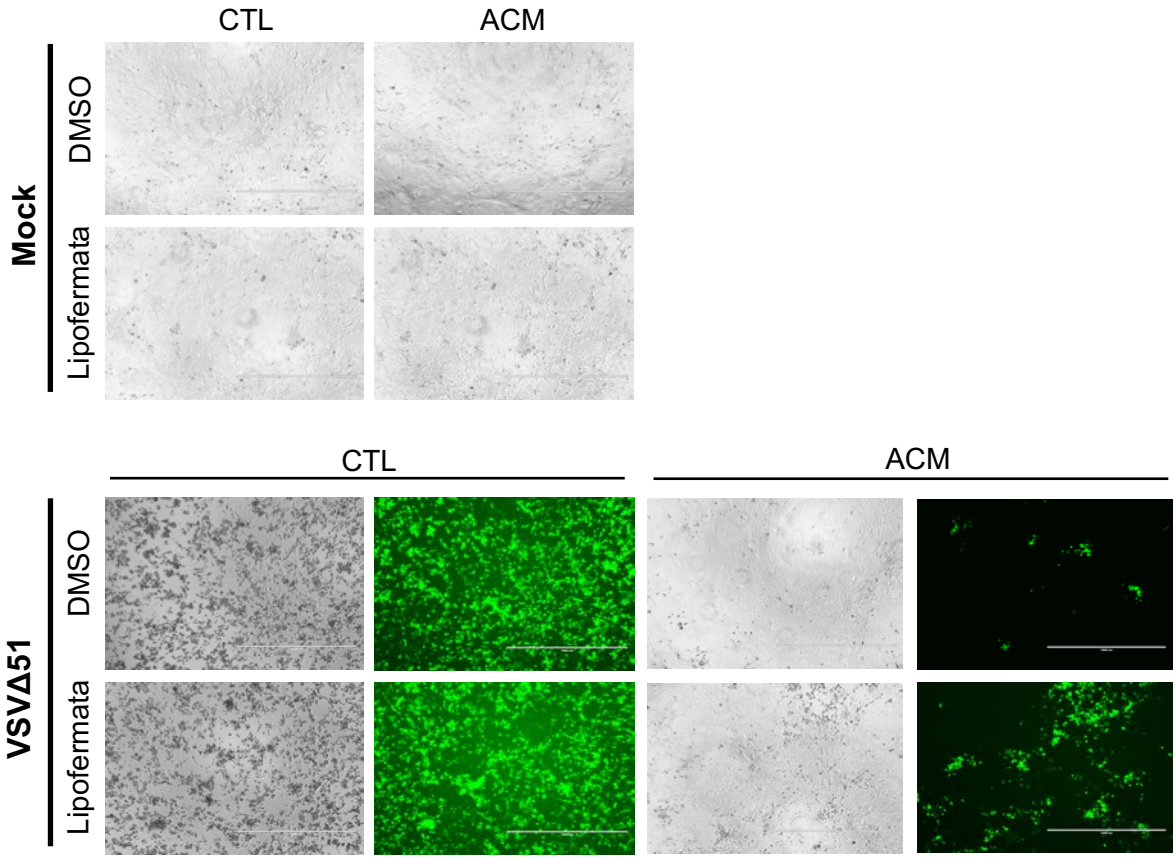

Figure 41: Combination treatment with Lipofermata increases OV infection *in vitro*. OVCAR8 cells in CTL media were treated with Lipofermata (0.24μM) overnight. Flow cytometry analysis of intracellular lipid accumulation was achieved with Bodipy staining (n=1 biological replicate) (A). Cells were treated with Lipofermata (0.24μM) and cultured in CTL media or ACM prior to infection with VSVΔ51-GFP (MOI 0.1, 48hrs). VSVΔ51 infection was visualized by IF (B) (Representative images of n=3 biological replicates). Scale bar represents 1000μm.

3.4 Using FATP inhibitors in combination treatment with OVs – *in vivo*

Given the promising *in vitro* data described in the previous section, we sought to evaluate the effect of OV combination treatment with FATP2 inhibitors *in vivo*.

Lipofermata is one of the best characterized inhibitors of FATP2 with compelling evidence for clinical promise.[213,214] In a syngeneic EO771 breast tumour model where tumours were seeded in the FP, neither Lipofermata or VSVΔ51 alone provided a survival benefit. When mice were treated in an OV combinatorial approach with Lipofermata, we observed a notable survival advantage over either monotherapy (**Figure 42B**). Tumour volume analysis demonstrated a trend towards increased tumour control in mice receiving combination treatment (**Figure 42C**). Preliminary studies evaluating the OV titer in mice receiving combination treatment showed a trend towards Lipofermata-driven increase in intratumoural OV infection (**Figure 43**).

In an intra-peritoneal ovarian tumour model (ID8-F3 p53-/-), combination treatment with Lipofermata provided the best survival advantage. Lipofermata treatment alone did not improve survival and VSVΔ51 alone only provided a modest survival benefit (**Figure 44**).

The findings from our studies in syngeneic mouse models demonstrated that combination treatment with Lipofermata can be a promising strategy to promote OV infection at the site of the tumour, decrease tumour burden and enhance overall survival *in vivo*.

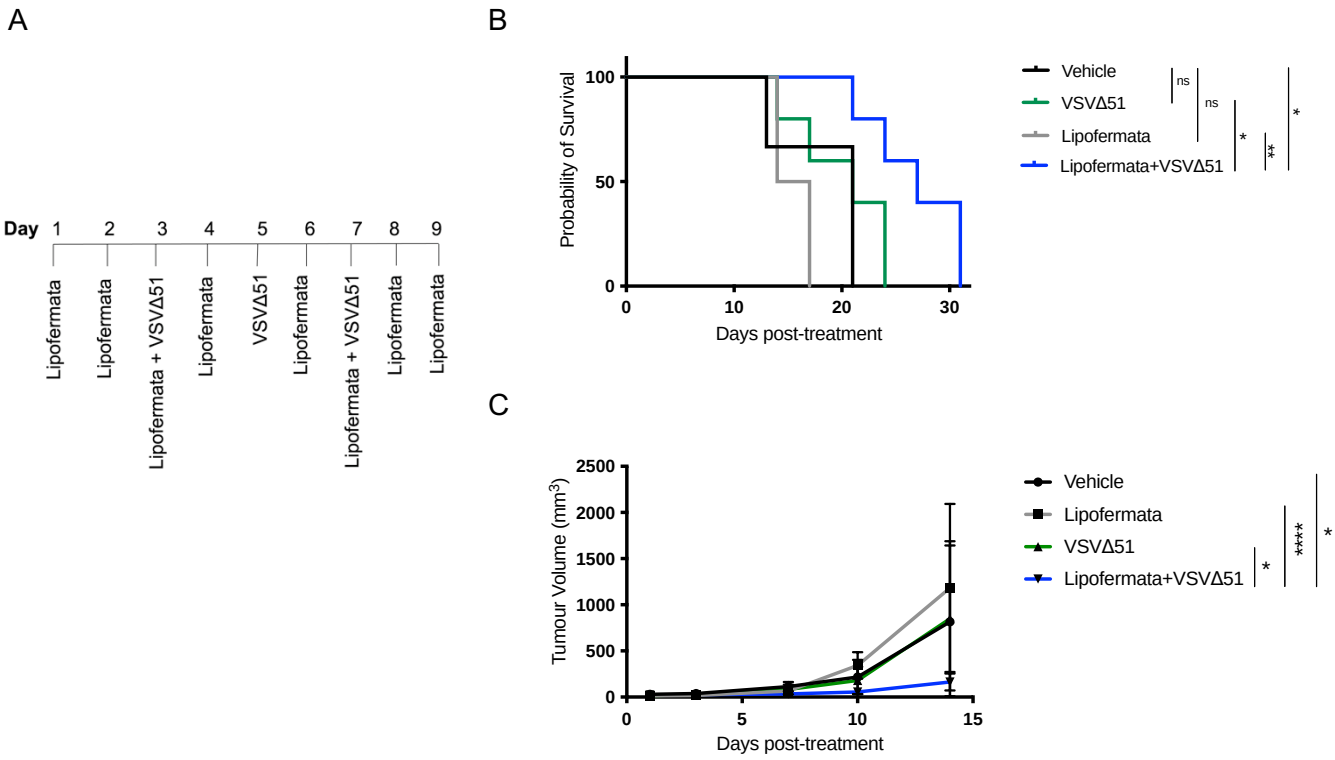

Figure 42: Combination treatment with Lipofermata and OV controls tumour growth and enhances overall survival in a murine syngeneic breast tumour model. EO771 fat-pad tumour bearing C57BL/6 mice received Vehicle (n=3), Lipofermata (3mg/kg) (n=4), VSVΔ51 (1E8 PFU) (n=5) or both Lipofermata and VSVΔ51 (n=5) by intratumoural delivery according to the schedule shown in (A). Kaplan Meier survival curve is shown in (B) and tumour volume up to the day before the first endpoint (Day 14) in shown in (C). Log-rank (Mantel-Cox) test for Panel B. 2-way ANOVA, Tukey's multiple comparison test for Panel C. Error bar represents SD. *p <0.05, **p <0.01, ****p < 0.0001.

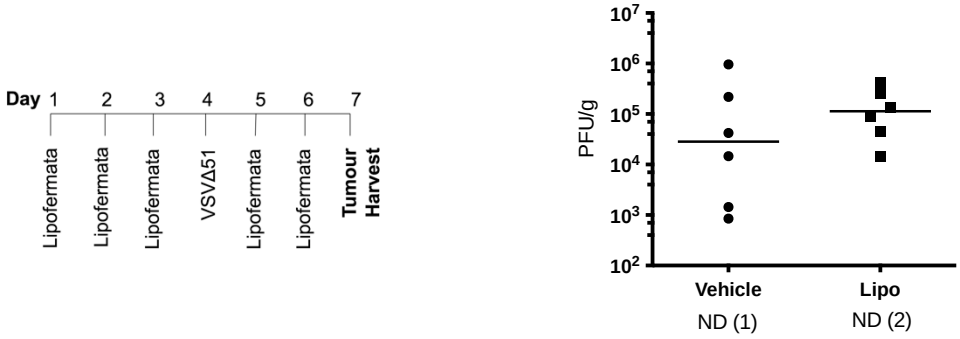

Figure 43: Combination treatment with Lipofermata and OV shows a trend towards increasing intratumoural OV titer. EO771 tumours (10 tumours/group) were intratumourally treated with a VSVΔ51 (3E8 PFU) alone or in combination with Lipofermata (2.5mg/kg) and the tumours were harvested for quantification by plaque assay 72hpi. Tumours <0.1g were excluded. Line indicates median. Two tailed, unpaired t-test.

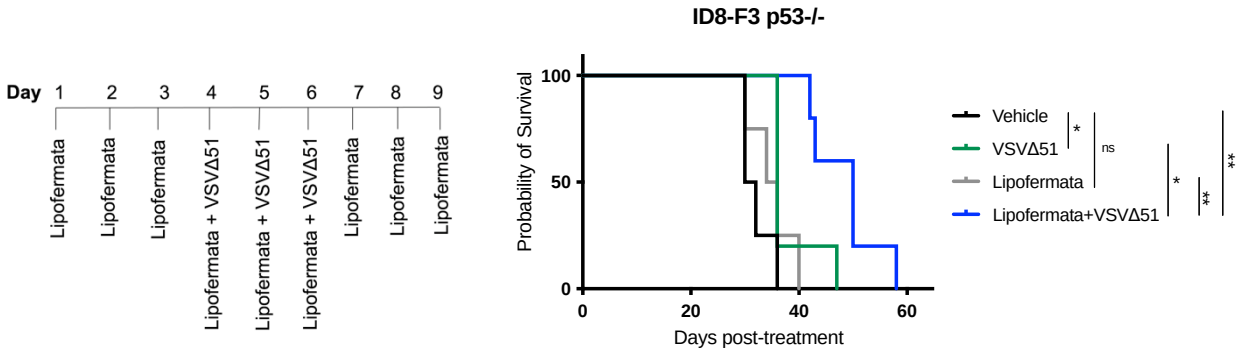

Figure 44: Combination treatment with Lipofermata and OV enhances overall survival in a murine syngeneic ovarian tumour model. ID8-F3 intraperitoneal (IP) tumour bearing C57BL/6 mice received Vehicle (n=4), Lipofermata (3mg/kg) (n=4), VSVΔ51 (3E8 PFU) (n=5) or both Lipofermata and VSVΔ51 (n=5) by IP delivery and assessed for survival. Log-rank (Mantel-Cox) test, *p <0.05, **p <0.01.

CHAPTER 3 – DISCUSSION & CONCLUDING STATEMENT

DISCUSSION

ACM-mediated OV resistance is a broad effect

In our studies, we showed that the inhibitory effect of ACM was consistent across OVs from 4 distinct families – Rhabdoviridae, Poxviridae, Herpesviridae and Paramyxoviridae. Not only are these viruses genetically diverse but they are unique in the host receptors they require for entry and their modes of infection.[173,215–217] Following cell entry, the viruses replicate in different compartments of the cell. Herpes virus can replicate in the nucleus while viruses from the other families replicate in the cytoplasm.[161,173,215–217] The replication of the genome is also distinct - VSV and Measles are RNA viruses while VACV and HSV have DNA genomes. The concordant inhibitory effect of ACM on a panel of viruses with such wide diversity in their methods of infection and replication insinuates that ACM mediated impediment to OV infection is more likely an indirect effect, for example, through alterations to the host cell, rather than a direct effect on the virions themselves. It must be noted that the panel of OVs tested did not include a non-enveloped OV. It would be interesting, and relevant, to elucidate the effect of ACM on naked OVs such as Reolysin, an FDA-approved treatment for numerous cancers, including metastatic breast tumours.[218]

Although the exact mechanism by which OV resistance occurs was not elucidated, we have accumulated some mechanistic clues about the potential mechanisms by which adipocyte secreted factors may contribute to OV resistance and they are explored in this Discussion. It is important to note that although initial evaluations of the inhibitory effect of ACM were determined in the context of diverse OV platforms from different families, for simplicity, the vast

majority of downstream studies were focused on Rhabdoviruses, namely VSVΔ51. The conclusions drawn from many of these studies must be validated in other OV platforms.

Impairment to OV infection occurs post-virus entry

Numerous independent experiments pointed to a post-virus entry mediated mechanism of OV resistance. This was exemplified by assays manipulating the timing of ACM exposure and evaluating its impact on OV infection. The relatively fast recovery in the sensitivity of cells to OV infection upon ACM removal, is interesting. This could be due to a quick clearing of intracellular lipids themselves or recovery of the ACM-induced impairments to cellular compartments that impede virus infection. Among the various assays performed, the VLP platform best elucidated that ACM does not impair virus entry. VLPs pseudotyped with VSV-G can be transduced into ACM-receiving cells unphased while infection with replicating VSVΔ51 particles were significantly hampered. The case for a post-entry mediated mechanism of resistance is further supported by the observation that the introduction of ACM post-virus entry can comparably inhibit OV infection (Appendix Figure 5) .

The virus particle, once engulfed by endocytosis, is trafficked through the endosomal trafficking pathway to the late endosome. Here, accumulating acidification triggers a conformational change in VSV-G, the glycoprotein of VSVΔ51, to mediate fusion and escape into the cytoplasm for replication of viral genes and eventually, viral assembly. [173] There are diverse conditions needed to trigger fusion in enveloped viruses; however, low pH remains to be a common requirement across all 3 classes of fusion proteins.[199,219] We sought to indirectly evaluate the potential effects of ACM on viral fusion by assessing the impact of ACM on acidic

compartments in the cell. Our preliminary study revealed a decrease in Lysotracker staining. At first glance, this finding appeared counter intuitive given that our work showed that ACM is enriched in FAs; however, FA-mediated decrease in intracellular acidity has been previously described. In a study by Liu *et al.*, excess long chain FAs, such as palmitate or oleate, decreased the acidity of endosomes by inducing disassembly of v-ATPase, a transmembrane pump that facilitates the movement of protons from the cytoplasm into the endosome for endosomal acidification.[220] It is reasonable to speculate that ACM-derived FAs contribute to the disassembly of v-ATPase that ultimately inhibits the fusion of VSVΔ51 particles into the cytoplasm for downstream oncolytic activity. To validate this hypothesis, the aforementioned preliminary Lysotracker studies must be repeated, and the state of v-ATPase assembly must be evaluated. Alternatively, viral fusion can be sensitive to the lipid composition of membranes which effects membrane fluidity.[187] Transmission electron microscopy studies could also provide visual indications of how virus trafficking unfolds in host cells receiving ACM.

The Lysotracker dye does not provide a direct measure of acidity. It is also known to induce an alkalizing effect on lysosomes when incubated for longer than 5mins. Alternatively, Lysosensor dye may be used in follow up studies to address intracellular acidity in the context of ACM, since it can be used to measure the pH of acidic organelles.

The role of interferon in ACM-mediated OV resistance

ACM-mediated OV resistance is not driven by Type I interferon

Interferons regulate the immune response to viral infections. To date, 3 classes of interferons have been identified – Type I, II and III. Specifically, type I interferon signaling is critical for mounting an anti-viral response in non-immune cells.

When cells in CTL media were infected with OVs, there was a significant upregulation in the expression of ISGs, as observed with RNA sequencing studies. Although cancer cells can be defective in their interferon response, some expression of ISGs in OV-infected cancer cells is expected since viral antigens will engage numerous extracellular and intracellular pattern recognition receptors to induce a Type I interferon mediated anti-viral response.[221] Due to intrinsic maladaptive characteristics in cancer cells, they remain susceptible to OV infection.[158,161] Comparatively, ACM-receiving OV infected cells were dampened in their ISG expression despite being significantly more resistant to OV infection. This result was contradictory to our expectations and further alluded to a mechanism of resistance alternative to Type I interferon signaling.

The binding of Type I interferons [13 partially homologous IFN-α subtypes, a single IFN-β, and several other poorly defined interferons (IFNε, IFNτ, IFNκ, IFNω, IFNδ and IFNζ)] to the IFNAR surface receptor induces cross-phosphorylation by Jak1 and Tyk2 on the cytoplasmic domains of the receptor subunits, as part of the JAK/STAT signaling pathway.[221] This subsequently triggers phosphorylation of STAT1 and signal transducer and activator of transcription 2 (STAT2) to form various complexes that translocate to the nucleus and bind the interferon sensitive response elements or gamma-activated sequences on the promoters of ISGs.[222] Our efforts to block IFNAR engagement with IFNAR blocking antibody or inhibit downstream JAK/STAT signaling with JAK

inhibitor did not improve OV infection in ACM conditions, further supporting a case for an Type I interferon alternative mechanism of OV resistance. It must be noted that an important caveat of these studies are that it precludes an anti-viral response due to ligand stimulation of intracellular viral sensors.[222]

The seemingly inert response in ISG expression in the face of OV infection was peculiar given that our studies showed that ACM does not hinder virus entry. ACM conditions appear to impair the cellular detection of internalized OV particles by some unknown mechanism. Though speculative, we hypothesize that this may be in line with the aforementioned theory suggesting a FA-mediated disruption of endosomal acidification that ultimately perturbs VSVΔ51 fusion. Endosome encapsulated VSVΔ51 particles may be protected from detection by cytoplasmic viral sensors and thus, do not engage Type I interferon mediated ISG expression.

This hypothesis however does not account for the stunted ISG expression observed in ACM-receiving cells treated with IFN-α. This phenomenon may be a product of another ACM-driven alteration to the host cell – lipid-mediated ER stress (will be further discussed in the section 'Exploring the potential role of lipid-mediated ER stress').

<u>The potential role of IFITM1 in ACM-mediated OV resistance</u>

RNA sequencing of cells receiving ACM showed an upregulated expression of IFITM1 (2.8X), a member of the IFN-induced transmembrane protein family. Although it has not been studied extensively, in both breast and ovarian cancers IFMIT1 is associated with tumour growth and invasion.[223,224]

IFITM1 has broad anti-viral activity.[225–229] IFITM1 is expressed at basal levels in most vertebrates and translocates to the plasma membrane to carry out its anti-viral activity. When it is mutated in a way that prohibits localization to the plasma membrane, its anti-viral activity is ablated.[225] Some studies have shown that IFITM1 can adopt more than one membrane topology and co-exist in the plasma membrane and in intracellular vesicles.[230,231] Moreover, IFITM1 inhibits semi-fusion across all classes of viral fusion proteins.[232] Notably, of the IFIT proteins, IFITM1 has been shown to preferentially inhibit viruses that fuse at the lysosome.[187,226] Mudhasani *et al.* showed that IFITM1 alters vesicle morphology. It enlarges the size of the vesicles and decreases its acidity, as shown by Lysotracker staining, the same dye used in our evaluation of intracellular acidic compartments in ACM-receiving cells.[230] IFITM1 has also been implicated in other processes relating to virus infection. For instance, IFITM1 is linked to the inhibition of cell-to-cell fusion (syncytia formation) in Measles infection as well as some post-entry mechanism in HIV infection.[227,232] Since the expression of IFIT genes can be expressed independent of IFNAR mediated Type I interferon signaling, our present studies with IFNAR blocking antibody or JAKi does not rule out the potential role of IFITM1 in promoting OV resistance in ACM-receiving cells.[233]

IFITM1 expression as a response to ACM culture is intriguing and may be a product of an undetermined link between IFITM1 and adipocyte secreted factors. Co-regulation of cellular bioenergetics and response to virus infection have been previously reported. For instance, in a study of cholesterol metabolism in macrophages, York *et al.* showed that altering cholesterol flux could engage a Type I interferon response to ultimately reduce murine gammaherpesvirus-68 viral load in bone-marrow derived macrophages.[234] Zhang *et al.* determined that the intracellular pattern recognition receptors, retinoic acid-inducible I -like receptors, are activated and its

activation is linked to glycolytic metabolism cross signaling with Type I interferon signaling.[235] IFIT proteins have been linked to cholesterol transport through interactions with vesicle associated membrane protein-associated protein A.[187] Thus, it is possible that IFITM1 expression is induced by intracellular metabolic shifts in response to the influx of adipocyte-derived lipid species. Future work can evaluate the expression of IFITM1 in cells receiving lipid-depleted ACM and separately, exploit siRNA targeting strategies to determine the role of IFITM1 in ACM-mediated OV resistance.

Lipids as the driver of OV resistance

The role of adipocyte-derived FAs

Although adipokines have previously been implicated in anti-cancer therapy resistance, in our studies using various methods to cleave or denature proteins, we demonstrated that OV resistance is unlikely to be spearheaded by a protein-derived biomolecule in ACM.[236]

The identification of lipid species as the primary driver of ACM-mediated OV resistance was a landmark finding in this project. Lipid-depletion of control media did not significantly impact OV infection or growth of the cells when evaluated by visual inspection, suggesting that our lipid-depletion protocol does not remove important factors from the serum that may negatively impact cells. Lipids can be received by cells in the form of lipoproteins, microvesicles, carrier proteins and/or free lipids.[39,237] CAAs in the TME are well characterized for capturing FAs in TAGs for storage, and releasing the stored FAs in times of demand; thus, evaluating the presence of FA species in ACM was an intuitive and logical next step.[23,27,65]

Analysis of ACM showed that ACM is enriched in FAs, and this was supported by RNA sequencing data that is suggestive of FA metabolism in ACM-receiving cells. As such, we evaluated

the effects of FA supplementation with palmitate and oleate on OV infection (**Figure 25, 32**). FA supplementation partially recapitulated the effects of ACM but was not as robust as ACM in inhibiting OV infection, as assessed by OV titer and cytotoxicity. Perhaps the oversimplification of evaluating a single species is insufficient to mimic the biochemical diversity of ACM. Although palmitate and oleate were chosen for their known abundance in human adipocytes, it is possible that other, less abundant FA species drive OV resistance. Studies have shown that FA identity can have differential effects on virus infection, as discussed in the Introduction of this thesis. In fact, cancer cells can have a demonstrated preference for certain FA species.[238,239] Moving forward, it could be beneficial to determine the identity of FA species in ACM and determine the biases for various FAs at the level of FA transport and its biochemical fate in the receiving cell.[240] Future work evaluating the transcriptome of cells receiving boiled ACM may provide more clues about the relative contribution of various biological macromolecules in ACM on receiving cancer cells.

In our *in vitro* studies, adipocyte derived factors were captured by harvesting ACM from an isolated culture of adipocytes. In tumours, CAAs undergo reciprocal communication with cancer cells and this has been shown to fuel de-lipidation by CAAs to release FAs for uptake by cancer cells.[21] A co-culture system would provide a more accurate depiction of the CAA phenotypes described in this thesis. We hypothesize that the observed lipid-driven effects may be an underestimation of true impact of adipocyte secreted lipids on OV infection in the TME.

While *in vivo* studies more accurately reflect the true nature of the TME, it is not devoid of experimental caveats. Specifically, OV spread within the tumour may be impacted by differing tumour sizes and stromal composition, ultimately impacting the intratumoural OV titer. Future studies may capitalize on tools such as IVIS imaging to evaluate OV spread in diverse TMEs.

Adipocyte secreted factors alter cancer cell metabolism

Agilent Seahorse XF Cell Mito Stress Test directly measures mitochondrial function by evaluating the OCR at intervals of meticulous injection of various modulators of the electron transport chain. We used this test to evaluate the mitochondrial metabolism of cells in the presence of ACM. Here, we found that the OCR signature of ACM and CTL media receiving cells were distinct, but the magnitude of these differences were modest in nature.

The more intriguing finding was the response of CTL media or ACM receiving cells to Etomoxir treatment. Etomoxir is a non-reversible inhibitor of CPT1, a key rate limiting enzyme for FA oxidation by β-oxidation. While CTL media receiving cells were unchanged by etomoxir treatment, it induced a striking and titratable decrease in the maximal respiration of cancer cells in ACM culture. Given reports of off-target effects by etomoxir at higher concentrations, we did not use concentrations above 5μM.[241] Our findings were suggestive of a shift in ACM-receiving cells towards using adipocyte derived lipids for FA oxidation. This metabolic shift was further substantiated by qPCR results demonstrating an increase in CPT1 expression (**Figure 27**). Future studies may seek to validate increased expression of CPT1 at the protein level by Western blotting. Transcriptome analysis also indicated that ACM-receiving cells were in a lipid-rich environment supporting FA metabolism (**Figure 28**). We observed an upregulation of CRAT, an enzyme which catalyzes the reversible transfer of acyl groups from carnitine to CoA, making it an important player in the cellular transport of FAs for β-oxidation. We also observed an upregulation of a variant of CPT1 typically found in neurons and cancer, CPT1c.[202] Taken together, these studies provided evidence of a metabolic shift in ACM-receiving cells favouring FA oxidation.

Perhaps this shift towards a substrate preference for FAs explains the decrease in maximal respiration observed in ACM receiving cells compared to the control. This finding was contrary to our expectations and numerous studies have reported opposite effects in cancer cells accumulating lipids.[36,146] The decrease in maximal respiration observed in ACM-receiving cells may be an artifact of a switch to FA metabolism and a lack of FAs in the Seahorse experimental medium. In a study of the impact of CAAs on acute lymphocytic leukemia cells, Tucci and colleagues observed a similar phenomenon of a reduction in bioenergetics in standard assay conditions in cells receiving adipocyte secreted products. They showed that this effect can be corrected by adding FAs to the experimental media. The addition of oleate to the media notably increased respiration in acute lymphocytic leukemia cells that were co-cultured with adipocytes, and this effect was absent in control conditions.[238] Future studies can seek to validate this presumed effect in our models in the way that Tocci and colleagues have done or alternatively, by exploiting Seahorse assays that were designed to assess FA oxidation directly, such as the Seahorse XF Palmitate Oxidation Stress Test Kit. More optimal assay conditions may also reveal the impact of acute delivery of Etomoxir on baseline respiration.

Exploring the potential role of lipid-mediated ER stress

Lipid metabolism and endoplasmic reticulum (ER) stress are closely linked and bi-directional in nature.[242,243] While ER stress can alter lipid metabolism, altered lipid homeostasis can also trigger an ER stress response.[242] Saturated FAs like palmitate have been shown to induce ER stress. [242,244,245]

RNA sequencing revealed TXNIP as an upregulated gene in ACM conditions (3.9X). TXNIP inhibits the antioxidative effects of thioredoxin, an important regulator in redox signaling; however, it is also implicated in regulating cellular metabolism and ER stress.[203,246] FA-induced upregulation of TXNIP has been previously described. In human aortic endothelial cells, high concentration of FAs increased expression of TXNIP.[247] This effect may be tissue specific since the opposite effect was observed in insulin secreting cells.[248]

ER is a key organelle involved in the synthesis, folding and modification of proteins. When the protein folding capacity of the ER is disrupted, increasing quantities of unfolded or misfolded proteins are detected by ER resident sensors and this activates the unfolded protein response, a number of mechanisms intended to reinstate ER homeostasis.[249] TXNIP, whose expression is triggered by the unfolded protein response, is an essential regulator of IL-1β production, a key player in inflammasome activation, a pro-inflammatory cellular response.[250] Transcriptomic analysis of ACM-receiving cells demonstrated an upregulation in IL-1β (6.0X), indicating a potential role for inflammasome activation in ACM-mediated OV resistance.

Viruses exploit the ER for replication, assembly and egress; thus, an impairment to ER function can form a significant barrier for successful infection.[251] There is some evidence to suggest that downregulating TXNIP may have a sensitizing effect on virus infection. In a study by Tiwarekar *et al.*, silencing of this gene increased Measles virus titer.[252]

Given the aforementioned evidence that is suggestive, albeit not confirming, of lipid-mediated ER stress in ACM-receiving cells, it is reasonable to hypothesize that the benefit of combinatorial treatment with the FATP2 inhibitor Lipofermata may at least partially derive from Lipofermata-mediated ER stress relief. Ahowesso *et al.* showed that Lipofermata attenuated

palmitate transport corresponded with a decrease in the expression of lipotoxicity mediated cell stress markers such as binding immunoglobulin protein and CCAAT/-enhancer-binding protein homologous protein.[213] Future studies can determine the role of TXNIP, ER stress and associated inflammasome activation by evaluating key genetic and protein markers of ER stress. We can also exploit chemical inhibitors of ER stress, such as 4-phenyl butric acid or tauroursodeoxycholic acid, to determine if relieving potential ER stress can re-sensitize cells to OV infection.[253,254]

Using lipid modulating drugs in combination approaches with OV therapy

Evaluating the benefit of using *de novo* lipogenesis inhibitors in an OV combination approach in lipid rich TMEs

Cancer cells divide rapidly, creating a high demand for lipids to support membrane synthesis and bioenergetic demands. As such, lipogenic enzymes are often overexpressed in cancer.[83] We showed through ACM lipid depletion studies that depleting exogenous lipid sources can provide a therapeutic advantage in the context of OV therapy. In an effort to recapitulate the effect exogenous lipid depletion on the intracellular lipid environment in cells receiving lipid-depleted ACM, we tested inhibitors of *de novo* lipogenesis enzymes in combination approaches with OVs.

ACC catalyzes the carboxylation of acetyl Co-A to form malonyl-CoA, the first committed step in the synthesis of long chain FAs. For the first time, we showed that combination treatment with TOFA, an inhibitor of ACC, can have a sensitizing effect on oncolytic rhabdovirus infection. In ACM conditions, the sensitizing effect of TOFA was ablated. This finding demonstrated that in a lipid-rich microenvironment, a lack of endogenous lipids can be replenished by nearby exogenous

sources and emphasized the need for alternative strategies to modulate lipid flux in lipid-rich TMEs. Future studies may seek to employ fluorescently labelled FAs to distinguish endogenous FAs from FAs that were uptaken from ACM.

The polyphenolic compound EGCG has at least in part been attributed to the anti-cancer activity of green tea.[255] Its FAS inhibitory activity has garnered significant interest as a therapeutic tool against obesity and cancer.[256,257] FAS catalyzes the formation palmitate from acetyl-CoA and malonyl-CoA in the presence of NADPH. It is commonly elevated in a wide variety of tumours and for this reason has been cited as both diagnostic and prognostic markers of cancer.[256] Combination treatment with EGCG has previously shown to potentiate oncolytic adenovirus killing in the context of prostate cancer.[207] Our preliminary studies with VSVΔ51 showed that combining EGCG with VSVΔ51 infection can enhance OV infection and overall cell death (Figure 34). Given that EGCG's mechanism of action is unknown and other phytochemicals have shown synergy with oncolytic adenovirus, we cannot attribute the OV potentiating effect of EGCG to its FAS inhibitory activity without further characterization. Future studies should make use of specific FAS inhibitors, such as the commonly studied C75 and cerulenin.[78] The effect of combination treatment with EGCG in ACM conditions will also be evaluated in future studies.

In our brief work evaluating the effects of FAS or ACC inhibition, we showed that inhibiting endogenous lipid synthesis can potentiate OV infection in the absence of ACM. *De novo* lipogenesis inhibitors have previously been shown to have differential effects on virus infection.[258,259] For instance, lipid-limiting drugs are actively being investigated for anti-viral use in pathogenic contexts.[260] This is unsurprisingly since new virions, especially enveloped virions, require lipids for the formation of new virus particles.

The virus potentiating or virus limiting effects of *de novo* lipogenesis inhibitors likely depends on overall host cell lipid homeostasis. In breast cancer, there is some evidence to suggest that the preference for *de novo* lipogenesis or uptake of exogenous FAs depends on the tumour subtype.[261] Watt *et al.*, in a model of prostate cancer, demonstrated that combining *de novo* lipogenesis inhibitors with FA blockade can have more potent anti-cancer effects than with either strategy alone.[38] Future approaches to anti-cancer therapeutic intervention may seek to delineate the specific lipid metabolic preferences of tumours in an effort to determine a tailored combinatorial approach that will maximize the therapeutic impact of OV therapy.

Targeting FATP-mediated FA transport

FAs can be transported by passive diffusion or facilitated transport. The latter facilitates the translocalization of larger FAs like long chain and very long chain FAs into the cell by making use of proteins like plasma membrane associated fatty acid binding protein, CD36, FATPs and others.[39]

FATPs are one of the most well studied group of proteins involved in the transport of FAs, as described in the Introduction of this thesis. DiRusso *et al.* generated a yeast model containing a structural deletion prohibiting the transport of exogenous FAs. When these cells were individually reconstituted with the mammalian isoforms of FATPs, only FATP1, FATP2 and FATP4 were able to facilitate FA transport, indicating that only these FATPs can directly participate in FA transport.[48] This gave precedence for the evaluation of targeting FATP1, FATP2 and FATP4-mediated FA transport in lipid-rich environments. When cancer cells were transiently silenced for

the expression of FATP1, FATP2 or FATP4, only FATP2 knockdown enhanced the sensitivity of ACM-receiving cells to OV infection.

The OV potentiating effect of FATP2 inhibition in comparison to other FATPs tested was interesting. Although FAs such as palmitate and oleate have previously been shown to increase the expression of proteins involved in FA transport including FATP2, no bias for FATP2 expression at baseline or increase in the presence of ACM was observed in our model (**Figure 39, Appendix Figure 2**).[214,262] FATPs are not static and the translocation of proteins involved in FA transport to the plasma membrane in times of demand have been previously described.[263] Future work may seek to determine the presence of FATP2 in the membrane fraction by Western blotting. Knockout studies may be pursued to validate the aforementioned results; however, caveats to this approach exist. Genetic deletion of FATP2 in the mouse liver resulted in the compensatory increase in the expression of other proteins involved in FA transport, such as FATP1 and CD36.[264] How FATP2 deletion impacts FA uptake in cancer and the resulting impact on OV infection is yet to be specifically examined.

FATP2 is highly expressed in the small intestine, liver, kidney, pancreas and placenta. [214] It has been shown to be upregulated in cancer, contributing to its proliferative and migratory capacities.[265] FATP2 has functions at both the plasma membrane and the ER. At the cell membrane, FAs are transported across the membrane and activated by a specific long chain acyl Co-A synthetase. In the ER, FAs that have entered the cell by some unknown mechanism, are activated by FATP2. [240,264]

FATP2 is the only FATP to have two splice variants, FATP2a and FATP2b. FATP2b lacks exon 2 encoding the ATP/AMP binding domain. While still adept at FA transport, this splice variant is

devoid of very long chain acyl CoA synthetase activity (ie. activation of FAs).[266] In contrast, point mutation studies in the ATP/AMP binding domain of FATP1 or FATP4, reduced or limited FA transport respectively.[267,268] The differential effects of losing the ATP/AMP motif on FA transport highlights the functional differences in FATP isoforms that are not yet well understood.

Moreover, FATP2 transports long and very long chain FAs but has a preference for polyunsaturated FAs (PUFAs), specifically n-3 FAs.[266] n-3 PUFAs have previously been demonstrated to have anti-viral activity by diverse mechanisms, including by interfering with binding to host entry receptors or inhibiting genome replication.[195,269] The inhibitory effects of FATP2 imported FAs may not be limited to n-3 PUFAs alone. FATP2-mediated transport of arachidonic acid, an n-6 PUFA, is a pre-cursor for prostaglandin E_2, a compound known to have differential effects on virus infection, including anti-viral outcomes.[270,271] Characterization of PUFA species and their relative quantity in ACM may provide clues about the lipid environment that contributes to FATP2-mediated OV resistance. The identified PUFAs can be employed in FA supplementation studies, similar to the palmitate and oleate supplementation studies, to evaluate its effects on OV infection and cell death.

Early reports suggest that intracellular trafficking of FATP2 imported exogenous FAs are dependent on carbon length and degree of saturation.[240] Melton *et al.* showed that FATP2 activated n-3 exogenous FAs are preferentially targeted into phosphatidylinositol. This is one of the first indications that FATP proteins can determine the metabolic fate of FAs. Phosphatidylinositols have been previously implicated in anti-viral roles; thus, it is reasonable to speculate a role of FATP2 derived phosphatidylinositol in OV resistance.[272]

It is worth mentioning that arachidonic acid and phosphatidylinositol have previously been observed to be enriched in malignant ovarian cancers when compared to benign ovarian tumours, suggesting a bias for FATP2-mediated FA transport in ovarian tumours. This suggestion remains speculative until further characterization of the metabolic fate of adipocyte-derived FAs in our models.[239]

The success of FATP2 inhibition as an OV sensitizing strategy in our model can be due to any of the aforementioned reasons described in this section. The role of FATP2 in ACM-mediated OV resistance was only evaluated in the context of VSVΔ51 to date. Future work should aim to determine if it can have broad OV sensitizing effects, and whether this effect persists across numerous cell lines.

Using FATP2 inhibitors in a combinatorial approach with OVs

Given the therapeutic benefit of FATP2 knockdown in the context of OV infection, we sought chemical inhibitors that target FATP2. Sandoval *et al.* identified 2 inhibitors of FATP2 in a yeast system expressing human FATP2 – Grassofermata and Lipofermata.[211]

Since FATP2 expression is enriched in the liver, it has been of keen interest in the study of diet-induced non-alcoholic fatty liver disease.[273] Blocking the uptake of FAs in the intestine has also been of longstanding interest as a strategy to blunt diet-induced obesity.[274] Both FATP2 inhibitors have been demonstrated to mitigate FA uptake in the hepatocellular carcinoma cell line, HepG2, and attenuate oleate absorption in the gut of mice, respectively.[212,213] Thus, FATP2 inhibitors Grassofermata and Lipofermata have demonstrated *in vivo* efficacy.

Lipofermata is one of the best characterized inhibitors of FATP2 with compelling evidence for clinical promise.[213,214] We demonstrated *in vitro* success in OV combination approaches with both Grassofermata and Lipofermata, but we moved forward with Lipofermata for *in vivo* studies for this reason. In both the FP breast tumour model (EO771) and IP ovarian tumour model (ID8 F3 p53-/-), OV combination therapy with Lipofermata provided the best survival advantage over either monotherapy.

Lipofermata has previously been shown to slow tumour growth *in vivo*; however, in our studies, Lipofermata monotherapy did not provide tumour control or survival benefit.[270,275] Given that Lipofermata has been demonstrated to have direct anti-cancer activity on cancer cells in a concentration specific manner *in vitro*, it is reasonable to hypothesize that the concentrations used in our studies likely did not meet the toxicity threshold.[37] We speculate that the non-toxic concentrations used in our *in vivo* study provided a sufficient FA limiting effect without inducing cellular toxicity that may impair productive OV replication, ultimately supporting the therapeutic benefit of combination therapy.

To date, a few studies have evaluated Lipofermata in the context of cancer. The investigators observed that the *in vivo* anti-tumour effects of Lipofermata is driven by modification of immune cells in the TME, specifically neutrophils, MDSCs and indirectly, T-cells.[270,275] Given the significance of the anti-tumour immune response in the anti-tumour effects of OV therapy *in vivo*, it would be interesting to determine the relative contribution of Lipofermata's effects on tumour cells and Lipofermata-driven modulation of immune cells of the TME, on the overall anti-cancer effects of OV combination treatment with Lipofermata, with studies that incorporate immune competent and immune deficient mouse models. Determining the effects of Lipofermarta on the

anti-cancer immune response and anti-OV immune response would also inform clinical translation of this approach.

Based on the existing literature and our studies, the success of Lipofermata in combination therapy will likely depend on numerous factors including FATP2 expression in the tumour, Lipofermata dosing and/or the relative presence of specific immune cell populations in the TME. The anti-cancer utility of this drug is only beginning to unfold. Here, for the first time, we showed the therapeutic impact of OV combination treatment with Lipofermata-mediated FATP2 inhibition in breast and ovarian tumours *in vivo*.

Future directions for OV combination therapy with a lipid-modulating strategy

Targeting FA uptake in OV combination therapy

Combination approaches that modulate lipid uptake have proven to be an effective strategy to curb adipocyte mediated anti-cancer therapy resistance, including in the context of OV therapy as described in this thesis.[37,38,146] A limitation of our study is that, to date, only the effects of combining OV therapy with blocking the FA transporter, FATP2, has been evaluated.

CD36 is a scavenger receptor that also has FA transport function.[276] The role of CD36-mediated FA transport in cancer progression has become of great interest in recent years, including in ovarian cancer.[36,38] We evaluated the expression of CD36 in OVCAR8 cells, the cell line in which the FATP study was conducted. We found that OVCAR8 cells had extremely low or non-existent expression of CD36 (**Figure 39**). OVCAR5 cells have a moderate expression of CD36, as determined by Cancer Cell Line Encylopedia.[277] In a preliminary experiment, we evaluated the effect of CD36 knockdown on OV infection and found that it increased the sensitivity of OVCAR5

cells to VSVΔ51-mediated cell death (**Appendix Figure 3**). This preliminary study did not include a condition testing ACM; however, the sensitizing effect in CTL media provides promise for lipid sensitizing effects in the presence of adipocyte-derived FAs. Given that CD36 has been implicated in driving both ovarian and breast cancers, it could be an attractive target in CD36-expressing tumours.[35,36] These findings serve as some of the first lines of evidence for tailoring FA blockade in a combinatorial strategy to maximize the anti-cancer effects of OVs. Future studies may seek to determine if simultaneously targeting more than one FA transporter enhances the therapeutic impact of OV combination therapy.

The need for clinical grade FA inhibitors is increasingly relevant as evidence accumulates for a role of TAGs in cancer risk, including in breast and ovarian cancers.[239,278,279] In ovarian cancer, many lipidomic changes occur across various lipid classes in early disease and intensifies with progression over time, including an increase in serum or plasma TAGs with long chain FAs.[280] A separate study showed that patients exhibit an overall decrease in most serum lipids, but certain TAG species were elevated and it was dependent on fatty acyl side chain composition.[239] To date, the beneficial effects of lowering lipids have largely been focused on limiting cholesterol levels and it is possible that this is an artifact of a lack of clinically approved drugs for the modulation of other lipid classes. FATP1 and FATP4 inhibitors have previously been identified in high throughput studies but have largely been unsuccessful *in vivo*.[214,281,282] Contrastingly, Lipofermata has numerous attributes of a good clinical drug target. It has limited tissue expression, specificity, proven efficacy in animal models against disease, and its cellular toxicity can be limited.[214] The homology between FATP proteins may facilitate the use of specific FATP inhibitors to target other related FATP family members. Despite being identified in a FATP2-specific screen and primarily

studied as an FATP2 inhibitor, Lipofermata has also been shown to block FATP1 mediated transport.[37] Furthermore, monoclonal antibodies have demonstrated as an effective FA blocking modality in murine models, especially in the context of CD36 blockade.[36,38] While the focus of lipid modifying drugs have largely been developed in the context of obesity and cardiovascular disease, there is growing demand for its use in anti-cancer therapeutic intervention.

Targeting CAAs in lipid rich TMEs

Perhaps one way to limit the availability of FAs for cancer cells is to limit the FAs released by adipocytes into periphery. Increasing insulin sensitivity in CAAs could be an effective strategy to limit adipocyte lipolysis. Rosiglitazone is an anti-diabetic drug which sensitizes adipocytes to insulin by binding PPAR in adipocytes.[283] Given that this drug has also demonstrated potential to decrease FATP2 expression by some unknown mechanism, it may prove to be an effective tool to promote anti-tumour effects in the TME by simultaneously targeting CAAs and cancer cells that employ FATP2 for exogenous FA uptake. [284] Unfortunately, this drug has been banned in numerous countries due to increased risk of heart attacks.[285] The identification of a safer drug with similar drug action could provide the beneficial effects described. An alternative strategy can be to target ATGL in adipocytes. ATGL is the first and rate-limiting enzyme in a series of reactions that liberate FA from storage in lipid droplets. Targeting ATGL in CAAs may limit exogenous lipid pools in the TME for uptake by cancer cells in the periphery. Additionally, tumour resident mesenchymal stem cells have been reported to have pro- or anti-tumour effects in the TME.[286] They are also a progenitor cell of adipocytes.[287] Blocking their differentiation may decrease the presence of adipocytes and thus, adipose-derived lipids in the TME.[58]

Beyond the adipocyte: acknowledging the role of adipose tissue resident cells and systemic factors that can contribute to OV resistance in lipid-rich TMEs *in vivo*

Adipose tissue is largely comprised of adipocytes but also harbours other cell types.[23,24] Given the increased presence of adipose tissue in tumours situated in fat-rich TMEs, the potential role of adipose tissue resident cells on responses to OV therapy cannot be disregarded, especially in the context of *in vivo* studies.

Macrophages are well described adipose tissue resident cells.[288,289] These cells were abundant in our brief evaluation of the adipose tissue front that borders STOSE tumours (Appendix Figure 4). The infiltration of the adipose tissue front into tumour tissue invites conjecture about the role of non-adipocyte cells, specifically immune cells, on tumour progression and responses to treatment. Macrophages, for instance, are the most widely described immune cell population in obese adipose tissue and can make up to 40% of adipose tissue in obese mice.[57] Macrophages can have anti- or pro-tumour phenotypes, and are referred to as M1 or M2 macrophages respectively. Further, plasticity in these cells allow them to react to changing TMEs.[290] Macrophage populations in the TME have been reported to have differential effects on OV therapy, enabling OV mediated tumour destruction or alternatively curbing its anti-tumour effects.[291,292] *In vitro* studies examining conditioned media from macrophages have been shown to induce ISG expression in breast and ovarian tumour cells which in turn reduce their sensitivity to oncolytic VSV infection.[293] Conversely, an oncolytic paramyxovirus study demonstrated that irrespective of polarization, macrophages in the TME potentiate breast tumour eradication.[294] The disparate effects of macrophages in the context of OV therapy suggests that its effects are highly context specific. A preliminary study evaluating the role of macrophages in the OV-infected TME are described in the Appendix of this

thesis (Appendix II). Future studies can evaluate the role of macrophages in the TME on response to OV infection with macrophage depletion studies using clodronate liposomes.[295]

Furthermore, adipose tissue also houses pluripotent stem cells, often described as adipose-derived stem cells (ADSCs). They have been well described to have roles in tumour progression and in treatment resistance, including in the context of breast cancer .[296,297] ADSCs can be permissive to OV infection; however, the mechanism by which this occurs is unclear.[298] In the context of glioblastoma, these cells were successfully exploited for their powerful ability to home to cancer cells, being used as a delivery vehicle for OVs to the site of the tumour.[299,300] These reports suggest that ADSCs could be harnessed to support the anti-tumour effects of OVs, pending further characterization in our models.

Moreover, the HFD model was an effective tool to evaluate the effect of a global change in adiposity on responses to OV infection. Our data showed that HFD-fed tumour-bearing mice have decreased intra-tumoural OV titers and this correlated with an increase in the presence of adipose tissue at the site of the tumour (Figure 4). A caveat of this model is the global effects of HFD-induced obesity on endocrine, metabolic and even immune parameters.[301] Since obesity is a risk factor for cancer and many patients are obese at the time of diagnosis, further characterization of this model holds immense value in how we approach OV therapy in these patients.[302]

CONCLUDING STATEMENT

The role of lipid homeostasis in breast and ovarian tumour progression and response to treatment, are only beginning to unfold.[61,140,144,145,239,303] Combination approaches to anti-cancer intervention, rather than monotherapy, have been repeatedly shown to provide the best results.[304] The work described in this thesis show that attenuating FA uptake in lipid-rich TMEs can enhance the cancer-killing potential of OVs (summarized in **Figure 45**). As the field of anti-cancer therapy continues to shift towards tailored therapies, the contributing role of proteins involved in FA transport must be considered and incorporated into rational therapy design in order to reap the maximum benefits of OV therapy. The findings from this work not only demonstrate how we can improve the prognosis of breast and ovarian cancer patients, but also shed light on how we can approach the treatment of other fatty tumours and tumours in obese individuals. To sum up, the work described in this thesis provides the impetus for the therapeutic strategy of attenuating FA uptake in combination approaches with OV therapy in a lipid-rich TME.

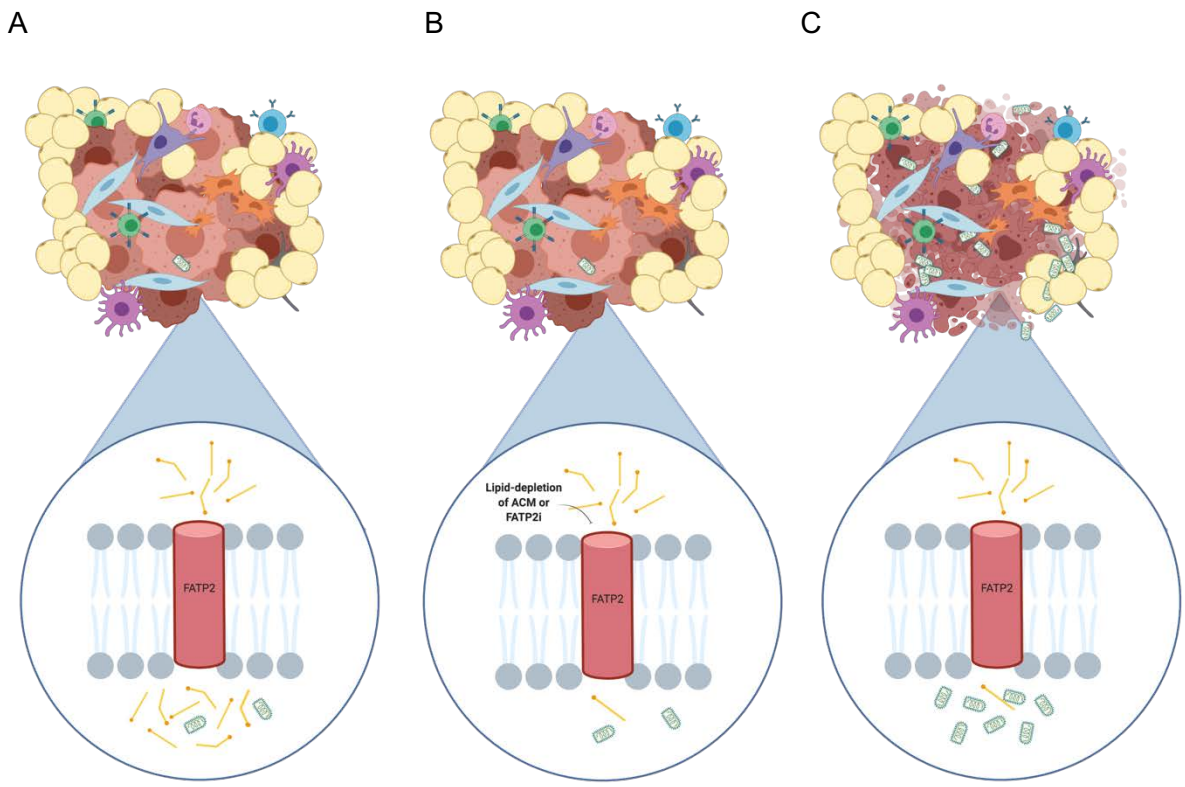

Figure 45: Working model of the effect of adipocyte-derived FAs on OV resistance and the OV sensitizing effect of FA blockade. Tumours in an adipocyte-rich tumour microenvironment accumulate intracellular lipids and this correlates with a decreased sensitivity to OV infection (A). Intracellular lipid accumulation is mitigated by blocking the uptake of exogenous adipocyte-derived FAs by depletion of lipid-derived constituents in ACM or by using FATP2 inhibitors, Lipofermata or Grassofermata (B). Cancer cells are re-sensitized to OV infection and OV-mediated cell death (C).

MATERIALS & METHODS

Cell lines & tissue culture

Cell lines

Cell lines (OVCAR8, SKOV3, OVCAR433, MDA MB 231, BT549, MCF-7, 4T1, EMT6, EO771, B16-F10, 3T3-L1) were purchased from American Type Culture Collection (ATCC, Masassas, VA), except ID8 p53-/- which was a gift from Dr. Iain McNeish (Barts Cancer Institute, Queen Mary University of London, UK), B16-F10 IFNAR-/- which was generated by Emily Brown (Master's student in the Bell lab) and STOSE cells which were a gift from Dr. Barbara Vanderhyden's lab (Ottawa Hospital Research Institute, Ottawa, ON). Cells were cultured in RPMI-1640 with 10% FBS and buffered with HEPES, except for MDA MB 231, MCF-7 and B16-F10 IFNAR -/- which were cultured in DMEM supplemented with 10% FBS and buffered with HEPES. Vero cells were cultured in media containing a %10 NCS/FBS mix (3:1 NCS: FBS). ID8 p53-/- cells were cultured in DMEM containing 5% FBS and ITS (5μg/mL insulin, 5μg/mL transferrin and 5ng/mL sodium selenite; Gibco).

Adipocyte Differentiation

Human breast and visceral pre-adipocytes (Zen-bio) were differentiated with the appropriate proprietary adipocyte differentiation medium (Zen-bio Cat #DM-2-500-ABF, Cat #OM-DM-500). Briefly, the preadipocytes were cultured in RPMI containing 10% FBS in T75 flasks until at least 80% confluency. The preadipocytes were then cultured in the appropriate differentiation medium for 10 days, with a media change every 3-4 days. Following differentiation, the cells were acclimatized to regular culture media (RPMI-1640 with 10% FBS and containing HEPES) for at least 5 days prior to the collection of adipocyte conditioned media (ACM). ACM was harvested every

48-72hrs. The media was centrifuged (1500rpm, 5mins) and the supernatant was stored at -20C until use. Murine 3T3-L1 cells were differentiated according to the appropriate murine differentiation media (Zenbio).

General

All cell lines were incubated at 37°C in a 5% CO_2 humidified incubator. All cells were tested with the e-Myco VALiD Myco PCR detection kit (FroggaBio) or Hoescht's staining to ensure they were devoid of mycoplasma contamination prior to the experiments described.

OV Propagation & Purification

VSVΔ51

Vero cells were seeded in roller bottles (1900cm^3 TC treated roller bottles; Ultident) at 4E7 cells per bottle for 3 days in ~200mL of DMEM media containing 10% FBS and 25mM HEPES in a rotating incubator. Cells were infected with VSVΔ51-GFP or VSVΔ51-Fluc and incubated until cytopathic effect was evident by microscopy (~50% cell death and/or detachment). The supernatant was harvested (1500rpm, 15mins, 4°C) and was subject to pre-clearing of cell debris with sequential filtration steps: first with 0.45μM bottle top filter (500mL PVDF filter, EMD Millipore) followed by a 0.22μM bottle top filter [500mL Stericup polyethersulfone (PES) filter, EMD Millipore]. The virus was pelleted by centrifugation (13500rpm, 1.5hrs, 4°C; Beckman Coulter Avanti JE centrifuge). The supernatant was aspirated, and the pellet was resuspended in cold Solution C (0.15M NaCl, 10mM EDTA, 50mM Tris-HCl pH 7.4). Virus stocks were aliquoted and stored at -80°C until use.

Other OVs

Oncolytic MeV, oncolytic HSV and oncolytic VACV (JX-594-GFP) were generously produced by Drs. Serge Neault, Kuan Zhang and Brian Keller, respectively. MG1-GFP and MG1ΔG stocks were generously produced by Dr. Carolina Ilkow.

Titer by plaque assay

VSV & HSV Titering

The day prior, 8E5 or 2E5 Vero cells were seeded on 6-well or 12-well, respectively. Infectious viral particles from the supernatant of VSVΔ51-infected cells or virus particles from the supernatant and cell-associated viral particles from HSV-infected cells were pooled (cell-associated viruses were liberated by bursting the cells with 3 freeze-thaw cycles by freezing the sample at -80°C and thawing in a 37°C water bath until thawed but before warm). The sample was clarified of cell debris by centrifugation (1500rpm, 10mins, 4°C). The virus samples were then diluted in a 10-fold serial dilution in cold serum-free DMEM media in deep-well plates. The media in the plates containing the Vero cells were aspirated and replaced with 500-600μL of the serially diluted virus (typically 4-6 dilutions from dilutions ranging from 10^{-3} to 10^{-11}, depending on the expected titer). The inoculated plates were incubated in the cell incubator (37°C) with gently rocking every 10-15mins. After 45mins, the inoculum was aspirated and replaced with an overlay media [1:1 mixture of 6% caboxymethyl cellulose (CMC; Sigma): DMEM (2X concentrated with 20% NCS/FBS mix)]. After a 48hr incubation, the overlay media was aspirated, the cells were gently washed with PBS twice and stained with crystal violet (0.1% crystal violet in 80% MeOH in water) for 20-30mins. The crystal violet was removed, the cells were gently washed with tap water and the plate was left to air dry overnight.

VACV Titering

Infected cells undergo 3 freeze-thaw cycles to release intracellular particles. Following centrifugal clarification of cell debris, the sample is tittered similarly to plaque assay of VSV described above, with a few modifications. The samples were tittered on U2OS cells and the overlay medium is made with 3% Carboxymethyl cellulose (CMC).

MeV Titering

The supernatant of Me-V infected cells was serially diluted in a 10-fold serial dilution. 10µL of the diluted viral stock was combined with 90µL of Vero cells prepared in a 150 000cells/mL solution in DMEM (10%FBS) in the wells of a 96-well plate. The plate was incubated in a 37°C incubator for 3 days. The titer was determined based on 50% tissue culture infective dose endpoint method according to Spearman–Karber.[305,306]

Titering ex vivo tumours

Tumours were harvested, weighed and transferred to 2mL Qiagen tubes containing 500uL of PBS-containing cOmplete™ Mini EDTA-free Protease inhibitor cocktail (1 tablet per 10mL PBS). The tumours were homogenized using a tissue lyser (TissueLyser II, Qiagen; frequency setting 30, 4mins per side with a 10min cooling session on ice between switch). The cell debris was spun down with a benchtop centrifuge (14000rpm, 10mins). Remaining cell debris was removed by passing the sample through a 70µm cell strainer (Fisherband). The sample was titered by plaque assay as

previously described; however, penicillin streptomycin (100U/mL; Thermo Fisher Scientific) was added to the overlay medium. The titers were reported as PFU per milligram of tumour.

Plaque counting

Wells containing plaques in the range of 10 to 100 were counted. The titers were calculated according to the following equation:

$$\frac{PFU}{mL} = \frac{\#\ plaques}{Dilution\ Factor\ x\ Volume\ (mL)}$$

Quantitative real-time PCR

Cell monolayer was washed twice with PBS and the total RNA was extracted using the NucleoZOL kit (Macherey-Nagel). The RNA pellets were resuspended in 20uL of nuclease free water. RNA quantification was achieved using the Nanodrop™ One Microvolume UV-Vis Spectrophotometer (Thermo Fisher Scientific). cDNA was generated using the iScriptTM cDNA Synthesis Kit (Bio-Rad) using 1μg of RNA. Amplification was achieved using the QuantiTect SYBR Green PCR Kit (Qiagen) in conjunction with analysis by the Applied Biosystems™ 7500 Fast Real-Time PCR System. Gene expression was determined relative to rPlp0 using the delta delta Ct method [2^(ΔΔCt)]. Primers were acquired from IDT (Integrated DNA Technologies) and primer optimization was determined using the standard curve method. Primer sequences are shown in Supplemental Table 1.

Flow cytometry

Visualization of neutral lipids was achieved with Bodipy 493/503 (Molecular Probes) using a previously described protocol.[307] Briefly, cells in 6-well plates are washed with PBS to remove

media and serum. They were then incubated with Bodipy staining solution (1:1000 diluted in PBS) for 15mins in the dark at 37°C. The cells were rinsed with PBS to remove the staining solution and trypsinized (Trypsin-EDTA 0.25%) to dislodge the cells from the well. The cells were resuspended in 5mL PBS, transferred to a 15mL conical tube and pelleted by centrifugation (1500rpm, 5mins). The cells were resuspended in 200µL of PBS and transferred to a 96-well V-bottom plate (Corning® 96-well Clear V-Bottom TC-treated Microplate). After centrifugation (1500rpm, 5mins) to pellet the cells, they were stained with fixable viability stain 510 (BD Horizon™; 0.5µL of stain was added per well in a total volume of 25µL PBS) and incubated for 15mins in the dark. The cells were diluted with 150µL PBS, and centrifuged (1500rpm, 5mins). The supernatant was discarded. The cells were washed with flow buffer once before they were resuspended in 200µL of flow buffer and transferred to 1.1mL tall microtubes (Thermo Scientific™ Microtubes for 1.1mL Microtube System). The samples were analyzed on the BD LSR Fortessa or BD Celesta flow cytometers at the University of Ottawa Flow Cytometry and Virometry core facility (Roger Guindon Hall, University of Ottawa). Data analysis was conducted on FlowJo software (FlowJo, LLC, Ashland, OR).

Cytotoxicity analysis by crystal violet staining

The media was aspirated and the cells were stained with crystal violet solution (0.5% crystal violet in 80% MeOH in water) for 40mins on a benchtop rocker. The crystal violet was removed, the monolayer was gently washed with tap water twice and left to air dry overnight. Qualitative analysis of the stained plates was achieved by scanning the plates. Cytotoxicity was quantified by lifting the crystal violet staining from the stained plates. The plates were incubated with 100%

methanol on a shaker for 40mins. The methanol containing crystal violet was transferred to a 96-well plate and the OD570 was read using the Multiskan Ascent plate reader.

Immunofluorescence microscopy

Brightfield and GFP filter images of cells seeded on plates were acquired with an AMG EVOS fluorescence microscope (Advanced Microscopy Group, Washington, USA).

Immunofluorescence images were also obtained of cells that were grown on glass coverslips. Lipid staining was achieved with Bodipy 493/503 (Molecular Probes) as per a previously described protocol.[307] Briefly, cells were washed with PBS and incubated with a Bodipy staining solution (1:1000 in PBS; 15mins, 37°C) in the dark. The cells were washed with PBS and fixed with 4% PFA (Thermo Fisher) for 20mins. The PFA was aspirated and the cells were washed twice with PBS before the coverslips were mounted on slides with mounting medium containing DAPI (ProLong™ Gold Antifade Mountant; Cat#P36931, Thermo Fisher Scientific). The slides were visualized with Zeiss Fluorescent Microscopes (ZEISS, Germany).

Evaluating interferon signaling

IFNAR blocking

ACM-receiving cells incurred a media change to ACM the evening before the day of the experiment. Anti-human IFNAR2 neutralizing monoclonal antibody (2ug; PBL Assay Science Cat#21385-1) was added to wells and, 4 hrs later, human IFN-α 2b (200U; Sigma Aldrich

cat#SRP4595) was added to the appropriate wells. 4hrs post IFN-α addition, the cells were infected with VSVΔ51-GFP (MOI 1).

JAK inhibition

OV titer & cytotoxicity analysis: Cell lines or ovarian patient ascites cells were cultured in ACM overnight. The next day the cells were treated with 1μM Jaki (EMD Millipore Cat# 420099) for 3hrs before receiving 200U/mL human IFN-α 2b (Sigma Aldrich). After 3hrs of IFN-α treatment, the cells were infected with VSVΔ51.

STAT1 Immunoblotting: 786O cells were treated with 1μM JAK I inhibitor (EMD Millipore Cat# 420099). After 4hrs, 200U/mL human IFN-α 2b (Sigma Aldrich) were added to the cells. Finally, 4hrs post -IFN-α addition, the cells were infected with VSVΔ51. In cells receiving both JAK I and IFN-α, a 2hr interval was given between IFN-α addition and VSVΔ51 infection. Cells were lysed with Ripa buffer (Pierce™ Riper Buffer; Thermo Scientific) containing a protease inhibitor cocktail (Sigma Aldrich, #P8340-5mL). The cell debris was clarified by centrifugation at 12000rpm on a benchtop centrifuge and the supernatant was transferred to a new tube and stored at -20°C until further analysis. The protein concentration was determined by using a BCA protein assay kit (Pierce™ BCA®Protein Assay Kits and Reagents; #23228; Thermo Scientific). An equal quantity of protein was prepared with loading dye (5X Laemmli loading buffer Bio-Rad) and boiled at 100°C for 5mins. The samples were then loaded on 4-12% gradient Bis-Tris gels (NuPAGE; Thermo Fisher Scientific) prepared in a system containing 1X MOPS running buffer (20X running buffer; 50mM MOPS, 50mM Tris Base, 0.1% SDS, 1mM EDTA, pH 7.7). The gel was run at 70V for the first 20mins, and then at 100V until the dye front reached the bottom of the gel. The gel was transferred onto

an ethanol-activated PDVF membrane using the Trans-Blot Turbo Transfer System (Bio-Rad). The membrane was cut into 2 sections based on where the target genes were expected based on size. The membranes were blocked in 5% milk (in TBST buffer) (generic skim milk powder; 50mM Tris-Cl pH 7.5, 150mM NaCl NaCL, 1% Tween-20) for 1hr. The appropriate membrane halves were incubated overnight on a gentle shaker at 4°C in 5% milk (in TBST) containing phospho STAT1 rabbit monoclonal antibody (Cat#: 7649S Cell signaling Technology; 1:1000) or rabbit GAPDH monoclonal antibody (cat#2118S; Cell Signaling Technology; 1:10000). The primary antibodies were removed and the membranes were washed 3 times with TBS-T (7mins/wash). The membranes were than incubated for 1hr at room temperature on a gentle shaker in 5% milk (in TBST) containing goat anti-rabbit IgG antibody HRP (cat#31490; Thermo Fisher Scientific; 1:5000). The secondary antibody was removed and the membranes were washed 3 times with TBS-T (7mins/wash) before a brief incubation with an ECL substrate (Clarity™ Western ECL Substrate; Bio-Rad). The membranes were developed on the Bio-Rad ChemiDoc imaging system.

Proteinase-K treatments, heat-inactivation & boiling studies

Each sample was treated with 1U of proteinase-K linked to agarose beads (Sigma-Aldrich) for 2-4hrs at 37°C. The proteinase-K linked agarose beads were removed by pelleting via centrifugation (500g, 5mins). Untreated ACM or proteinase-K treated ACM were run on an SDS-PAGE gel and stained with Coomassie blue. The efficacy of protein digestion was evaluated by monitoring the density of the band corresponding to BSA.

The effect of heat inactivation or boiling of ACM was evaluated by incubation of ACM in a 56°C water bath or boiling (95-100°C) on a heat block, respectively, for 30mins, before cooling to room temperature and transferring to cells. The cells were then infected with VSVΔ51.

LRA-mediated lipid depletion

Lipid Removal Agent (MilliporeSigma™ Supelco™) was mixed with PBS to a achieve a working solution of 100mg/mL. The LRA solution was added to CTL or ACM media to achieve a final LRA concentration of 4.3mg/mL. This concentration was determined based on optimization experiments that sought to minimize cellular toxicity. CTL media or ACM treated with LRA solution were incubated on a benchtop shaker for 30mins. Next, the samples were spun down (1500rpm, 10mins) at a decreased deceleration speed (setting 6), and the supernatant was transferred to a new tube. The supernatant was gently drawn up while leaving a 1-2mL buffer between the pellet and the tip of the serological pipette. Centrifugation of the supernatant was repeated 2 more times to eliminate any LRA contaminants. The lipid-depleted media was transferred to cells.

FA quantification

Quantification of FAs in the ACM was achieved using the Free Fatty Acid Quantification Colorimetric/Fluorometric Kit (BioVision).

FA supplementation

Preparation of FA stocks

Sodium palmitate (cat#P9767-5G; Sigma-Aldrich) or sodium oleate (Cat#O7501-1Gl; Sigma-Aldrich) was combined with heated 100% ethanol and vortexed for 15 seconds. The FA solution was then heated for 5-10mins at 65°C with periodic vortexing. It was then combined with an equal volume of heated sterile water and vortexed immediately. The FA solution was stored at -20°C until use.

Preparation of BSA-FA supplemented media

A 2% BSA containing media solution was prepared by adding BSA (FA free BSA, cat# A8806-5G; Sigma-Aldrich) to serum-free RPMI media. The sample was briefly mixed by swirling and warmed in a 37°C water bath to facilitate dissolving of the BSA. The BSA containing media was filtered with a 0.22μM syringe filter. The stock of sodium-palmitate or sodium-oleate in 50% ethanol was warmed on a heat block at 65°C until the FA was in solution. While still warm, the sodium-FA solution was added to the 2% BSA containing media in a dropwise fashion, immediately capped and vortexed. The FA supplemented media was incubated in a 37°C water bath for 3hrs. The prepared FA-BSA media was supplemented with 10% FBS right before being adding to cells. Cytotoxicity quantification of lifted crystal violet or OV titers were normalized to samples containing equivalent volume of 2% BSA containing media.

Assessment of mitochondrial respiration using seahorse technology

Oligomycin (1.5µM), trifluoromethoxy carbonylcyanide phenylhydrazone (FCCP) (0.5µM) and antimycin and rotenone (0.5µM) treatment were injected at designated intervals as per the manufacturer's instructions for Seahorse XF Cell Mito Stress Test Kit (Agilent). The effect of acute etomoxir (Cayman Chemical company; #11969) treatment was evaluated by injection of the drug after 3 baseline readings.

OV pre-incubation with ACM

VSVΔ51-GFP or VACV was incubated in Eppendorf tubes containing RPMI-1640 (10% FBS, HEPES) or ACM in a 37°C incubator or at RT for various length of time. This viral stock was then used to infect cancer cells.

Modified plaque assay to assess virus entry

The modified plaque assay to assess virus entry was adapted from Xu *et al*.[196] Briefly, OVCAR8 cells were incubated in ACM at the indicated lengths of time prior to infection with 150PFU of VSVΔ51-GFP. After a 1hr period of infection, the media containing the virus inoculum was removed and replaced with overlay medium (1:1 mixture of 6% CMC: 2X DMEM with 20% NCS/FBS mix). After 48hrs, the overlay medium was removed, the cell monolayer was washed with PBS and the wells were stained with crystal violet solution (0.1% crystal violet with 80% MeOH). The plates were left to air dry overnight and the PFUs were counted the next day.

Evaluating the timing of ACM exposure on OV resistance

The media in the wells were changed to ACM 16hrs before the experiment ('pre-incubation' media). During 'infection' the media was aspirated and changed to CTL or ACM media and inoculated with VSVΔ51. After 1hr, the media containing the inoculum was aspirated and replaced with fresh CTL media or ACM ('post-infection' media). Three possible time-frames peri-infection and two different medias produced 6 different combinations of cell exposure to CTL media or ACM peri-infection.

Using VLPs to assess viral entry

GFP loaded VLPs pseudotyped with VSV-G glycoprotein were generated using a previously described protocol.[308] Briefly, following transfection of plasmids encoding VLP components in 2.5E5 HEK293T cells (ATCC), VLPs were harvested and concentrated as per manufacturer's instructions (Lenti-X concentrator; Takara, #631232) to a 1mL suspension in PBS. OVCAR8 cells at 80% confluency in 6-well plates were cultured in ACM for at least 4hrs before they were transduced with 30µL of VLPs [aided with 0.8µg/mL polybrene (Sigma; #TR-1003-G)] or infected with VSVΔ51-GFP (MOI 0.1). After 24hrs, the cells were harvested, stained with propidium iodide and assessed by flow cytometry.

Assessing intracellular pH

The cells were stained with 1µM Lysotracker™ Green DND-26 (Cat#L7526, Thermo Fisher Scientific) for 20mins. The cells were washed with PBS and stained with propidium iodide. The cells were washed twice, resuspended in 200µL of flow buffer and analyzed by flow cytometry.

siRNA knockdown of genes involved in FA transport

siRNAs [SMARTpool ON-TARGETplus Non-targeting Control Pool (D-001810-10-20; Dharmacon); SMARTpool ON-TARGETplus Human SLC27A1 (Cat# L-010759-01-0005; Dharmacon); SMARTpool ON-TARGETplus Human SLC27A2 (Cat# L-007498-00-0005; Dharmacon); SMARTpool ON-TARGETplus Human SLC27A4 (Cat# L-007500-01-0005; Dharmacon); SMARTpool ON-TARGETplus Human CD36 (Cat#L-010206-00-0005; Dharmacon)] were resuspended in siRNA Buffer (5X siRNA Buffer; Cat#B-002000-UB-100; Dharmacon) to generate 20μM stocks.

For transfection, 5μL of Lipofectamine™ RNAiMAX Transfection Reagent (Thermo Fisher Scientific) was combined with 250μL Opti-MEM and incubated for 5mins. The RNAiMAX complex was then combined with siRNAs diluted in Opti-MEM (2μL of siRNA with 250μL of Opti-MEM) in a gentle dropwise fashion. The siRNA-RNAiMAX complex was then incubated for 20mins at room temperature and added to wells with 5E5 cells suspended in 1.5mL RMPI-1640 (containing 10% FBS). 18-24hpt, designated wells were infected with VSVΔ51-GFP for 40mins. The inoculum containing media was removed and replaced with CTL media or ACM (50% v/v).

Lipid modulating drugs

TOFA

Cells were treated with 0.1, 0.5, 1, 2, 5, 8 or 10μM of 5-tetradecyloxy-2-furoic (TOFA; Cat#54857-86-2; Millipore Sigma) for 3hrs. The media was then changed to CTL media or ACM media containing half the previous concentration of TOFA in the well. 2hrs later, the cells were infected with VSVΔ51 (MOI 0.1).

(–)-Epigallocatechin gallate (EGCG)

SKOV3 cells were treated with 100μM EGCG (Sigma Aldrich #E4143-50MG) for at least 4hrs before infection with VSVΔ51 (MOI 0.1).

Grassofermata & Lipofermata

Grassofermata (Cayman Chemical Company, Cat#26202) was diluted in CTL media (RPMI containing 10% FBS and HEPES). The media in the wells was aspirated and replaced with Grassofermata or Vehicle (DMSO) containing media at half the well volume. Following a 4hr incubation period, the cells were infected with VSVΔ51 for 30-60mins. The wells were then supplemented with an equal well volume of CTL media or ACM.

For Lipofermata studies, cells were infected with VSVΔ51 for 40mins. The inoculum containing media was removed and replaced with CTL media containing Lipofermata (Cayman Chemical Company, Cat#25869-50) at the indicated concentration for 2hrs before equivalent volume of CTL media or ACM was added to the wells. For *in vivo* studies, Lipofermata was prepared from a 25mg/mL stock (in DMSO) to its working concentrating with dilution with DMSO alone or DMSO and 30% v/v of Kolliphor®EL (Sigma Aldrich Cat#C5135-500G). The target injection volume was 25uL to minimize DMSO toxicity to receiving mice.

H&E staining protocol

Tumours were fixed in formalin as per standard protocols and were stained by the Pathology Department at the Ottawa Hospital.

RNA Sequencing analysis

OVCAR8 cells were cultured in CTL media or ACM for 18hrs or cultured in CTL media or ACM for 6hrs and infected with VSVΔ51 for 12hrs. The wells were washed with sterile PBS and the RNA was extracted (NucleoZOL kit; Macherey-Nagel). Tidyverse, EdgeR[309] and Heatmaply were used for bioinformatics analysis and the generation of a heatmap.

RNA sequencing raw files: https://drive.google.com/file/d/1sP5LErigDW46dXh56tzPWhgXyF-w4rht/view?usp=sharing

Animal studies & tumour models

6-8 week old Balb/c or C57BL/6 female mice were acquired from Charles River Laboratories. All animal studies were handled in accordance with ethical guidelines with protocols approved by the Institutional Animal Care Committee of the University of Ottawa. Treatment regiments are described in the figure legends. Mice were euthanized when they reached humane endpoint. Tumour volume was calculated using the following formula: $\text{tumor volume} = 1/2(\text{length} \times \text{width}^2)$.

HFD (TD.06414) or a RD control (T. 08806) fed C57BL/6 mice received a specialized diet from Harlan Laboratories (Teklad Custom Diet; Envigo) for 8-10 weeks until a substantial change in the

average mouse weight was observed (at least 20-25%). The mice remained on the diet until the end of the experiment.

Cells for implantation were cultured until 60-70% confluency. The cells were washed twice with PBS and passed through a 70μM cell strainer. 2E5 cells (EMT6, 4T1, EO771) or 5E6 cells (ID8-F3 p53-/-) resuspended in sterile PBS were implanted SC/FP or IP, respectively. Tumour models in mice were generated by implanting syngeneic tumour cells in the FP, or subcutaneously. Intrabursal STOSE models were generated by surgical implantation as previously described.[310]

Statistical Analysis

Statistical significance was determined using an unpaired t-test, one-way or two-way analysis of variance (ANOVA) as indicated in the figure legend. Log-rank Mantel-Cox test was used to assess survival. The number of biological and/or technical replicates and the statistical test used are indicated in the figure legend. Error bars represent standard error of mean or standard deviation as indicated. P-values less than 0.05 were deemed significant. If no indication is shown, the results are non-significant. Statistical analyses were performed using GraphPad Prism 9 software (San

REFERENCES

1 Weinberg RA. How cancer arises. *Sci Am* 1996; **275**: 62–70.

2 Jones PA, Baylin SB. The epigenomics of cancer. *Cell* 2007; **128**: 683–692.

3 Ames BN, Gold LS, Willett WC. The causes and prevention of cancer. *Proc Natl Acad Sci U S A* 1995; **92**: 5258–5265.

4 Krump NA, You J. Molecular mechanisms of viral oncogenesis in humans. *Nat Rev Microbiol* 2018; **16**: 684–698.

5 Brenner DR, Weir HK, Demers AA, Ellison LF, Louzado C, Shaw A *et al.* Projected estimates of cancer in Canada in 2020. *CMAJ* 2020; **192**: E199–E205.

6 Canadian Cancer Statistics. Canadian Cancer Society. 2021.https://cdn.cancer.ca/-/media/files/research/cancer-statistics/2021-statistics/2021-pdf-en-final.pdf?rev=2b9d2be7a2d34c1dab6a01c6b0a6a32d&hash=01DE85401DBF0217F8B64F2B7DF43986 (accessed Feb2022).

7 Achard C, Surendran A, Wedge M-E, Ungerechts G, Bell J, Ilkow CS. Lighting a Fire in the Tumor Microenvironment Using Oncolytic Immunotherapy. *EBioMedicine* 2018; **31**: 17–24.

8 Paget S. The distribution of secondary growths in cancer of the breast. 1889. *Cancer Metastasis Rev* 1989; **8**: 98–101.

9 Shi Y, Liu CH, Roberts AI, Das J, Xu G, Ren G *et al.* Granulocyte-macrophage colony-stimulating factor (GM-CSF) and T-cell responses: what we do and don't know. *Cell Res* 2006; **16**: 126–133.

10 Waldmann TA. Cytokines in Cancer Immunotherapy. *Cold Spring Harb Perspect Biol* 2018; **10**. doi:10.1101/cshperspect.a028472.

11 Roma-Rodrigues C, Mendes R, Baptista PV, Fernandes AR. Targeting Tumor Microenvironment for Cancer Therapy. *Int J Mol Sci* 2019; **20**. doi:10.3390/ijms20040840.

12 Szebeni GJ, Vizler C, Nagy LI, Kitajka K, Puskas LG. Pro-Tumoral Inflammatory Myeloid Cells as Emerging Therapeutic Targets. *Int J Mol Sci* 2016; **17**. doi:10.3390/ijms17111958.

13 Fend L, Accart N, Kintz J, Cochin S, Reymann C, Le Pogam F *et al.* Therapeutic effects of anti-CD115 monoclonal antibody in mouse cancer models through dual inhibition of tumor-associated macrophages and osteoclasts. *PLoS One* 2013; **8**: e73310.

14 Coscia M, Quaglino E, Iezzi M, Curcio C, Pantaleoni F, Riganti C *et al.* Zoledronic acid repolarizes tumour-associated macrophages and inhibits mammary carcinogenesis by targeting the mevalonate pathway. *J Cell Mol Med* 2010; **14**: 2803–2815.

15 Sounni NE, Noel A. Targeting the tumor microenvironment for cancer therapy. *Clin Chem* 2013; **59**: 85–93.

16 He X, Yang Y, Li L, Zhang P, Guo H, Liu N *et al.* Engineering extracellular matrix to improve drug delivery for cancer therapy. *Drug Discov Today* 2020; **25**: 1727–1734.

17 Huang X, Ding L, Liu X, Tong R, Ding J, Qian Z *et al.* Regulation of tumor microenvironment for pancreatic cancer therapy. *Biomaterials* 2021; **270**: 120680.

18 Najafi M, Farhood B, Mortezaee K. Extracellular matrix (ECM) stiffness and degradation as cancer drivers. *J Cell Biochem* 2019; **120**: 2782–2790.

19 Diop-Frimpong B, Chauhan VP, Krane S, Boucher Y, Jain RK. Losartan inhibits collagen I synthesis and improves the distribution and efficacy of nanotherapeutics in tumors. *Proc Natl Acad Sci U S A* 2011; **108**: 2909–2914.

20 Rio M-C. The Role of Cancer-Associated Adipocytes (CAA) in the Dynamic Interaction Between the Tumor and the Host. In: Mueller MM, Fusenig NE (eds). *Tumor-Associated Fibroblasts and their Matrix: Tumor Stroma*. Springer Netherlands: Dordrecht, 2011, pp 111–123.

21 Zhao C, Wu M, Zeng N, Xiong M, Hu W, Lv W *et al.* Cancer-associated adipocytes: emerging supporters in breast cancer. *J Exp Clin Cancer Res* 2020; **39**: 156.

22 Duong MN, Geneste A, Fallone F, Li X, Dumontet C, Muller C. The fat and the bad: Mature adipocytes, key actors in tumor progression and resistance. *Oncotarget* 2017; **8**: 57622–57641.

23 Nieman KM, Romero IL, Van Houten B, Lengyel E. Adipose tissue and adipocytes support tumorigenesis and metastasis. *Biochim Biophys Acta* 2013; **1831**: 1533–1541.

24 Sethi JK, Vidal-Puig AJ. Thematic review series: adipocyte biology. Adipose tissue function and plasticity orchestrate nutritional adaptation. *J Lipid Res* 2007; **48**: 1253–1262.

25 Rosen ED, Spiegelman BM. Adipocytes as regulators of energy balance and glucose homeostasis. *Nature* 2006; **444**: 847–853.

26 Duncan RE, Ahmadian M, Jaworski K, Sarkadi-Nagy E, Sul HS. Regulation of lipolysis in adipocytes. *Annu Rev Nutr* 2007; **27**: 79–101.

27 Wang H, Airola MV, Reue K. How lipid droplets "TAG" along: Glycerolipid synthetic enzymes and lipid storage. *Biochimica et Biophysica Acta (BBA) - Molecular and Cell Biology of Lipids* 2017; **1862**: 1131–1145.

28 Sztalryd C, Brasaemle DL. The perilipin family of lipid droplet proteins: Gatekeepers of intracellular lipolysis. *Biochim Biophys Acta Mol Cell Biol Lipids* 2017; **1862**: 1221–1232.

29 Green H, Kehinde O. An established preadipose cell line and its differentiation in culture. II. Factors affecting the adipose conversion. *Cell* 1975; **5**: 19–27.

30 Farmer SR. Transcriptional control of adipocyte formation. *Cell Metab* 2006; **4**: 263–273.

31 Lefterova MI, Lazar MA. New developments in adipogenesis. *Trends Endocrinol Metab* 2009; **20**: 107–114.

32 Jaworski K, Sarkadi-Nagy E, Duncan RE, Ahmadian M, Sul HS. Regulation of triglyceride metabolism. IV. Hormonal regulation of lipolysis in adipose tissue. *Am J Physiol Gastrointest Liver Physiol* 2007; **293**: G1-4.

33 Schweiger M, Eichmann TO, Taschler U, Zimmermann R, Zechner R, Lass A. Measurement of lipolysis. *Methods Enzymol* 2014; **538**: 171–193.

34 Tian W, Zhang W, Zhang Y, Zhu T, Hua Y, Li H *et al.* FABP4 promotes invasion and metastasis of colon cancer by regulating fatty acid transport. *Cancer Cell Int* 2020; **20**: 512.

35 Zhao J, Zhi Z, Wang C, Xing H, Song G, Yu X *et al.* Exogenous lipids promote the growth of breast cancer cells via CD36. *Oncol Rep* 2017; **38**: 2105–2115.

36 Ladanyi A, Mukherjee A, Kenny HA, Johnson A, Mitra AK, Sundaresan S *et al.* Adipocyte-induced CD36 expression drives ovarian cancer progression and metastasis. *Oncogene* 2018; **37**: 2285–2301.

37 Zhang M, Di Martino JS, Bowman RL, Campbell NR, Baksh SC, Simon-Vermot T *et al.* Adipocyte-Derived Lipids Mediate Melanoma Progression via FATP Proteins. *Cancer Discov* 2018; **8**: 1006–1025.

38 Watt MJ, Clark AK, Selth LA, Haynes VR, Lister N, Rebello R *et al.* Suppressing fatty acid uptake has therapeutic effects in preclinical models of prostate cancer. *Sci Transl Med* 2019. doi:10.1126/scitranslmed.aau5758.

39 Schwenk RW, Holloway GP, Luiken JJFP, Bonen A, Glatz JFC. Fatty acid transport across the cell membrane: regulation by fatty acid transporters. *Prostaglandins Leukot Essent Fatty Acids* 2010; **82**: 149–154.

40 Anderson CM, Stahl A. SLC27 fatty acid transport proteins. *Mol Aspects Med* 2013; **34**: 516–528.

41 Stahl A. A current review of fatty acid transport proteins (SLC27). *Pflugers Arch* 2004; **447**: 722–727.

42 Doege H, Stahl A. Protein-mediated fatty acid uptake: novel insights from in vivo models. *Physiology* 2006; **21**: 259–268.

43 Gimeno RE. Fatty acid transport proteins. *Curr Opin Lipidol* 2007; **18**: 271–276.

44 Pei Z, Fraisl P, Berger J, Jia Z, Forss-Petter S, Watkins PA. Mouse very long-chain Acyl-CoA synthetase 3/fatty acid transport protein 3 catalyzes fatty acid activation but not fatty acid transport in MA-10 cells. *J Biol Chem* 2004; **279**: 54454–54462.

45 DiRusso CC, Darwis D, Obermeyer T, Black PN. Functional domains of the fatty acid transport proteins: studies using protein chimeras. *Biochim Biophys Acta* 2008; **1781**: 135–143.

46 Faergeman NJ, DiRusso CC, Elberger A, Knudsen J, Black PN. Disruption of the Saccharomyces cerevisiae homologue to the murine fatty acid transport protein impairs uptake and growth on long-chain fatty acids. *J Biol Chem* 1997; **272**: 8531–8538.

47 Zou Z, DiRusso CC, Ctrnacta V, Black PN. Fatty acid transport in Saccharomyces cerevisiae. Directed mutagenesis of FAT1 distinguishes the biochemical activities associated with Fat1p. *J Biol Chem* 2002; **277**: 31062–31071.

48 DiRusso CC, Li H, Darwis D, Watkins PA, Berger J, Black PN. Comparative biochemical studies of the murine fatty acid transport proteins (FATP) expressed in yeast. *J Biol Chem* 2005; **280**: 16829–16837.

49 Anastasiou D. Tumour microenvironment factors shaping the cancer metabolism landscape. *Br J Cancer* 2017; **116**: 277–286.

50 Xiong X, Wen Y-A, Fairchild R, Zaytseva YY, Weiss HL, Evers BM *et al.* Upregulation of CPT1A is essential for the tumor-promoting effect of adipocytes in colon cancer. *Cell Death Dis* 2020; **11**: 736.

51 Balaban S, Lee LS, Schreuder M, Hoy AJ. Obesity and cancer progression: is there a role of fatty acid metabolism? *Biomed Res Int* 2015; **2015**: 274585.

52 Schlaepfer IR, Rider L, Rodrigues LU, Gijón MA, Pac CT, Romero L *et al.* Lipid catabolism via CPT1 as a therapeutic target for prostate cancer. *Mol Cancer Ther* 2014; **13**: 2361–2371.

53 De Pergola G, Silvestris F. Obesity as a major risk factor for cancer. *J Obes* 2013; **2013**: 291546.

54 Buschemeyer WC 3rd, Freedland SJ. Obesity and prostate cancer: epidemiology and clinical implications. *Eur Urol* 2007; **52**: 331–343.

55 Bousquenaud M, Fico F, Solinas G, Rüegg C, Santamaria-Martínez A. Obesity promotes the expansion of metastasis-initiating cells in breast cancer. *Breast Cancer Res* 2018; **20**: 104.

56 Liu Y, Metzinger MN, Lewellen KA, Cripps SN, Carey KD, Harper EI *et al.* Obesity Contributes to Ovarian Cancer Metastatic Success through Increased Lipogenesis, Enhanced Vascularity, and Decreased Infiltration of M1 Macrophages. *Cancer Res* 2015; **75**: 5046–5057.

57 Weisberg SP, McCann D, Desai M, Rosenbaum M, Leibel RL, Ferrante AW Jr. Obesity is associated with macrophage accumulation in adipose tissue. *J Clin Invest* 2003; **112**: 1796–1808.

58 Cao Y. Adipocyte and lipid metabolism in cancer drug resistance. *J Clin Invest* 2019; **129**: 3006–3017.

59 Dirat B, Bochet L, Dabek M, Daviaud D, Dauvillier S, Majed B *et al.* Cancer-associated adipocytes exhibit an activated phenotype and contribute to breast cancer invasion. *Cancer Res* 2011; **71**: 2455–2465.

60 Heydt Q, Xintaropoulou C, Clear A, Austin M, Pislariu I, Miraki-Moud F *et al.* Adipocytes disrupt the translational programme of acute lymphoblastic leukaemia to favour tumour survival and persistence. *Nat Commun* 2021; **12**: 5507.

61 Dai L, Song K, Di W. Adipocytes: active facilitators in epithelial ovarian cancer progression? *J Ovarian Res* 2020; **13**: 115.

62 Attané C, Muller C. Drilling for Oil: Tumor-Surrounding Adipocytes Fueling Cancer. *Trends Cancer Res* 2020; **6**: 593–604.

63 Quail DF, Joyce JA. Microenvironmental regulation of tumor progression and metastasis. *Nat Med* 2013; **19**: 1423–1437.

64 Engfeldt P, Arner P. Lipolysis in human adipocytes, effects of cell size, age and of regional differences. *Horm Metab Res Suppl* 1988; **19**: 26–29.

65 Wang Y-X, Zhu N, Zhang C-J, Wang Y-K, Wu H-T, Li Q *et al.* Friend or foe: Multiple roles of adipose tissue in cancer formation and progression. *J Cell Physiol* 2019; **234**: 21436–21449.

66 Nieman KM, Kenny HA, Penicka CV, Ladanyi A, Buell-Gutbrod R, Zillhardt MR *et al.* Adipocytes promote ovarian cancer metastasis and provide energy for rapid tumor growth. *Nat Med* 2011; **17**: 1498–1503.

67 Yang D, Li Y, Xing L, Tan Y, Sun J, Zeng B *et al.* Utilization of adipocyte-derived lipids and enhanced intracellular trafficking of fatty acids contribute to breast cancer progression. *Cell Commun Signal* 2018; **16**: 32.

68 Pavlides S, Whitaker-Menezes D, Castello-Cros R, Flomenberg N, Witkiewicz AK, Frank PG *et al.* The reverse Warburg effect: aerobic glycolysis in cancer associated fibroblasts and the tumor stroma. *Cell Cycle* 2009; **8**: 3984–4001.

69 Incio J, Ligibel JA, McManus DT, Suboj P, Jung K, Kawaguchi K *et al.* Obesity promotes resistance to anti-VEGF therapy in breast cancer by up-regulating IL-6 and potentially FGF-2. *Sci Transl Med* 2018; **10**. doi:10.1126/scitranslmed.aag0945.

70 Khalid A, Wolfram J, Ferrari I, Mu C, Mai J, Yang Z *et al.* Recent Advances in Discovering the Role of CCL5 in Metastatic Breast Cancer. *Mini Rev Med Chem* 2015; **15**: 1063–1072.

71 Laurent V, Guérard A, Mazerolles C, Le Gonidec S, Toulet A, Nieto L *et al.* Periprostatic adipocytes act as a driving force for prostate cancer progression in obesity. *Nat Commun* 2016; **7**: 10230.

72 Strong AL, Ohlstein JF, Biagas BA, Rhodes LV, Pei DT, Tucker HA *et al.* Leptin produced by obese adipose stromal/stem cells enhances proliferation and metastasis of estrogen receptor positive breast cancers. *Breast Cancer Res* 2015; **17**: 112.

73 Lee JO, Kim N, Lee HJ, Lee YW, Kim SJ, Park SH *et al.* Resistin, a fat-derived secretory factor, promotes metastasis of MDA-MB-231 human breast cancer cells through ERM activation. *Sci Rep* 2016; **6**: 18923.

74 Xiong Y, Russell DL, McDonald LT, Cowart LA, LaRue AC. Hematopoietic Stem Cell-derived Adipocytes Promote Tumor Growth and Cancer Cell Migration. *Int J Cancer Res Mol Mech* 2017; **3**. doi:10.16966/2381-3318.130.

75 Arcidiacono B, Chiefari E, Laria AE, Messineo S, Bilotta FL, Britti D *et al.* Expression of matrix metalloproteinase-11 is increased under conditions of insulin resistance. *World J Diabetes* 2017; **8**: 422–428.

76 Koundouros N, Poulogiannis G. Reprogramming of fatty acid metabolism in cancer. *Br J Cancer* 2020; **122**: 4–22.

77 Mounier C, Bouraoui L, Rassart E. Lipogenesis in cancer progression (review). *Int J Oncol* 2014; **45**: 485–492.

78 Zhang J-S, Lei J-P, Wei G-Q, Chen H, Ma C-Y, Jiang H-Z. Natural fatty acid synthase inhibitors as potent therapeutic agents for cancers: A review. *Pharm Biol* 2016; **54**: 1919–1925.

79 Mullen GE, Yet L. Progress in the development of fatty acid synthase inhibitors as anticancer targets. *Bioorg Med Chem Lett* 2015; **25**: 4363–4369.

80 Swinnen JV, Vanderhoydonc F, Elgamal AA, Eelen M, Vercaeren I, Joniau S *et al.* Selective activation of the fatty acid synthesis pathway in human prostate cancer. *Int J Cancer* 2000; **88**: 176–179.

81 Milgraum LZ, Witters LA, Pasternack GR, Kuhajda FP. Enzymes of the fatty acid synthesis pathway are highly expressed in in situ breast carcinoma. *Clin Cancer Res* 1997; **3**: 2115–2120.

82 Wang C, Ma J, Zhang N, Yang Q, Jin Y, Wang Y. The acetyl-CoA carboxylase enzyme: a target for cancer therapy? *Expert Rev Anticancer Ther* 2015; **15**: 667–676.

83 Montesdeoca N, López M, Ariza X, Herrero L, Makowski K. Inhibitors of lipogenic enzymes as a potential therapy against cancer. *FASEB J* 2020; **34**: 11355–11381.

84 Bray F, Ferlay J, Soerjomataram I, Siegel RL, Torre LA, Jemal A. Global cancer statistics 2018: GLOBOCAN estimates of incidence and mortality worldwide for 36 cancers in 185 countries. *CA Cancer J Clin* 2018; **68**: 394–424.

85 DeSantis CE, Ma J, Gaudet MM, Newman LA, Miller KD, Goding Sauer A *et al.* Breast cancer statistics, 2019. *CA Cancer J Clin* 2019; **69**: 438–451.

86 Weigelt B, Geyer FC, Reis-Filho JS. Histological types of breast cancer: how special are they? *Mol Oncol* 2010; **4**: 192–208.

87 Suryawanshi YR, Zhang T, Essani K. Oncolytic viruses: emerging options for the treatment of breast cancer. *Med Oncol* 2017; **34**: 43.

88 Chen M-T, Sun H-F, Zhao Y, Fu W-Y, Yang L-P, Gao S-P *et al.* Comparison of patterns and prognosis among distant metastatic breast cancer patients by age groups: a SEER population-based analysis. *Sci Rep* 2017; **7**: 9254.

89 Eiro N, Gonzalez LO, Fraile M, Cid S, Schneider J, Vizoso FJ. Breast Cancer Tumor Stroma: Cellular Components, Phenotypic Heterogeneity, Intercellular Communication, Prognostic Implications and Therapeutic Opportunities. *Cancers* 2019; **11**. doi:10.3390/cancers11050664.

90 Hill BS, Sarnella A, D'Avino G, Zannetti A. Recruitment of stromal cells into tumour microenvironment promote the metastatic spread of breast cancer. *Semin Cancer Biol* 2020; **60**: 202–213.

91 Welch DR, Hurst DR. Defining the Hallmarks of Metastasis. *Cancer Res* 2019; **79**: 3011–3027.

92 Massa M, Gasparini S, Baldelli I, Scarabelli L, Santi P, Quarto R *et al.* Interaction Between Breast Cancer Cells and Adipose Tissue Cells Derived from Fat Grafting. *Aesthet Surg J* 2016; **36**: 358–363.

93 Carter JC, Church FC. Mature breast adipocytes promote breast cancer cell motility. *Exp Mol Pathol* 2012; **92**: 312–317.

94 Iyengar P, Combs TP, Shah SJ, Gouon-Evans V, Pollard JW, Albanese C *et al.* Adipocyte-secreted factors synergistically promote mammary tumorigenesis through induction of anti-apoptotic transcriptional programs and proto-oncogene stabilization. *Oncogene* 2003; **22**: 6408–6423.

95 He J-Y, Wei X-H, Li S-J, Liu Y, Hu H-L, Li Z-Z *et al.* Adipocyte-derived IL-6 and leptin promote breast Cancer metastasis via upregulation of Lysyl Hydroxylase-2 expression. *Cell Commun Signal* 2018; **16**: 100.

96 D'Esposito V, Liguoro D, Ambrosio MR, Collina F, Cantile M, Spinelli R *et al.* Adipose microenvironment promotes triple negative breast cancer cell invasiveness and dissemination by producing CCL5. *Oncotarget* 2016; **7**: 24495–24509.

97 Rybinska I, Mangano N, Tagliabue E, Triulzi T. Cancer-Associated Adipocytes in Breast Cancer: Causes and Consequences. *Int J Mol Sci* 2021; **22**. doi:10.3390/ijms22073775.

98 Weigelt B, Peterse JL, van 't Veer LJ. Breast cancer metastasis: markers and models. *Nat Rev Cancer* 2005; **5**: 591–602.

99 Morris EV, Edwards CM. The role of bone marrow adipocytes in bone metastasis. *J Bone Oncol* 2016; **5**: 121–123.

100 Justesen J, Stenderup K, Ebbesen EN, Mosekilde L, Steiniche T, Kassem M. Adipocyte tissue volume in bone marrow is increased with aging and in patients with osteoporosis. *Biogerontology* 2001; **2**: 165–171.

101 Templeton ZS, Lie W-R, Wang W, Rosenberg-Hasson Y, Alluri RV, Tamaresis JS *et al.* Breast Cancer Cell Colonization of the Human Bone Marrow Adipose Tissue Niche. *Neoplasia* 2015; **17**: 849–861.

102 Nutter F, Holen I, Brown HK, Cross SS, Evans CA, Walker M *et al.* Different molecular profiles are associated with breast cancer cell homing compared with colonisation of bone: evidence using a novel bone-seeking cell line. *Endocr Relat Cancer* 2014; **21**: 327–341.

103 Nimri L, Peri I, Yehuda-Shnaidman E, Schwartz B. Adipocytes Isolated from Visceral and Subcutaneous Depots of Donors Differing in BMI Crosstalk with Colon Cancer Cells and Modulate their Invasive Phenotype. *Transl Oncol* 2019; **12**: 1404–1415.

104 Zha JM, Di WJ, Zhu T, Xie Y, Yu J, Liu J *et al.* Comparison of gene transcription between subcutaneous and visceral adipose tissue in Chinese adults. *Endocr J* 2009; **56**: 935–944.

105 Trayes KP, Cokenakes SEH. Breast Cancer Treatment. 2021.https://www.aafp.org/afp/2021/0800/p171.html (accessed 27 Feb2022).

106 Howlader N, Cronin KA, Kurian AW, Andridge R. Differences in Breast Cancer Survival by Molecular Subtypes in the United StatesU.S. Breast Cancer Survival by Molecular Subtypes. *Cancer Epidemiol Biomarkers Prev* 2018; **27**: 619–626.

107 Torre LA, Trabert B, DeSantis CE, Miller KD, Samimi G, Runowicz CD *et al.* Ovarian cancer statistics, 2018. *CA Cancer J Clin* 2018; **68**: 284–296.

108 Landen CN Jr, Birrer MJ, Sood AK. Early events in the pathogenesis of epithelial ovarian cancer. *J Clin Oncol* 2008; **26**: 995–1005.

109 Li W, Wang H, Wang J, L F V, Zhu X, Wang Z. Ovarian metastases resection from extragenital primary sites: outcome and prognostic factor analysis of 147 patients. *BMC Cancer* 2012; **12**: 278.

110 Bigorie V, Morice P, Duvillard P, Antoine M, Cortez A, Flejou JF *et al.* Ovarian metastases from breast cancer: report of 29 cases. *Cancer* 2010; **116**: 799–804.

111 Karnezis AN, Cho KR, Gilks CB, Pearce CL, Huntsman DG. The disparate origins of ovarian cancers: pathogenesis and prevention strategies. *Nat Rev Cancer* 2017; **17**: 65–74.

112 Pimentel C, Becquet M, Lavoue V, Henno S, Leveque J, Ouldamer L. Ovarian Metastases from Breast Cancer: A Series of 28 Cases. *Anticancer Res* 2016; **36**: 4195–4200.

113 Hansen JM, Coleman RL, Sood AK. Targeting the tumour microenvironment in ovarian cancer. *Eur J Cancer* 2016; **56**: 131–143.

114 Yang Y, Yang Y, Yang J, Zhao X, Wei X. Tumor Microenvironment in Ovarian Cancer: Function and Therapeutic Strategy. *Front Cell Dev Biol* 2020; **8**: 758.

115 Lan C, Heindl A, Huang X, Xi S, Banerjee S, Liu J *et al.* Quantitative histology analysis of the ovarian tumour microenvironment. *Sci Rep* 2015; **5**: 16317.

116 Zhang B, Chen F, Xu Q, Han L, Xu J, Gao L *et al.* Revisiting ovarian cancer microenvironment: a friend or a foe? *Protein Cell* 2018; **9**: 674–692.

117 Clark R, Krishnan V, Schoof M, Rodriguez I, Theriault B, Chekmareva M *et al.* Milky spots promote ovarian cancer metastatic colonization of peritoneal adipose in experimental models. *Am J Pathol* 2013; **183**: 576–591.

118 Tan DSP, Agarwal R, Kaye SB. Mechanisms of transcoelomic metastasis in ovarian cancer. *Lancet Oncol* 2006; **7**: 925–934.

119 Lengyel E. Ovarian cancer development and metastasis. *Am J Pathol* 2010; **177**: 1053–1064.

120 Wang Y, Niu XL, Qu Y, Wu J, Zhu YQ, Sun WJ *et al.* Autocrine production of interleukin-6 confers cisplatin and paclitaxel resistance in ovarian cancer cells. *Cancer Lett* 2010; **295**: 110–123.

121 Calle EE, Rodriguez C, Walker-Thurmond K, Thun MJ. Overweight, obesity, and mortality from cancer in a prospectively studied cohort of U.S. adults. *N Engl J Med* 2003; **348**: 1625–1638.

122 Mukherjee A, Chiang C-Y, Daifotis HA, Nieman KM, Fahrmann JF, Lastra RR *et al.* Adipocyte-Induced FABP4 Expression in Ovarian Cancer Cells Promotes Metastasis and Mediates Carboplatin ResistanceFABP4 and Omental Metastasis. *Cancer Res* 2020; **80**: 1748–1761.

123 Brasaemle DL, Subramanian V, Garcia A, Marcinkiewicz A, Rothenberg A. Perilipin A and the control of triacylglycerol metabolism. *Mol Cell Biochem* 2009; **326**: 15–21.

124 Stewart C, Ralyea C, Lockwood S. Ovarian Cancer: An Integrated Review. *Semin Oncol Nurs* 2019; **35**: 151–156.

125 Chien J, Poole EM. Ovarian Cancer Prevention, Screening, and Early Detection: Report From the 11th Biennial Ovarian Cancer Research Symposium. *Int J Gynecol Cancer* 2017; **27**: S20–S22.

126 Behan JW, Yun JP, Proektor MP, Ehsanipour EA, Arutyunyan A, Moses AS *et al.* Adipocytes impair leukemia treatment in mice. *Cancer Res* 2009; **69**: 7867–7874.

127 Chen D-R, Lu D-Y, Lin H-Y, Yeh W-L. Mesenchymal stem cell-induced doxorubicin resistance in triple negative breast cancer. *Biomed Res Int* 2014; **2014**: 532161.

128 Chiu Y-J, Yang J-S, Hsu H-S, Tsai C-H, Ma H. Adipose-derived stem cell conditioned medium attenuates cisplatin-triggered apoptosis in tongue squamous cell carcinoma. *Oncol Rep* 2018; **39**: 651–658.

129 Pramanik R, Sheng X, Ichihara B, Heisterkamp N, Mittelman SD. Adipose tissue attracts and protects acute lymphoblastic leukemia cells from chemotherapy. *Leuk Res* 2013; **37**: 503–509.

130 Liu Z, Xu J, He J, Liu H, Lin P, Wan X *et al.* Mature adipocytes in bone marrow protect myeloma cells against chemotherapy through autophagy activation. *Oncotarget* 2015; **6**: 34329–34341.

131 Coelho P, Silva L, Faria I, Vieria M, Monteiro A, Pinto G *et al.* Adipocyte Secretome Increases Radioresistance of Malignant Melanocytes by Improving Cell Survival and Decreasing Oxidative Status. *Radiat Res* 2017; **187**: 581–588.

132 Chi M, Chen J, Ye Y, Tseng H-Y, Lai F, Tay KH *et al.* Adipocytes contribute to resistance of human melanoma cells to chemotherapy and targeted therapy. *Curr Med Chem* 2014; **21**: 1255–1267.

133 Duong MN, Cleret A, Matera E-L, Chettab K, Mathé D, Valsesia-Wittmann S *et al.* Adipose cells promote resistance of breast cancer cells to trastuzumab-mediated antibody-dependent cellular cytotoxicity. *Breast Cancer Res* 2015; **17**: 57.

134 Ehsanipour EA, Sheng X, Behan JW, Wang X, Butturini A, Avramis VI *et al.* Adipocytes cause leukemia cell resistance to L-asparaginase via release of glutamine. *Cancer Res* 2013; **73**: 2998–3006.

135 Booth A, Magnuson A, Fouts J, Foster M. Adipose tissue, obesity and adipokines: role in cancer promotion. *Horm Mol Biol Clin Investig* 2015; **21**: 57–74.

136 Pang J, Shi Q, Liu Z, He J, Liu H, Lin P *et al.* Resistin induces multidrug resistance in myeloma by inhibiting cell death and upregulating ABC transporter expression. *Haematologica* 2017; **102**: 1273–1280.

137 Lehuédé C, Li X, Dauvillier S, Vaysse C, Franchet C, Clement E *et al.* Adipocytes promote breast cancer resistance to chemotherapy, a process amplified by obesity: role of the major vault protein (MVP). *Breast Cancer Res* 2019; **21**: 7.

138 Sheng X, Tucci J, Parmentier J-H, Ji L, Behan JW, Heisterkamp N *et al.* Adipocytes cause leukemia cell resistance to daunorubicin via oxidative stress response. *Oncotarget* 2016; **7**: 73147–73159.

139 Ye H, Adane B, Khan N, Sullivan T, Minhajuddin M, Gasparetto M *et al.* Leukemic Stem Cells Evade Chemotherapy by Metabolic Adaptation to an Adipose Tissue Niche. *Cell Stem Cell* 2016; **19**: 23–37.

140 Yang J, Zaman MM, Vlasakov I, Roy R, Huang L, Martin CR *et al.* Adipocytes promote ovarian cancer chemoresistance. *Sci Rep* 2019; **9**: 13316.

141 Choi J, Cha YJ, Koo JS. Adipocyte biology in breast cancer: From silent bystander to active facilitator. *Prog Lipid Res* 2018; **69**: 11–20.

142 Menendez JA, Vellon L, Colomer R, Lupu R. Pharmacological and small interference RNA-mediated inhibition of breast cancer-associated fatty acid synthase (oncogenic antigen-519) synergistically enhances Taxol (paclitaxel)-induced cytotoxicity. *Int J Cancer* 2005; **115**: 19–35.

143 Rae C, Haberkorn U, Babich JW, Mairs RJ. Inhibition of Fatty Acid Synthase Sensitizes Prostate Cancer Cells to Radiotherapy. *Radiat Res* 2015; **184**: 482–493.

144 Sounni NE, Cimino J, Blacher S, Primac I, Truong A, Mazzucchelli G *et al.* Blocking lipid synthesis overcomes tumor regrowth and metastasis after antiangiogenic therapy withdrawal. *Cell Metab* 2014; **20**: 280–294.

145 Puig T, Aguilar H, Cufí S, Oliveras G, Turrado C, Ortega-Gutiérrez S *et al.* A novel inhibitor of fatty acid synthase shows activity against HER2+ breast cancer xenografts and is active in anti-HER2 drug-resistant cell lines. *Breast Cancer Res* 2011; **13**: R131.

146 Alicea GM, Rebecca VW, Goldman AR, Fane ME, Douglass SM, Behera R *et al.* Changes in Aged Fibroblast Lipid Metabolism Induce Age-Dependent Melanoma Cell Resistance to Targeted Therapy via the Fatty Acid Transporter FATP2. *Cancer Discov* 2020; **10**: 1282–1295.

147 Iwamoto H, Abe M, Yang Y, Cui D, Seki T, Nakamura M *et al.* Cancer Lipid Metabolism Confers Antiangiogenic Drug Resistance. *Cell Metab* 2018; **28**: 104-117.e5.

148 Sudhakar A. History of Cancer, Ancient and Modern Treatment Methods. *J Cancer Sci Ther* 2009; **1**: 1–4.

149 Esfahani K, Roudaia L, Buhlaiga N, Del Rincon SV, Papneja N, Miller WH Jr. A review of cancer immunotherapy: from the past, to the present, to the future. *Curr Oncol* 2020; **27**: S87–S97.

150 Dobosz P, Dzieciątkowski T. The Intriguing History of Cancer Immunotherapy. *Front Immunol* 2019; **10**: 2965.

151 Kelly E, Russell SJ. History of oncolytic viruses: genesis to genetic engineering. *Mol Ther* 2007; **15**: 651–659.

152 Lin E, Nemunaitis J. Oncolytic viral therapies. *Cancer Gene Ther* 2004; **11**: 643–664.

153 Russell L, Peng K-W. The emerging role of oncolytic virus therapy against cancer. *Chin Clin Oncol* 2018; **7**: 16.

154 Liang M. Oncorine, the World First Oncolytic Virus Medicine and its Update in China. *Curr Cancer Drug Targets* 2018; **18**: 171–176.

155 Eissa IR, Bustos-Villalobos I, Ichinose T, Matsumura S, Naoe Y, Miyajima N *et al.* The Current Status and Future Prospects of Oncolytic Viruses in Clinical Trials against Melanoma, Glioma, Pancreatic, and Breast Cancers. *Cancers* 2018; **10**. doi:10.3390/cancers10100356.

156 Maroun J, Muñoz-Alía M, Ammayappan A, Schulze A, Peng K-W, Russell S. Designing and building oncolytic viruses. *Future Virol* 2017; **12**: 193–213.

157 Hanahan D, Weinberg RA. Hallmarks of cancer: the next generation. *Cell* 2011; **144**: 646–674.

158 Pikor LA, Bell JC, Diallo J-S. Oncolytic Viruses: Exploiting Cancer's Deal with the Devil. *Trends Cancer Res* 2015; **1**: 266–277.

159 Choi AH, O'Leary MP, Fong Y, Chen NG. From Benchtop to Bedside: A Review of Oncolytic Virotherapy. *Biomedicines* 2016; **4**: 18.

160 Anderson BD, Nakamura T, Russell SJ, Peng K-W. High CD46 receptor density determines preferential killing of tumor cells by oncolytic measles virus. *Cancer Res* 2004; **64**: 4919–4926.

161 Kaufman HL, Kohlhapp FJ, Zloza A. Oncolytic viruses: a new class of immunotherapy drugs. *Nat Rev Drug Discov* 2015; **14**: 642–662.

162 Ricca JM, Oseledchyk A, Walther T, Liu C, Mangarin L, Merghoub T *et al.* Pre-existing Immunity to Oncolytic Virus Potentiates Its Immunotherapeutic Efficacy. *Mol Ther* 2018; **26**: 1008–1019.

163 Havunen R, Santos JM, Sorsa S, Rantapero T, Lumen D, Siurala M *et al.* Abscopal Effect in Non-injected Tumors Achieved with Cytokine-Armed Oncolytic Adenovirus. *Mol Ther Oncolytics* 2018; **11**: 109–121.

164 Hu F, Hu X-H, Yu P, Zhang J-X, Lou G-G, Liu H-L *et al.* [Abscopal effect on metastatic tumor induced by oncolytic virus of H101 combining with local heating]. *Ai Zheng* 2006; **25**: 919–924.

165 Lichty BD, Breitbach CJ, Stojdl DF, Bell JC. Going viral with cancer immunotherapy. *Nat Rev Cancer* 2014; **14**: 559–567.

166 Dang CV, Reddy EP, Shokat KM, Soucek L. Drugging the “undruggable” cancer targets. *Nat Rev Cancer* 2017; **17**: 502–508.

167 Freedman JD, Duffy MR, Lei-Rossmann J, Muntzer A, Scott EM, Hagel J *et al.* An Oncolytic Virus Expressing a T-cell Engager Simultaneously Targets Cancer and Immunosuppressive Stromal CellsOncolytic Adenovirus Expressing FAP BiTE. *Cancer Res* 2018; **78**: 6852–6865.

168 Arulanandam R, Batenchuk C, Angarita FA, Ottolino-Perry K, Cousineau S, Mottashed A *et al.* VEGF-Mediated Induction of PRD1-BF1/Blimp1 Expression Sensitizes Tumor Vasculature to Oncolytic Virus Infection. *Cancer Cell* 2015; **28**: 210–224.

169 Jin S, Wang Q, Wu H, Pang D, Xu S. Oncolytic viruses for triple negative breast cancer and beyond. *Biomark Res* 2021; **9**: 71.

170 Chaurasiya S, Fong Y, Warner SG. Oncolytic Virotherapy for Cancer: Clinical Experience. *Biomedicines* 2021; **9**. doi:10.3390/biomedicines9040419.

171 Pol J, Bloy N, Obrist F, Eggermont A, Galon J, Cremer I *et al.* Trial Watch:: Oncolytic viruses for cancer therapy. *Oncoimmunology* 2014; **3**: e28694.

172 Balachandran S, Barber GN. Vesicular stomatitis virus (VSV) therapy of tumors. *IUBMB Life* 2000; **50**: 135–138.

173 Lichty BD, Power AT, Stojdl DF, Bell JC. Vesicular stomatitis virus: re-inventing the bullet. *Trends Mol Med* 2004; **10**: 210–216.

174 Payne S. Chapter 19 - Family Rhabdoviridae. In: Payne S (ed). *Viruses*. Academic Press, 2017, pp 165–172.

175 Bukreyev A, Skiadopoulos MH, Murphy BR, Collins PL. Nonsegmented negative-strand viruses as vaccine vectors. *J Virol* 2006; **80**: 10293–10306.

176 Stojdl DF, Lichty BD, tenOever BR, Paterson JM, Power AT, Knowles S *et al.* VSV strains with defects in their ability to shutdown innate immunity are potent systemic anti-cancer agents. *Cancer Cell* 2003; **4**: 263–275.

177 Jayakar HR, Murti KG, Whitt MA. Mutations in the PPPY motif of vesicular stomatitis virus matrix protein reduce virus budding by inhibiting a late step in virion release. *J Virol* 2000; **74**: 9818–9827.

178 Newcomb WW, Tobin GJ, McGowan JJ, Brown JC. In vitro reassembly of vesicular stomatitis virus skeletons. *J Virol* 1982; **41**: 1055–1062.

179 Hastie E, Grdzelishvili VZ. Vesicular stomatitis virus as a flexible platform for oncolytic virotherapy against cancer. *J Gen Virol* 2012; **93**: 2529–2545.

180 Naik S, Nace R, Federspiel MJ, Barber GN, Peng K-W, Russell SJ. Curative one-shot systemic virotherapy in murine myeloma. *Leukemia* 2012; **26**: 1870–1878.

181 Merchan JR, Patel M, Cripe TP, Old MO, Strauss JF, Thomassen A *et al.* Relationship of infusion duration to safety, efficacy, and pharmacodynamics (PD): Second part of a phase I-II study using VSV-IFNβ-NIS (VV1) oncolytic virus in patients with refractory solid tumors. *J Clin Orthod* 2020; **38**: 3090–3090.

182 Cook J, Peng KWW, Witzig TE, Broski SM, Villasboas JC, Paludo J *et al.* Clinical Activity of Single Dose Systemic Oncolytic VSV Virotherapy in Patients with Relapsed Refractory T-Cell Lymphoma. *Blood Adv* 2022. doi:10.1182/bloodadvances.2021006631.

183 Search of: VSV - List Results - ClinicalTrials.gov. https://clinicaltrials.gov/ct2/results?cond=&term=VSV&cntry=&state=&city=&dist= (accessed 8 Mar2022).

184 Brun J, McManus D, Lefebvre C, Hu K, Falls T, Atkins H *et al.* Identification of genetically modified Maraba virus as an oncolytic rhabdovirus. *Mol Ther* 2010; **18**: 1440–1449.

185 Pol JG, Atherton MJ, Bridle BW, Stephenson KB, Le Boeuf F, Hummel JL *et al.* Development and applications of oncolytic Maraba virus vaccines. *Oncolytic Virother* 2018; **7**: 117–128.

186 Heaton NS, Randall G. Multifaceted roles for lipids in viral infection. *Trends Microbiol* 2011; **19**: 368–375.

187 Schoggins JW, Randall G. Lipids in innate antiviral defense. *Cell Host Microbe* 2013; **14**: 379–385.

188 Chukkapalli V, Heaton NS, Randall G. Lipids at the interface of virus-host interactions. *Curr Opin Microbiol* 2012; **15**: 512–518.

189 Pfaender S, Heyden J, Friesland M, Ciesek S, Ejaz A, Steinmann J *et al.* Inactivation of hepatitis C virus infectivity by human breast milk. *J Infect Dis* 2013; **208**: 1943–1952.

190 Morniroli D, Consales A, Crippa BL, Vizzari G, Ceroni F, Cerasani J *et al.* The Antiviral Properties of Human Milk: A Multitude of Defence Tools from Mother Nature. *Nutrients* 2021; **13**. doi:10.3390/nu13020694.

191 Dodge JA, Sagher FA. Antiviral and antibacterial lipids in human milk and infant formula. Arch. Dis. Child. 1991; **66**: 272–273.

192 Vázquez-Calvo A, Saiz J-C, Sobrino F, Martín-Acebes MA. Inhibition of enveloped virus infection of cultured cells by valproic acid. *J Virol* 2011; **85**: 1267–1274.

193 Bartolotta S, García CC, Candurra NA, Damonte EB. Effect of fatty acids on arenavirus replication: inhibition of virus production by lauric acid. *Arch Virol* 2001; **146**: 777–790.

194 Hornung B, Amtmann E, Sauer G. Laurie acid inhibits the maturation of vesicular stomatitis virus. *J Gen Virol* 1994; **75**: 353–361.

195 Kapadia SB, Chisari FV. Hepatitis C virus RNA replication is regulated by host geranylgeranylation and fatty acids. *Proc Natl Acad Sci U S A* 2005; **102**: 2561–2566.

196 Xu B, Ma R, Russell L, Yoo JY, Han J, Cui H *et al.* An oncolytic herpesvirus expressing E-cadherin improves survival in mouse models of glioblastoma. *Nat Biotechnol* 2018. doi:10.1038/nbt.4302.

197 Ci Y, Yang Y, Xu C, Shi L. Vesicular stomatitis virus G protein transmembrane region is crucial for the hemi-fusion to full fusion transition. *Sci Rep* 2018; **8**: 10669.

198 Schnell MJ, Johnson JE, Buonocore L, Rose JK. Construction of a novel virus that targets HIV-1-infected cells and controls HIV-1 infection. *Cell* 1997; **90**: 849–857.

199 Lay Mendoza MF, Acciani MD, Levit CN, Santa Maria C, Brindley MA. Monitoring Viral Entry in Real-Time Using a Luciferase Recombinant Vesicular Stomatitis Virus Producing SARS-CoV-2, EBOV, LASV, CHIKV, and VSV Glycoproteins. *Viruses* 2020; **12**. doi:10.3390/v12121457.

200 Bastin D, Aitken AS, Pelin A, Pikor LA, Crupi MJF, Huh MS *et al.* Enhanced susceptibility of cancer cells to oncolytic rhabdo-virotherapy by expression of Nodamura virus protein B2 as a suppressor of RNA interference. *J Immunother Cancer* 2018; **6**: 62.

201 Le Boeuf F, Diallo J-S, McCart JA, Thorne S, Falls T, Stanford M *et al.* Synergistic interaction between oncolytic viruses augments tumor killing. *Mol Ther* 2010; **18**: 888–895.

202 Casals N, Zammit V, Herrero L, Fadó R, Rodríguez-Rodríguez R, Serra D. Carnitine palmitoyltransferase 1C: From cognition to cancer. *Prog Lipid Res* 2016; **61**: 134–148.

203 Zhou J, Chng W-J. Roles of thioredoxin binding protein (TXNIP) in oxidative stress, apoptosis and cancer. *Mitochondrion* 2013; **13**: 163–169.

204 Hodson L, Skeaff CM, Fielding BA. Fatty acid composition of adipose tissue and blood in humans and its use as a biomarker of dietary intake. *Prog Lipid Res* 2008; **47**: 348–380.

205 Aggarwal V, Tuli HS, Tania M, Srivastava S, Ritzer EE, Pandey A *et al.* Molecular mechanisms of action of epigallocatechin gallate in cancer: Recent trends and advancement. *Semin Cancer Biol* 2020. doi:10.1016/j.semcancer.2020.05.011.

206 Brusselmans K, De Schrijver E, Heyns W, Verhoeven G, Swinnen JV. Epigallocatechin-3-gallate is a potent natural inhibitor of fatty acid synthase in intact cells and selectively induces apoptosis in prostate cancer cells. *Int J Cancer* 2003; **106**: 856–862.

207 Adam V, Ekblad M, Sweeney K, Müller H, Busch KH, Johnsen CT *et al.* Synergistic and Selective Cancer Cell Killing Mediated by the Oncolytic Adenoviral Mutant AdΔΔ and Dietary Phytochemicals in Prostate Cancer Models. *Hum Gene Ther* 2012; **23**: 1003–1015.

208 McCune SA, Harris RA. Mechanism responsible for 5-(tetradecyloxy)-2-furoic acid inhibition of hepatic lipogenesis. *J Biol Chem* 1979; **254**: 10095–10101.

209 Chiu H-C, Kovacs A, Blanton RM, Han X, Courtois M, Weinheimer CJ *et al.* Transgenic expression of fatty acid transport protein 1 in the heart causes lipotoxic cardiomyopathy. *Circ Res* 2005; **96**: 225–233.

210 Wu Q, Ortegon AM, Tsang B, Doege H, Feingold KR, Stahl A. FATP1 is an insulin-sensitive fatty acid transporter involved in diet-induced obesity. *Mol Cell Biol* 2006; **26**: 3455–3467.

211 Sandoval A, Chokshi A, Jesch ED, Black PN, Dirusso CC. Identification and characterization of small compound inhibitors of human FATP2. *Biochem Pharmacol* 2010; **79**: 990–999.

212 Saini N, Black PN, Montefusco D, DiRusso CC. Fatty acid transport protein-2 inhibitor Grassofermata/CB5 protects cells against lipid accumulation and toxicity. *Biochem Biophys Res Commun* 2015; **465**: 534–541.

213 Ahowesso C, Black PN, Saini N, Montefusco D, Chekal J, Malosh C *et al.* Chemical inhibition of fatty acid absorption and cellular uptake limits lipotoxic cell death. *Biochem Pharmacol* 2015; **98**: 167–181.

214 Black PN, Ahowesso C, Montefusco D, Saini N, DiRusso CC. Fatty Acid Transport Proteins: Targeting FATP2 as a Gatekeeper Involved in the Transport of Exogenous Fatty Acids. *Medchemcomm* 2016; **7**: 612–622.

215 McFadden G. Poxvirus tropism. *Nat Rev Microbiol* 2005; **3**: 201–213.

216 Ibáñez FJ, Farías MA, Gonzalez-Troncoso MP, Corrales N, Duarte LF, Retamal-Díaz A *et al.* Experimental Dissection of the Lytic Replication Cycles of Herpes Simplex Viruses in vitro. *Front Microbiol* 2018; **9**: 2406.

217 Moss WJ, Griffin DE. Global measles elimination. *Nat Rev Microbiol* 2006; **4**: 900–908.

218 Stoeckel J, Hay JG. Drug evaluation: Reolysin--wild-type reovirus as a cancer therapeutic. *Curr Opin Mol Ther* 2006; **8**: 249–260.

219 White JM, Delos SE, Brecher M, Schornberg K. Structures and mechanisms of viral membrane fusion proteins: multiple variations on a common theme. *Crit Rev Biochem Mol Biol* 2008; **43**: 189–219.

220 Liu Y, Steinbusch LKM, Nabben M, Kapsokalyvas D, van Zandvoort M, Schönleitner P *et al.* Palmitate-Induced Vacuolar-Type H+-ATPase Inhibition Feeds Forward Into Insulin Resistance and Contractile Dysfunction. *Diabetes* 2017; **66**: 1521–1534.

221 McNab F, Mayer-Barber K, Sher A, Wack A, O'Garra A. Type I interferons in infectious disease. *Nat Rev Immunol* 2015; **15**: 87–103.

222 Mesev EV, LeDesma RA, Ploss A. Decoding type I and III interferon signalling during viral infection. *Nat Microbiol* 2019; **4**: 914–924.

223 Kim NH, Sung HY, Choi EN, Lyu D, Choi HJ, Ju W *et al.* Aberrant DNA methylation in the IFITM1 promoter enhances the metastatic phenotype in an intraperitoneal xenograft model of human ovarian cancer. *Oncol Rep* 2014; **31**: 2139–2146.

224 Liang R, Li X, Zhu X. Deciphering the Roles of IFITM1 in Tumors. *Mol Diagn Ther* 2020; **24**: 433–441.

225 Smith SE, Busse DC, Binter S, Weston S, Diaz Soria C, Laksono BM *et al.* Interferon-Induced Transmembrane Protein 1 Restricts Replication of Viruses That Enter Cells via the Plasma Membrane. *J Virol* 2019; **93**. doi:10.1128/JVI.02003-18.

226 Huang I-C, Bailey CC, Weyer JL, Radoshitzky SR, Becker MM, Chiang JJ *et al.* Distinct patterns of IFITM-mediated restriction of filoviruses, SARS coronavirus, and influenza A virus. *PLoS Pathog* 2011; **7**: e1001258.

227 Lu J, Pan Q, Rong L, He W, Liu S-L, Liang C. The IFITM proteins inhibit HIV-1 infection. *J Virol* 2011; **85**: 2126–2137.

228 Wang J, Wang C-F, Ming S-L, Li G-L, Zeng L, Wang M-D *et al.* Porcine IFITM1 is a host restriction factor that inhibits pseudorabies virus infection. *Int J Biol Macromol* 2020; **151**: 1181–1193.

229 Zhang Y, Wang L, Zheng J, Huang L, Wang S, Huang X *et al.* Grouper Interferon-Induced Transmembrane Protein 1 Inhibits Iridovirus and Nodavirus Replication by Regulating Virus Entry and Host Lipid Metabolism. *Front Immunol* 2021; **12**: 636806.

230 Mudhasani R, Tran JP, Retterer C, Radoshitzky SR, Kota KP, Altamura LA *et al.* IFITM-2 and IFITM-3 but not IFITM-1 restrict Rift Valley fever virus. *J Virol* 2013; **87**: 8451–8464.

231 Li K, Jia R, Li M, Zheng Y-M, Miao C, Yao Y *et al.* A sorting signal suppresses IFITM1 restriction of viral entry. *J Biol Chem* 2015; **290**: 4248–4259.

232 Li K, Markosyan RM, Zheng Y-M, Golfetto O, Bungart B, Li M *et al.* IFITM proteins restrict viral membrane hemifusion. *PLoS Pathog* 2013; **9**: e1003124.

233 Diamond MS, Farzan M. The broad-spectrum antiviral functions of IFIT and IFITM proteins. *Nat Rev Immunol* 2013; **13**: 46–57.

234 York AG, Williams KJ, Argus JP, Zhou QD, Brar G, Vergnes L *et al.* Limiting Cholesterol Biosynthetic Flux Spontaneously Engages Type I IFN Signaling. *Cell* 2015; **163**: 1716–1729.

235 Zhang W, Wang G, Xu Z-G, Tu H, Hu F, Dai J *et al.* Lactate Is a Natural Suppressor of RLR Signaling by Targeting MAVS. *Cell* 2019; **178**: 176-189.e15.

236 Germain N, Dhayer M, Boileau M, Fovez Q, Kluza J, Marchetti P. Lipid Metabolism and Resistance to Anticancer Treatment. *Biology* 2020; **9**. doi:10.3390/biology9120474.

237 Eisenberg S, Levy RI. Lipoprotein metabolism. *Adv Lipid Res* 1975; **13**: 1–89.

238 Tucci J, Chen T, Margulis K, Orgel E, Paszkiewicz RL, Cohen MD *et al.* Adipocytes Provide Fatty Acids to Acute Lymphoblastic Leukemia Cells. *Front Oncol* 2021; **11**: 665763.

239 Braicu EI, Darb-Esfahani S, Schmitt WD, Koistinen KM, Heiskanen L, Pöhö P *et al.* High-grade ovarian serous carcinoma patients exhibit profound alterations in lipid metabolism. *Oncotarget* 2017; **8**: 102912–102922.

240 Melton EM, Cerny RL, DiRusso CC, Black PN. Overexpression of human fatty acid transport protein 2/very long chain acyl-CoA synthetase 1 (FATP2/Acsvl1) reveals distinct patterns of trafficking of exogenous fatty acids. *Biochem Biophys Res Commun* 2013; **440**: 743–748.

241 O'Connor RS, Guo L, Ghassemi S, Snyder NW, Worth AJ, Weng L *et al.* The CPT1a inhibitor, etomoxir induces severe oxidative stress at commonly used concentrations. *Sci Rep* 2018; **8**: 6289.

242 Basseri S, Austin RC. Endoplasmic reticulum stress and lipid metabolism: mechanisms and therapeutic potential. *Biochem Res Int* 2012; **2012**: 841362.

243 Han J, Kaufman RJ. The role of ER stress in lipid metabolism and lipotoxicity. *J Lipid Res* 2016; **57**: 1329–1338.

244 Guo W, Wong S, Xie W, Lei T, Luo Z. Palmitate modulates intracellular signaling, induces endoplasmic reticulum stress, and causes apoptosis in mouse 3T3-L1 and rat primary preadipocytes. *Am J Physiol Endocrinol Metab* 2007; **293**: E576-86.

245 Wei Y, Wang D, Topczewski F, Pagliassotti MJ. Saturated fatty acids induce endoplasmic reticulum stress and apoptosis independently of ceramide in liver cells. *Am J Physiol Endocrinol Metab* 2006; **291**: E275-81.

246 Oslowski CM, Hara T, O'Sullivan-Murphy B, Kanekura K, Lu S, Hara M *et al.* Thioredoxin-interacting protein mediates ER stress-induced β cell death through initiation of the inflammasome. *Cell Metab* 2012; **16**: 265–273.

247 Li W, Zhang D, Yuan W, Wang C, Huang Q, Luo J. Humanin Ameliorates Free Fatty Acid-Induced Endothelial Inflammation by Suppressing the NLRP3 Inflammasome. *ACS Omega* 2020; **5**: 22039–22045.

248 Panse M, Kluth O, Lorza-Gil E, Kaiser G, Mühlbauer E, Schürmann A *et al.* Palmitate and insulin counteract glucose-induced thioredoxin interacting protein (TXNIP) expression in insulin secreting cells via distinct mechanisms. *PLoS One* 2018; **13**: e0198016.

249 Chen X, Cubillos-Ruiz JR. Endoplasmic reticulum stress signals in the tumour and its microenvironment. *Nat Rev Cancer* 2021; **21**: 71–88.

250 Zhou R, Tardivel A, Thorens B, Choi I, Tschopp J. Thioredoxin-interacting protein links oxidative stress to inflammasome activation. *Nat Immunol* 2010; **11**: 136–140.

251 Ravindran MS, Bagchi P, Cunningham CN, Tsai B. Opportunistic intruders: how viruses orchestrate ER functions to infect cells. *Nat Rev Microbiol* 2016; **14**: 407–420.

252 Tiwarekar V, Wohlfahrt J, Fehrholz M, Scholz C-J, Kneitz S, Schneider-Schaulies J. APOBEC3G-Regulated Host Factors Interfere with Measles Virus Replication: Role of REDD1 and Mammalian TORC1 Inhibition. *J Virol* 2018; **92**. doi:10.1128/JVI.00835-18.

253 Uppala JK, Gani AR, Ramaiah KVA. Chemical chaperone, TUDCA unlike PBA, mitigates protein aggregation efficiently and resists ER and non-ER stress induced HepG2 cell death. *Sci Rep* 2017; **7**: 3831.

254 Rellmann Y, Gronau I, Hansen U, Dreier R. 4-Phenylbutyric Acid Reduces Endoplasmic Reticulum Stress in Chondrocytes That Is Caused by Loss of the Protein Disulfide Isomerase ERp57. *Oxid Med Cell Longev* 2019; **2019**: 6404035.

255 Vergote D, Cren-Olivé C, Chopin V, Toillon R-A, Rolando C, Hondermarck H *et al.* (-)-Epigallocatechin (EGC) of green tea induces apoptosis of human breast cancer cells but not of their normal counterparts. *Breast Cancer Res Treat* 2002; **76**: 195–201.

256 Chakravarty B, Gu Z, Chirala SS, Wakil SJ, Quiocho FA. Human fatty acid synthase: structure and substrate selectivity of the thioesterase domain. *Proc Natl Acad Sci U S A* 2004; **101**: 15567–15572.

257 Wang X, Tian W. Green tea epigallocatechin gallate: a natural inhibitor of fatty-acid synthase. *Biochem Biophys Res Commun* 2001; **288**: 1200–1206.

258 Royle J, Donald CL, Merits A, Kohl A, Varjak M. Differential effects of lipid biosynthesis inhibitors on Zika and Semliki Forest viruses. *Vet J* 2017; **230**: 62–64.

259 Merino-Ramos T, Vázquez-Calvo Á, Casas J, Sobrino F, Saiz J-C, Martín-Acebes MA. Modification of the Host Cell Lipid Metabolism Induced by Hypolipidemic Drugs Targeting the Acetyl Coenzyme A Carboxylase Impairs West Nile Virus Replication. *Antimicrob Agents Chemother* 2016; **60**: 307–315.

260 Gaunt ER, Cheung W, Richards JE, Lever A, Desselberger U. Inhibition of rotavirus replication by downregulation of fatty acid synthesis. *J Gen Virol* 2013; **94**: 1310–1317.

261 Monaco ME. Fatty acid metabolism in breast cancer subtypes. *Oncotarget* 2017; **8**: 29487–29500.

262 Chabowski A, Żendzian-Piotrowska M, Konstantynowicz K, Pankiewicz W, Mikłosz A, Łukaszuk B *et al.* Fatty acid transporters involved in the palmitate and oleate induced insulin resistance in primary rat hepatocytes. *Acta Physiol* 2013; **207**: 346–357.

263 Stahl A, Evans JG, Pattel S, Hirsch D, Lodish HF. Insulin causes fatty acid transport protein translocation and enhanced fatty acid uptake in adipocytes. *Dev Cell* 2002; **2**: 477–488.

264 Perez VM, Gabell J, Behrens M, Wase N, DiRusso CC, Black PN. Deletion of fatty acid transport protein 2 (FATP2) in the mouse liver changes the metabolic landscape by increasing the expression of PPARα-regulated genes. *J Biol Chem* 2020; **295**: 5737–5750.

265 Feng K, Ma R, Li H, Yin K, Du G, Chen X *et al.* Upregulated SLC27A2/FATP2 in differentiated thyroid carcinoma promotes tumor proliferation and migration. *J Clin Lab Anal* 2022; **36**: e24148.

266 Melton EM, Cerny RL, Watkins PA, DiRusso CC, Black PN. Human fatty acid transport protein 2a/very long chain acyl-CoA synthetase 1 (FATP2a/Acsvl1) has a preference in mediating the channeling of exogenous n-3 fatty acids into phosphatidylinositol. *J Biol Chem* 2011; **286**: 30670–30679.

267 Stuhlsatz-Krouper SM, Bennett NE, Schaffer JE. Substitution of alanine for serine 250 in the murine fatty acid transport protein inhibits long chain fatty acid transport. *J Biol Chem* 1998; **273**: 28642–28650.

268 Milger K, Herrmann T, Becker C, Gotthardt D, Zickwolf J, Ehehalt R *et al.* Cellular uptake of fatty acids driven by the ER-localized acyl-CoA synthetase FATP4. *J Cell Sci* 2006; **119**: 4678–4688.

269 Goc A, Niedzwiecki A, Rath M. Polyunsaturated ω-3 fatty acids inhibit ACE2-controlled SARS-CoV-2 binding and cellular entry. *Sci Rep* 2021; **11**: 5207.

270 Veglia F, Tyurin VA, Blasi M, De Leo A, Kossenkov AV, Donthireddy L *et al.* Fatty acid transport protein 2 reprograms neutrophils in cancer. *Nature* 2019; **569**: 73–78.

271 Sander WJ, O'Neill HG, Pohl CH. Prostaglandin E2 As a Modulator of Viral Infections. *Front Physiol* 2017; **8**: 89.

272 Numata M, Kandasamy P, Nagashima Y, Fickes R, Murphy RC, Voelker DR. Phosphatidylinositol inhibits respiratory syncytial virus infection. *J Lipid Res* 2015; **56**: 578–587.

273 Krammer J, Digel M, Ehehalt F, Stremmel W, Füllekrug J, Ehehalt R. Overexpression of CD36 and acyl-CoA synthetases FATP2, FATP4 and ACSL1 increases fatty acid uptake in human hepatoma cells. *Int J Med Sci* 2011; **8**: 599–614.

274 Wang TY, Liu M, Portincasa P, Wang DQ-H. New insights into the molecular mechanism of intestinal fatty acid absorption. *Eur J Clin Invest* 2013; **43**: 1203–1223.

275 Adeshakin AO, Liu W, Adeshakin FO, Afolabi LO, Zhang M, Zhang G *et al.* Regulation of ROS in myeloid-derived suppressor cells through targeting fatty acid transport protein 2 enhanced anti-PD-L1 tumor immunotherapy. *Cell Immunol* 2021; **362**: 104286.

276 Jay AG, Hamilton JA. The enigmatic membrane fatty acid transporter CD36: New insights into fatty acid binding and their effects on uptake of oxidized LDL. *Prostaglandins Leukot Essent Fatty Acids* 2018; **138**: 64–70.

277 Cancer Cell Line Encyclopedia (CCLE). https://sites.broadinstitute.org/ccle/ (accessed 4 Apr2022).

278 Ulmer H, Borena W, Rapp K, Klenk J, Strasak A, Diem G *et al.* Serum triglyceride concentrations and cancer risk in a large cohort study in Austria. *Br J Cancer* 2009; **101**: 1202–1206.

279 Lofterød T, Mortensen ES, Nalwoga H, Wilsgaard T, Frydenberg H, Risberg T *et al.* Impact of pre-diagnostic triglycerides and HDL-cholesterol on breast cancer recurrence and survival by breast cancer subtypes. *BMC Cancer* 2018; **18**: 654.

280 Niemi RJ, Braicu EI, Kulbe H, Koistinen KM, Sehouli J, Puistola U *et al.* Ovarian tumours of different histologic type and clinical stage induce similar changes in lipid metabolism. *Br J Cancer* 2018; **119**: 847–854.

281 Matsufuji T, Ikeda M, Naito A, Hirouchi M, Kanda S, Izumi M *et al.* Arylpiperazines as fatty acid transport protein 1 (FATP1) inhibitors with improved potency and pharmacokinetic properties. *Bioorg Med Chem Lett* 2013; **23**: 2560–2565.

282 Blackburn C, Guan B, Brown J, Cullis C, Condon SM, Jenkins TJ *et al.* Identification and characterization of 4-aryl-3,4-dihydropyrimidin-2(1H)-ones as inhibitors of the fatty acid transporter FATP4. *Bioorg Med Chem Lett* 2006; **16**: 3504–3509.

283 Balfour JA, Plosker GL. Rosiglitazone. *Drugs* 1999; **57**: 921–30; discussion 931-2.

284 Schaiff WT, Knapp FF (russ), Barak Y, Biron-Shental T, Nelson DM, Sadovsky Y. Ligand-Activated Peroxisome Proliferator Activated Receptor γ Alters Placental Morphology and Placental Fatty Acid Uptake in Mice. *Endocrinology* 2007; **148**: 3625–3634.

285 Cheung BM. Behind the rosiglitazone controversy. *Expert Rev Clin Pharmacol* 2010; **3**: 723–725.

286 Aravindhan S, Ejam SS, Lafta MH, Markov A, Yumashev AV, Ahmadi M. Mesenchymal stem cells and cancer therapy: insights into targeting the tumour vasculature. *Cancer Cell Int* 2021; **21**: 158.

287 Chen Q, Shou P, Zheng C, Jiang M, Cao G, Yang Q *et al.* Fate decision of mesenchymal stem cells: adipocytes or osteoblasts? *Cell Death Differ* 2016; **23**: 1128–1139.

288 Murano I, Barbatelli G, Parisani V, Latini C, Muzzonigro G, Castellucci M *et al.* Dead adipocytes, detected as crown-like structures, are prevalent in visceral fat depots of genetically obese mice. *J Lipid Res* 2008; **49**: 1562–1568.

289 Ferrante AW Jr. The immune cells in adipose tissue. *Diabetes Obes Metab* 2013; **15 Suppl 3**: 34–38.

290 Mehla K, Singh PK. Metabolic Regulation of Macrophage Polarization in Cancer. *Trends Cancer Res* 2019; **5**: 822–834.

291 Kwan A, Winder N, Atkinson E, Al-Janabi H, Allen RJ, Hughes R *et al.* Macrophages Mediate the Antitumor Effects of the Oncolytic Virus HSV1716 in Mammary TumorsMacrophage Response to Oncolytic Viruses in Mammary Tumors. *Mol Cancer Ther* 2021; **20**: 589–601.

292 Denton N, Chen C-Y, Hutzen B, Leddon J, Wang P-Y, Scott T *et al.* 518. Tumor Associated Macrophages Mitigate Oncolytic Herpes Simplex Virus Efficacy in Part Through TGF-β Signaling. *Mol Ther* 2016; **24**: S206–S207.

293 Liu Y-P, Suksanpaisan L, Steele MB, Russell SJ, Peng K-W. Induction of antiviral genes by the tumor microenvironment confers resistance to virotherapy. *Sci Rep* 2013; **3**: 2375.

294 Tan DQ, Zhang L, Ohba K, Ye M, Ichiyama K, Yamamoto N. Macrophage response to oncolytic paramyxoviruses potentiates virus-mediated tumor cell killing. *Eur J Immunol* 2016; **46**: 919–928.

295 Weisser SB, van Rooijen N, Sly LM. Depletion and reconstitution of macrophages in mice. *J Vis Exp* 2012; : 4105.

296 Scioli MG, Storti G, D'Amico F, Gentile P, Kim B-S, Cervelli V *et al.* Adipose-Derived Stem Cells in Cancer Progression: New Perspectives and Opportunities. *Int J Mol Sci* 2019; **20**. doi:10.3390/ijms20133296.

297 Yeh W-L, Tsai C-F, Chen D-R. Peri-foci adipose-derived stem cells promote chemoresistance in breast cancer. *Stem Cell Res Ther* 2017; **8**: 177.

298 Josiah DT, Zhu D, Dreher F, Olson J, McFadden G, Caldas H. Adipose-derived stem cells as therapeutic delivery vehicles of an oncolytic virus for glioblastoma. *Mol Ther* 2010; **18**: 377–385.

299 Brower V. Search and destroy: recent research exploits adult stem cells' attraction to cancer. *J Natl Cancer Inst* 2005; **97**: 414–416.

300 Power AT, Bell JC. Cell-based delivery of oncolytic viruses: a new strategic alliance for a biological strike against cancer. *Mol Ther* 2007; **15**: 660–665.

301 de Heredia FP, Gómez-Martínez S, Marcos A. Obesity, inflammation and the immune system. *Proc Nutr Soc* 2012; **71**: 332–338.

302 Stone TW, McPherson M, Gail Darlington L. Obesity and Cancer: Existing and New Hypotheses for a Causal Connection. *EBioMedicine* 2018; **30**: 14–28.

303 Preethika A, Suchetha KN. EFFECT OF FATTY ACID BASED FUNCTIONAL LIPIDOMICS IN WOMEN WITH BREAST CANCER. *Asian J Pharm Clin Res* 2019; : 138–141.

304 Vanneman M, Dranoff G. Combining immunotherapy and targeted therapies in cancer treatment. *Nat Rev Cancer* 2012; **12**: 237–251.

305 Spearman C. The method of Right and Wrong cases (Constant Stimuli) without Gauss's formulae. British Journal of Psychology; London, etc. 1908; **2**: 227.

306 Kärber G. Beitrag zur kollektiven Behandlung pharmakologischer Reihenversuche. *Naunyn-Schmiedebergs Archiv für experimentelle Pathologie und Pharmakologie* 1931; **162**: 480–483.

307 Qiu B, Simon MC. BODIPY 493/503 Staining of Neutral Lipid Droplets for Microscopy and Quantification by Flow Cytometry. *Bio Protoc* 2016; **6**. doi:10.21769/BioProtoc.1912.

308 Mangeot PE, Risson V, Fusil F, Marnef A, Laurent E, Blin J *et al.* Genome editing in primary cells and in vivo using viral-derived Nanoblades loaded with Cas9-sgRNA ribonucleoproteins. *Nat Commun* 2019; **10**: 45.

309 Robinson MD, McCarthy DJ, Smyth GK. edgeR: a Bioconductor package for differential expression analysis of digital gene expression data. *Bioinformatics* 2010; **26**: 139–140.

310 McCloskey CW, Goldberg RL, Carter LE, Gamwell LF, Al-Hujaily EM, Collins O *et al.* A new spontaneously transformed syngeneic model of high-grade serous ovarian cancer with a tumor-initiating cell population. *Front Oncol* 2014; **4**: 53.

CONTRIBUTIONS OF COLLABORATORS

The contents of this thesis would not be possible without the guidance and support from summer students, colleagues & external collaborators:

Curtis McCloskey and Carolina Ilkow generated the data shown in Figure 3D. The data shown in Figure 4 was generated by Carolina Ilkow & Theresa Falls. Data shown in Figure 9 & 10 was generated by Justin Mayer & Carolina Ilkow. The titers and IF images for VSVΔ51 & VACV in Figure 6 and the data shown in Figure 11A & Appendix Figure 4 was generated by Carolina Ilkow. Data shown in Figure 33A-C was generated by Justin Mayer.

All mouse work was assisted by technicians Christiano de Souza, Julia Petryk or Bradley Austin. A portion of the injections in Figure 42-44 were assisted by Joanna Poutou & Taylor Jamieson.

Titering assistance was provided by Joanna Poutou and Taylor Jamieson in Figure 3A-C, Serge Neault for MeV titering in Figure 6A and Sarah Tucker & Victoria Taylor for Figure 37B. Titer data in Figure 32B was generated by Shainyn Garrett. HSV, MeV and VACV virus stocks were generously provided by Kuan Zhang, Serge Neault & Brian Keller, respectively.

VLP generation and transduction was completed by Jaahnavi Dave in Figure 14.

The following was completed with the assistance of Victoria Taylor: RNA extraction, cDNA synthesis and qPCR plate set-up in Figure 15,23,27, 38-39, Appendix Figure 2; immunofluorescence imaging in Figure 19, 41B; cell growth data for Figure 8.

RNA sequencing analysis featured in Figures 18, 28 and 39 were completed by Reza Rezaei.

Data shown in Figure 20, 21, 33E, Appendix Figure 20 was generated with assistance from Emily Brown. B16-F10 IFNAR KO cells was made by Emily Brown.

Immunofluorescence images in Figure 24 was generated by Brenna Wylie.

Seahorse experiments were conducted by Christine Lawson (Tai Lab, University of Sherbrooke).

Flow cytometry assistance from Harsimrat Birdi for Figure 29, 40A.

Tumour processing for immunoprofiling experiments in Appendix II with assistance from Nouf Alluqmani, Joanna Poutou & Taylor Jamieson. Cell staining and flow cytometry analysis completed by Nouf Alluqmani.

Appendix Figures 11-13 and cytotoxicity assay in Appendix Figure 11 in Appendix III was completed with assistance from Ben McSweeney.

APPENDIX I – SUPPLEMENTARY FIGURES & TABLES

SUPPLEMENTARY FIGURES

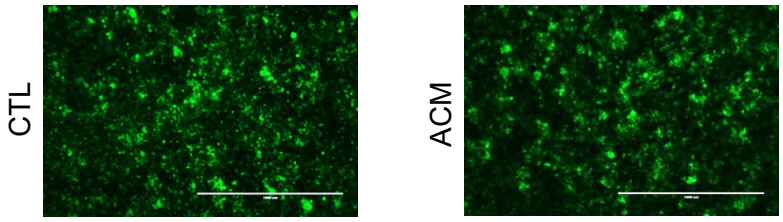

Appendix Figure 1: Pre-incubation of VACV with ACM does not significantly impact its infectivity. GFP-expressing VACV was pre-incubated in CTL media or ACM prior to using the inoculum for infection of OVCAR8 cells. OV infection was assessed by immunofluorescence microscopy (MOI 1, 48hpi) (n=1 biological). Scale bar represents 1000um.

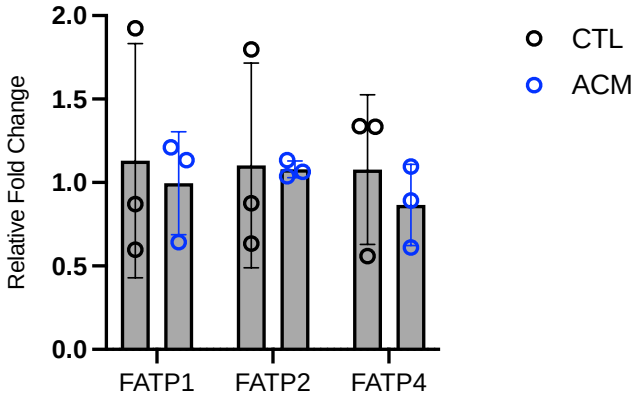

Appendix Figure 2: ACM does not alter FATP1, FATP2 or FATP4 expression. OVCAR8 cells receiving CTL media or ACM for 24hrs were harvested for RNA extraction. FATP expression relative to rPlp0 was determined by qPCR (n=3 biological). Error bars represent SD. 2-way ANOVA. Bonferroni's multiple comparison test.

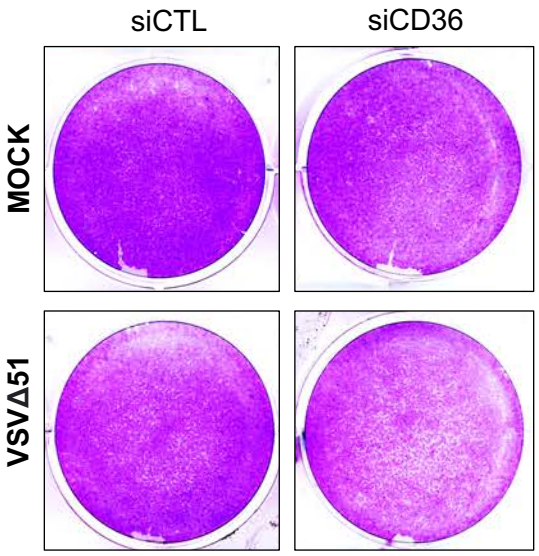

Appendix Figure 3: siRNA-mediated knockdown of CD36 increases sensitivity to OV-mediated cell death in OVCAR5 cells. OVCAR5 cells were transfected with the indicated siRNAs for 16hr prior to infection with VSVΔ51 (MOI 0.1). Cytotoxicity was determined with crystal violet staining 24hpi (n=1 biological).

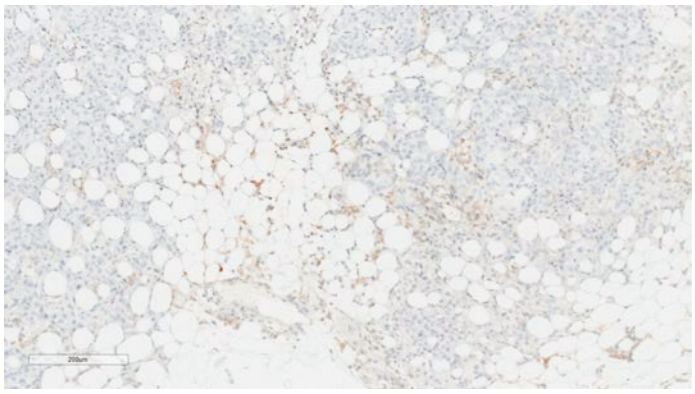

Appendix Figure 4: Macrophages are present in infiltrating adipose tissue of STOSE tumour. H&E staining of uninfected STOSE tumour derived from FP. Macrophages were visualized by anti-CD68 staining.

A

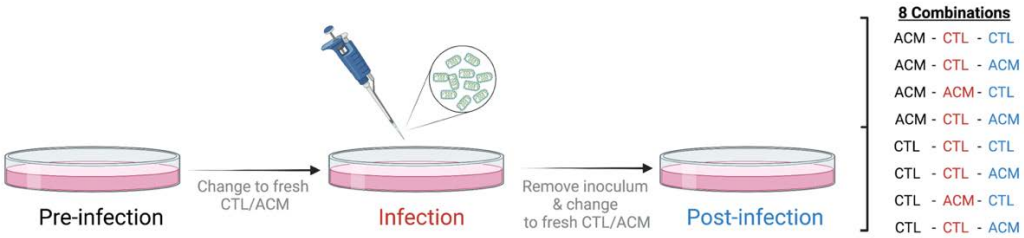

B

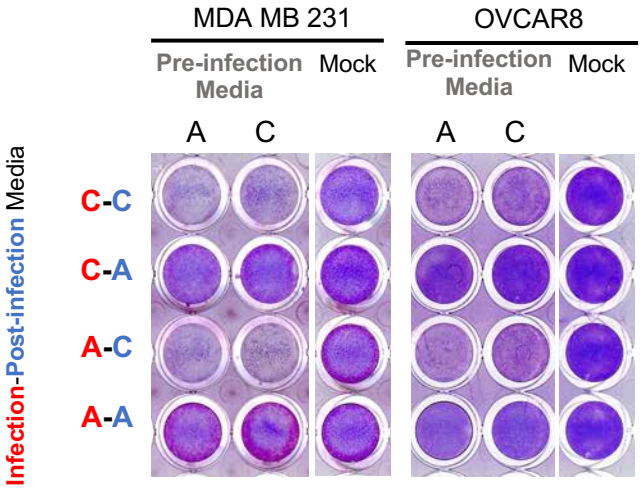

C

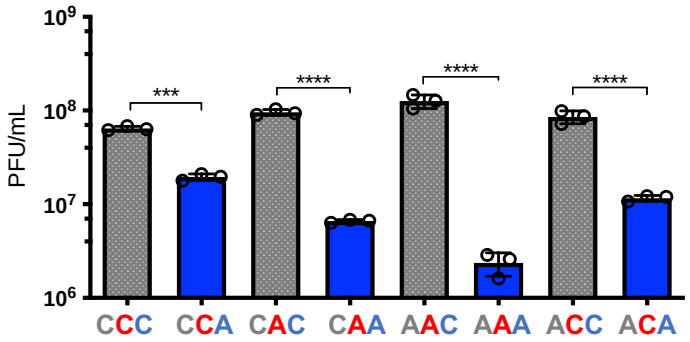

Appendix Figure 5: Evaluating the effect of the timing of ACM exposure on OV infection. OVCAR8 cells were cultured overnight ('pre-infection') in CTL media or ACM, and the media was changed to CTL or ACM media at the time of VSVΔ51 inoculation ('infection'; MOI 0.1). Following a 1hr period of infection, the media containing the inoculum was removed and changed to fresh CTL media or ACM ('post-infection') (A). The monolayer was stained with crystal violet to assess cytotoxicity 48 hpi) (B). Viral titer from OVCAR8 infected cells was quantified by plaque assay (n=3 biological replicates) (C). Representative crystal violet staining of n=2 biological replicates shown. Error bar represents SD. 1-way ANOVA, Tukey's multiple comparison test, ***p<0.001, ****p < 0.0001. All blue bar comparisons, CCC vs ACC, CAC vs ACC are ns. CCC vs CAC p<0.05. CCC vs AAC p<0.0001. CAC vs AAC p<0.05. AAC vs ACC p<0.01.

SUPPLEMENTARY TABLES

Supplemental Table 1: qPCR Primer Sequences

Gene	Forward Sequence (5'- 3')	Reverse Sequence (5'- 3')
MG1-L	GGCAAGAATCGTTCTTCAGC	TCGAAGCATTTGATGAGTGG
DDX58	TGTGGGCAATGTCATCAAAA	GAAGCACTTGCTACCTCTTGC
IFITM1	ACTCCGTGAAGTCTAGGGACA	GACCATAAGCCGAGACACTGT
STAT1	TGTATGCCATCCTCGAGAGC	AGACATCCTGCCACCTTGTG
OAS1	AAGGTGGTAAAGGGTGGCTC	GCTGTCTCCTAATTTCCTGG
CPT1a	CCTCCAGTTGGCTTATCGTG	TTCTTCGTCTGGCTGGACAT
FATP1	GCATCTGGGGAAAAGTTTGA	TGAGCCGTCCTTTGTAGTAG
FATP2	TGTCGCCAGAACTACAAGCA	TGAGAACGGAACGCCTGATT
FATP4	CCAGGCCTACCTTACTGGTG	GACTCGACGTGTTTTGTCCT
CD36	CGGA ACTGTGGGCTCAT	GGTCTCCAACTGGCATTAGA A
RPLP0	TTAAACCCTGCGTGGCAATCC	TTAAACCCTGCGTGGCAATCC

* All are human target genes (except MG1-L)

Supplemental Table 2: Antibodies used for immune-profiling flow cytometry experiment

	Marker	Fluorophore	Antibody dilution	Manufacturer & Catalog#
General	Viability	FV510	1:1000	BD Biosciences #564406
	Neutral lipids (Bodipy)	FITC	1:1000	Molecular Probes #D3922
	CD45	BV786	1:1000	BD Biosciences #564225
T-cell panel	CD3	AF700	1:50	BD Biosciences #564406
	CD4	V450	1:1000	BD Biosciences #560468
	CD8	PercPcy5.5	1:100	BD Biosciences #551162
	CD25	PE	1:100	BD Biosciences #12-0251-82
	CD69	BV605	1:100	BD Biosciences #563290
	PD-1	APC-Cy-7	1:50	BioLegend #135223
APC panel	CD11b	APC	1:100	BD Biosciences #553312
	CD19	BV421	1:100	BD Biosciences #562701
	CD86	ACPR700	1:100	BD Biosciences #565479
	F4/80	APC-Cy7	1:50	Biolegend #123118
	Gr1	PE	1:100	BD Biosciences #553128

APPENDIX II – ASSESSING THE INTRATUMOURAL IMMUNE-PROFILE OF OV-INFECTED DIET-INDUCED OBESE MICE

INTRODUCTION

The anti-tumour immune response is an important player in the therapeutic impact of OVs. Both innate and adaptive immune cells in the TME can mount powerful anti-tumour effects through inflammatory cytokine secretion and direct cytotoxic effects. In brief, the anti-tumour immune response begins with the local inflammation induced by OV infection. The release of danger signals and pro-inflammatory signals recruit immune cells to the site of the tumour, including antigen presenting cells like dendritic cells. Dendritic cells engulf tumour-associated antigens (TAAs) and present them to T cells to stimulate their activation. TAA-specific cytotoxic lymphocytes will exert its cytotoxic activity against the tumour through the secretion of pore-forming protein, perforin and, the cytolytic molecule, Granzyme B.[1] In addition to T cells recruitment, B cells are also recruited to exert anti-tumour functions though the secretion of effector cytokines and even direct cytotoxicity.[2] The anti-tumour immune response includes coordinated responses from innate immune cells such as macrophages. Macrophages exert their anti-tumour functions through the expression of inflammatory cytokines such as interleukin-12 and TNF-α.[3] Moreover, granulocytes are frequently found to be increased in the TME.[4] Together, the host-derived immune response to OV infection and the release of TAAs in the TME promote tumour de-bulking.

Obesity is a risk factor for cancer.[5] In obesity, low-grade chronic inflammation is derived from numerous events in the obese adipose tissue milieu. Excessive nutrient levels cause adipocyte hypertrophy and subsequent cell stress. The combination of an increasingly hypoxic environment and cell apoptosis due to cell stress results in the infiltration of inflammatory

mediators such as macrophages.[6] In fact, obese adipose tissue is often characterized to have crown-like structures – the distinct arrangement of macrophages surrounding dead adipocytes.[7]

Excess adipose tissue and adipocyte-derived lipids have been implicated in anti-cancer therapy resistance across a myriad of platforms including cancer immunotherapies, as described in the Introduction of this thesis. The impact of obesity-induced metabolic changes on the immune microenvironment in the context of OV therapy has not yet been studied. In the main body of this thesis, we showed that increased adiposity in the local TME can reduce intratumoural OV infection. We also showed that an increase in global adiposity with a high-fat diet (HFD) correspondingly increased local TME adiposity and induced similar effects on intratumoural OV titers. Here, we present the data from a preliminary study broadly determining the intratumoural immune landscape in the TME of HFD or regular diet (RD)-fed mice receiving oncolytic VSV (VSVΔ51) therapy. We assessed the presence of CD4+ and CD8+ T cell subsets including activation markers, CD25 and CD69, and the checkpoint molecule, PD-1. We also determined the presence of CD19+ B cells and the activation marker, CD86. Finally, we probed for the presence of myeloid cells including dendritic cells, macrophages as well as the presence of granulocytes.

MATERIALS & METHODS

VSVΔ51 propagation, purification & titering

Please refer to the method section in the main body of this thesis.

In vivo treatment regimen

EO771 tumours were seeded in the FP of C57BL/6 mice that were fed RD (T.08806) or HFD (TD.06414) (Teklad Custom Diet; Envigo) until substantial weight gain was observed in the HFD group (at least 20%). After the tumours reached sufficient size (~5mm x 5mm), they were intratumourally treated with 3 doses of VSVΔ51-Fluc (1E8 PFU) or equivalent volume of PBS every other day. After 10 days since the first treatment, the tumours were harvested.

Tumour processing & staining for flow cytometry analysis

The tumours were dissociated according to the manufacturer's instructions using a Tumour Dissociation kit (Miltenyi Biotec, cat#130-096-730) in conjunction with the gentleMACS™ Dissociator (Miltenyi Biotec). The samples were resuspended in 5mL RMPI [10% heat-inactivated (HI)-FBS] and passed through a 100μm cell strainer. Any solid pieces of tumour were forcefully squished through the strainer as much as possible. Another 5mL RMPI (10% HI FBS) was used to remove tumour cells along the sides of the tubes and passed through the cell strainer. The samples were centrifuged (500g, 5mins) and the supernatant was discarded. Red blood cells were lysed with 1-2mL (depending on the size of the pellet) Ammonia Chloride Potassium (ACK) lysis buffer (Gibco ACK Lysing Buffer, Thermo Scientific cat#A1049201) for 2mins and the reaction was

stopped by added 20mL of RMPI (10% HI-FBS). The samples were centrifuged (500g, 5mins) and the cells were resuspended in 5mL RMPI (10% HI-FBS). The cells were diluted (1:40) before being counted on an automated cell counter (Vi-CELL XR Cell Viability Analyzer; Beckman Coulter). 100µL of 1.5E7 viability cells/mL were transferred to a 96-well round bottom plate for flow staining. 100uL of flow buffer was added to the wells and the cells were spun down (500g, 5mins). The supernatant was discarded, and the cells were stained with 100µL of PBS containing viability dye. Following a 15min incubation in the dark, 100µL of FACS buffer was added to the wells and the cells were spun down (500g, 5mins). 25µL of Fc Block (Mouse BD Fc Block™; BD Biosciences) diluted 100X in flow buffer was added to the cells and incubated at 4°C in the dark for 5mins. An antibody mix was prepared with the indicated dilutions to a target volume of 25µL/sample. The cells were spun down (500g, 5mins) and incubated with the antibodies at 4°C for 30mins in the dark (antibodies are listed in Supplementary Table 2). The cells were washed twice with flow buffer and resuspended in 200µL of 1%PFA. Compensation beads (OneComp eBeads™ Compensation Beads; cat# 01-1111-41 Thermo Fisher Scientific) were used to prepare fluorescence minus one (FMO) controls. The samples were analyzed on the BD LSR Fortessa flow cytometer (Flow Cytometry and Virometry core facility, University of Ottawa) and the data was analyzed on FlowJo software (FlowJo, LLC, Ashland, OR).

RESULTS

Leukocytes

The percentage of infiltrating leukocytes and intracellular lipid accumulation in these leukocytes remained unphased by diet-induced obesity and/or OV infection (**Appendix Figure 6**).

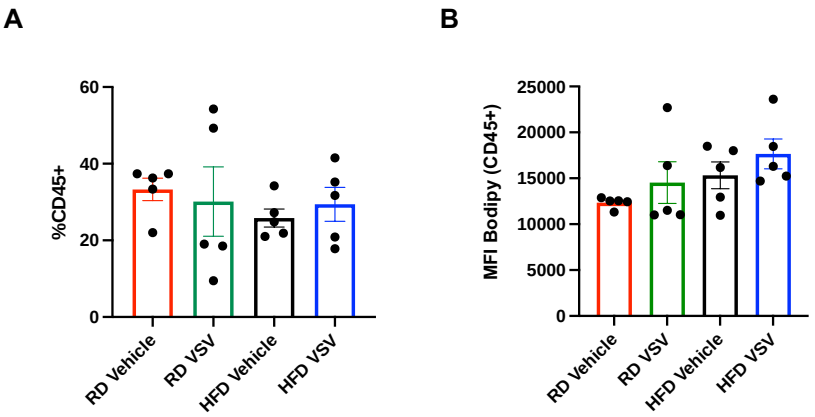

Appendix Figure 6: Leukocyte population in HFD or RD-fed mice infected with oncolytic VSV. %CD45+ of live cells (A) and the lipid accumulation in these cells as assessed by Bodipy staining (B) are shown. EO771 FP tumours. 1-way ANOVA Tukey's multiple comparisons test. Error bars denote SEM.

T-cells

We then sought to assess the presence of T cells and key T cell markers. HFD-fed mice showed an overall lower presence of T cells in the TME compared to their RD-fed counterparts as shown by the assessment of CD3+ cells from pooled data of uninfected or OV-infected groups ($p=0.0024$, two-tailed unpaired t-test). CD4+ subpopulation remained unchanged across different diet groups and in the presence or absence of OV infection. The infiltration of CD8+ cells is boosted by OV infection in both groups; however, this effect is only statistically significant in RD groups, with a stunted increase in HFD-fed mice ($p=0.2111$). The analysis of the T cell activation markers CD25 and CD69 revealed a decreasing trend upon OV infection in both HFD or RD groups. For CD25, this trend is statistically significant in CD4+ cells and is a less robust in CD8+ cells.

Contrastingly, CD69+ populations were more significantly decreased upon OV infection in CD8+ T cells compared to CD4+ where only a modest trend was observed. In both CD4+ and CD8+ populations, OV infection induced a decreasing trend in the expression of the immune checkpoint molecule PD1 in both HFD and RD-fed groups. This effect is more pronounced in RD groups than HFD groups (p= 0.0273 RD, p= 0.0744 HFD for CD4+ cells; p= 0.2786 for RD, p= 0.7100 in HFD for CD8+ cells). Lastly, T-cells do not significantly accumulate lipids depending on diet; however, the slight increasing trend in response to OV infection may be in response to stress due to infection (Appendix Figure 7).

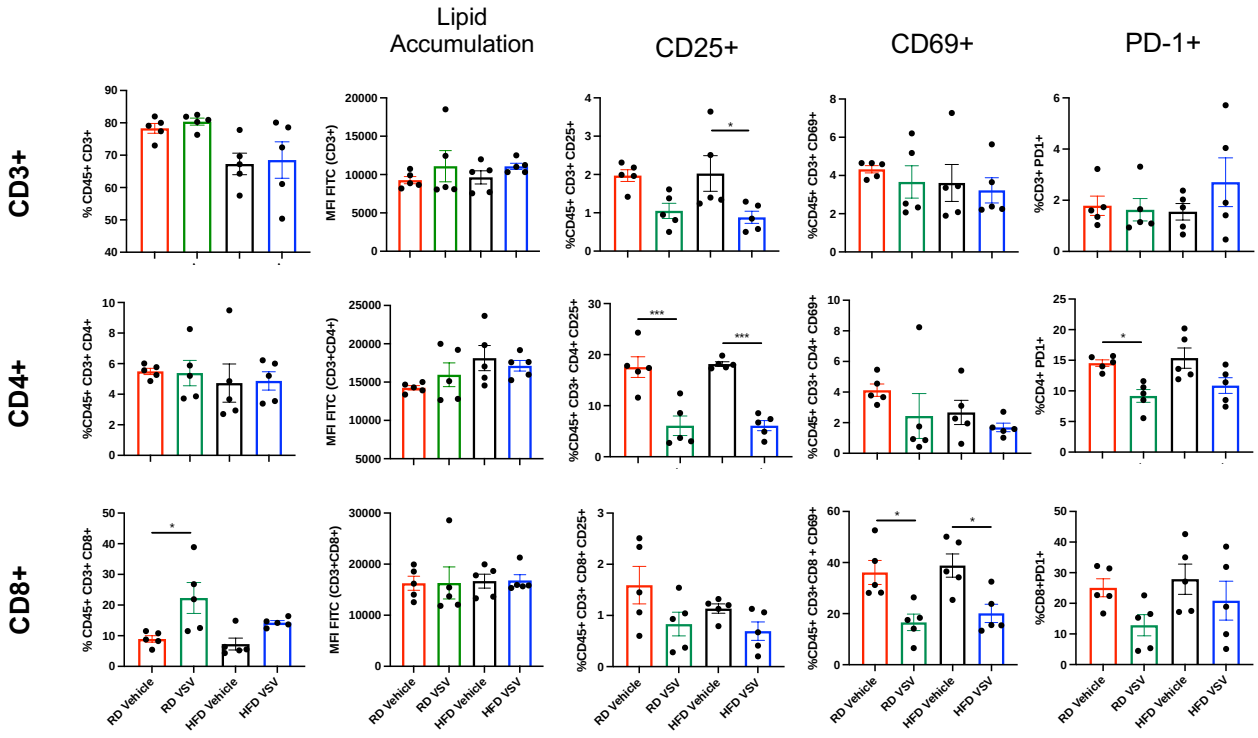

Appendix Figure 7: T cells in HFD or RD-fed mice infected with oncolytic VSV. CD4+ or CD8+ populations of CD45+CD3+ live cells were assessed for lipid accumulation by Bodipy staining, activation markers CD25 or CD69 and the expression of PD-1. EO771 FP tumours. 1-way ANOVA Tukey's multiple comparisons test. Error bars denote SEM. *p <0.05, ***p < 0.001

B cells

Although the presence of CD19+ B cells remained constant across diet and treatment groups, there was a differential response to B cell activation in response to OV treatment. In RD-fed mice, OV infection boosted B cell activation to near statistical significance (p=0.0514); however, HFD-fed mice remained unchanged (Appendix Figure 8).

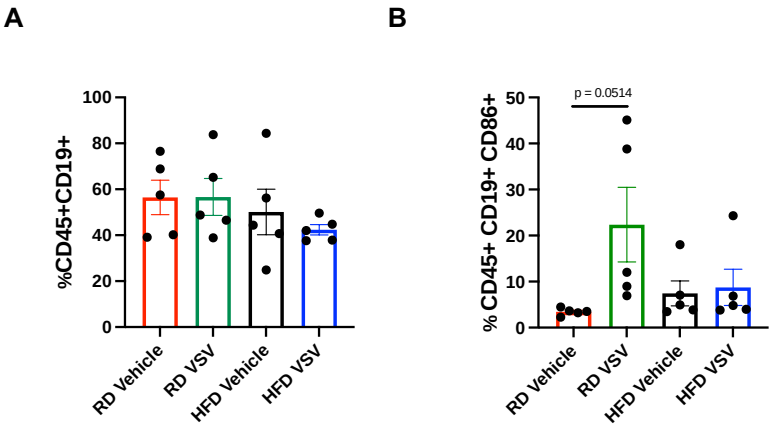

Appendix Figure 8: B cells in HFD or RD-fed mice infected with oncolytic VSV. %CD19 of CD45+ cells (A) and their activation as assessed by CD86 expression (B). EO771 FP tumours. 1-way ANOVA Tukey's multiple comparisons test. Error bars denote SEM.

Myeloid cells

No significant changes or trends were induced by diet or OV infection in dendritic cell, macrophage or granulocyte populations in our study (Appendix Figure 9).

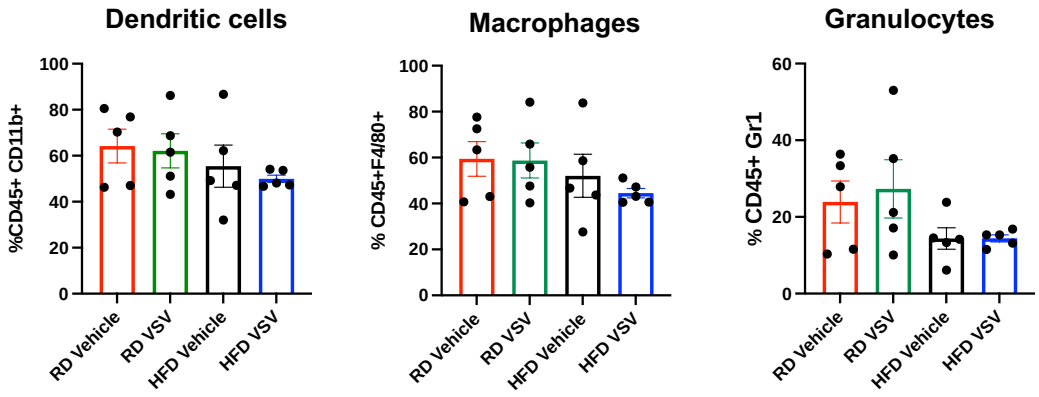

Appendix Figure 9: Other cell populations of interest in HFD or RD-fed mice infected with oncolytic VSV. CD11b+, F4/80+ or Gr1+ populations in CD45+ cells were assessed to determine the populations of DCs, macrophages and granulocytes respectively. EO771 FP tumours. 1-way ANOVA Tukey's multiple comparisons test. Error bars denote SEM.

DISCUSSION

Our findings indicated no changes in intracellular lipid accumulation in T cell populations. This aligns with reports by Ringel *et al*. investigating lipid accumulation in CD8+ T cells from HFD or RD-fed mice. The authors showed that the tumour cells respond to the abundance of lipids in the TME by upregulating pathways to mobilize free FAs; however, contrary to their expectations, CD8+ T cells did not. It is possible that in our models the lack of changes in T cell intracellular lipid accumulation is due to competitive uptake of FAs by tumour cells.

Across both uninfected and OV-infected groups, there was a decrease in the CD3+ population in HFD groups. Notably, the stunted increase CD8+ T cells in OV-infected HFD group aligns with findings presented by Ringel *et al.* showing a decrease in CD8+ T cell infiltration in HFD mice. The authors also showed that this was associated with a decrease in T cell function, as demonstrated by a decrease in the expression of Granzyme B in CD8+ T cells in a EO771 breast tumour model, the model used in our work.

Moreover, work by others have shown differential effects of HFD on CD8+PD1+ T cells in the tumour; however, in our studies no significant differences in CD8+PD1+ populations was observed due to differences in diet alone.[8,9] In OV-infected mice, CD4+PD1+ populations were decreased in RD-fed mice but this effect was dwarfed in HFD mice. This data suggests that HFD-fed mice may benefit from OV combination treatment with anti-PD-1 checkpoint blockade.

We also assessed T cell activation markers, CD25 and CD69. Contrary to our expectations, we observed that these populations were decreased following OV infection. It is possible that the diminished population of activated T cells is due to their death after carrying out the effector functions following OV infection.[10] Since the immunoprofiling experiment was conducted 10 days

post-infection, it is likely that we missed an earlier and more optimal time point for assessment of these markers. Future studies should determine CD25+ and CD69+ populations at earlier time points (~5 days).

There is limited information about the effects of obesity on B cells; however, there is some evidence to suggest that a HFD diminishes its functional capacity.[11,12] In our studies, we observed that B cell activation shows a trend towards distinct responses to OV infection in RD versus HFD mice (RD-VSV vs HFD-VSV p=0.2120). While RD-fed mice showed a notable increase in activation upon OV infection (p=0.0514), this effect was absent in HFD mice. The phenomenon of a dampened response to viral infection in obese animals have been previously reported by Kosaraju *et al.*, where they showed that mice fed a Western diet (higher fat content) had decreased antibodies against influenza infection compared to a RD control.[13] It is reasonable to speculate that the resistance to B cell activation in OV-infected HFD mice may stunt the anti-tumour effects of OVs by dampening the anti-tumour immune response.

We also evaluated the presence of dendritic cells, macrophages and neutrophils. Dendritic cells promote tissue recruitment and activation of macrophages in the TME.[14] In our studies, we did not observe any notable differences in the presence of dendritic cells or macrophages across diets or treatment groups. Granulocyte numbers in OV-infected mice showed an interesting trend. HFD mice have lower overall intratumoural granulocytes compared to RD-fed mice in pooled data of uninfected and infected groups (p=0.0273; two tailed, unpaired t-test). OV infection did not significantly alter granulocyte numbers in neither RD or HFD groups. Among granulocytes, neutrophils are noted to be the most abundant; however, other types of granulocytes make up the granulocyte population, including eosinophils, basophils and mast cells. In clinical evaluation

of neutrophils from obese individuals, neutrophils appear to be in a priming state and this has been attributed to furthering obesity pathogenesis.[15] Future work may evaluate the functional characteristics of tumour infiltrating neutrophils to determine how it shapes the TME of OV-infected tumours in HFD mice.

Our findings show numerous trends but lack statistical power. Future studies should aim to repeat and affirm our findings from this work. Nonetheless, our preliminary study is suggestive of HFD-induced tendency towards immunosuppression in the context of OV therapy. This is supported by a trend towards increased PD1+ populations in OV-infected HFD mice, a reduced population of CD8+ cells in OV-infected HFD mice, and the absence of OV infection mediated B cell activation in the HFD group.

Summary Table of Results

	RD	RD + OV	HFD	HFD + OV
CD3+ T cells	Normal %		↓*	
CD4+ T cells	No Δ	No Δ	No Δ	No Δ
CD4+ PD-1+	Normal %	↓*	Normal %	↓
CD8+ T cells	Normal %	↑*	Normal %	↑
CD8+ PD-1+	Normal %	↓	Normal %	↓ (lesser extent)
CD19+ B cells	No Δ	No Δ	No Δ	No Δ
CD19+CD86+ (B cell Activation)	Normal %	↑	Normal % (slightly higher than RD)	Normal % (slightly higher than RD)
Myeloid cells – Dendritic cells & macrophages	No Δ	No Δ	No Δ	No Δ
Myeloid cells – Granulocytes	Normal %		↓*	

*statistically significant trend; merged cells indicate pooled analysis

CONCLUDING STATEMENT

Obesity has global effects on the body, effecting endocrine, metabolic and even immune parameters.[16] Given that obesity is a risk factor for cancer, it is important to understand the unique intratumoural immune landscape in obese individuals receiving immunotherapies, including OV therapy. Our preliminary study broadly assessing the intratumoural immune profile of OV-infected tumours from HFD or RD-fed mice demonstrated that diet-induced obesity can alter the immune response to OV infection. Future studies will be focused on validating our findings and determining the effect of diet-induced obesity on OV mediated tumour control and overall survival.

REFERENCES

1 Achard C, Surendran A, Wedge M-E, Ungerechts G, Bell J, Ilkow CS. Lighting a Fire in the Tumor Microenvironment Using Oncolytic Immunotherapy. *EBioMedicine* 2018; **31**: 17–24.

2 Sarvaria A, Madrigal JA, Saudemont A. B cell regulation in cancer and anti-tumor immunity. *Cell Mol Immunol* 2017; **14**: 662–674.

3 Poh AR, Ernst M. Targeting Macrophages in Cancer: From Bench to Bedside. *Front Oncol* 2018; **8**: 49.

4 Kamir J. Hiam- Galvez BMAAMHS. Systemic immunity in cancer. *Nature Reviews Cancer* 2021; **21**: 345–359.

5 De Pergola G, Silvestris F. Obesity as a major risk factor for cancer. *J Obes* 2013; **2013**: 291546.

6 Woodall MJ, Neumann S, Campbell K, Pattison ST, Young SL. The Effects of Obesity on Anti-Cancer Immunity and Cancer Immunotherapy. *Cancers* 2020; **12**. doi:10.3390/cancers12051230.

7 Murano I, Barbatelli G, Parisani V, Latini C, Muzzonigro G, Castellucci M *et al.* Dead adipocytes, detected as crown-like structures, are prevalent in visceral fat depots of genetically obese mice. *J Lipid Res* 2008; **49**: 1562–1568.

8 Ringel AE, Drijvers JM, Baker GJ, Catozzi A, García-Cañaveras JC, Gassaway BM *et al.* Obesity Shapes Metabolism in the Tumor Microenvironment to Suppress Anti-Tumor Immunity. *Cell* 2020; **183**: 1848-1866.e26.

9 Wang Z, Aguilar EG, Luna JI, Dunai C, Khuat LT, Le CT *et al.* Paradoxical effects of obesity on T cell function during tumor progression and PD-1 checkpoint blockade. *Nat Med* 2019; **25**: 141–151.

10 Lu B, Finn OJ. T-cell death and cancer immune tolerance. *Cell Death Differ* 2008; **15**: 70–79.

11 Srikakulapu P, McNamara CA. B Lymphocytes and Adipose Tissue Inflammation. *Arterioscler Thromb Vasc Biol* 2020; **40**: 1110–1122.

12 Pham TD, Chng MHY, Roskin KM, Jackson KJL, Nguyen KD, Glanville J *et al.* High-fat diet induces systemic B-cell repertoire changes associated with insulin resistance. *Mucosal Immunol* 2017; **10**: 1468–1479.

13 Kosaraju R, Guesdon W, Crouch MJ, Teague HL, Sullivan EM, Karlsson EA *et al.* B Cell Activity Is Impaired in Human and Mouse Obesity and Is Responsive to an Essential Fatty Acid upon Murine Influenza Infection. *J Immunol* 2017; **198**: 4738–4752.

14 Stefanovic-Racic M, Yang X, Turner MS, Mantell BS, Stolz DB, Sumpter TL *et al.* Dendritic cells promote macrophage infiltration and comprise a substantial proportion of obesity-associated increases in CD11c+ cells in adipose tissue and liver. *Diabetes* 2012; **61**: 2330–2339.

15 Brotfain E, Hadad N, Shapira Y, Avinoah E, Zlotnik A, Raichel L *et al.* Neutrophil functions in morbidly obese subjects. *Clin Exp Immunol* 2015; **181**: 156–163.

16 de Heredia FP, Gómez-Martínez S, Marcos A. Obesity, inflammation and the immune system. *Proc Nutr Soc* 2012; **71**: 332–338.

APPENDIX III – EVALUATING THE THERAPEUTIC BENEFIT OF GOT2 METABOLITE SUPPLEMENTATION WITH OV THERAPY

PREFACE

This section showcases the preliminary work evaluating the therapeutic benefit of supplementation with glutamate oxaloacetate transaminase 2 (GOT2) metabolites, α-ketoglutarate and L-aspartate, on OV therapy. This work was largely inspired by the elegant work of *Wang et al.*, where the authors showed that GOT2 metabolites can enhance virus mediated cytotoxicity in an interferon-independent manner.[1] The findings from this work support the reoccurring theme in this thesis showcasing that metabolites can greatly influence OV infection and OV-mediated cell death. Herein, we present the therapeutic impact of supplementation with GOT2 metabolites in an effort to boost the anti-cancer effects of OV therapy.

INTRODUCTION

Cancer metabolism is an emerging hallmark of cancer.[2] The rapid growth and proliferation of tumours results a significantly altered metabolic signature in the TME.[3] Glucose and glutamine are the primary carbon sources in mammalian cells; however, in cancer, glucose is typically directed away from the TCA cycle, as postulated by the Warburg effect. When glucose is low, cells typically shift to glutominolysis to maintain ATP and NADP production by the TCA cycle.[4]

Glutominolysis is process of converting glutamine into TCA cycle metabolites and is considered a hallmark of cancer. Glutamine is critical for many fundamental cellular processes, including the generation of anti-oxidants, synthesis of non-essential amino acids, purines, pyrimidines, FA synthesis and activation of cell signaling.[5] Glutamine is first hydrolyzed into glutamate by an enzyme, glutaminase. The glutamate can be further metabolized by 3 different enzymes, one of which is GOT2. GOT2 functions as a homodimer involved in the reversible transamination between oxaloacetic acid and L-glutamic acid into α-ketoglutarate and L-aspartate.[6] α-ketoglutarate and L-aspartate molecules then go on to feed bioenergetic demands of the cell or contribute to anabolic pathways.[7]

A recent study by Wang *et al.* showed that long non-coding RNA (lncRNA)-ACOD1 is expressed in response to virus infection independent of Type I interferon. This effect was broadly observed across numerous viruses. lncRNAs are conventionally known for their roles in epigenetic regulation; however, their roles in various other biological functions are now beginning to unfold.[8] In knockout studies, lncRNA-ACOD1 deletion protected mice from viral lethality. The effect of lncRNA-ACOD1 mediated virus potentiation was attributed to its direct binding of GOT2 and a corresponding increase in GOT2 catalytic activity. The researchers show that the lncRNA-ACOD1

or GOT2 overexpression or the administration of GOT2 metabolites, L-aspartate and α-ketoglutarate, increased viral burden.[1] Thus, this publication invited conjecture on the therapeutic benefits of GOT2 metabolites where a high viral load is desirable, such as OV therapy.

Viruses are obligate intracellular parasites and as such, the metabolites they require for their successful replication are derived from the host cell. They rely on host resources to produce viral proteins, nucleic acids and membranes to form viral particles.[9] The mechanisms employed by viruses to exploit and manipulate the host cell environment for progeny production is largely elusive and is only beginning to unfold. Given that glutominolysis is an important player in cancer metabolism, we sought to determine if GOT2 metabolites, α-ketoglutarate and L-aspartate, can be exploited to potentiate the therapeutic impact of OVs.

MATERIALS & METHODS

Cell lines & OV stocks

4T1 murine breast cancer cell line and 786O human renal cell carcinoma cell lines were acquired from ATCC. They were cultured in DMEM (supplemented with 10% FBS). VSVΔ51-GFP stock was acquired as described in the methods below. Oncolytic Vaccinia stocks, JX-594 and Cope B14KO, were generously provided by Dr. Brian Keller and Brianna Samson (Master's student in the Bell Lab), respectively.

VSVΔ51-GFP propagation, purification & titering

Please refer to the method section in the main body of this thesis.

Titering VACV

Please refer to the method section in the main body of this thesis.

Generating AKG & L-Asp supplemented media

α-ketoglutaric acid (Sigma-Aldrich K1128-100G) or L-aspartic acid (Sigma-Aldrich A7219-100G) were dissolved into DMEM media (ThermoFisher Scientific) with constant stirring. Once all of the powder was dissolved, the pH of the solution was adjusted to 7.4 with 10N NaOH in a dropwise fashion. The supplemented media was sterile filtered (0.22μM Millipore® Stericup® filter; Millipore Sigma). A 400mM stock of α-ketoglutarate and a 37mM stock of L-aspartate was prepared and stored at 4°C until use. The media was supplemented with fresh 10% FBS before adding to cells. Cells were pre-incubated with supplemented media for at least 4hrs before infection with an OV.

Crystal violet staining

Cells were stained with crystal violet (0.5% crystal violet in 80% MeOH in water) for 40mins on a benchtop rocker. The crystal violet was removed, the monolayer was gently washed with tap water twice and the plate was left to air dry overnight. Qualitative analysis of the stained plates was achieved by scanning the plates.

Microscopy

Brightfield and GFP filter images were acquired with an AMG EVOS fluorescence microscope (Advanced Microscopy Group, Washington, USA).

RESULTS

To begin our studies, we chose cell lines and OV platforms that would provide a broad platform for testing our hypothesis. We chose 2 cell lines that are well characterized to be highly resistant to OV infection – 4T1 and 786O. 4T1 is a murine breast tumour cell line. 786O is a human renal cell carcinoma. With the use of these 2 cell lines, we were able to simultaneously test our hypothesis across 2 distinct tumour models and across 2 species. By using resistant models, we hoped to more readily capture any potentiating effects on OV infection. Moreover, we tested 2 different species of OVs – Vaccinia virus (Copenhagen, Wyeth) and Rhabdovirus (VSV). These viruses have unique and distinct methods of infection, replication and defences against anti-viral mechanisms.[10,11]

786O cells are strongly resistant to many OV platforms. This is at least in part due to its robust interferon response to viral infection.[12,13] In an earlier section of this thesis, we showed that they are extremely resistant to VSVΔ51 infection (**Figure 21**). When 786O cells were supplemented with α-ketoglutarate they more susceptible to VSVΔ51-mediated cell death than in controls (**Appendix Figure 10A**). When the supernatant was titered by plaque assay, we observed a ~2.6X increase in infectious particles (**Appendix Figure 10B**).

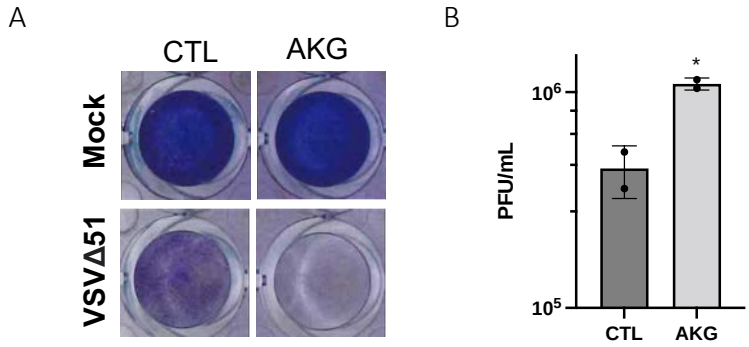

Appendix Figure 10: α-ketoglutarate supplementation enhances oncolytic VSV-mediated cytotoxicity and titers in 786O cells. 786O cells were cultured α-ketoglutarate (AKG) supplemented media (40mM) for at least 4hrs prior to infection with VSVΔ51 (MOI 1). The monolayer was stained for crystal violet for cytotoxicity analysis (72hpi; n=3 biological replicates) (A). Supernatant was collected for plaque assay (48hpi; n=2 biological replicates) (B). Unpaired, two-tailed t-test.

In 4T1 cells, a similar pattern of α-ketoglutarate-mediated potentiation of OV infection was observed. We observed a disruption in the cell monolayer of uninfected controls receiving the highest concentration of α-ketoglutarate. Viruses are obligate intracellular parasites that require relatively healthy cells for successful infection. Given the successful infection of 4T1 cells at this concentration of α-ketoglutarate and anecdotal evidence for the lifting of 4T1 cells more readily than other cell lines in overconfluent conditions, we hypothesize that this disruption to the monolayer is likely due to cell overconfluency. Moreover, preliminary studies with VSV-infected L-aspartate-supplemented cells showed a decreasing trend in cell viability, with an anomaly at 20mM concentration. The highest concentration of L-aspartate (34mM) induced the greatest decrease in cell viability (p=0.2698) (**Appendix Figure 11**).

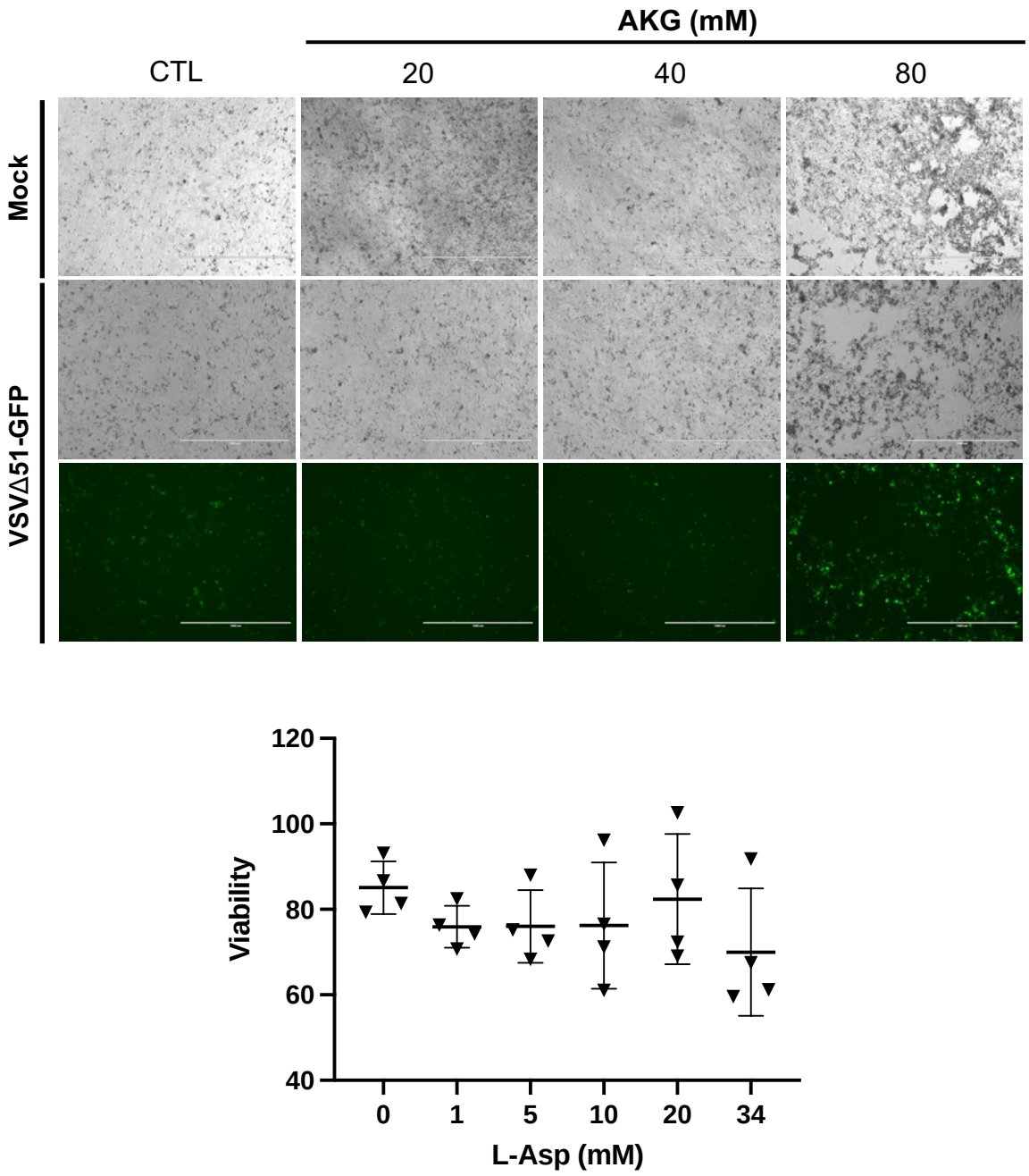

Appendix Figure 11: α-ketoglutarate supplementation enhances oncolytic VSV infection in 4T1 cells. 4T1 cells were cultured α-ketoglutarate (AKG) supplemented media at indicated concentrations for at least 4hrs prior to infection with VSVΔ51 (MOI 3). The infection was visualized by immunofluorescence microscopy (24hpi). Representative images shown (n=3 technical replicates) (A). L-aspartate (L-Asp)-receiving cells were infected with VSVΔ51 (MOI 1) and assessed for viability (n=4 technical replicates) (B). Normalized to mock to L-aspartate concentration controls. 1-way ANOVA, Dunnet's multiple comparison test. Scale bar indicates 1000μm.

Next, we evaluated the effect of GOT2 metabolite supplementation on oncolytic VACV infection. α-ketoglutarate-receiving 4T1 cells were more susceptible to VACV mediated cell-death than control cells (Appendix Figure 12A). This correlated with a trend in increasing VACV titers (Appendix Figure 12B). When the media was supplemented with increasing concentrations of L-aspartate, a similar trend was observed. L-aspartate supplementation boosted VACV titers (Appendix Figure 12C). Notably, the highest concentration of L-Asp tested (37mM) showed a ~7X increase in titer ($p=0.0591$). L-aspartate supplementation also showed an increase in VACV infection in 786O cells, as observed by an immunofluorescence analysis of GFP from GFP-expressing oncolytic VACV (Appendix Figure 13). An important caveat of this experiment is the lack of mock infected cells. Given the intact monolayer in infected cells, we presume that L-aspartate supplementation does not have toxic effects on these cells. Future studies will include this important control.

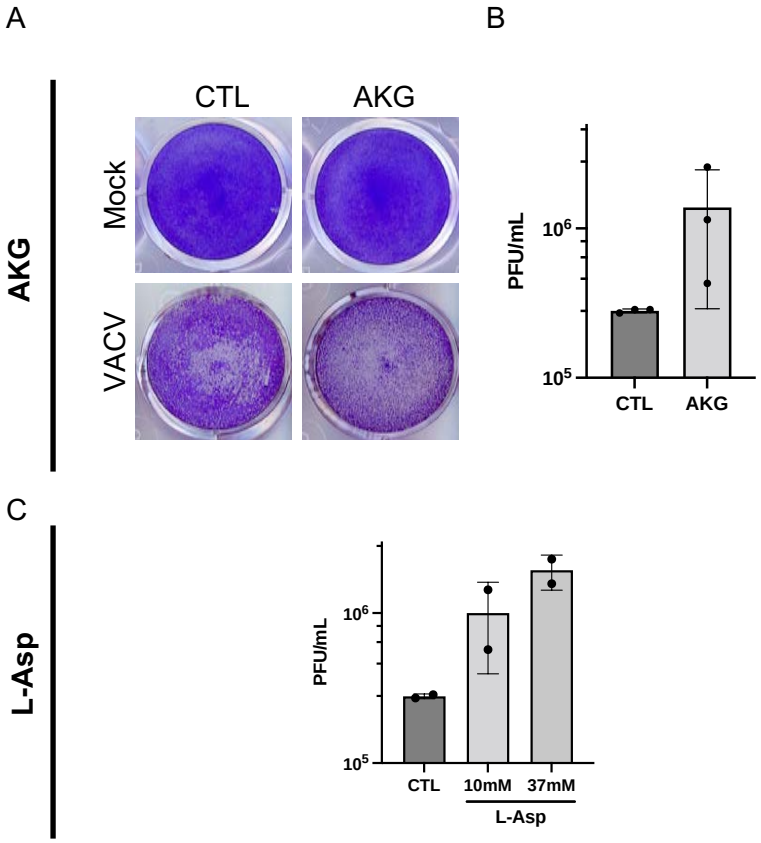

Appendix Figure 12: α-ketoglutarate or L-aspartate supplementation enhances oncolytic VACV-mediated cytotoxicity and titers in 4T1 cells. 4T1 cells were supplemented with α-ketoglutarate (AKG; 40mM) and infected with Cope B14KO (MOI 1, 24hrs). The monolayer was stained with crystal violet to assess cytotoxicity (A). Titers from AKG-receiving JX-594-infected cells (MOI 1, 48hpi) are shown in (B) (n=3 biological replicates). L-aspartate (L-Asp) supplemented cells were infected with JX-594 (MOI 1, 48hpi) (n=2 biological replicates) (C). Cells were incubated in supplemented media for at least 4hrs before infection with OV. Titers were determined by plaque assay. Ns; Unpaired, two tailed t-test or one-way ANOVA (Dunnet's multiple comparison test).

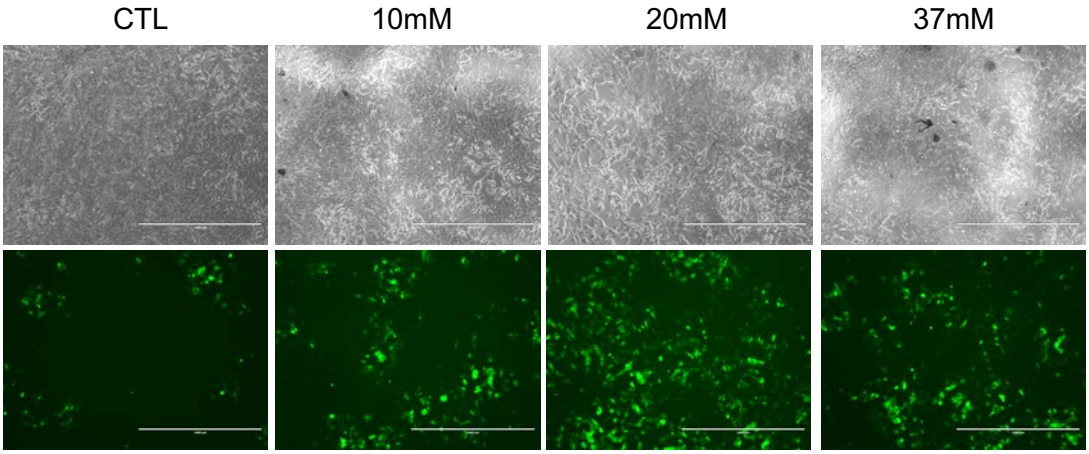

Appendix Figure 13: L-aspartate supplementation enhances oncolytic VACV infection in 786O cells. 786O cells supplemented with L-aspartate at the indicated concentrations and infected with JX-594 (MOI 1). The infection was visualized by immunofluorescence microscopy (24hpi). Representative images shown (n=3 technical). Scale bar indicates 1000µm.

DISCUSSION

Here, we showed that supplementation with GOT2 metabolites α-ketoglutarate and L-aspartate can potentiate the anti-tumour effects of OVs. Our data suggests that this is at least in part due to an enhancement in OV infection. This effect was observed across both GOT2 metabolites (α-ketoglutarate and L-Asp), 2 unique OV platforms and 2 disparate tumour cell lines.

In some cases, the replication of OVs was very modest, such as in the case of a mere 2.6X increase in VSV titer in α-ketoglutarate supplemented 786O cells (**Appendix Figure 9**). Given that this is below the threshold for titering error (<3X), the data suggested that some mechanism, other than enhanced OV infection, is contributing to the observed cytotoxic effects. Interestingly, α-ketoglutarate has been reported to have anti-tumourigenic properties although the mechanism of action remains elusive.[7] Accumulation of this TCA intermediate in the primary tumour was correlated with an anti-metastatic effect in an *in vivo* murine breast tumour model.[14] There is

evidence to suggest that α-ketoglutarate can alleviate hypoxia to potentially alleviate therapy resistance in certain contexts.[15,16] Given that reactive oxygen species are abundant in tumours, the antioxidative role of α-ketoglutarate can be beneficial in mitigating the pro-tumorigenic roles of reactive oxygen species in the TME.

Future studies will include *in vivo* evaluation of OV combinatorial therapy with α-ketoglutarate and L-aspartate supplementation. This will allow us to determine how GOT2 metabolites may influence stromal cells in the TME, such as T-cells. Klysz *et al.* showed that when culture media was lacking an α-ketoglutarate precursor, glutamine, Tregs, an immunosuppressive T-cell subset, became prevalent despite the fact that cells were differentiated in the appropriate cytokines to produce Th1 cells.[17] It is possible that α-ketoglutarate supplementation in combinatorial approaches with OVs may simultaneously enhance OV-mediated tumour cell killing and promote anti-tumour T-cells in the TME.

These studies served as a preliminary evaluation of the potential therapeutic impact of OV combination treatment with α-ketoglutarate and L-Asp. Future studies will aim to encode GOT2 or lncRNA-ACOD1 or both into an oncolytic VACV platform. VACV is of particular interest due to its ease of genetic manipulation and a demonstrated reliance on glutamine, or more specifically its catabolite α-ketoglutarate, to generate VACV viral products.[18] These OVs will enhance intracellular α-ketoglutarate pools to ultimately enhance VACV replication and VACV-mediated cell death. This approach can be particularly advantageous in tumours with low glutamine pools or low GOT2 expression. In tumours where GOT2 expression is high, an OV expressing lncRNA-ACOD1 alone can be used to boost GOT2 catalytic activity. Thus, the utility of these engineered viruses can be tailored to the metabolic features of the tumour in question. In some tumours, α-ketoglutarate

has been shown to enhance growth while in others it has been shown to prohibit its proliferation.[19] By employing viruses that preferentially replicate in cancer cells, we can mitigate the potential risks of α-ketoglutarate-derived tumour growth since these OV-infected cells will eventually succumb to the viral load.

CONCLUDING STATEMENT

Our preliminary work shows that combining GOT2 metabolites with OV infection can have beneficial anti-tumour effects. By using an approach that seeks to enhance the bioavailability of naturally occurring cellular metabolites, contrasting the conventional approach of introducing cytotoxic agents, we can enhance OV therapeutic efficacy while mitigating risk. Future work will focus on building on our supplementation studies and generating GOT2 and/or lncRNA-ACOD1 expressing OVs.

REFERENCES

1 Wang P, Xu J, Wang Y, Cao X. An interferon-independent lncRNA promotes viral replication by modulating cellular metabolism. *Science* 2017; **358**: 1051–1055.

2 Hanahan D, Weinberg RA. Hallmarks of cancer: the next generation. *Cell* 2011; **144**: 646–674.

3 Hsu PP, Sabatini DM. Cancer cell metabolism: Warburg and beyond. *Cell* 2008; **134**: 703–707.

4 Glutaminolysis. doi:10.1016/B978-0-12-396521-9.00014-0.

5 Yang L, Venneti S, Nagrath D. Glutaminolysis: A Hallmarkof Cancer Metabolism. *Annu Rev Biomed Eng* 2017; **19**: 163–194.

6 Toney MD. Aspartate aminotransferase: an old dog teaches new tricks. *Arch Biochem Biophys* 2014; **544**: 119–127.

7 Vatrinet R, Leone G, De Luise M, Girolimetti G, Vidone M, Gasparre G *et al.* The α-ketoglutarate dehydrogenase complex in cancer metabolic plasticity. *Cancer Metab* 2017; **5**: 3.

8 Wu Z, Liu X, Liu L, Deng H, Zhang J, Xu Q *et al.* Regulation of lncRNA expression. *Cell Mol Biol Lett* 2014; **19**: 561–575.

9 Merrick AE, Ilett EJ, Melcher AA. JX-594, a targeted oncolytic poxvirus for the treatment of cancer. *Curr Opin Investig Drugs* 2009; **10**: 1372–1382.

10 McFadden G. Poxvirus tropism. *Nat Rev Microbiol* 2005; **3**: 201–213.

11 Lichty BD, Power AT, Stojdl DF, Bell JC. Vesicular stomatitis virus: re-inventing the bullet. *Trends Mol Med* 2004; **10**: 210–216.

12 Bastin D, Aitken AS, Pelin A, Pikor LA, Crupi MJF, Huh MS *et al.* Enhanced susceptibility of cancer cells to oncolytic rhabdo-virotherapy by expression of Nodamura virus protein B2 as a suppressor of RNA interference. *J Immunother Cancer* 2018; **6**: 62.

13 Le Boeuf F, Diallo J-S, McCart JA, Thorne S, Falls T, Stanford M *et al.* Synergistic interaction between oncolytic viruses augments tumor killing. *Mol Ther* 2010; **18**: 888–895.

14 Atlante S, Visintin A, Marini E, Savoia M, Dianzani C, Giorgis M *et al.* α-ketoglutarate dehydrogenase inhibition counteracts breast cancer-associated lung metastasis. *Cell Death Dis* 2018; **9**: 1–18.

15 MacKenzie ED, Selak MA, Tennant DA, Payne LJ, Crosby S, Frederiksen CM *et al.* Cell-permeating alpha-ketoglutarate derivatives alleviate pseudohypoxia in succinate dehydrogenase-deficient cells. *Mol Cell Biol* 2007; **27**: 3282–3289.

16 Muz B, de la Puente P, Azab F, Azab AK. The role of hypoxia in cancer progression, angiogenesis, metastasis, and resistance to therapy. *Hypoxia (Auckl)* 2015; **3**: 83–92.

17 Klysz D, Tai X, Robert PA, Craveiro M, Cretenet G, Oburoglu L *et al.* Glutamine-dependent α-ketoglutarate production regulates the balance between T helper 1 cell and regulatory T cell generation. *Sci Signal* 2015; **8**: ra97.

18 Fontaine KA, Camarda R, Lagunoff M. Vaccinia virus requires glutamine but not glucose for efficient replication. *J Virol* 2014; **88**: 4366–4374.

19 Rzeski W, Walczak K, Juszczak M, Langner E, Pożarowski P, Kandefer-Szerszeń M *et al.* Alpha-ketoglutarate (AKG) inhibits proliferation of colon adenocarcinoma cells in normoxic conditions. *Scand J Gastroenterol* 2012; **47**: 565–571.

APPENDIX IV – DETECTION OF SARS-COV-2 RECEPTOR-BINDING DOMAIN ANTIBODY USING A HiBiT-BASED BIOREPORTER

PREFACE

In March 2020, the world was swept by Coronavirus disease 2019 (COVID19) caused by severe acute respiratory syndrome coronavirus 2 (SARS-CoV-2) infections. In light of the COVID19 global pandemic, the Bell and Ilkow labs pivoted to COVID19 research in an effort to contribute to global efforts to understand this lethal virus and develop an effective vaccine platform.

The following publication showcases a concerted effort by members of the Bell and Ilkow labs to generate a biosensor that can quickly and reliably quantify anti-SARS-CoV-2 antibodies, including from patient serum samples. The publication is included in this doctoral dissertation with written permission from JoVE.

jove

Detection of SARS-CoV-2 Receptor-Binding Domain Antibody using a HiBiT-Based Bioreporter

Reza Rezaei[1,2], **Abera Surendran**[1,2], **Ragunath Singaravelu**[1,2], **Taylor R. Jamieson**[1,2], **Parisa Taklifi**[3], **Joanna Poutou**[1,2], **Taha Azad**[1,2], **Carolina S. Ilkow**[1,2]

[1] Ottawa Hospital Research Institute [2] Department of Biochemistry, Microbiology and Immunology, University of Ottawa [3] Department of Biotechnology, University of Tehran

Corresponding Author

Carolina S. Ilkow
cilkow@ohri.ca

Citation

Rezaei, R., Surendran, A., Singaravelu, R., Jamieson, T.R., Taklifi, P., Poutou, J., Azad, T., Ilkow, C.S. Detection of SARS-CoV-2 Receptor-Binding Domain Antibody using a HiBiT-Based Bioreporter. *J. Vis. Exp.* (174), e62488, doi:10.3791/62488 (2021).

Date Published

August 12, 2021

DOI

10.3791/62488

URL

jove.com/video/62488

Abstract

The emergence of the COVID-19 pandemic has increased the need for better serological detection methods to determine the epidemiologic impact of severe acute respiratory syndrome coronavirus 2 (SARS-CoV-2). The increasing number of SARS-CoV-2 infections raises the need for better antibody detection assays. Current antibody detection methods compromise sensitivity for speed or are sensitive but time-consuming. A large proportion of SARS-CoV-2-neutralizing antibodies target the receptor-binding domain (RBD), one of the primary immunogenic compartments of SARS-CoV-2. We have recently designed and developed a highly sensitive, bioluminescent-tagged RBD (NanoLuc HiBiT-RBD) to detect SARS-CoV-2 antibodies. The following text describes the procedure to produce the HiBiT-RBD complex and a fast assay to evaluate the presence of RBD-targeting antibodies using this tool. Due to the durability of the HiBiT-RBD protein product over a wide range of temperatures and the shorter experimental procedure that can be completed within 1 h, the protocol can be considered as a more efficient alternative to detect SARS-CoV-2 antibodies in patient serum samples.

Introduction

The recent emergence of a new coronavirus, SARS-CoV2[1], has caused more than 2,800,000 fatalities and 128 million infections as of March 30th, 2021[2]. Due to the lack of a reliable and well-established treatment procedure for SARS-CoV-2 clinical therapies, many endeavors have been made to restrict further viral transmission and more importantly, to develop an effective and robust treatment or a vaccine[3]. To date, there are more than 50 COVID-19 vaccine candidates in trials reported by the World Health Organization[4]. Detection of antibodies against SARS-CoV-2 is of paramount importance to determine the long-term stability of humoral response upon administration of the vaccine as well as in recovered patients of COVID-19[5]. Some studies have demonstrated that there is a possibility

that recovered SARS-CoV-2 patients lose most of the RBD-binding antibodies after 1 year[5,6,7,8,9]. Further investigation is required to better understand lasting immunity, and more sensitive antibody detection platforms can help further such work. Reports of sustained immunity of mild SARS-CoV-2 infections, which suggest long-term antibody responses, is also an interesting and worthwhile area of study. A fast and accurate method of detection is essential for monitoring antibodies in individuals' sera to provide more information about immunity in the population.

Like other coronaviruses, SARS-CoV-2 uses protruding spike glycoprotein to bind to angiotensin-converting enzyme-2 (ACE2) to initiate a cascade of events that lead to the fusion of the viral and cell membranes[6,7]. Several studies have recently proved the RBD of the Spike protein to have a crucial role in eliciting powerful and specific antibody response against SARS-CoV2[8,9,10,11]. In particular, correlations observed by Premkumar et al. between the titer of RBD-binding antibody and SARS-CoV-2 neutralization potency of patients' plasma are consistent with RBD being an immunogenic compartment of the virus structure[9]. With that in mind, many diagnostic tests available for SARS-CoV-2 antibody detection are time and cost-intensive, require a lengthy procedure of incubation and washing (enzyme-linked immunosorbent assay [ELISA]), or lack sensitivity and accuracy (lateral flow immunoassay [LFIA])[12]. Therefore, a quantitative and rapid complementary serological method of COVID-19-derived antibody detection with high sensitivity, fast response, and relatively low cost would serve the need for a reliable serologic test for SARS-CoV-2 epidemiologic surveillance.

Collectively, the limitations of current serological assays prompted the investigation of the bioluminescent reporting system as a potential diagnostic agent in future serosurveys. Bioluminescence is a naturally occurring enzyme/substrate reaction, with light emission. Nanoluc luciferase is the smallest (19 kDa), yet the brightest system compared to *Renilla* and firefly luciferase (36 kDa and 61 kDa, respectively)[13,14]. Further, Nanoluc has the highest signal to noise ratio and stability among the previously mentioned systems. The high signal intensity of Nanoluc supports the detection of even very low amounts of reporter fusions[15]. Nanoluc Binary Technology (NanoBiT) is a split version of the Nanoluc system, which is comprised of two segments: small BiT (11 amino acids; SmBiT) and large BiT (LgBiT) with relatively low-affinity interactions (K_D = 190 µM) to form a luminescent complex[16]. NanoBiT is extensively used in various studies involving the identification of protein-protein interactions[15,17,18,19] and cellular signaling pathways[11,20,21].

Recently, another small peptide with a distinctly higher affinity to LgBiT (K_D = 0.7 nM) was introduced, namely the HiBiT Nano-Glo system, in place of SmBiT. The high affinity and strong signal of the Nano-Glo "add-mix-read" assay makes HiBiT a suitable, quantitative, luminescent peptide tag. In this approach, the HiBiT tag is appended to the target protein by developing a construct imposing minimal structural interference. HiBiT-protein fusion would actively bind to the LgBiT counterpart, producing a highly active luciferase enzyme to generate detectable bioluminescence in the presence of detection reagents (**Figure 1**). Similarly, we developed a HiBiT Nano-Glo-based system to readily measure the neutralizing antibody titer in the sera of SARS-CoV-2 recovered individuals and recently developed a HiBiT-tagged SARS-CoV-2 RBD. This paper describes the protocol for producing the HiBiT-RBD bioreporter using standard laboratory procedures and equipment, and shows how this

bioreporter can be used in a fast and efficient assay to detect SARS-CoV-2 RBD-targeting antibodies.

Protocol

NOTE: The protocol described below adheres to all ethics guidelines according to protocol code 20200371-01H.

1. Production and evaluation of the HiBiT-RBD bioreporter

1. Producing a sufficient quantity of HiBiT-RBD bioreporter
    1. Prepare for cell culture
        1. Prepare complete Dulbecco's modified Eagle medium (DMEM) containing 10% fetal bovine serum and 1% penicillin/streptomycin. Then, warm the media in a 37 °C water bath.
        2. Turn the biological safety cabinet (BSC) on, and use 70% v/v ethanol for sterilizing the cabinet surface.
    2. Culture the cell line.
        1. Take out the cell line from -80 °C or liquid nitrogen, and thaw it in a 37 °C water bath.
           NOTE: An appropriate cell line is easy to maintain in culture, has high transfection efficiency, and is suitable for exogenous protein production. Human embryonic kidney, HEK293 cells were used for this protocol.
        2. Mix the thawed cells with at least 10 mL of complete medium, pipette the cell suspension to a 10 cm Petri dish, and swirl the plate to distribute cells in the dish uniformly. Place the dish in a cell culture incubator at 37 °C, 5% CO_2, and 85-95% humidity.
        3. Observe the cells under the microscope until the confluency level reaches 80-90%. At high confluency, remove the medium, wash the cells with warm phosphate-buffered saline (PBS), and add 1 mL of 0.25% trypsin-ethylenediamine tetraacetic acid to detach the cells from the surface.
           NOTE: The HEK293 cells are fairly easily detached. Hence, the washing step should be done very gently to prevent accidental detachment and loss of cells.
        4. After approximately 5 min, look at the cells under a microscope. If all cells are floating, add at least 4 mL of medium, and transfer the cell suspension into a new sterile tube. Count the cells using a hemocytometer, and add 1 × 10^6 cells into each well of a 6-well plate for transfection.
           NOTE: After 24 h, cells should be at 80% or more confluent.
3. Transfection of the HiBiT-RBD plasmid
    1. Use 1 µg of the HiBiT-RBD expression plasmid with a suitable transfection reagent. Incubate for 10-15 min at room temperature, and then add the total volume to each well of the plate, drop-wise.
       NOTE: Follow the manufacturer's transfection protocol. In this case, a mixture (a specified amount) of the transfection reagent with DMEM was added to the diluted plasmid (1 µg) in DMEM (see the **Table of Materials**). Use a marker containing (e.g., green fluorescent

protein [GFP]) plasmid as a control to monitor the transfection efficiency.

2. On the next day, replace the medium containing the transfection mixture with complete medium. Observe the transfection control well 48 h after transfection.
   NOTE: If the transfection was positive and efficient (more than 80% GFP-positive), the cells should be ready for harvesting the HiBiT-RBD bioreporter. The construct also contains His-tag, which can be used to obtain purified protein in place of the total supernatant.
3. Collect the supernatant in 1.5 mL microtubes. Add 500 µL of 1x passive lysis buffer (PLB) to the cells; incubate and shake the plate for 15 min at room temperature for cell lysis.
   NOTE: The supernatant and the lysate solution can be preserved at -20 °C with minor loss of integrity for at least 6 months. According to Azad et al.[22], the reporter is stable at a wide range of pH (4-12) and temperature (4-42 °C).

2. Evaluation of the luminescent signal from the bioreporter by luciferase assay
   1. Preparing the reaction components
      1. Use the supernatant as the source of the bioreporter.
         NOTE: Both supernatant and lysate contain the HiBiT-RBD bioreporter and can be used for the assay. However, the supernatant is recommended as the source due to reasons explained in the following notes.
      2. Dilute the LgBiT and substrate to 1x before use (stock concentration is 100x).
         NOTE: See the **Table of Materials** for details about the LgBiT.
   2. Luciferase assay
      1. Transfer 50 µL of the supernatant from each well or tube to a 96-well plate, and add 50 µL of 1x LgBiT to each well. Incubate for 5 min at room temperature.
      2. Open the luminometer software, add 50 µL of 1x substrate (furimazine) to each well, place the plate in the luminometer, and run the software.
         NOTE: Add the substrate immediately before reading the plate to prevent consumption of the substrate by the active enzymes before signal measurement.

2. Detecting anti-RBD antibody with a fast and sensitive assay

1. HiBiT-RBD antibody detection assay
   1. Prepare the HiBiT-RBD bioreporter as described in section 1.1 of the protocol.
      NOTE : It is recommended to use the supernatant for the following assay as it is simpler to collect and contains the mature glycosylated version of the protein. Moreover, the lysate has several other proteins that could interfere with the HiBiT-RBD-antibody interaction.
   2. Combine 50 µL of the HiBiT-RBD-containing supernatant with 1 µg of the commercial SARS-CoV-2-RBD antibody in a 1.5 mL microtube. Add 20 µL of immunoglobulin-binding protein (protein G) to the solution. Bring up the total volume to 300 µL by adding PBS.

NOTE: The total volume of the mixture can be decreased to 150 µL. Lower total volumes are not recommended as it could result in inadequate mixing of antibodies with the bioreporter.

3. Incubate the tube(s) on a tube shaker or rotator for 30 min. Centrifuge at 12,000 × *g* for 30 s, discard the supernatant, and wash with PBS. Repeat the process three times to remove free HiBiT-RBD. Resuspend in 50 µL of PBS and transfer to a 96-well plate.
4. Add 50 µL of 1x LgBiT and wait for 5 min. Then, add 50 µL of 1x NanoLuc substrate. Immediately read the luminescent signal with a luminometer.

3. High-throughput detection of the SARS-CoV-2-specific antibodies from patient serum samples

1. Prepare larger quantities of the HiBiT-RBD bioreporter for a high-throughput assay by following section 1.1 of the protocol.
2. Combine 20 µL of magnetic protein G with 50 µL of the HiBiT-RBD supernatant in a well of 96-well plate for each sample. Add 10 µL of the serum sample to each well and bring up the total volume to 150 µL by adding PBS.
   NOTE: Use both nonspecific IgG (negative control) and neutralizing SARS-CoV-2 antibody (positive control) at 1 µg/mL concentration as described in step 2.1.2. Moreover, serum samples from vaccinated mice can also be assessed for antibodies. In this test, serum samples were obtained from Ottawa Hospital General Campus under an approved procedure and with informed consent from individuals.
3. Incubate for 30 min on a shaker at room temperature. Place the plate on a magnetic washer to precipitate the protein G-antibody complex.
   NOTE: The specific structure of the magnetic washer will precipitate the complex on the side walls of each well.
4. Discard the solution in the middle section of each well, and add PBS for washing. Repeat the washing step at least three times to remove excess HiBiT-RBD. Add 50 µL of 1x PBS and 50 µL of 1x LgBiT. Incubate for at least 5 min at room temperature.
5. Prepare the luminometer software, and then add 50 µL of 1x substrate. Place the plate in the machine, run the software, and record the signals. Compare the signals from serum samples, control samples, and background (empty wells).

Representative Results

The signals from both the HiBit-RBD-containing cell lysate and supernatant of the transfected cells were recorded (**Figure 2**) to evaluate the appropriate protein source. HiBiT-RBD and LgBit were separately used as controls, and the data showed low background compared to a strong signal when both parts were combined. Hence, HiBiT-RBD interaction with LgBiT is necessary to generate active enzyme for substrate digestion and bioluminescence activity (**Figure 1**).

The addition of protein G will help antibody precipitation (**Figure 3**). The assay was used to compare the signal from a commercial SARS-CoV-2-neutralizing antibody with a control IgG. The specific antibody signal was robust, while the control antibody had close to the luminescent background level (**Figure 4A**). Recombinant attenuated oncolytic vesicular stomatitis virus (VSV) with a mutation at position 51 of the M protein (**Δ51)** expressing exogenous RBD was used to vaccinate mice. The serum collected from vaccinated mice produced a robust signal compared to no signal in mice injected with control VSV (**Figure 4B**).

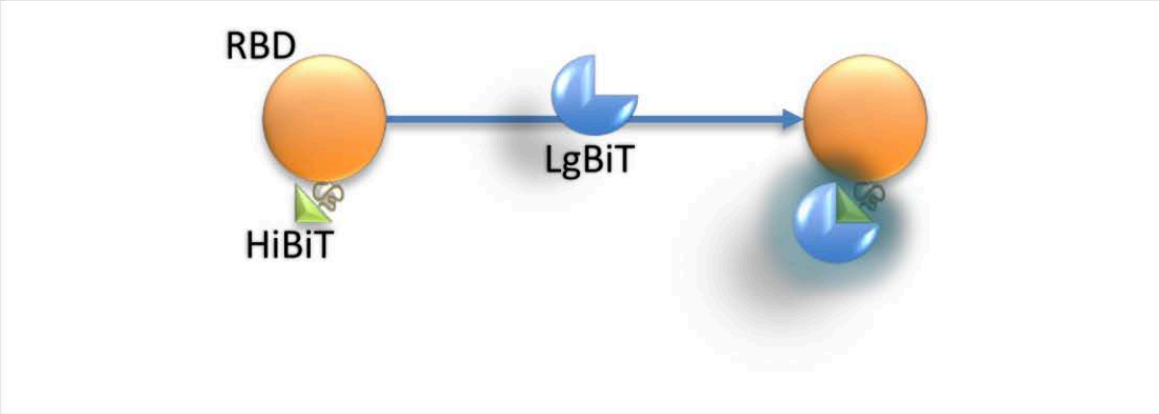

Figure 1: LgBiT interaction with HiBiT connected to RBD. Upon interaction of the small portion of the nanoluciferase, HiBiT, with the large subunit of the enzyme, LgBiT, the active enzyme complex can produce a luminescent signal after substrate consumption. The RBD does not interfere with this process. Abbreviations: RBD = receptor-binding domain. Please click here to view a larger version of this figure.

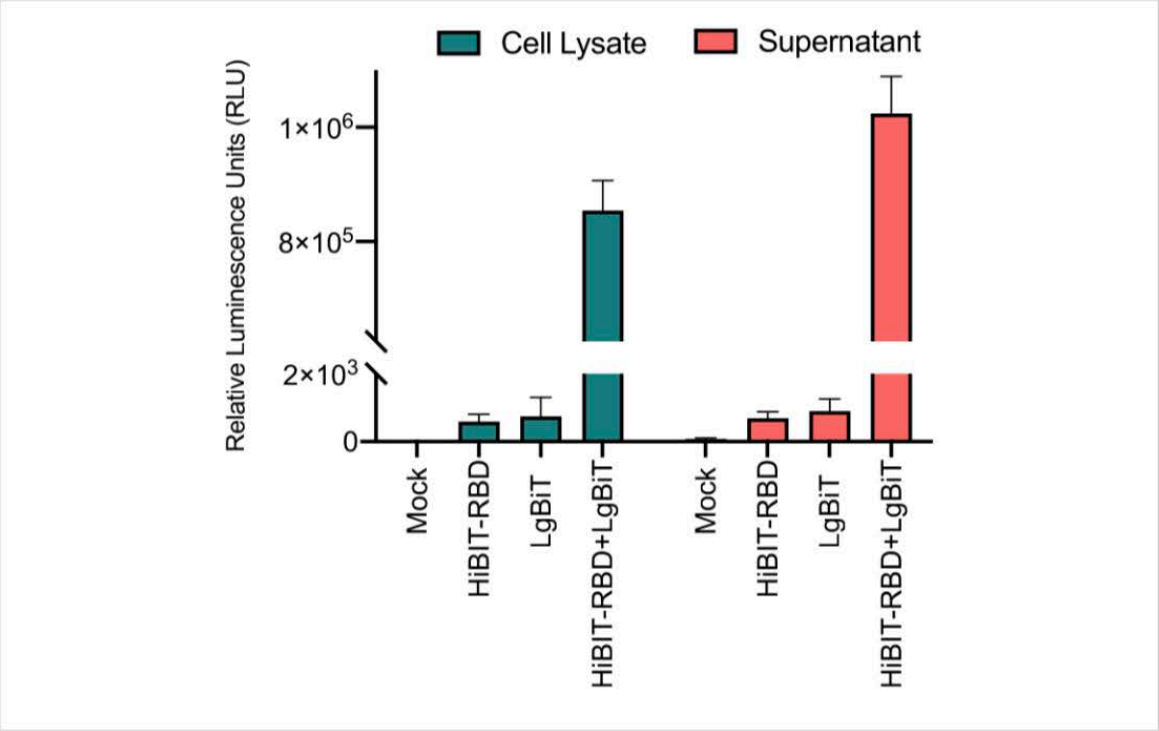

Figure 2: Robust reporter activity from both lysate and supernatant of transfected cells. The protein is present in both supernatant and lysate and produces a strong signal. Control groups' luminescent signals were close to the background. Error bars represent Standard Deviation (SD). Please click here to view a larger version of this figure.

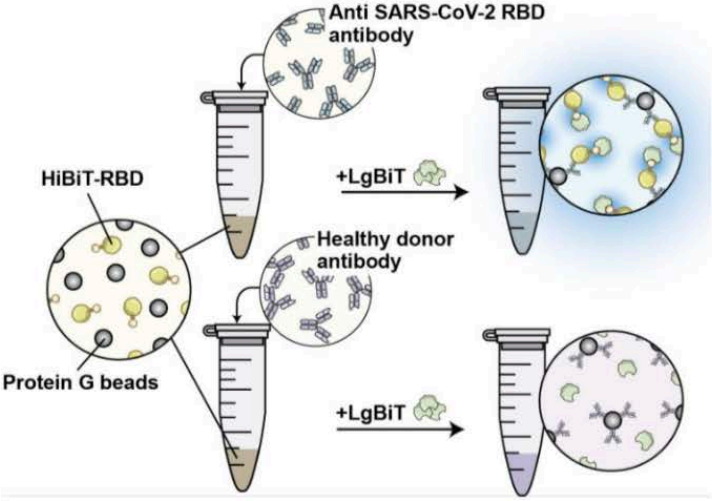

Figure 3: Schematic of the HiBiT-RBD interaction with antibodies bound to protein G. The schematic depicts the antibody precipitation by protein G and interaction with HiBiT-RBD. The addition of the LgBit to the mixture will produce a robust signal when the antibody is specific for RBD. Please click here to view a larger version of this figure.

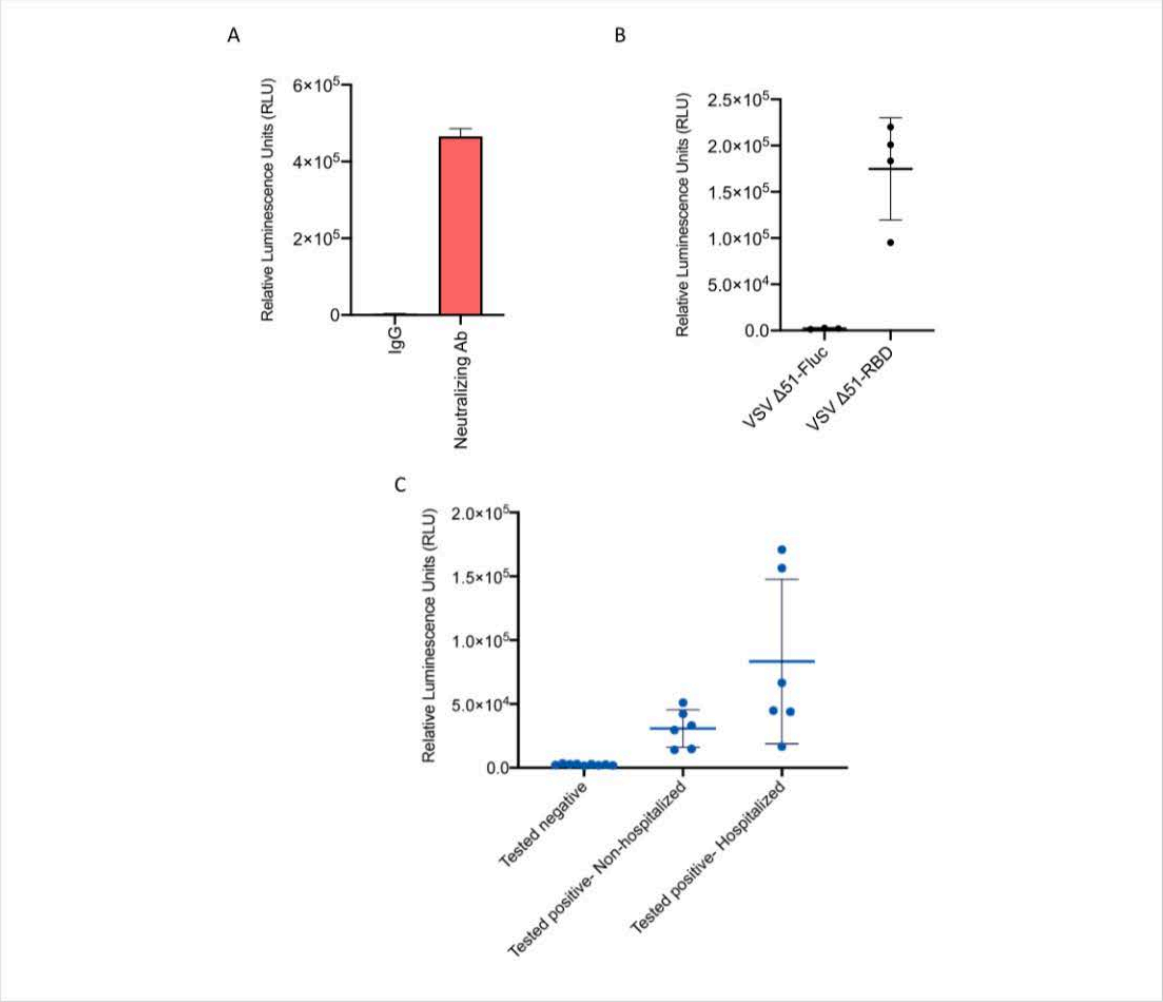

Figure 4: HiBiT-RBD bioreporter generates strong bioluminescence with purified neutralizing antibodies, vaccinated mouse serum, and patient serum samples. (**A**) HiBiT-RBD interacts with RBD-specific neutralizing antibody and generates significantly high signal compared to the negligible signal for nonspecific IgG. (**B**) The bioreporter can detect SARS-CoV-2 antibodies in vaccinated mouse serum. Abbreviations: RBD = receptor-binding domain; IgG = immunoglobulin G; Ab = antibody; VSV = vesicular stomatitis virus; Fluc = firefly luciferase. (**C**) Detection of the SARS-CoV-2 antibodies in patient serum samples, reproduced from Azad et al.[22]. Please click here to view a larger version of this figure.

Discussion

The increasing number of people infected with the SARS-CoV-2 and the ongoing effort for global vaccination necessitates sensitive and fast serologic tests that can be used in large-scale serosurveys. Recent research shows that split nanoluciferase-based bioreporters can be used to develop such assays. We recently developed the HiBiT-RBD bioreporter to design a test that can be used to detect SARS-CoV-2-specific antibodies in patient serum in a fast and reliable fashion (**Figure 4C**).

There are a few critical steps in this assay. Because the system's efficiency depends on RBD protein expression, the protein levels should be validated by western blotting. Moreover, it is necessary to use a positive control, such as a commercial antibody against RBD, and a negative control antibody. Addition of a Nanoluciferase protein is recommended to be used as a positive control for bioluminescence detection. The protein product also contains a His-tag, which can be used for purification for a large number of serum samples.

There are several advantages to using this bioreporter compared to other competing methods. First, an experienced user can perform the complete assay procedure in less than one hour, which is considerably faster than existing tests such as ELISA. Second, the minimum preparation and testing requirements make this test highly valuable for large-scale production at a low cost. Moreover, the detection limit of the assay is as low as 1 ng of the SARS-CoV-2-neutralizing antibody as described by Azad et al.[22]. A drawback of this approach is the inability to differentiate between different antibody isotypes. Moving forward, the sensitivity of the test should be compared to other routinely used serologic tests.

Azad et al.[22] had used serum samples from patients to evaluate the applicability of the assay. It is also essential that the system is tested for antibody detection in blood samples from patients. This tool could also be very impactful in the assessment of the correlation between the severity of COVID-19 and the presence of SARS-CoV-2-specific antibodies. Overall, such serologic tests could have a substantial impact in estimating the epidemiological impact of the SARS-CoV-2 and can be a convenient substitute for time-consuming and less sensitive detection methods.

Disclosures

The authors declare no conflict of interest.

Acknowledgments

We appreciate and thank the technical assistance of Xiaohong He, Ricardo Marius, Julia Petryk, Bradley Austin, and Christiano Tanese De Souza. We also thank Mina Ghahremani for Graphic Design. We would also like to thank all the individuals who participated and donated their blood samples for this study. DWC is supported in part by uOttawa Faculty and Department of Medicine.

References

1. Ullah, H., Ullah, A., Gul, A., Mousavi, T., Khan, M. W. Novel coronavirus 2019 (COVID-19) pandemic outbreak: A comprehensive review of the current literature. *Vacunas.* (2020).
2. *Coronavirus update (Live) Worldometer.* https://www.worldometers.info/coronavirus/. (2021).
3. Cacciapaglia, G., Cot, C., Sannino, F. Second wave COVID-19 pandemics in Europe: a temporal playbook. *Scientific Reports.* **10** (1), 15514 (2020).

4. World Health Organization. *COVID-19 vaccines.* https://www.who.int/emergencies/diseases/novel-coronavirus-2019/covid-19-vaccines. (2021).
5. Hueston, L. et al. The antibody response to SARS-CoV-2 infection. *Open Forum Infectious Diseases.* 7 (9), ofaa387 (2020).
6. Lan, J. et al. Structure of the SARS-CoV-2 spike receptor-binding domain bound to the ACE2 receptor. *Nature.* **581** (7807), 215-220 (2020).
7. Azad, T. et al. Implications for SARS-CoV-2 vaccine design: fusion of Spike glycoprotein transmembrane domain to receptor-binding domain induces trimerization. *Membranes.* **10** (9), 215 (2020).
8. Piccoli, L. et al. Mapping neutralizing and immunodominant sites on the SARS-CoV-2 Spike receptor-binding domain by structure-guided high-resolution serology. *Cell.* **183** (4), 1024-1042.e21 (2020).
9. Premkumar, L. et al. The receptor-binding domain of the viral spike protein is an immunodominant and highly specific target of antibodies in SARS-CoV-2 patients. *Science Immunology.* **5** (48), eabc8413 (2020).
10. Walls, A. C. et al. Elicitation of potent neutralizing antibody responses by designed protein nanoparticle vaccines for SARS-CoV-2. *Cell.* **183** (5), 1367-1382.e17 (2020).
11. Azad, T. *Nanoluciferase complementation-based biosensor reveals the importance of N- linked glycosylation of SARS-CoV-2 Spike for viral entry.* S1525-0016(21)0074-5 (2021).
12. Bastos, M. L. et al. Diagnostic accuracy of serological tests for covid-19: systematic review and meta-analysis. *BMJ.* **370**, m2516 (2020).
13. Promega. *Bioluminescent Reporters | Reporter Gene Applications | An Introduction to Reporter Genes.* https://www.promega.ca/resources/guides/cell-biology/bioluminescent-reporters/#references-6d127eb8-eeae-40b7-86e9-fe300545e8fa. (2021).
14. Fleiss, A., Sarkisyan, K. S. A brief review of bioluminescent systems (2019). *Current Genetics.* **65** (4), 877-882 (2019).
15. Nouri, K. et al. A kinome-wide screen using a NanoLuc LATS luminescent biosensor identifies ALK as a novel regulator of the Hippo pathway in tumorigenesis and immune evasion. *The FASEB Journal.* **33** (11), 12487-12499 (2019).
16. Boute, N. et al. NanoLuc Luciferase - a multifunctional tool for high throughput antibody screening. *Frontiers in Pharmacology.* **7**, 27 (2016).
17. Nouri, K. et al. Identification of celastrol as a novel YAP-TEAD inhibitor for cancer therapy by high throughput screening with ultrasensitive YAP/TAZ-TEAD biosensors. *Cancers.* **11** (10), 1596 (2019).
18. Azad, T. et al. SARS-CoV-2 S1 NanoBiT: A nanoluciferase complementation-based biosensor to rapidly probe SARS-CoV-2 receptor recognition. *Biosensors and Bioelectronics.* **180**, 113122 (2021).
19. Brown, E. E. F. et al. Characterization of critical determinants of ACE2-SARS CoV-2 RBD interaction. *International Journal of Molecular Sciences.* **22** (5), 2268 (2021).
20. Azad, T. et al. A gain-of-functional screen identifies the Hippo pathway as a central mediator of receptor

tyrosine kinases during tumorigenesis. *Oncogene*. **39** (2), 334-355 (2020).

21. Schwinn, M. K. et al. CRISPR-Mediated tagging of endogenous proteins with a luminescent peptide. *ACS Chemical Biology*. **13** (2), 467-474 (2018).

22. Azad, T. et al. A high-throughput NanoBiT-based serological assay detects SARS-CoV-2 seroconversion. *Nanomaterials*. **11** (3), 807 (2021).

CURRICULUM VITAE

EDUCATION

PhD – Microbiology & Immunology, September 2016 – Present (transfer from MSc April 2018)
Faculty of Medicine, University of Ottawa, Ottawa, Ontario, Canada

HBSc – Biochemistry (Biomedical Research Spc.) Co-op, *Summa cum laude*, Class of 2016
McMaster University, Hamilton, Ontario, Canada

SCHOLARSHIPS & AWARDS

NSERC PGS-D Scholarship ($21,000/year, Sep 2020 – Present)
University of Ottawa Nominee for Let's Talk Science National Award 2019, 2021
Best Student Plenary Presentation Award – Summit4CI Conference ($1000, Oct 2018)
Ontario Graduate Scholarship ($15,000/year, Sep 2018 – Aug 2020)
BioCanRx Travel Award – Summit 4CI (July 2018)
BioCanRx Travel Award – ICMS Conference ($1000, June 2018)
University of Ottawa Admission Scholarship ($3000, Sep 2017 – Aug 2018)
University of Ottawa Excellence Scholarship (Varied, Sep 2016 – Aug 2017, Sep 2018– present)
QEII Graduate Scholarship in Science & Technology ($15,000, Sep 2016 – Aug 2017)
OHRI Summer Student Seminar Silver Award – Peer Category (Aug 2016)
IRIC Next Generation Internship Award ($4250, Summer 2013)
McMaster President's Award Entrance Scholarship ($3000, 2011)

RESEARCH EXPERIENCE

PhD Student – Ilkow & Bell Labs **Sep 2016 – Present**
Ottawa Hospital Research Institute, University of Ottawa, Ottawa, ON

Molecular Biology Co-op Student **May – Dec 2015**
Biologics Division, Admare BioInnovations, Vancouver, BC

Honours Thesis Student **Sep 2014 – April 2015**
Brain-body Institute, St. Joseph's Hospital, Hamilton, ON

Downstream Platform Co-op Student **Jan – Aug 2014**
Downstream Platform, Bioprocess R&D, Sanofi Pasteur, Toronto, ON

IRIC Summer Intern – Verreault Lab **May – Aug 2013**
Institute for Research in Immunology and Cancer, University of Montréal, Montréal, QC

PUBLICATIONS

Manuscript In-progress

Modulating lipid flux in a fatty tumour microenvironment sensitizes tumours to oncolytic virus therapy. **Surendran A**, Taylor V, Brown E, de Souza CT, Petryk J, Poutou J, Lawson C, McCloskey C, Mayer J, Rezaei R, Birdi H, Neault S, Jamieson T, Dave J, Wylie B, Tucker S, Austin B, Falls T, Azad T, Vanderhyden B, Tai L, Bell J, Ilkow C.

Published Articles

Virally programmed extracellular vesicles sensitize cancer cells to oncolytic virus and small molecule therapy. Wedge ME, Jennings V, Crupi M, Poutou J, Jamieson T, Pugliese J, Souza CS, Petryk J, Laight B, Boileau M, Taha Z, Alluqmani N, McKay H, Pikor L, Khan ST, Azad T, Rezaei R, Austin B, He X, Mansfield D, Pelin A, Rose E, Brown E, Crawford N, Alkayya Al, **Surendran A**, Singaravelu R, Roy D, Migneco G, McSweeney B, Cottee ML, Jacobus E, Keller B, Yamaguchi T, Boutros P, Geoffrion M, Rayner K, Chatterjee A, Auer R, Diallo JS, Gibbings D, tenOever B, Melcher A, Bell J, Ilkow C. Nature Communications. Accepted 2022 Mar 7

Rangsitratkul C, Lawson C, Bernier-Godon F, Niavarani SR, Boudaud M, Rouleau S, Gladu-Corbin AO, **Surendran A**, Ekindi-Ndongo N, Koti M, Ilkow CS. Intravesical immunotherapy with a GM-CSF armed oncolytic vesicular stomatitis virus improves outcome in bladder cancer. Molecular Therapy-Oncolytics. 2022 Mar 17;24:507-21

Boulton S, Poutou J, Martin NT, Azad T, Singaravelu R, Crupi MJ, Jamieson T, He X, Marius R, Petryk J, de Souza CT, Austin B, Taha Z, Whelan J, Khan ST, Pelin A, Rezaei R, **Surendran S**, Tucker S, Brown EEF, Dave J, Diallo JS, Auer R, Angel JB, Cameron W, Cailhier JF, Lapointe R, Potts K, Mahoney DJ, Bell JC, Ilkow CS. Single-dose replicating poxvirus vector-based RBD vaccine drives robust humoral and T cell immune response against SARS-CoV-2 infection. Molecular Therapy. 2021 Oct 20

Rezaei R, **Surendran A**, Singaravelu R, Jamieson TR, Taklifi P, Poutou J, Azad T, Ilkow CS. Detection of SARS-CoV-2 Receptor-Binding Domain Antibody using a HiBiT-Based Bioreporter. Journal of Visualized Experiments: Jove. 2021 Aug 12(174).

Azad T, Rezaei R, Singaravelu R, Jamieson TR, Crupi MJ, **Surendran A**, Poutou J, Taklifi P, Cowan J, Cameron DW, Ilkow CS. A High-Throughput NanoBiT-Based Serological Assay Detects SARS-CoV-2 Seroconversion. Nanomaterials. 2021 Mar;11(3):807

Brown EE, Rezaei R, Jamieson TR, Dave J, Martin NT, Singaravelu R, Crupi MJ, Boulton S, Tucker S, Duong J, Poutou J, Pelin A, Yasavoli-Sharahi H, Taha Z, Arulanandam R, **Surendran A**, Ghahremani M, Austin B, Matar C, Diallo JS, Bell JC, Ilkow CS, Azad T. Characterization of critical determinants of ACE2–SARS CoV-2 RBD interaction. International journal of molecular sciences. 2021 Jan;22(5):2268.

Azad T, Singaravelu R, Crupi MJ, Jamieson T, Dave J, Brown EE, Rezaei R, Taha Z, Boulton S, Martin NT, Surendran A. Implications for SARS-CoV-2 vaccine design: Fusion of spike glycoprotein transmembrane domain to receptor-binding domain induces trimerization. Membranes. 2020 Sep;10(9):215.

Azad T, Rezaei R, Surendran A, Singaravelu R, Boulton S, Dave J, Bell JC, Ilkow CS. Hippo signaling pathway as a central mediator of receptors tyrosine kinases (RTKs) in tumorigenesis. Cancers. 2020 Aug;12(8):2042.

Achard C*, Surendran A*, Wedge ME, Ungerechts G, Bell J, Ilkow CS. Lighting a fire in the tumor microenvironment using oncolytic immunotherapy. EBioMedicine. 2018 May 1;31:17-24.

Yu Z, Karkaria T, Espina M, Hunjun M, Surendran A, Luu T, Telychko J, Yang YP. Comparing multi-module connections in membrane chromatography scale-up. Journal of Biotechnology. 2015 Jul 20;206:38-41.

Book Chapters

Keller BA, Wedge MÈ, Surendran A, Ilkow CS. Generating Primary Models of Human Cancer to Aid in the Development of Clinically Relevant Oncolytic Viruses. InOncolytic Viruses 2020 (pp. 271-284). Humana, New York, NY.

INTERNSHIPS

Strategy & Integration Intern **July – Aug 2019**
Policy, Integration & Performance Branch, National Research Council, Ottawa, ON

TEACHING ACTIVITIES

Certificate in University Teaching **Sep 2020 – Present**
Teaching & Learning Support Service, University of Ottawa

Undergraduate Course Guest Lecture – TMM 4101 **April 2021**
University of Ottawa

- Title: 'The tumour immune microenvironment & immunotherapies'

Teaching Assistantships **Jan 2017 – Dec 2021**
Faculty of Medicine and Faculty of Science, University of Ottawa

- Proteins: Structure, Function & Disease - Corrector (BIO 3151/TMM3102; Nov–Jan 2021, Oct–Dec 2021)
- Pathogenic Bacteriology – Corrector (MIC 4124; Jan – April 2021)
- Molecular Biology Demonstrator (BIO 3151; Jan – April 2020)
- Biochemistry Lab II Demonstrator (BIO 3346; Jan – April 2017)

Undergraduate lab mentorship May 2019 – Aug 2021
Ottawa Hospital Research Institute, Ottawa General Hospital
- BioCanRx Summer Student (May – Aug 2021)
- Two TMM Rotation Students (Jan – April 2020)
- Summer Student (May – July 2019)

EXTRACURRICULAR ACTIVITIES

Plain Language Facilitator Feb 2021
Summit for Cancer Immunotherapy Speaker Series
- Title: 'Engineered biovesicles – a new platform for cancer immunotherapeutics'

Let's Talk Science Nov 2016 – Aug 2021
Ottawa, ON
- Let's Talk Cancer Co-ordinator (Aug 2020–May 2021)
- Team Leader (Nov 2018–Aug 2021)
- Demonstrator (Nov 2016–Aug 2021)

University of Ottawa Journal of Medicine Sep 2018 – Aug 2021
University of Ottawa
- Editorial Team (Sep 2018 – Aug 2021)
- Vice-President of Finance (Sep 2018 – Aug 2019)

The Ottawa hospital Grade 9 Job Shadow Day Nov 2020
Ottawa General Hospital, Ottawa, ON
- https://www.youtube.com/watch?v=jBhLyIYY3AY&feature=youtu.be&fbclid=IwAR22-e5iDxYaJMqlw3Opibp-nEyo-9SmWNgGXd5GDu4NRemJvfKYpovbKMI

Graduate Student Mentorship Program – Mentor Sep 2018 – Aug 2019
University of Ottawa

CONFERENCE PARTICIPATION

Conference	Nature of Participation
Biochemistry, Microbiology & Immunology Seminar Day, University of Ottawa, Ottawa, ON	2017, 2019 – Poster 2020 – Seminar (pre-recorded) 2021 – Seminar
Ottawa Hospital Research Institute Research Day, Ottawa, ON	2016-2019 – Poster 2020 – Oral Presenter
BioCanRx Summit for Cancer Immunotherapy	2019 – Poster (Victoria, BC) 2018 – Oral Presenter (Banff, AB) 2017 – Speed-talk (Gatineau, QC)
8th International Conference on Tumour Microenvironment Progression, Therapy and Prevention, Lisbon, Portugal (2018)	Poster
Canadian Cancer Research Conference, Vancouver, BC (2017)	Poster